UNIVERSITA' VITA-SALUTE SAN RAFFAELE

CORSO DI DOTTORATO DI RICERCA INTERNAZIONALE IN MEDICINA MOLECOLARE

Curriculum in Gene and Cell Therapy

DEVELOPMENT OF CHIMERIC LYSOSOMAL ENZYMES WITH IMPROVED BIOAVAILABILITY TO ADVANCE GENE THERAPY STRATEGIES FOR GLOBOID CELL LEUKODYSTROPHY

DoS: Dr. Angela Gritti

Second Supervisor: Dr. Marta Serafini

Tesi di DOTTORATO di RICERCA di Federica Cascino

Matr. 015646

Ciclo di dottorato XXXV

SSD: BIO/11, BIO/13

Anno Accademico 2021/2022

CONSULTAZIONE TESI DI DOTTORATO DI RICERCA

Il/la sottoscritto/*I* Cascino Federica

Matricola / *registration number* *015646*

nata/ *born at* Palermo

il/*on* 15/02/1991

autore della tesi di Dottorato di ricerca dal titolo / *author of the PhD Thesis titled*

DEVELOPMENT OF CHIMERIC LYSOSOMAL ENZYMES WITH IMPROVED BIOAVAILABILITY TO ADVANCE GENE THERAPY STRATEGIES FOR GLOBOID CELL LEUKODYSTROPHY.

X AUTORIZZA la Consultazione della tesi / AUTHORIZES *the public release of the thesis*

□ NON AUTORIZZA la Consultazione della tesi per …… mesi /DOES NOT AUTHORIZE *the public release of the thesis for …… months*

a partire dalla data di conseguimento del titolo e precisamente */ from the PhD thesis date, specifically*

Dal / *from* ……/……/…… Al / *to* ……/……/……

Poiché /*because*:

□ l'intera ricerca o parti di essa sono potenzialmente soggette a brevettabilità/ *The whole project or part of it might be subject to patentability;*

□ ci sono parti di tesi che sono già state sottoposte a un editore o sono in attesa di pubblicazione/ *Parts of the thesis have been or are being submitted to a publisher or are in press;*

□ la tesi è finanziata da enti esterni che vantano dei diritti su di esse e sulla loro pubblicazione/ *the thesis project is financed by external bodies that have rights over it and on its publication.*

Data /Date 02/11/22 Firma /Signature Federica Cascino

DECLARATION

This thesis has been:

- composed by myself and has not been used in any previous application for a degree. Throughout the text I use both 'I' and 'We' interchangeably.
- has been written according to the editing guidelines approved by the University.

All the results presented here were obtained by myself, with the following specific contributions:

1) **Lentiviral vector production and titration*:***

Lentiviral vectors productions were performed by Doctor Lucia Sergi Sergi, Doctor Francesca Ornaghi and Doctor Luigi Tiradani (San Raffaele Telethon Institute for gene therapy, SR-Tiget; Milan, Italy). Lentiviral vectors titrations were performed by myself with technical help by Doctor Francesca Ornaghi and Doctor Luigi Tiradani (Results, paragraphs 2.1, 2.4).

2) **ImageStream acquisitions and analyses*:***

were performed by Desirée Zambroni (Results, paragraph 2.3, Figure 17H), carried out in ALEMBIC, San Raffaele Scientific Institute, Milan, Italy.

3) **Quantification of GALC enzymatic activity*:***

All the measurements of GALC enzymatic activity were performed by Professor Sabata Martino and Doctor Francesco Morena, Department of Chemistry, Biology and Biotechnologies, University of Perugia, Perugia; Italy. All the data analyses were performed by myself.

4) **Cell culturing, mouse conditioning and HSPC transplant*:***

were performed by myself with technical help by Marta Freschi and Doctor Alessandra Ricca.

All sources of information are acknowledged by means of reference.

Part of the results have been published in:
https://www.frontiersin.org/articles/10.3389/fmolb.2020.00167/full

Where specified in Figure legends, graphical elements from Biorender are used and acknowledged as per license of Ospedale San Raffaele – SR Tiget's Plan active at the time of submission.

Abstract

Globoid cell leukodystrophy (GLD) is a neurodegenerative lysosomal storage disease (LSD) due to the genetic deficiency of ß-galactosylceramidase (GALC). The most frequent infantile forms display an unrelenting progression with a severe central and peripheral neurological deterioration. The only treatment option is the hematopoietic stem/progenitor cell transplant (HSPC-T), although this is poorly effective. Thus, GLD is considered an untreatable disorder.

Gene therapy (GT) provides therapeutic benefit in other LSDs that share with GLD the severe and rapid central nervous system (CNS) deterioration. However, only moderate benefit was obtained in preclinical studies for GLD and none of them was able to halt this rapid and complex multi-organ pathology. Previous studies showed that modifications to the lysosomal enzymes sequence to enhance their secretion and capability to cross the blood brain barrier (BBB) boost the GT efficacy in different animal models of LSDs. Thus, the use of a similar chimeric GALC enzyme may be crucial to successfully increase the GALC bioavailability and GT success.

We generated lentiviral vectors (LVs) encoding for the murine GALC enzyme fused with the mCherry fluorescent reporter and we engineered it by: i) replacing the GALC signal peptide (sp) with that of highly secreted lysosomal enzymes (iduronate-2-sulphatase -IDS- or α-L-iduronidase -IDUA-) to increase GALC secretion; ii) adding a low-density lipoprotein receptor binding domain peptide to enhance BBB crossing. We tested generated LVs in murine GLD neural and hematopoietic stem/progenitor cells and progeny, relevant cell types in the context of GT platforms.

We showed safe overexpression and enzymatic activity of chimeric GALC enzymes in transduced GLD cells, with an advantage in terms of GALC production and secretion given by the IDSsp and even more by the IDUAsp. The chimeric enzymes were secreted by transduced cells and recaptured by GALC-deficient neural cells, mediating clearance of galactosylceramide storage in cross-corrected cells.

These results strongly support the rationale of testing the safety and efficacy of chimeric GALC enzymes in LV-mediated HSPC-GT approaches in neonatal GLD mice. To this end, we compared Busulfan and total body irradiation as myeloablative conditioning regimens in this challenging murine model and selected a protocol that has been applied in preliminary experiments to test the safety and efficacy of HSPC-GT approaches using the optimized GALC chimeric construct.

The final goal of this project is to develop novel and more effective GT strategies for this untreatable disease.

Table of Contents

Acronyms and abbreviations

Aa: amino acid
AAV: adeno-associated virus
ACD: acid ceramidase
ACK: ammonium-chloride-potassium
Apo: apoliprotein
ARSA: arylsulfatase A
BBB: blood-brain barrier
BM: bone marrow
Bp: base pair
BUS: Busulfan
BSA: bovine serum albumin
C-: carboxyl terminus
CA: caudal
CAG: chicken beta-actin
CB: cerebellum
CD: cluster of differentiation
CFC: colony forming cell assay
CGT: ceramide galactosyltransferase
CH: mCherry
CLN2: lipofuscinosis 2
CLX: calnexin
CNS: central nervous system
CSF: cerebrospinal fluid
CSF1R: colony stimulating factor 1 receptor
CST: galactosylceramide sulfotransferase
Di: diencephalon
DMEM: dulbecco's modified eagle medium
DRG: dorsal root ganglia
E.g.: for example
EGF: epidermal growth factor
eGFP: enhanced green fluorescent protein
ER: endoplasmic reticulum
ERT: enzyme replacement therapy
FACS: fluorescence-activated cell sorting

FBS: fetal bovine serum
FGF2: fibroblast growth factor 2
FW: forward
GALC: β-galactosylceramidase
GalCer: galactosylceramide
Galc-iKO: inducible Galc knockout
GAPDH: glyceraldehyde-3-phosphate dehydrogenase
GC: glucocerebrosidase
GFAP: glial fibrillary acidic protein
GFP: green fluorescent protein
GAPDH: glyceraldehyde-3-phosphate dehydrogenase
GLD: globoid cell leukodystrophy
GNS: glucosamine-6-sulfatase
GT: gene therapy
H: hours
H-: hydrophobic core
HA: hemagglutinin
HC: hematopoietic cell
HCC: hepatocellular carcinoma
HEK293: human embryonic kidney 293
HET: heterozygous
HEXA: hexosaminidase A
HIV: human immunodeficiency virus
hFlt3L: human FMS-related tyrosine kinase 3 ligand
HRP: horseradish peroxidase
HS: heparan sulfate
HSPC: hematopoietic stem/progenitor cell
HSPC-T: hematopoietic stem/progenitor cell transplant
Iba1: activated macrophages/microglia, and ionized
IC: intracranial
ICV: intracerebroventricular
IDUA: L-iduronase
IDS: iduronate-2-sulphatase
I.e.: id est, latin for "that is"
IL: interleukin
IF: immunofluorescence
IFN- γ: interferon-γ

IGFR: insulin-like growth factor receptor
IgG: human immunoglobulin G
IP: intraperitoneal
iPSCs: induced pluripotent stem cells
IR: insulin receptor
IT: intrathecal
IV: intravenous
Kb: kilobase
kDa: kilodalton
LAMP1: lysosome-associated membrane protein 1
LC: liquid culture
LDLR: low density lipoprotein receptor
LIMP-2: lysosomal integral membrane protein 2
Lin-: lineage negative
LL: long linker
LRP: low density lipoprotein receptor related protein
LSD: lysosomal storage disorder
LV: lentiviral vector
M: molar
MLD: metachromatic leukodystrophy
Min: minutes
M6P: mannose 6-phosphate
M6PR: mannose 6-phosphate receptor
MOI: multiplicities of infection
MPS: Mucopolysaccharidosis
MRI: magnetic resonance imaging
MSC: mesenchymal stem cell
mSCF: murine stem cell factor
mTPO: murine thrombopoietin
MW: molecular weight
N-: amino terminus
NAGLU: N-acetyl-glucosaminidase
NGS: normal goat serum
NHP: non-human primate
NPC: neural progenitor cell
NPs: nanoparticles
NSPC: neural stem/progenitor cell

O4: oligodendrocyte O4 marker
O/n: overnight
PAS: periodic acid–Schiff
PB: peripheral blood
PC: pharmacological chaperone
PCR: polymerase chain reaction
PFA: paraformaldehyde
PGK: human phosphoglycerate kinase
PH: potential of hydrogen
PLX: Pexidartinib
PND: post-natal day
PNS: peripheral nervous system
PRA: Pravastatin
P/S: Penicillin/Streptomycin
PSA-NCAM: polysialylated neuronal cell adhesion molecule
Psy: psychosine or galactosylsphingosine
RAD: absorbed radiation dose
REV: reverse
RO: rostral
RT: real-time
SapA: saponin A
SC: spinal cord
Sec: seconds
Sema3A: semaphorin 3A
SGSH: N-sulfoglucosamine sulfohydrolase
SIM: Simvastatin
SIN: self-inactivating
SL: short linker
SN: sciatic nerve
Sp: signal peptide
SR-Tiget: San Raffaele Telethon Institute for gene therapy
SRT: substrate reduction therapy
SUMF1: sulfatase-modifying factor 1
Sup: supernatant
SVZ: subventricular zone
Tat: transactivator of transcription
TBI: total body irradiation

tBM: total bone marrow

tBM-T: total bone marrow transplant

TEL: telencephalon

TELO: telomerase

TfR: transferrin receptor 1

TGN: trans-Golgi network

TNF-α: tumor necrosis factor alpha

Trs: transgenic

TU: transducing units

TuJ1: neuron-specific class III beta-tubulin

UCB: umbilical cord blood

UT: untreated

VCN: vector copy number

Vg: vector genome

Vs.: versus

VSV: vesicular stomatitis virus

TWI: twitcher

WB: western blotting

WT: wild-type

List of figures and tables

Introduction

1. Lysosomal storage disorders (LSDs).

1.1 Lysosomal enzymes: function and intracellular sorting pathways.

Lysosomes are mammalian cytoplasmic acidic organelles. They contain more than 60 different hydrolases required for the degradation of macromolecules as well as efflux permeases that facilitate the inside-out translocation of small molecules generated through macromolecule catabolism (Bagshaw et al., 2005). Lysosomes play a central role in the clearance of cellular and extracellular components coming from multiple routes within the endosomal-autophagic-lysosomal pathway (Walkley, 2007), being the primary centre for the breakdown of intracellular and extracellular different biomaterials and macromolecules. Substances for digestion are acquired by the lysosomes via a series of processes including endocytosis, phagocytosis, and autophagy. The molecules resulting from these digestive events are translocated from the intra-lysosomal compartment across the membrane and released into the cytoplasm for reuse. Besides this degradative role, lysosomes are also involved in other cellular functions, such as plasma membrane repair, protein secretion, cell growth and cell death (Bagshaw et al., 2005; Ballabio & Bonifacino, 2020).

Lysosomal enzymes are synthesised as precursor polypeptides in which the amino terminus (N-) sequence of 20–25 amino acids (signal peptide, sp) is responsible for co-translational translocation into the lumen of the endoplasmic reticulum (ER) and direction to the secretory pathway as well as the lysosomal localisation pathway. In the ER, after the cleavage of the sp by signal peptidases, high-mannose oligosaccharides are transferred to selected asparagine residues and the resulting products are transferred by vesicular transport to the cis-Golgi network. In the Golgi, specific enzymes catalyse the addition of a phosphate group to one or two mannose residues of each N-linked oligosaccharide, creating mannose 6-phosphate (M6P) groups. Soluble proteins have several oligosaccharides and, consequently, M6P modifications that enhance their recognition by the mannose 6-phosphate receptors (M6PRs), which are mainly present in the trans-Golgi network (TGN) and endosomal compartment and, to a lesser extent, on the plasma membrane. These receptor-protein complexes are packaged into clathrin-coated vesicles that depart from the TGN and are transported to the late endosomes and mature lysosomes. The acidic potential of hydrogen (pH) of these organelles (pH 6) causes the dissociation of the lysosomal proteins from the M6PRs, which are recycled to the Golgi or to the plasma

membrane. The phosphate groups are also removed from the M6P-tag, to prevent the whole protein returning to the Golgi apparatus. Furthermore, the acid pH triggers proteolytic processing steps for several lysosomal proteins for their maturation and folding and the final formation of active homo/hetero-multimers (Stern et al., 2008; Braulke & Bonifacino, 2009; Bajaj et al., 2019). Lysosomal proteins, both soluble enzymes and non-enzymatic proteins, can be also trafficked to lysosomes in a M6P-independent way that involves alternative receptors, such as sortilin, the lysosomal integral membrane protein 2 (LIMP-2), and low-density lipoprotein receptor (LDLR) and related protein 1 (LRP1) (Braulke & Bonifacino, 2009; Saftig & Klumperman, 2009; Markmann et al., 2015). A fraction (5–20%) of lysosomal enzymes in their precursor form escapes the intracellular sorting and is secreted in the extracellular milieu (Figure 1).

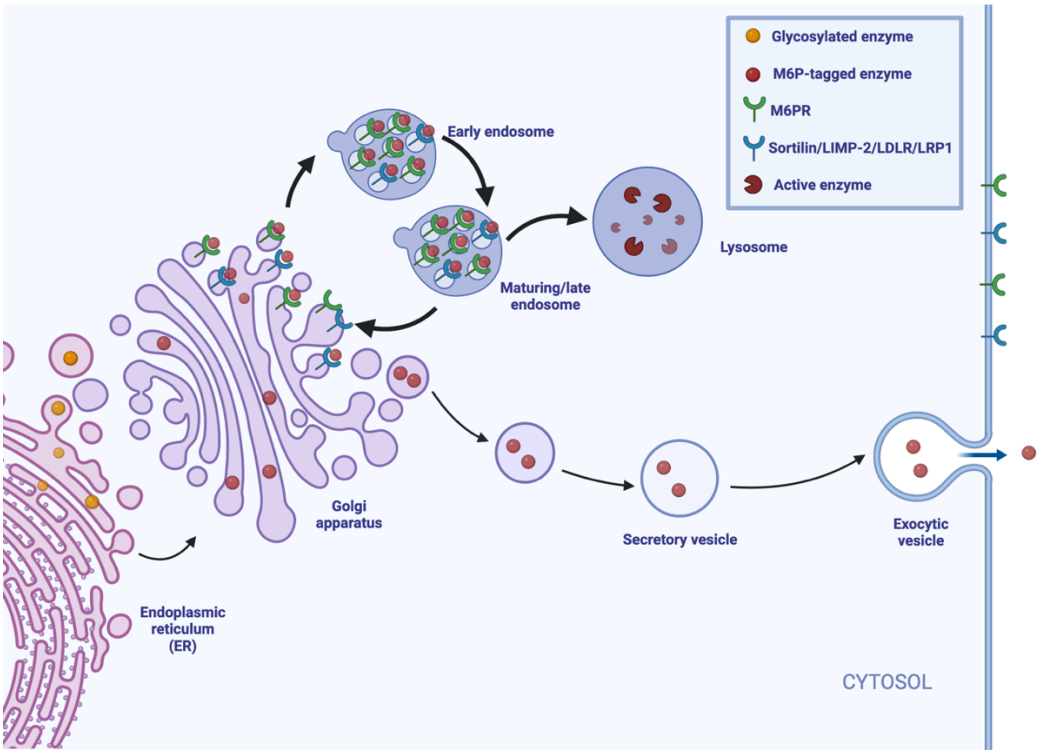

Figure 1. Lysosomal enzyme sorting pathways*. Lysosomal enzymes are glycosylated in the endoplasmic reticulum (ER) and tagged with M6P residues in the Golgi. Here, M6P-tagged enzymes bind to M6PR or other receptors, like sortilin, LIMP-2, LDLR, and LRP1. The majority (heavy arrows) of the enzymes bind to the receptors and are sorted to mature lysosomes (Lys) through endosomal compartments. In the endosomes, the acidic pH causes the dissociation of these complexes: the enzymes remain in the lumen during endosomal maturation and final fusion with lysosomes, where they are activated; the receptors are retrieved to the Golgi. A minority (fine arrows) of the lysosomal enzymes is secreted. Created with BioRender.com.*

The secreted enzymes can bind to M6PRs on the cell surface, being then internalized and transported to the lysosomes, where they become activated. In addition, they could be uptaken by surrounding cells that express M6PRs, in the

mechanism known as "cross-correction". If the enzyme secreted by healthy or genetically-modified cells is reuptaken by enzyme-deficient cells, the endocytosed functional enzymes can be directed to lysosomes, where they are activated and can fulfil their functions (Solomon & Muro, 2017) (Figure 2).

Thus, the cross-correction mechanism is at the bases of therapeutic strategies collectively named "enzyme replacement strategies", further described in paragraph 2.5.

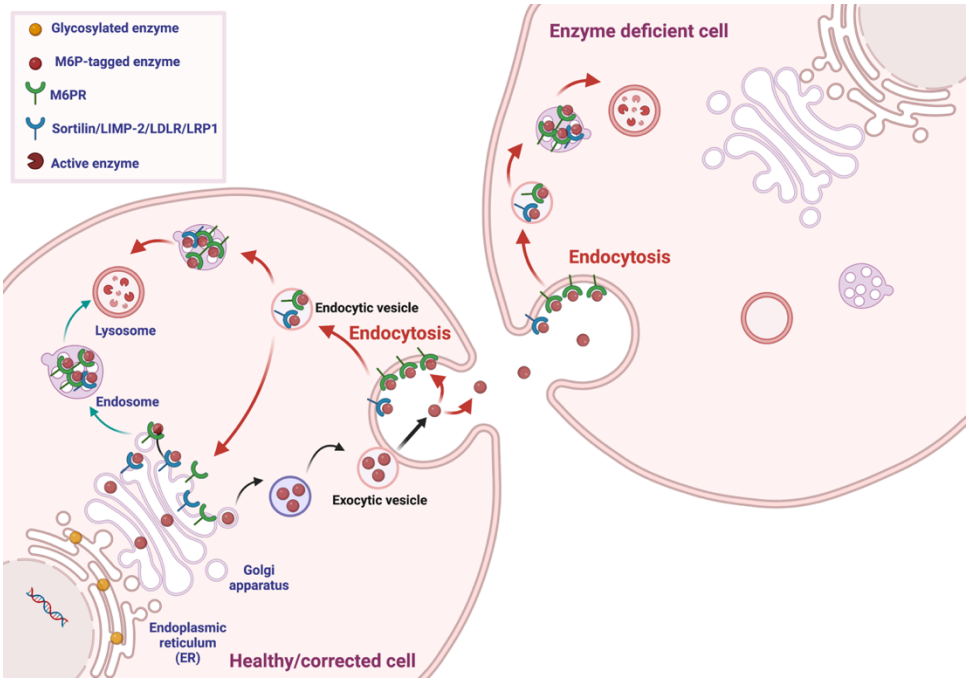

Figure 2. Cross-correction mechanism*. Lysosomal enzymes are glycosylated in the endoplasmic reticulum (ER) and tagged with M6P residues in the Golgi. They are then sorted to lysosomes (green arrows) and activated. A fraction of the lysosomal enzymes is secreted (black arrows). In the extracellular space, the secreted enzymes can bind the M6PRs or other receptors on the plasma membrane of surrounding cells. The interaction is followed by the endocytosis of the enzymes and their subsequent sorting to the lysosomes of the acceptor cells (red arrows). The receptors are retrieved to the Golgi (red arrows). The functional enzyme secreted by healthy/genetically-modified cells can be recaptured by surrounding enzyme-deficient cells, which become metabolically cross-corrected. Created with BioRender.com.*

1.2 Lysosomal storage disorders (LSDs): molecular genetics and pathophysiology.

Lysosomal storage disorders (LSDs) are a group of 70 rare inherited monogenic diseases caused by mutations in genes encoding proteins that are involved in key lysosomal functions, namely: hydrolases, transferases, integral membrane proteins, lipid and ion transporters, cofactors and enzymes activators, as well as several non-lysosomal proteins that participate in lysosome-associated processes (Li, 2018; Parenti, Andria, & Ballabio, 2015a; Platt et al., 2018).

LSDs are inherited in an autosomal recessive manner, except for three of them which are X-linked disorders: i) Fabry disease and mucopolysaccharidosis type II (MPS-II or Hunter disease), which are recessive disorders; ii) Danon disease (Sugie et al., 2003) with dominant inheritance. Individually, LSDs have an incidence ranging from 1:50,000 to 1:250,000 live births; taken together they have an incidence of 1:5,000 to 1:5,500 live births (Platt et al., 2018).

The deficiency of a specific lysosomal protein/activity or, in a few cases, of non-lysosomal proteins implicated in lysosomal biogenesis or protein maturation, causes abnormal storage of macromolecular substrates within lysosomes of affected cells (primary storage). This, in turn, triggers alterations in downstream cellular functions (Schulze & Sandhoff, 2011). This may lead to the accumulation of additional lysosomal substrates (secondary storage) due to a disruption in lysosomal trafficking. Primary and secondary storage trigger defects in calcium homeostasis, signalling abnormalities, and lysosomal membrane permeabilization. The autophagy pathway is also impaired due to a defective fusion between lysosomes and autophagosomes, causing the accumulation of autophagic substrates such as aggregate-prone proteins and dysfunctional mitochondria (tertiary storage).

Thus, LSDs are complex diseases in which the direct and indirect consequences of lysosomal engulfment affect fundamental cellular processes such as intracellular trafficking, cell signalling, calcium homeostasis, lipid biosynthesis and autophagy (Ballabio & Gieselmann, 2009; Marques & Saftig, 2019).

1.3 Classification of LSDs, clinical phenotype, and therapies.

According to the major storage compound, LSDs are most frequently classified in mucopolysaccharidoses, glycoproteinosis, sphingolipidoses, glycogen storage disease, lysosomal transport defect, and others (Futerman & Van Meer, 2004; Blau, 2014). A list of the most common LSDs is reported in Figure 3.

	Alternative titles	Enzyme deficiency	OMIM
Mucopolysaccharidoses			
MPS type I	Hurler syndrome, Scheie syndrome	Alpha-L-iduronidase	252800
MPS type II	Hunter syndrome	Iduronate 2-sulfatase	309900
MPS type IIIA	Sanfilippo A syndrome	Heparan *N*-sulfatase	252900
MPS type IIIB	Sanfilippo B syndrome	Alpha-*N*-acetylglucosaminidase	252920
MPS type IIIC	Sanfilippo C syndrome	Acetyl-CoA: alpha-glucosaminide acetyltransferase	252930
MPS type IIID	Sanfilippo D syndrome	*N*-Acetylglucosamine 6-sulfatase	252940
MPS type IVA	Morquio A syndrome	*N*-Acetylgalactosamine-6-sulfate sulfatase	253000
MPS type IVB	Morquio B syndrome	Beta-galactosidase	253010
MPS type VI	Maroteaux-Lamy syndrome	*N*-Acetylgalactosamine-4-sulfatase	253200
MPS type VII	Sly syndrome	Beta-glucuronidase	253220
MPS IX	Natowicz syndrome	Hyaluronidase	601492
Glycoproteinoses			
Aspartylglucosaminuria		Glycosylasparaginase	208400
Fucosidosis		Alpha-L-fucosidase	230000
Galactosialidosis	Goldberg syndrome	Cathepsin A/beta-galactosidase/neuraminidase	256540
α-Mannosidosis		Alpha-mannosidase	248500
β-Mannosidosis		Beta-mannosidase	248510
Mucolipidosis I	Sialidosis Type II	Alpha-neuraminidase	256550
Mucolipidosis II	I-cell disease	*N*-Acetylglucosamine-1-phosphotransferase	252500
Mucolipidosis III	Pseudo-Hurler polydystrophy	*N*-Acetylglucosamine-1-phosphotransferase	252600
Schindler disease	Neuroaxonal dystrophy	Alpha-*N*-acetylgalactosaminidase	609241
Sphingolipidoses			
Fabry disease	Anderson-Fabry disease	Alpha-galactosidase A	301500
Farber disease	Farber lipogranulomatosis	*N*-Acylsphingosine amidohydrolase	613468
Gaucher disease		Acid beta-glucosidase	230800
GM1 gangliosidosis		Beta-galactosidase-1	230500
Krabbe disease	Globoid cell leukodystrophy	Galactosylceramidase	245200
Metachromatic leukodystrophy		Arylsulfatase A	250100
Multiple sulfatase deficiency	Austin disease		272200
Niemann-Pick disease type A		Acid sphingomyelinase	257220
Niemann-Pick disease type B		Acid sphingomyelinase	607616
GM2-gangliosidosis type II	Sandhoff disease	Beta-hexosaminidase	268800
GM2-gangliosidosis type I	Tay-Sachs disease	Alpha-hexosaminidase	272800
Glycogen storage disease			
Glycogen storage disorder type II	Pompe disease	Acid-alpha-glucosidase	232300
Glycogen storage disorder type IIb	Danon disease	LAMP-2	300257
Lysosomal transport defects			
Cystinosis		Cystinosin	219800
Mucolipidosis IV	Sialolipidosis	Mucolipidin	252650
Sialuria	Salla disease	Vesicular excitatory amino acid transporter (VEAT)	604369
Others			
Neuronal ceroid lipofuscinosis		Cathepsin D	610127
Niemann-Pick disease type C		NPC1 protein	257220
Lysosomal acid lipase deficiency	Wolman disease	Lysosomal acid lipase	278000
Pycnodysostosis		Cathepsin K	265800

Figure 3. Classification of lysosomal storage disorders. *The defective protein and the primary accumulated substrate are indicated for each disease. Adapted from Blau, 2014.*

This classification is useful and accepted in clinical practice but in most LSDs more than one compound is accumulated. Alternatively, LSDs can be classified based on the molecular defect (Filocamo & Morrone, 2011) in:

i) non-enzymatic lysosomal protein defects;

ii) transmembrane protein defects (transporters and structural proteins);
iii) lysosomal enzyme protection defects;
iv) post-translational processing defects of lysosomal enzymes;
v) trafficking defects in lysosomal enzymes;
vi) polypeptide degradation defects;
vii) neuronal ceroid lipofuscinoses.

Despite LSDs are monogenic disorders, different disease-causing mutations for the same disorder are usually described, including missense, nonsense and splice-site mutations, partial deletions, and insertions. Mutations in the genes encoding for lysosomal enzymes lead to the reduction or complete loss of enzyme activity (Ballabio & Gieselmann, 2009). Different levels of residual enzyme activity, associated with the different disease-causing mutations, are partially responsible for the clinical heterogeneity of LSDs. The severity of the pathological phenotype is usually related to the residual enzyme activity, which is undetectable in the most acute forms and around 5% of the physiological activity in the milder forms. However, for most LSDs there is not a direct genotype-phenotype correlation, and the course of the disease can be highly variable even between affected siblings in the same family, suggesting that other mechanisms may be involved in the onset and progression of the disease (e.g., environmental factors, modifying genes, or epigenetic factors) (Futerman & Van Meer, 2004; Gieselmann, 2005).

Most lysosomal enzymes are ubiquitously expressed, but each LSD manifestation is different according to the tissues/organs that are mainly affected by the storage, such as hypertrophic cardiomyopathy in Pompe disease patients, central nervous system (CNS) deficits in children with neuronal ceroid lipofuscinosis 2 (CLN2) or hepatosplenomegaly in Gaucher disease type I patients (Platt et al., 2018). The most severe manifestations involve the CNS and are present in about 75% of all LSDs. Clinical signs include cognitive delay, auditory and visual defects, movement disorders, seizures, and peripheral neuropathy (Bellettato & Scarpa, 2010).

The age of onset can vary within a single disease, but LSDs are prevalently paediatric disorders. Some LSDs have been classified into clinical subtypes based on the time of onset of symptoms (such as the Hurler/Scheie definitions of MPS-I or the infantile-/juvenile-/adult-onset forms of Pompe disease), but most LSDs have a wide range of clinical severity and age of presentation (Fuller et al., 2006).

The diagnosis is difficult because affected children are initially asymptomatic. Since an early diagnosis is crucial for the efficacy of the treatments, prenatal or new-born screening diagnoses are applied in case of family history (Platt et al., 2018). Expanded new-born screening programs, thanks to the introduction of novel tandem

mass spectrometry and molecular genetic techniques, are under evaluation and represent an important tool to identify pre-symptomatic patients and provide a more efficient therapy option (Peake & Bodamer, 2017; Jones et al., 2022; Ruoppolo et al., 2022; Sikonja et al., 2022).

Besides the support therapy for LSD patients' care (i.e., ventilatory and nutritional support, surgical interventions, physical therapy, and managing of neurological, cardiac, and renal complications) (Sun, 2018), specific treatments have been developed for some LSDs to correct the metabolic defect. Enzyme replacement therapy (ERT) (Desnick & Schuchman, 2012), hematopoietic stem/progenitor cell transplant (HSPC-T), and pharmacological chaperones (PC) (Platt & Lachmann, 2009; Parenti, Andria, & Valenzano, 2015b; Pereira et al., 2018; Tan et al., 2019) are applied to provide enzymatic activity *de novo* (in the case of null mutations) or to increase the residual enzymatic activity of defective enzymes. Substrate reduction therapy (SRT) is an alternative strategy to reduce the production of storage by blocking the biosynthetic enzymes upstream of the mutated one with specific inhibitors (Platt et al., 2018). Gene therapy (GT) is emerging as the most promising therapeutic strategy for the treatment of LSDs. In fact, the life-long correction of enzyme deficiency can be achieved by genetic modification of patient's cells to force the expression of the functional enzyme, also in the organs that are more difficult to be targeted and more resilient to correction, like the CNS, the bone/cartilage, and the heart. Over the last 10 years, several clinical trials based on GT strategies have started, some of them resulting in outstanding results and significant therapeutic benefits for treated patients (Platt et al., 2018; Leal et al., 2020; Naldini, 2019). More details of these therapeutic approaches are provided in paragraph 2.5 specifically for globoid cell leukodystrophy (GLD).

2. Globoid cell leukodystrophy.

Globoid cell leukodystrophy (GLD; OMIM #245200, OIMA #1140/000578) is a severe neurodegenerative LSD caused by the genetic deficiency of β-galactosylceramidase (GALC), a lysosomal enzyme that degrades galactolipids (Suzuki & Suzuki, 1970). It is also called Krabbe disease since Doctor Knud H. Krabbe first reported the clinical and histological manifestations in five affected children (Krabbe, 1916).

GLD is an autosomal recessive disease with an incidence that varies from 0.4 to 1.9 in 100,000 live births, according to the population study (Tappino et al., 2010;

Orsini et al., 2018). A higher incidence has been reported in Muslim Arabs in Jerusalem and Druze in Israel, due to consanguineous marriages (Das et al., 2020).

Different mutations (about 200) have been reported in the *GALC* gene of affected patients, without preferences for a specific region and no evident direct genotype-phenotype correlation, even if large gene deletions (of 30 kilobases, kb), truncations, frameshift and nonsense mutations are associated with severe clinical manifestations (Luzi et al., 1995; Shin et al., 2016; Bradbury et al., 2021). Mutations in the *GALC* gene cause the reduction or absence of GALC enzymatic activity and the consequent accumulation of undegraded galactolipids-derived substrate, like galactosylceramide (GalCer), a glycolipid found in central and peripheral myelin, and galactosylsphingosine (psychosine, psy), a cytotoxic lipid (Mikulka & Sands, 2016).

Since galactolipids are found almost exclusively in myelin sheets, GLD is considered as a primary myelin disorder ("leuko" white, "dys" ill, trophy "growth") and it is characterized by progressive and severe neurodegeneration caused by damage to myelin-forming cells: oligodendrocytes in the CNS and Schwann cells in the peripheral nervous system (PNS) (Suzuki, 2003; Bradbury et al., 2021). The unbalance of myelin galactolipids causes both dysmyelination (i.e., disturbances of myelination affecting the developing myelin sheaths) and demyelination (i.e., damages of myelin after its maturation is finished). This results not only in abnormal nerve conduction (Jones et al., 1999; Dolcetta et al., 2005; Toyoshima et al., 1986), but also in microglia and astrocytes activation, which induce neuroinflammation and macrophages infiltration. Neuroinflammation may result in brain atrophy, where the white matter is replaced by gliotic tissue. Taken together, they induce a rapid deterioration of cognitive, nervous, and motor functions in GLD patients (Sasaki et al., 1991; Potter & Petryniak, 2016).

The specific histological feature of GLD is the multinucleated morphology assumed by the macrophages infiltrating the CNS, which are named globoid cells. These cells contain periodic acid–Schiff (PAS)–positive tubular or filamentous inclusions and are abundant in regions of active demyelination, often clustered around blood vessels. They are mainly present within the affected white matter but can accumulate in central gray matter structures as well. These cells display microglia-specific markers and were utilized in the past as markers for post-mortem diagnosis (Itoh et al., 2002; Avola et al., 2016; Nicaise et al., 2016). Globoid cells are not present in the PNS, but endoneurial macrophages and Schwann cells contain tubular inclusions similar to those found in globoid cells (Suzuki, 2003; Kofler et al., 2022).

GLD patients are divided into different clinical subtypes according to the age of onset of symptoms: early-infantile (0 months - 6 months); late-infantile or later-

onset (6 months – 3 years); juvenile (3 years – 8 years); adult (8+ years) (Suzuki, 2003; Liao et al., 2014). The most frequent and severe form is the early infantile (representing about 85-90% of all cases) which is typically divided into four stages. Patients develop normally in the first month of life and appear normal, only to start crying frequently without an apparent cause and show feeding difficulties and gastro-oesophageal reflux. This first stage is followed by the second stage (occurring between 1 and 6 months of age), characterized by gradual and rapid mental and neural degeneration, hyper-irritability, spasticity, stiffness, hypertonicity (extended and crossed legs), trunk hyperextension (opisthotonos) and first optical degeneration with optic atrophy and sluggish pupillary reactions to light. The third stage is characterized by seizure, blindness, deafness, arrest of motor and mental development and episodes of temperature elevation without infection, possibly caused by involvement of the hypothalamus. This is followed by the last stage with myoclonic jerks of arms and legs and mental regression that progresses to a severe decerebrate condition and psychomotor deterioration. Affected children lose contact with their surroundings and usually die before two years of age from infections and respiratory failure or gradual disease progression (Wenger et al., 2000; Orsini et al., 2018).

The remaining 10%-15% of all cases are considered later-onset GLD disease. They include the late infantile form and the less represented juvenile and adult forms. Later-onset and juvenile patients are clinically heterogeneous, progress slowly, and survival varies widely among patients, with a median of eight years after symptom onset. The adult form is the most variable in terms of clinical symptomatology and course of progression. Patients may have a rapid degenerative course or an indolent progression leading a normal life (Wenger et al., 2000; Liao et al., 2014; Bascou et al., 2018; Orsini et al., 2018).

It is not possible to distinguish between early-onset and later-onset variants by comparing residual enzyme activities and, similar to other LSDs, GLD patients with similar or identical genotypes may have variable clinical presentations and disease progression. In addition, less than 10% of normal GALC activity levels have been found in healthy people (Wenger et al., 2000), suggesting a threshold that therapeutic approaches has to reach/overcome to provide benefit.

2.1 The GALC enzyme.

The human *GALC* gene (OMIM# 606890) contains 17 exons and 16 introns spanning approximately 60 kb of genomic DNA on chromosome 14q31 and encodes for a 3.8 kb mRNA (Zlotogora et al., 1990; Luzi et al., 1995b; Sakai et al., 1998).

In line with the process of lysosomal enzyme maturation described above, the GALC protein is synthesised as a precursor protein of 80 kilodaltons (kDa) and N-glycosylated in the ER, tagged with M6P in the Golgi, recognized by M6PR in the TGN and sorted to the lysosomal compartment. In the acidic lysosomal environment, it is proteolytically cleaved into a 50 kDa N-terminal and a 30 kDa carboxyl-terminal (C-) subunit, which subsequently combine to form a functional enzyme complex (Nagano et al., 1998; Spratley & Deane, 2016). In 2013, Hill and colleagues resolved the crystal structure of GALC. They showed that the functional enzyme is composed of a central dimer of Saponin A (SapA), the GALC co-factor, bound to two molecules of GALC, to form a 2:2 heterotetrameric complex (Figure 4, Hill et al., 2013, 2018).

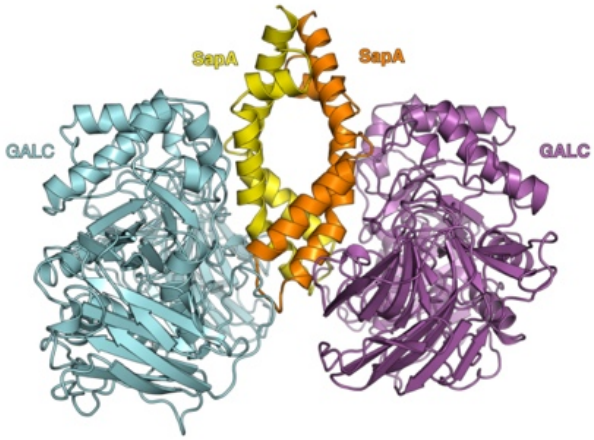

Figure 4. Crystal structure of the human GALC enzyme and Saponin A. *Two GALC molecules (cyan and magenta) and two SapA molecules (yellow and orange) are assembled in a pseudo-symmetric 2:2 heterotetramer (Hill et al., 2018).*

The highest molecular weight (MW) form (700 kDa) of GALC is the most abundant and displays the highest enzymatic activity (Ben-Yoseph et al., 1980). The cofactor SapA plays an important role in presenting the substrates' galactose group to the GALC catalytic site. Indeed, mutations in the SapA cofactor cause phenotypical alterations resembling the later-onset forms of GLD (Matsuda et al., 2001).

As for the other lysosomal enzymes, a fraction (5-20%) of the GALC precursor protein escapes the sorting pathway and is secreted in the extracellular space, where it can be reuptaken by the producing cell or by surrounding cells in the cross-correction mechanism (Lattanzi et al., 2010; Spratley & Deane, 2016).

As mentioned before, multiple receptors are involved in the traffic of lysosomal proteins. The inhibition of M6PR reduces but does not abolish GALC uptake in cultured skin fibroblasts derived from GLD patients and mice (50% and 77%, respectively) and murine neuronal/glial cells derived from GLD mice (~20-30%), suggesting that several receptors might also be involved in GALC sorting in a cell type-specific

manner (Wenger et al., 1997; Neri et al., 2011; Zhang et al., 2008). However, to date, no specific receptor has been identified.

The GALC enzyme hydrolyses several glycosphingolipids (with a terminal galactose moiety in the β-anomeric configuration), which are essential structural components of membranes and regulate a vast number of cellular processes (e.g., proliferation, survival, and apoptosis) (Spiegel & Milstien, 2003; Garcia-Ruiz et al., 2015). The CNS, which displays the highest lipid content and at the highest density, is the most affected organ in GLD. Interestingly, sphingolipids are specific for each brain region and cell type, i.e., gangliosides are the most abundant glycosphingolipid class in neurons (and thus in the gray matter), while sphingomyelin, GalCer, and sulfatides are more expressed by oligodendrocytes (white matter) and Schwann cells. Furthermore, their expression is finely regulated during mammalian development, post-natal life, and ageing, from the simpler to the more complex glycosphingolipids, with a peak which corresponds to the phase of neuronal differentiation, dendritic and axonal outgrowth, and synaptogenesis (Olsen & Færgeman, 2017).

The main substrates of GALC are GalCer and its lysolipid derivative psy (Hill et al., 2015). GalCer is the primary lipid constituent of myelin mass. It is produced from ceramide by the enzyme ceramide galactosyltransferase (CGT) and from sphingosine by the enzyme arylsulfatase A (ARSA). It is involved in pathways regulating oligodendrocyte differentiation (Hayashi & Su, 2004) and axon-glia interaction (Marcus & Popko, 2002) and its peak of expression coincides with active myelination (during the first post-natal 1.5 years in humans and between 15 and 25 post-natal days in rodents; Graziano & Cardile, 2015). Since GalCer can also be hydrolysed by the galactosylceramide sulfotransferase enzyme (CST), its concentration in GLD patients remains similar to those observed in healthy subjects (Kobayashi et al., 1985; Graziano & Cardile, 2015).

Psy derives from the transfer of galactose to sphingosine by the enzyme CGT (the same enzyme responsible for GalCer synthesis) (Won et al., 2013) and from the deacylation of GalCer by acid ceramidase (ACD) (Li et al., 2019). CGT is more expressed in the myelinating cells with respect to neurons, making oligodendrocytes more susceptible to accumulating psy (Nicaise et al., 2016). Differentially from GalCer, psy cannot be hydrolysed by other enzymes besides GALC and thus progressively accumulates in the CNS tissues of GLD patients. In physiological conditions, psy is present at nanomolar concentration in CNS tissues, while in GLD patients and animal models accumulates up to 100x the normal level, reaching micromolar concentrations (Svennerholm & Vanier, 1980). A scheme of the main pathways of glycosphingolipid metabolism involving GALC is shown in Figure 5.

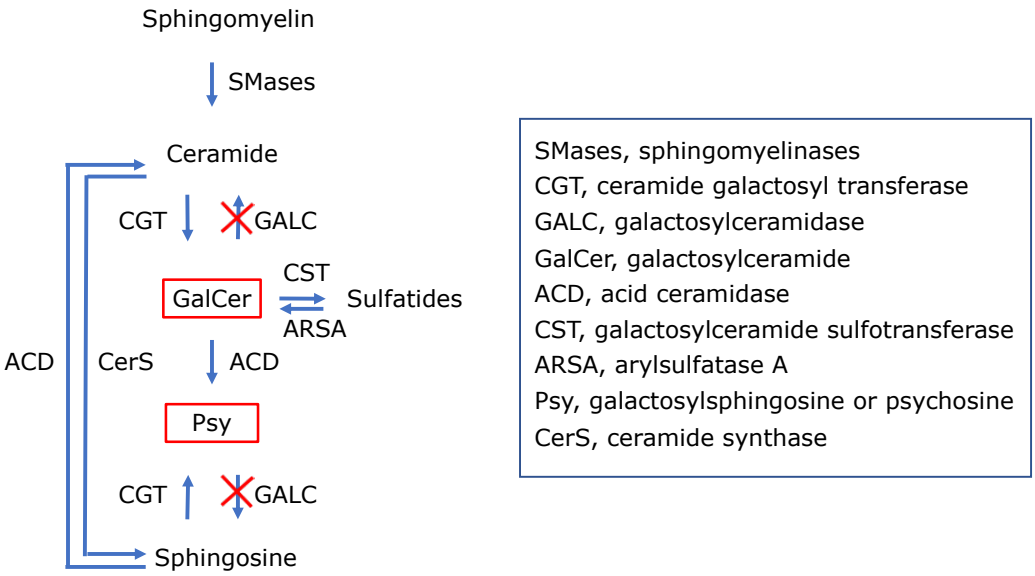

Figure 5. Main pathways of glycosphingolipid synthesis/degradation involving the GALC enzyme. *Adapted from (Gowrishankar et al., 2020).*

2.2 The GLD pathogenesis.

Neurodegeneration and neuroinflammation caused by the impaired degradation of GalCer and psy are the hallmarks of GLD pathology.

GLD is considered as an atypical LSD because its major substrate GalCer does not accumulate in the lysosomes of affected cells nor in myelin sheaths (Kobayashi et al., 1985; Graziano & Cardile, 2015). However, the PAS–positive tubular or filamentous inclusions in the cytoplasm of microglia/macrophages within the affected white and gray matter mainly consist of GalCer and cholesterol crystals (Anzil et al., 1972; Suzuki, 2003; Nicaise et al., 2016; Weinstock et al., 2020a). GalCer induces what has been defined as the "globoid reaction" in GALC-deficient macrophages, i.e., the increased expression of proinflammatory cytokines and effectors of the integrated stress, underling that this substrate plays an important role in GLD pathology and impaired macrophage function (Weinstock, et al., 2020b).

The detergent-like property of psy causes its accumulation in the lysosomal compartment and the destruction of the organelle, ultimately inducing the apoptosis of oligodendrocytes as well as neurons (Haq et al., 2003; Cantuti-Castelvetri et al., 2013; D'auria et al., 2017). In neurons, psy accumulation induces neurofilament dephosphorylation and inhibition of the fast axonal transport with consequent accumulation of vesicular cargoes and axonal swellings (Cantuti-Castelvetri et al., 2013) that leads to neurotoxicity. In oligodendrocytes, psy accumulation causes: i) alteration of membrane architecture (White et al., 2009, 2011); ii) alteration of mitochondria and peroxisomal functions (Haq et al., 2003, 2006); iii) alteration of

signal transduction pathways (Ballabio & Gieselmann, 2009), axonal cytoskeleton, and transport (Smith et al., 2011; Cantuti-Castelvetri et al., 2011, 2012); iv) apoptotic cell death (Jatana et al., 2002; Haq et al., 2003; Zaka & Wenger, 2004); v) formation of microglia and macrophage-derived multinuclear globoid cells (Kanazawa et al., 2000; Kozutsumi et al., 2002; Ijichi et al., 2013); vi) astrogliosis and microgliosis (Suzuki, 2003).

It is known that myelin and cellular debris from dead cells activate microglial cells, which became phagocytic and secrete pro-inflammatory cytokines, e.g., tumor necrosis factor alpha (TNF-α), interferon-γ (IFN- γ), and interleukin 1 beta (IL- 1β), which enhance and perpetuate microgliosis as well as induce astrogliosis (Avola et al., 2016; Potter & Petryniak, 2016). In addition, the macrophage infiltration in the site of injury and the production of cytotoxic metabolites contribute to increased gliosis over time as demyelination aggravates (Snook et al., 2014; Avola et al., 2016). The infiltration of immune cells in the nervous tissue is further facilitated by alteration of the microvasculature and dysfunction of the blood-brain barrier (BBB), which have been described in the brain of GLD patients as well as in the mouse model (Belleri et al., 2013; Giacomini et al., 2015; Belleri & Presta, 2016). Psy is responsible for inhibiting endothelial cell proliferation and migration, increasing BBB permeability, and reducing the response to proangiogenic stimuli, thus hampering neovascularization (Belleri et al., 2013). A summary of GLD pathogenic events is shown in Figure 6.

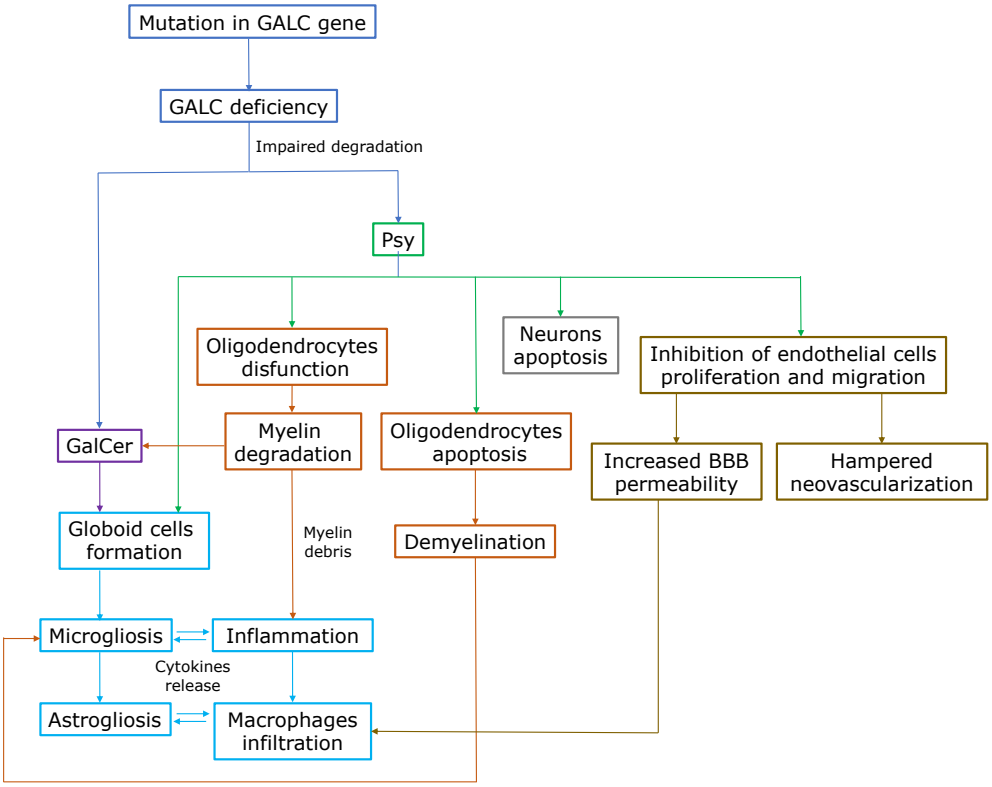

Figure 6. Role of Galactosylceramide and Psychosine in the pathogenic cascade of GLD. *GALC deficiency impairs GalCer and psy degradation, leading to loss of oligodendrocytes and neurons, increase in BBB permeability, and neuroinflammation.*

The availability of the GLD animal models has been extremely important for laboratory research to investigate the pathogenic events of GLD (see paragraph 2.4), and the establishment of primary neural cultures derived from GLD mice (Cantuti-Castelvetri et al., 2011; Santambrogio et al., 2012) has represented important *in vitro* tools to study of specific molecular phenotypes in target cell types. Despite GLD animal models recapitulate the disease phenotypes, they are limited in reproducing some specific mutations of human patients and the associated phenotype (see paragraph 2.4). For these reasons, *in vitro* models that closely recapitulate the human mutations have been generated, namely patient-specific fibroblasts (Ribbens et al., 2013; Spratley & Deane, 2016), hematopoietic cells (Martino et al., 2009), and human induced pluripotent stem cells (iPSCs) lines (Mangiameli et al., 2021), as well as epithelial cell lines in which GALC mutations have been induced (Lee et al., 2010; Shin et al., 2016).

Even if the genetic defects and the principal pathogenic events of GLD are well identified, many details of the pathogenic cascade that finally leads to cell damage and death are still poorly elucidated.

2.3 GLD diagnosis.

Current diagnosis is based on the assessment of absent/low GALC activity, detection of mutations by sequence analysis of *GALC*, and clinical examination, which includes cerebrospinal fluid (CSF) total protein test, magnetic resonance imaging (MRI) of the head, and nerve conduction velocity test (Liao et al., 2017; Orsini et al., 2018). Despite a direct genotype-phenotype correlation is missing, two mutations are specifically associated to the infantile form of GLD: a 30 kb deletion encompassing much of the *GALC* gene and a single point mutation (T513M) (Luzi et al., 1995b; Bradbury et al., 2021b). The missense mutation p.G270D is common in later-onset patients, while three pseudodeficiency alleles (p.R168C, p.D232N, and p.I546T) are known to cause reduced GALC activity but do not cause GLD (Wenger et al., 2019). In 2006, the New York state started a newborn screening program for GLD with the perspective to identify presymptomatic cases and increase the chances of successful therapy for early infantile affected children. The diagnosis is based on GALC activity evaluation, gene sequencing to detect *GALC* mutations, and psy dosage in dried blood spots. Other ten states in the United States included GLD in their newborn screening program (Orsini et al., 2016; Wasserstein et al., 2016; Kwon et al., 2018). Also in Israel, where GLD is frequent in two Moslem Arab villages in the Jerusalem area and in a Druze community in northern Israel, the prenatal and newborn screening are in place. Thanks to this program, GLD incidence has been reduced from 1.6 per 1,000 live births to 0.82 per 1,000 live births (Macarov et al., 2011). In Europe, the newborn screening programs include a more limited number of disorders (Hoffmann et al., 2014). In Italy, aminoacidemias, organic acidemias, urea cycle defects, and fatty acid oxidation disorders are included in the newborn screening (Ruoppolo et al., 2022). The DGRT n 909/2018 implemented the newborn screening program in Northeast Italy by including three LSDs, namely Pompe and Fabry diseases and MPS-I, based on successful pilot projects (Spada et al., 2006; Paciotti et al., 2012; Burlina et al., 2018). However, to date, there is not a GLD newborn screening program in Europe.

Still, reduced GALC activity and DNA sequencing do not reliably predict disease onset or severity. Thus, children identified as high risk at newborn screening may remain asymptomatic for years and false positives are also possible, highlighting several ethical concerns that limit the full exploitation of newborn screening for GLD (Ehmann & Lantos, 2019; Orsini, 2019).

2.4 GLD animal models.

Besides the *in vitro* human cellular models used to recapitulate the main pathological features of the diseases and to monitor the response to therapies (e.g. patients' fibroblasts, iPSCs, and epithelial cell lines) (Lee et al., 2010; Ribbens et al.,

2013; Shin et al., 2016; Spratley & Deane, 2016; Mangiameli et al., 2021) the animals' models are an essential tool for basic and even more for translational research. Both naturally occurring and genetically modified animal models are available for neurodegenerative LSDs, including GLD. Despite with limitations due to species-specific differences, these models allow understanding the complex neuropathological changes that occur downstream of the genetic mutation and to evaluate the outcome of therapeutic approaches once *in vitro* testing has been carried out (Hemsley & Hopwood, 2010; Gurda & Vite, 2019).

The biochemical defect associated to GLD was identified in human patients in 1970, but already in 1963 Fankhauser and colleagues described the characteristic pathological features of GLD in Cairn and West Highland White terriers, and a dog colony was established for research (Wenger et al., 1999). The following cloning of mouse (Sakai et al., 1996), dog (Victoria et al., 1996), and non-human primate (NHP, rhesus monkey, Luzi et al., 1997) GALC genes led to the identification of the disease-causing mutations and the study of pathogenetic mechanisms.

GLD dogs, which share about 90% of the amino acid (aa) sequence with humans, display low GALC activity and a progressive accumulation of psy in the brain. Between 6 and 12 weeks of age they show brain lesions with an MRI signal identical to that of human patients, dysmetria, weakness and tremor (Victoria et al., 1996; Wenger et al., 1999).

GLD NHPs, which share about 97% of the aa sequence with humans, are characterized by no residual GALC activity, the onset of symptoms within the 3–6 months of life and rapid progression to an early death, at around 1 year of age, similarly to early infantile patients (Luzi et al., 1997). Affected animals display globoid cells in the white matter and gliosis, CNS and PNS demyelination, and decreased nerve conduction velocity (Borda et al., 2008).

The similarities in genome and pathophysiology to humans, coupled with the complexity of brain structures and the possibility to use the same equipment and techniques used in human patients, make large animal models ideal for evaluating the safety and efficacy of therapies prior to human trials (Gurda & Vite, 2019). However, the limited number of affected animals relying on spontaneous mutations for the onset and progression of the disease, the genetic heterogeneity, as well as the long gestational period and the high maintenance costs, are major limitations to the use of large animal models. Ethical issues and legal restrictions are other relevant limitations (Xu et al., 2016; Ribitsch et al., 2020).

The availability of mouse models of GLD is crucial for *in vivo* studies, as mice can be easily housed, bred, and treated. Another important advantage of using mouse

models is the possibility of generating several models carrying different mutations in single or mixed backgrounds to reproduce different disease features and patient-specific mutations (Suzuki, 2003; Favret et al., 2020; Rydell-Törmänen & Johnson, 2019; Vandamme, 2014). The first GDL murine model with a naturally occurring mutation in the *Galc* gene was discovered in 1976 at the Jackson Laboratory and was referred to as twitcher mouse (Suzuki & Suzuki, 1983).

In the twitcher mouse (TWI) an autosomal recessive non-sense mutation in the *Galc* gene (chromosome 12), that has no counterpart in humans (Kobayashi et al., 1980), is responsible for a G>A transition at position 1017 of the cDNA. This leads to the formation of a premature termination codon (W339X), the degradation of synthesised mRNA due to non-sense mediated mRNA decay, and the resulting loss of GALC enzymatic activity (Lee et al., 2006; Sakai et al., 1996). TWI and unaffected littermates are indistinguishable at birth and begin to show clinical signs only around the post-natal day (PND) 21, becoming less active and developing muscular weakness, the typical limb and particularly head tremors (twitching) and limb incoordination. The disease progression is very rapid, with more intense tremors, paralysis of hind legs and neck muscles and progressive weight loss, also due to feeding difficulties. The lifespan of TWI mice with a C57BL/6J background rarely extends beyond PND 40 (Suzuki & Suzuki, 1995).

Pathological features are almost limited to the nervous system, comprising psy accumulation, severe demyelination and axonal degeneration, astrogliosis, microgliosis and presence of PAS+ globoid cells, as for affected GLD patients. More in detail, TWI mice show time-dependent characteristic pathological hallmarks of the CNS which comprises: i) accumulation of psy that in oligodendrocytes can be detected as early as PND 5, with subsequent oligodendroglia death; ii) infiltration of PSA+ macrophages in the spinal cord (SC), cerebellar white matter, and brainstem starting from PND 20, expanding then in the cerebral white matter after PND 25, and in the cerebellar and cerebral gray matter after PND 30; iii) severe astrogliosis caused by numerous glial fibrillary acidic protein (GFAP)-immunoreactive astrocytes throughout the CNS axis, including the gray matter. The cerebral cortex and other regions of the gray matter are almost unaffected, except for scattered PAS+ perivascular or perineuronal microglial cells (Taniike & Suzuki, 1994).

Even if TWI mice accurately recapitulate CNS lesions in GLD patients, some differences are present. In patients, the total lipid in the brain is drastically decreased whereas the water content increased, while in the brain of TWI mice these events are minimal (Suzuki & Taniike, 1995; Vanier & Svennerholm, 1974). Moreover, GalCer inclusions have been found in the TWI kidneys and macrophages in the lymph

nodes, but not in post-mortem tissues of GLD patients (Ida et al., 1982; Igisu et al., 1983; Suzuki & Suzuki, 1970; Takahashi et al., 1983). Differentially from GLD patients, the PNS of TWI mice is more severely affected than the CNS, as early as PND 10, possibly due to the early death of affected mice before CNS pathology fully develops. Consequently, TWI showed flaccid hind limb paralysis, whereas the decerebrate rigidity and opisthotonos observed in GLD patients are not developed. The peripheral nerves of TWI mice are grossly abnormal, with widespread segmental demyelination associated with macrophage infiltration, astrogliosis and severe endoneural oedema. Schwann cells of myelinating fibres often contain characteristic GLD inclusions, but without signs of death (Suzuki & Suzuki, 1990; Kunihiko Suzuki & Suzuki, 1995; Taniike & Suzuki, 1994).

TWI mice also showed progressive loss of immune competence. Age-related lymphoid organ failure, detectable as early as PND 15 and complete around the fifth week of life, is due to a progressive and irreversible depletion of catecholaminergic and cholinergic axons and denervation of the thymic cortex and medulla, resulting in thymic involution (Galbiati et al., 2007).

Besides TWI, other GLD murine models with different mutations in the *Galc* gene and progressive forms are available:

i) GALCtwi-5J mice (strain BXD32/TyJ) show spontaneous homozygous missense mutation in the exon 4 (G388A) of the *Galc* gene, that is identical to E130K missense mutation in a subset of infantile GLD patients. These animals show GALC precursor protein but not enzymatic activity, severe PNS hypomyelination, and the onset of the pathological phenotype sooner than TWI (at PND 14), with consequent lower median survival (23.5 days vs. around 40 of TWI) (Potter et al., 2013).

ii) Transgenic (trs) mouse model generated by homologous recombination, bearing a polymorphism (H168C) found in the human *GALC* gene, display residual GALC activity (5-10% of normal levels), lower psy accumulation and less severe CNS and PNS involvement, leading to slower disease progression and longer lifespan (around 60 days) (Luzi et al., 2001).

iii) Twitcher mice on the mixed background of C57BL/6J and FVB, generated at the San Raffaele Telethon Institute for gene therapy (SR-Tiget, Lattanzi et al., 2010; Visigalli et al., 2009), have larger litters and slowly progressive form of GLD than canonical TWI. CNS and PNS characteristic features are the same of TWI mice, and life expectancy is slightly increased (40-45 days). However, the mixed background presents limitations since influences the disease phenotype, e.g., diverse hippocampal neuron

vulnerability was observed in TWI mouse on C57BL/6J or mixed C57BL/6J-129SvEv backgrounds, and can gradually move to a pure background (Tominaga et al., 2004).

iv) Inducible GALC knockout mouse models (Galc-iKO) were generated to activate *Galc* ablation at different post-natal time points and identify a critical period of vulnerability to GALC deficiency. GALC deficiency prior to PND 4 (Galc-iKO ≤ P4) resulted in more severe phenotype and psy accumulation as well as lower survival with respect to mice in which *Galc* depletion was induced after PND 6 (Galc-iKO ≥ P6, median survival of 60 vs 90 days, respectively) (Weinstock, et al., 2020b). Galc-iKO mice in which the *Galc* knockout is restricted to the Schwann cells in the PNS (Galc SC cKO) allowed to define the role of GALC in myelination and neurodegeneration in this simply and anatomically isolated tissue (Weinstock, et al., 2020a).

v) A GLD mouse model was also obtained by knockout of its activator SapA, using the Cre/loxP system to induce amino acid substitution (C106F). $SapA^{-/-}$ mice developed a later-onset chronic form of GLD (onset of symptoms at ~2.5 months), with severe PNS involvement and a similar but milder phenotype than the canonical TWI. This leads to a slower progression of the disease and increased survival (122 ± 17 days) (Matsuda et al., 2001).

A putative GLD model was developed in zebrafish (Danio rerio) by genetic knockdown of the *GALC* orthologues genes *galca* and *galcb* (Zizioli et al., 2014). The mutant fishes do not present psy accumulation in any tissue, so they do not really represent a GLD model. Still, the developmental brain abnormalities and the increased apoptosis in the CNS point to psy-independent effect of GALC deficiency in the nervous system.

2.5 Therapeutic approaches for GLD.

Several therapeutic approaches have been tested in GLD animal models and patients, and many of them have provided various degrees of correction of the biochemical and clinical-pathological phenotype, as described below. Still, all of them fail to address the complex multi-organ pathology of GLD and are not able to arrest the disease.

Allogeneic hematopoietic stem/progenitor cell transplant (HSPC-T)

The transplantation of allogeneic HSPCs, derived from the bone marrow (BM) or the umbilical cord blood (UCB), is currently the standard of care and the only treatment available for GLD patients (Escolar et al., 2005; Krivit et al., 1998) The rationale for transplanting healthy donor HSPCs in LSDs, including GLD, relies on the possibility of repopulating the patient's hematopoietic system with metabolically competent healthy cells that are able to migrate into all the affected organs and provide a lifelong source of functional lysosomal enzymes that can act locally as well as being released and available for cross-correction (see paragraph 1.1). Also the brain, the most affected tissue in GLD, can potentially be corrected by the HSPC myeloid progeny that migrates and engrafts in this tissue as macrophages/microglial cells (Prasad & Kurtzberg, 2010). However, clinical evidence suggests that HSPC-T delays the onset and the progression of pathological manifestations in GLD affected children – still without arresting the disease progression – only if performed before the onset of symptoms (Allewelt et al., 2018; Escolar et al., 2005; Wright et al., 2017). The outcome of HSPC-T depends on the severity and progression of the disease at the time of diagnosis and treatment (Orsini et al., 2018). In addition, the procedure requires HLA-matched donors and a myeloablation and immunosuppressive regimen, which has significant impacts on HSPC-T morbidity and mortality (Wasserstein et al., 2016).

Since HSPC-T is not resolutive for GLD, many therapeutic approaches based on pharmacological approach and enzyme replacement strategies, as a single therapy or in combination, are being tested in preclinical studies and are discussed below.

Enzyme Replacement Therapy (ERT)

ERT is based on the periodic intravenous (IV) administration of a functional recombinant lysosomal enzyme. Currently, ERT is approved for Gaucher (imiglucerase, taliglucerase-α, velaglucerase-α), Fabry (agalsidase-α, agalsidase- β), and Pompe (alglucosidase) diseases, acid lipase deficiency (sebelipase-α), and MPS types I (laronidase), II (idursulfase), and VI (galsulfase) (Li, 2018; Parenti, Andria, & Ballabio, 2015a). The main obstacle to systemic ERT lies in the inability of the recombinant enzymes to cross the BBB, making this therapy effective only in LSDs with predominant peripheral manifestations, e.g., Gaucher and Fabry diseases (Giugliani, Vairo, et al., 2018; Spratley & Deane, 2016)

Preclinical studies in murine models of GLD have shown that a very low amount of functional enzyme reaches the brains of treated mice after systemic (Lee et al., 2005; Matthes et al., 2015) or even direct intracerebroventricular injection (ICV) of GALC (Lee et al., 2007), which in principle bypasses the BBB obstacle. This strategy leads

to a moderate increase in the lifespan of GLD mice without obvious benefits to the nervous system. To specifically target the brain, Del Grosso and colleagues exploited the intraperitoneal (IP) delivery of nanoparticles (NPs) engineered with brain-targeting peptides and loaded with the recombinant GALC protein. NPs-GALC injection led to significant recovery of GALC activity in different tissues, including the brain but not the SC and PNS, assessed 4 hours after treatment (Grosso et al., 2019).

The natural degradation of infused enzymes and the difficulty in reaching the CNS would require weekly administrations of GALC at high doses, with important issues related to potential immune responses, high costs, and quality of patient's life (Eng et al., 2001; Lenders & Brand, 2018; Linthorst et al., 2004; Parenti, Andria, & Ballabio, 2015a; Spratley & Deane, 2016)

Substate Reduction Therapy (SRT)

SRT is based on the inhibition of the biosynthetic enzymes upstream of the mutated one using specific small proteins, in order to reduce the storage of undegraded substrates. The advantages of SRT over ERT are the possibility of oral administration and the absence of immune reactions (Coutinho et al., 2016). SRT has shown promise in some LSDs and is approved for the treatment of Gaucher type I (miglustat, eliglustat tartrate) and Niemann-Pick disease type C (miglustat) (Parenti et al., 2021; Parenti, Andria, & Ballabio, 2015a).

Specifically for GLD, the subcutaneous administration of L-Cycloserine, an irreversible inhibitor of 3-ketodyhydrosphingosine synthase (responsible for the synthesis of sphingosine) able to cross the BBB, resulted in a slight increase in lifespan and amelioration of pathological signs in TWI mice, which was further enhanced when coupled to other therapies like HSPC-T or GT (Hawkins-Salsbury et al., 2015; LeVine et al., 2000; Li et al., 2021) However, L-cycloserine is not approved for human use because of its toxicity when used at high doses (LeVine & Tsau, 2022). Several compounds have been tested to inhibit safely and more specifically the enzymes involved in the final steps of GalCer and psy synthesis, but the majority of them were inefficient in prolonging TWI survival besides showing important side effects (Babcock et al., 2021; Fujikawa et al., 2001; Yamada et al., 1989), highlighting the limitations of SRT in treating all the LSDs.

Pharmacological chaperone therapy

Pharmacological chaperone therapy (or enzyme enhancement therapy) is based on the use of small molecules (pharmacological chaperones, PCs) that can interact with mutant proteins favouring their native conformation, enhancing their stability,

and allowing for correct trafficking, with the final aim to enhance the residual enzymatic activity of misfolded or unstable enzymes. Migalastat has shown clinical efficacy and is approved for the treatment of Fabry disease with amenable galactosidase-α gene mutations (Parenti et al., 2021; Parenti, Andria, & Valenzano, 2015b). The advantages of using PCs are their excellent biodistribution profile (including BBB crossing) upon oral administration, the reversible mode of action, and the overall little impact on the patient's quality of life. Thus, PCs are a promising tool for LSDs affecting the nervous system. However, this approach can only be applied to patients carrying chaperone-responsive mutations (Parenti et al., 2021; Pastores & Sathe, 2006). Several possible candidates for PC therapy for GLD have been identified (Hill et al., 2015; Hossain et al., 2015; Spratley & Deane, 2016) but their selectivity for the GALC enzyme is low and, consequently, the concentrations needed to enhance enzyme activity would be extremely high (Graziano et al., 2016), posing major safety issues.

Stem cell-based therapies

Besides HSPCs, other stem cell types can be exploited for LSDs treatment. The rationale for transplanting healthy donor mesenchymal stem cells (MSCs) or early neural progenitor cells (NPCs) lies in their immunomodulatory action and capability to engraft in host tissues and provide a stable source of the defective enzyme (Martino & Pluchino, 2006; Wicks et al., 2011). This therapeutic approach has been tested in the preclinical study and clinical trials to treat LSDs as well as other neurodegenerative diseases, e.g., Parkinson disease (clinical trial ID: NCT03128450), amyotrophic lateral sclerosis (clinical trial ID: NTC01640067), and neuronal ceroid lipofuscinosis (clinical trials ID: NCT00337636, NCT01238315) (Issa et al., 2022; Luciani et al., 2020; Shihabuddin & Cheng, 2011).

MSCs systemically infused or injected in the striatum of TWI mice provided minimal clinical improvement and low engraftment in the CNS (Miranda et al., 2011; Wicks et al., 2011). In contrast, NPCs injected in the CNS of TWI mice stably engraft and differentiate along neuronal lineages, without perturbing the brain cytoarchitecture, thus representing a promising therapeutic approach. Injected NPCs provide rescue of GALC activity up to 50% of the WT level not only in the telencephalon (TEL), the site with the majority of engrafted donor cells, but also in the cerebellum (CB) and SC (Neri et al., 2011). Despite the significant enzymatic supply and the immunomodulatory and neuroprotective actions mediated by NPCs, NPC transplant as a single therapy only slightly delays the disease onset without

counteracting the disease progression, particularly the severe PNS demyelination (Martino & Pluchino, 2006; Neri et al., 2011; Pellegatta et al., 2006).

Gene therapy (GT)

GT is based on the direct correction of patients' cells to restore the expression of a functional enzyme. This can be achieved by correcting the mutated gene (gene editing) or by transferring one or more copies of the functional gene into patients' cells via a vector delivery system – usually adeno-associated virus (AAV) or lentivirus (LV)- or a non-viral delivery system (e.g., NPs) (Gillmore et al., 2021; Naldini, 2019; Platt et al., 2018; Reghupaty & Sarkar, 2019). GT is a promising therapeutic option for all LSDs, as they are monogenic disorders and could also benefit from the cross-correction mechanisms, meaning that few modified cells might be in principle needed to rescue the disease (Platt et al., 2018).

The transfer of the corrected gene can be obtained using *in vivo* or *ex vivo GT* procedures. In the *in vivo* procedure, the corrected gene is delivered directly into the patient's target tissues (in situ administration) or injected into the blood or CSF circulation. These methods could be more or less invasive, depending on the target tissue (e.g., CNS), and may lead to off-target gene transfer (e.g., AAV in the liver, heart, and muscle upon systemic and even intrathecal delivery) (Goertsen et al., 2022; Gong et al., 2019; Hordeaux et al., 2022; Srivastava, 2016). In the *ex vivo* approach, patients' HSPCs are isolated and engineered *in vitro* before being reinfused into the host (Figure 7). This procedure is less challenging for the patients since it requires a myeloablation treatment but avoids the need for an immunosuppressive regimen (Cantore et al., 2022; Gonzalez & Baldo, 2017; Sands & Davidson, 2006).

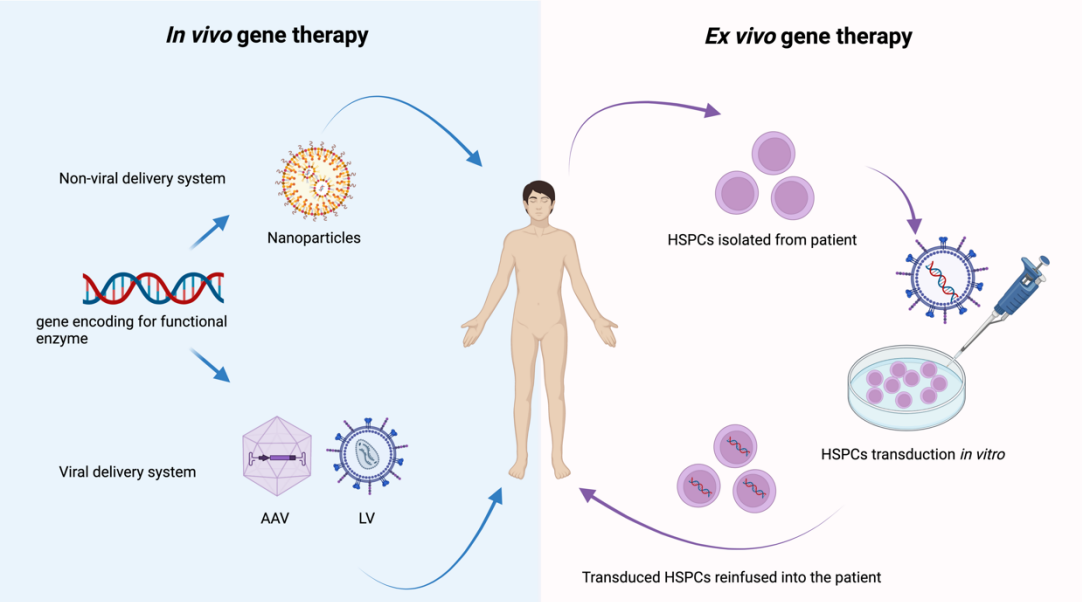

Figure 7. In vivo and ex vivo GT strategies. *In the in vivo gene therapy, genetic material encoding for the functional enzyme is directly delivered to patients via a non-viral (nanoparticles) or viral (adeno-associated virus, AAV; lentivirus, LV) delivery system. In the ex vivo gene therapy, hematopoietic stem/progenitor cells (HSPCs) are isolated from the patient, genetically modified in vitro by transduction with LV carrying the functional enzyme gene, and then reinfused into the patient. Created with BioRender.com.*

As mentioned before (paragraph 1.1.3), several *in vivo* and *ex vivo* GT approaches are under clinical evaluation for different LSDs, including metachromatic leukodystrophy (MLD), mucopolysaccharidosis (MPS) types I, II, IIIA, VI, and Pompe, Fabry and Gaucher diseases. Many of them have shown encouraging results and significant therapeutic benefits for treated patients (Leal et al., 2020; Massaro et al., 2021; Naldini, 2019; Platt et al., 2018; Sevin & Deiva, 2021).

For LSDs with CNS involvement, several delivery routes and vector capsids or envelopes (for AAV and LV, respectively) have been tested in *in vivo* GT approaches to maximise functional enzyme supply in this tissue and, when systemically infused, to favour the BBB crossing and transduction of neuronal/glial cells (Goertsen et al., 2022; Platt et al., 2018). Several *in vivo* GT approaches have been tested on GLD animal models over the past two decades.

Single or multiple intracranial injections (IC) of AAV1 (3×10^{10} vector genomes, vg, into each site of injection, Rafi et al., 2005) or AAV2/5 (2.4×10^{9} vg into each site of injection, Lin et al., 2005) to vehicle corrected *Galc* gene in neonatal GLD mice (TWI and Trs) resulted in elevated GALC activity in the brain and a slight improvement in the behavioural deficits and lifespan. However, no benefit in PNS was achieved.

The combination of ICV, intracerebellar, and IV of AAVrh10-GALC (1.5×10^{9} vg into each site of injection) in neonate TWI mice resulted in increased survival (up to 8 months), amelioration of pathological phenotype and neuroinflammation and ability to mate (Rafi et al., 2012). Similarly, neonatal TWI mice treated with AAV9-GALC via three delivery routes (IC, intrathecal -IT-, and IV) at a dosage of 4.2×10^{11} vg in total, showed an extensive AAV distribution and psy reduction in the CNS and PNS, leading to increased lifespan (Marshall et al., 2018). In these studies, the AAV biodistribution in the different organs besides the CNS and PNS was not analysed, thus it is not possible to exclude potential off-targets.

To evaluate the safety and efficacy of AAV-mediated GT in large animal models, Bradbury and colleagues tested the combination of IV and ICV injections of AAVrh10-GALC (IV injection at 3 days; ICV injection at 6 weeks of age, prior to the onset of neurological dysfunction) at different doses (1.2×10^{12} vg low dose, 3.8×10^{13} vg high dose) in the naturally occurring canine model of GLD. The treatment resulted in

delayed onset of clinical signs, extended lifespan, correction of biochemical defects, and attenuation of neuropathology, with the best results in the high dose group. Despite targeting both the peripheral and the central nervous systems, this approach failed to completely attenuate myelin loss or prevent storage accumulation, indicating that the optimal doses were not yet reached (Bradbury et al., 2018). Two years later, the same group demonstrated that a single IT injection of AAV9-GALC (10^{14} vg, higher than in the previous work) into the cisterna magna of GLD dogs resulted in increased GALC enzyme activity, normalization of psy concentration, improved myelination, and attenuated inflammation in both the CNS and PNS. Moreover, AAV-mediated therapy successfully prevented clinical neurological dysfunction, allowing treated dogs to live beyond 2.5 years of age, more than 7 times longer than untreated dogs. Importantly, they highlighted that a 5x lower dose resulted in an attenuated form of the disease, indicating that reaching a threshold dose is critical for full efficacy. Finally, they showed that injection of high-dose AAV9-GALC in dogs at 6 weeks of age (post-symptomatic) significantly extended the lifespan of treated animals, suggesting a potential treatment option for patients for whom HSPC-T is not applicable (Bradbury et al., 2020). Similarly, Hordeaux and colleagues demonstrated that a single IT injection of AAVhu68-GALC significantly increases the survival of GLD mice (1×10^{11} vg) and dogs (3×10^{13} vg) and demonstrated the feasibility of clinical translation by testing this approach on healthy NHPs (from 5×10^{10} vg of the low dose to 5×10^{11} vg of the high dose) (Hordeaux et al., 2022). A Phase I/II clinical study based on these results started in February 2021 and the recruitment is ongoing (clinical trial ID: NCT04771416). The viral vector biodistribution analysis in treated dogs showed AAV delivery not only in CNS but also in peripheral organs, including the heart, kidney, liver, and spleen (Bradbury et al., 2018, 2020; Hordeaux et al., 2022). Although any adverse histopathological findings were detected, the AAV distribution in off-target organs is an important safety parameter to be evaluated.

Despite the outstanding results obtained in the pre-clinical models, all the AAV-mediated GT approaches tested so far do not arrest the progression of the disease and still fail to completely normalize some of the more critical pathological hallmarks, such as demyelination and inflammation. The use of elevated AAV doses and multiple delivery routes pose obvious safety concerns. For example, Li and colleagues described a high incidence of hepatocellular carcinoma (HCC) in TWI and WT neonatal mice after AAV9-GALC IC and IT injections, in combination with HSPC-T and/or L-cycloserine administration. Ten out of 10 tumours analysed showed AAV integrations within the *Rian* locus (Li et al., 2021). The incidence of HCC upon AAV-GT was detected in different models, especially in mice treated at the neonatal stage

(Sabatino et al., 2022). Other safety concerns arising from: i) high level of pre-existing anti-AAV antibodies in the population, leading to immune-mediated toxicity as well as the loss of transgene expression (Hinderer et al., 2018; Perez et al., 2020; Rabinowitz et al., 2019; Vandamme et al., 2017); ii) integration of AAV genome into the mice, NHPs, and humans genomes, despite the DNA episomal state, entailing a risk of insertional mutagenesis and genotoxicity (Bijlani et al., 2022; Kaeppel et al., 2013; Li et al., 2021; Russell, 2007; Sabatino et al., 2022); iii) degeneration of dorsal root ganglia (DRG) neurons which has been described in some treated NHPs, in contrast to dogs, suggesting that DRG pathology cannot be accurately predicted based on animal models (Bradbury et al., 2020; Hinderer et al., 2018; Hordeaux et al., 2020, 2022; Perez et al., 2020). A correlation between vector copy number (VCN) and integration events after AAV-deliver was highlighted in AAV-treated haemophilia A dogs, with a preference for transcription units (Nguyen et al., 2021). Further analyses, some of those already presented at the European Society of Gene and Cell Therapy 29th Annual Meeting by Doctor Hordeaux, from the University of Pennsylvania, will clarify AAV dose-related toxicities in NHPs. To overcome some of these issues, the switch of the delivery route from IV to IT appears to be less expensive in terms of vector amount and partially safer, with a reduction of anti-AAV-neutralizing antibodies but still with the delivery of AAV to off-target tissues (Gray et al., 2013; Hordeaux et al., 2018). The use of cell/gene-specific promoters possibly reduces the risk of HCC upon AAV gene integration. Human alpha-1 antitrypsin enhancer-promoter, besides the common strong chicken beta-actin (CAG) and thyroxin-binding globulin elements which are known to cause genotoxicity (Bell et al., 2006; Donsante et al., 2001), did not cause tumorigenesis even when integrated into the *Rian* locus (Chandler et al., 2015).

The LV vectors, obtained from the human immunodeficiency virus (HIV), mediate gene transfer in proliferating and non-proliferating cells and the DNA integration into the cell genome, thus allowing long-term transgene expression. The use of LVs instead of AAVs was attractive for several technical and safety aspects: i) the accommodation of larger gene (up to 8kb); ii) the high safety with low immunogenicity upon intracerebral or systemic delivery (Cantore et al., 2015; Lattanzi et al., 2014); iii) the highly efficient transduction of mammalian neuronal and glial cells (Abordo-Adesida et al., 2005; Lattanzi et al., 2010; Naldini, 2019; Wong et al., 2006; Zheng et al., 2018); iv) the integration into the host genome prevents loss of transgene expression even in continuously dividing cells such as hepatocytes (Cantore et al., 2015; Milani et al., 2022). However, the main risk is associated with the integration of LV into the cell genome, which could induce

mutagenesis and oncogenes activation (Corre et al., 2022; Zheng et al., 2018). To overcome this issue, several works have been aimed at improving the safety profile of LVs by limiting their ability to randomly integrate or by including "transcriptional insulators" that decrease the chance to transcriptionally activate bystander genes. The third-generation, self-inactivating (SIN) LVs have further improved safety and drastically reduced the risk of insertional oncogenesis (Cesana et al., 2014; Modlich et al., 2009; Montini et al., 2009; Zhou et al., 2010).

LVs have been exploited for *in vivo* and *ex vivo* GT approaches for GLD.

A single IC injection of LV-GALC (2×10^6 TU) in TWI neonatal and adult mice was able to provide a rapid and long-lasting source of enzyme in CNS tissues (30-40% of physiological activity). This level of enzymatic reconstitution resulted in partial amelioration of CNS pathology and a slight increase in the survival of TWI mice treated at the neonatal stage (Lattanzi et al., 2010; Ricca et al., 2015). Importantly, the safety of IC injections of LV-GALC (one injection in the thalamus and one in the internal capsule, 3.5×10^7 transducing units -TU- in total) was also demonstrated in the GLD NHP model, in which this treatment led to widespread reconstitution of GALC activity in CNS tissues up to 70% of physiological levels in the brain and 40% in the SC, with evidence of GALC enzyme secretion in the CSF (Meneghini et al., 2016). These results support the feasibility and potential efficacy of this procedure in humans. However, low doses of LV-GALC, which results in GALC activity remaining below physiological levels in the CNS and even lower in the PNS, are not sufficient as a single therapy to correct GLD pathology.

The *ex vivo* LV-mediated HSPC-GT approach shares the same rationale described for HSPC-T, i.e., to exploit the metabolically competent HSPC myeloid progeny engrafted in all enzyme-deficient tissues/organs (CNS, PNS, periphery) as a long-lasting source of functional enzyme. The advantage of HSPC-GT over HSPC-T lies in the possibility of inducing the overexpression of the lysosomal enzyme in the donor cell populations, thus increasing its availability in the affected tissues. Furthermore, the LV-mediated insertion of a transgene into the patient's HSPC genome ensures the transmission of the functional gene to the HSPC progeny and the maintenance of life-long gene correction. Finally, the autologous setting overcomes the issue of immune rejection by the host, avoiding the need for an immunosuppression regimen (Naldini, 2019). The clinical benefit of this approach was demonstrated in Phase I/II clinical trials for MLD (clinical trial ID: NCT01560182) and MPS type I (clinical trial ID: NCT03488394), LSDs which shares with GLD the early onset and the severe neurological involvement (Biffi et al., 2013; Fumagalli et al., 2022; Gentner et al., 2021; Sessa et al., 2016; Visigalli et al., 2010). *Ex vivo* gene therapy for MLD is

maybe the most successful example of HSPC-GT. In Phase I/II trial, pre-symptomatic patients were treated with autologous HSPCs transduced with LV encoding ARSA (Biffi et al., 2013). Results from a follow-up study (Penati et al., 2017; Sessa et al., 2016) showed that disease onset was prevented or the progression was halted in eight out of nine patients, providing evidence of the safety and efficacy of this approach that led to its authorization (Libmeldy) in the European Union (by the European Medicines Agency). Preclinical studies demonstrated that HSPC-GT is effective also in other lysosomal disorders, such as MPS-II (Wakabayashi et al., 2015) and MPS-I (Visigalli et al., 2010), representing an attractive therapeutic option also for GLD.

When tested in GLD mice, the HSPC-GT approach results in only moderate amelioration of pathological hallmarks and a slight increase in survival. Similarly to what was observed after LV-GALC IC injection, only partial GALC activity restoration was achieved in the CNS (~30% of physiological levels) (Gentner et al., 2010; Ungari et al., 2015).

The similar results obtained by the two therapeutic approaches suggested that no sufficient GALC overexpression/bioavailability and/or cross-correction of GALC-deficient cells are achieved to halt the rapid and aggressive course of the disease. Supraphysiological GALC activity in the CNS are fast needed to counteract the psy accumulation, already present at birth/early in life in GLD mice (Ricca et al., 2015; Santambrogio et al., 2012) and in patients (Siddiqi et al., 2006a, 2006b) and increasing over time. The transplantation of HSPCs is not sufficient to rescue GALC activity, since the engraftment of donor cells is a process slower than disease progression. Moreover, GALC protein is found at a low level in the tissues (Chen et al., 1993; Chen & Wenger, 1993) and its overexpression is very hard to obtain without very high vector doses and/or multiple injections, which determined a better outcome but raises safety concerns. To overcome these issues, modifications of the gene encoding for the lysosomal enzyme in order to increase its expression and/or secretion represent an attractive and safer option (see paragraph 3). Another strategy is the combination of different approaches that, as described below, aim to address the need for early intervention and robust rescue of GALC activity in all the tissues and especially in the CNS and PNS to rapidly and steadily reduce the psy storage.

Combined therapies

Most of the combined approaches evaluated in GLD murine models included total bone marrow (tBM) transplantation coupled to: i) SRT with L-cycloserine, alone (Biswas & Levine, 2002) or in combination with AAV9-GALC IC and IT injections (Li

et al., 2021) or AAV2/5-GALC IC injection (Hawkins-Salsbury et al., 2015); ii) systemic or IT ERT (Qin et al., 2012); iii) IC/IT injection of AAV vectors (Lin et al., 2007; Marshall et al., 2018; Reddy et al., 2011); iv) systemic injection of LV-GALC (Galbiati et al., 2009). These pre-clinical studies showed a variable extent of synergy of the treatments and often provided unclear or controversial results (Mikulka & Sands, 2016). The contribution of tBM-T in ameliorating CNS and PNS pathology is not fully defined, ranging from moderate (Galbiati et al., 2009; Hawkins-Salsbury et al., 2015; Lin et al., 2007) to ineffective (Reddy et al., 2011).

Our previous study showed that tBM-T synergized with LV-GALC IC injection (2×10^6 TU) or IC transplantation of GALC-overexpressing NPCs (~3x the GALC activity measured in WT NPCs; Ricca et al., 2015). Indeed, the combined treatment provided a significant delay in disease progression, enhancement of lifespan (up to 290 days), and substantial amelioration of pathological hallmarks. Interestingly, no synergy was observed in terms of GALC activity achieved in CNS tissues, which was around 30-40% of physiological levels, highlighting how supraphysiological levels of GALC activity are hard to achieve in CNS tissues without elevated vector doses.

On the same line, Rafi and colleagues combined tBM-T with IV injection of AAVrh10-mGALC at elevated doses (from 4×10^{11} vg/kg up to 6×10^{14} vg/kg). The results showed a significant extension of lifespan (up to 400 days) as well as amelioration of myelin in the sciatic nerve (SN) in mice treated with the highest dose. However, pathological changes were detected in the liver of a few animals, but none of them were neoplastic (Rafi et al., 2020). These promising results, together with those obtained by Bradbury and colleagues using the same vector (Bradbury et al., 2018), led to the start of Phase I/II clinical study in which GLD patients will be treated with IV injection of AAVrh10-GALC after HSPC-T (RESKUE, clinical trial ID: NCT04693598).

Overall, these data suggest that the combination of different therapeutic approaches could provide an advantage in terms of widespread distribution of GALC enzyme in all the tissues and especially in the CNS. The GT (both *in vivo* and *ex vivo*) can induce lifelong GALC overexpression, but vector doses and therapeutic protocols are not sufficient to halt disease progression so far. Therefore, there is an urgent clinical need for this devastating disease.

3. Chimeric lysosomal enzymes.

The main obstacle to the efficient treatment of LSDs with neurological involvement is the limited and timely availability of functional enzymes in the CNS and PNS before

irreparable damage occurs. All the experimental and clinical evidence obtained so far in GLD animal models and patients strongly suggest that when the first pathological manifestations begin to appear, the disease progression is irreversible, indicating a narrow therapeutic window for GLD. As anticipated in paragraph 2.5 (gene therapy), possible solutions to these issues are to increase vector doses to force GALC overexpression and/or to use combined therapeutic approaches to fast target different sites of pathology. An alternative and safer strategy is to increase GALC bioavailability by modifying its sequence.

In this view, several groups modified lysosomal enzymes by: i) changing the sp to increase lysosomal enzyme production/secretion; ii) adding alternative receptor-binding domains to enhance the BBB crossing of the modified enzyme. All these modifications (single or combined) are aimed at increasing the bioavailability of chimeric enzymes in all tissues, especially in the CNS.

As mentioned in paragraph 1.1, the sp is responsible for directing the nascent protein through the secretory pathway as well as for targeting intracellular localization. The sp consists of 25-30 residues and includes three different domains: i) the N-positive charged region, responsible for efficient proteins translocation: ii) the hydrophobic core region (H-region), involved in the binding to signal recognition particle and consequentially to ribosomes, in stabilising nascent mRNA and in directing the protein to the secretory pathway; iii) the C-region, acting as cleavage site that is recognised and cleaved off by signal peptidase on the luminal side of the ER membrane. Although all sp sequences have this general structure, they are remarkably heterogeneous (von Heijne, 1990).

It was demonstrated that modifications to sp sequences or the use of alternative sps can lead to increased protein expression and/or secretion (Knappskog et al., 2007; Kober et al., 2013; Stern et al., 2008). For example, the substitution of interleukin-25 (IL-25) sp sequence with that of Trypsin-1 (aa 1-15) and a part of Trypsin-1 pro-peptide sequence (aa 16-23) lead to an increase IL-25 secretion by 5x in transiently transfected human embryonic kidney 293 (HEK293) cells (Mullin et al., 2021). Increased protein secretion can be obtained also increasing the basicity of the N-region and the hydrophobicity of the H-region of the sp sequence, as demonstrated by Zhang and colleagues. They replaced the placental alkaline phosphatase and endostatin sp sequences with that of modified IL-2sp, obtaining an increased secretion of both enzymes by around 2.5x and 3-5x, respectively, from the M14 melanoma cell lines (Zhang et al., 2005). Güler-Gane and colleagues, in a study on the HEK293 cells, also showed that the modification of specific aa in the sp sequence has a positive or negative effect on the secretion of the protein alkaline phosphatase

(Güler-Gane et al., 2016). Specifically for the lysosomal enzymes, Sorrentino and colleagues demonstrated that the substitution of N-sulfoglucosamine sulfohydrolase (SGSH) sp with that of the highly secreted iduronate-2-sulphatase (IDS) enzyme increases the chimeric enzyme secretion by ~3x in transfected embryonic fibroblast derived from MPS-IIIA mice (Sorrentino et al., 2013). However, Chen and colleagues showed increased secretion of the same chimeric construct by only ~30% in the HEK293 cells (Chen et al., 2018), highlighting how modifications to sp influence the enzyme secretion in an enzyme- and cell type- specific manner (Cheng et al., 2021; Güler-Gane et al., 2016). Starting from this consideration, Cheng and colleagues screened nine different sp sequences, derived from different types of protein (antibody, serum protein, and exocrine), to increase the secretion of two lysosomal enzymes (the N-acetyl-**α**-glucosaminidase -NAGLU- and the glucosamine-6-sulfatase) by chinese hamster ovary cell lines, as most of the lysosomal enzymes used as ERT for MPS are purified by this cell line (Cheng et al., 2021).

In all the reported works, any cellular toxicity related to sp modification was described and the intracellular enzymatic activity of the different chimeric enzymes was not decreased, suggesting that modification did not impact enzyme folding.

While modification of sp may achieve increased enzyme bioavailability by enhancing its secretion, the problem of BBB crossing remains.

To overcome this issue and boost lysosomal enzyme availability in the CNS the addition of molecules that bind receptor-mediated transporters, expressed on the plasma membrane of the brain capillary endothelium, may favour the BBB crossing of the modified enzyme. Receptors highly expressed in endothelial cells include the leptin receptor (Boado et al., 1998), insulin receptor (IR) (Kurata et al., 2013; Pardridge et al., 1995), the transferrin receptor 1 (TfR) (Bickel et al., 1994; Jefferies et al., 1984), the insulin-like growth factor receptor (IGFR), (Garcia-Segura et al., 1997), the LDLR (Molino et al., 2017), and the LRP1 (Storck et al., 2016).

One of the strategies to modify lysosomal enzymes is based on their fusion to immunoglobulin G (IgG), that act as a Trojan horse to transport chimeric enzymes into the brain through insulin and transferrin receptors (Figure 8).

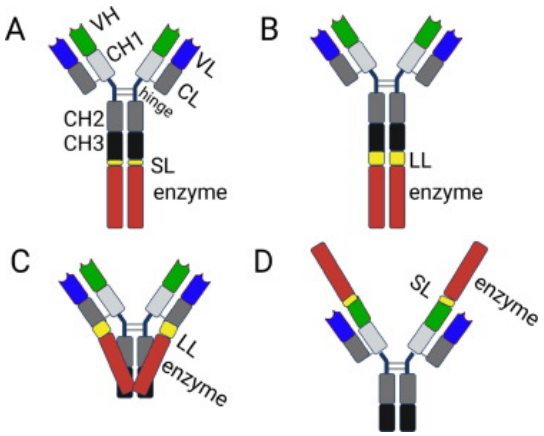

Figure 8. Chimeric lysosomal enzymes fused to IgG. *The lysosomal enzyme is fused to IgG to the C-terminus of the heavy chain of the IgG via a short linker (SL, in A) or via a long linker (LL, in B), or to the light chain of the IgG via a LL (in C). D. Enzyme can also be fused to the N-terminus of the IgG heavy chain via an SL (in D) (Pardridge, 2022).*

L-iduronase (IDUA) and IDS enzymes fused to IgG to target human IR (HIRMAb) or mouse or human TfR (TfRMAb) were produced to enhance the delivery of the enzymes in the brain of primates or mice, respectively. IV injection of HIRMAb-IDUA and HIRMAb-IDS was safe and rapidly provided chimeric enzymes in the CNS and peripheral organs (Boado et al., 2014; Boado, Hui, Lu, & Pardridge, 2013; Boado, Hui, Lu, Sumbria, et al., 2013; Boado & Pardridge, 2017), even if chronic treatment can cause an increase in anti-drug antibodies against both IDUA and HIRMAb domains (Boado, Hui, Lu, Sumbria, et al., 2013). Similarly, TfRMAb-IDUA as well as TfRMAb-IDS chronic IV injection reduced GAGs and heparan sulfate (HS) storage in all the tissues, including CNS, in MPS-I and MPS-II mouse models, respectively (Boado et al., 2011; Morimoto et al., 2021; Tanaka et al., 2018). Similar results were obtained for chimeric SGSH, NAGLU, ARSA, and hexosaminidase A (HEXA) when tested in NHPs and mouse models of MPS-IIA, MPS-IIB, MLD, Tay Sachs disease, respectively (Pardridge, 2022). Starting from these promising data, clinical trials were performed to test the efficacy of HIRMAb-IDUA (valanafusp alfa; clinical trials ID: NCT03053089, NCT03071341) (Giugliani, Giugliani, et al., 2018; Wraith et al., 2007) and TfRMAb-IDS (pabinafusp alfa; clinical trials ID: NCT03359213, NCT03568175) (Okuyama et al., 2021) in treating MPS-I and MPS-II patients, respectively. The results show no toxicity related to chimeric enzyme infusion and provide evidence for efficacy in terms of partial reduction of CSF storage, and stabilization of cognitive functions and total gray matter volume of treated patients (Giugliani, Giugliani, et al., 2018; Okuyama et al., 2021; Pardridge, 2022; Wraith et al., 2007). However, the absence in these studies of control groups treated side-by-

side with unmodified enzymes precludes an evaluation of the real advantage of the chimeric proteins.

An innovative strategy was applied by Ullman and colleagues in producing a chimeric IDS enzyme in which IDS is fused to the fragment crystallizable region of the human IgG1 engineered to bind to the human TfR (ETV:IDS). ETV:IDS, once IV infused in MPS-II mice expressing hTfR, crossed the BBB and reduced the storage in different CNS cell types (neurons, astrocytes and microglia) and peripheral tissues, also achieving the complete correction of disease-relevant pathologies in the brain (Ullman et al., 2020). This chimeric enzyme is currently under clinical development for MPS-II treatment (clinical trial ID: NCT04251026).

Besides the IgG, shorter sequences encoding for alternative binding domains have been fused to lysosomal enzymes to induce the BBB crossing after systemic infusion.

The addition of the transactivator of transcription (Tat) protein derived from the HIV enhanced brain delivery of chimeric β-galactosidase (Schwarze et al., 1999). Similar results were obtained by fusing IDUA or ARSA enzymes to a single or tandem repeat of different regions of the apolipoprotein E (ApoE), a ligand of the LDLR family (Böckenhoff et al., 2014; Wang et al., 2013). Zhang and colleagues showed that the Tat domain fused to the GALC enzyme improved enzyme secretion *in vitro* in the LV-transduced monkey kidney fibroblast-like cell line and reduced GalCer storage in TWI fibroblasts (Zhang et al., 2008).

The ERT strategy based on the use of chimeric enzymes has the same limitations as the classical ERT, namely the necessary chronic administrations which are costly both in terms of time and resources and can cause immune reactions.

An interesting possibility is to exploit chimeric enzymes in the context of *in vivo* and/or *ex vivo* GT. Previous studies demonstrated that the presence of ApoB fused to glucocerebrosidase (GC) promoted brain delivery upon *in vivo* LV IV and IP injections (Spencer & Verma, 2007). The addition of a tandem repeat of the ApoE II binding domain increased the BBB crossing and CNS delivery of chimeric IDS upon LV-mediated HSPC-GT in MPS-II mice. The chimeric enzyme led to a complete normalization of HS storage in the brain of treated mice, with the full rescue of lysosomal pathology and astrocytosis, which were not achieved using the unmodified enzyme (Gleitz et al., 2018).

The ApoE modification has been previously exploited to modify the GALC enzyme. The use of either a myeloid- or an erythroid/megakaryocyte-specific promoter and the addition of ApoE I binding domain resulted in a safe LV-mediated expression of chimeric GALC enzymes in HSPCs. TWI mice IP injected with a combination of tBM collected from wild-type (WT) mice and WT HSPCs engineered to express the chimeric

GALC showed a lifespan comparable to that observed with the canonical tBM-T (Hu et al., 2016). The unknown amount of GALC overexpression in LV-transduced HSPCs coupled to the transplantation performed at PND 9, when CNS involvement is already present in TWI mice, have possibly limited the efficacy of this treatment.

In order to further improve the bioavailability of lysosomal enzymes in the CNS, the modification of sp may be coupled to the addition of alternative binding domains or enzyme activators. As mentioned before, the replacement of endogenous sp with that of the highly secreted IDS enzyme increased the secretion of a chimeric SGSH (IDSsp.SGSH) *in vitro* in embryonic fibroblast derived from MPS-IIIA mice (Sorrentino et al., 2013). The addition of the ApoB binding domain (IDSsp.SGSH.ApoB) did not further impact the enzyme secretion, similar to that of IDSsp.SGSH. To test generated construct *in vivo*, MPS-IIIA mice were IV injected with AAV2/8 encoding for the chimeric enzymes and unmodified counterpart, in order to transduce the liver and evaluate the enzyme distribution in the brain and the rescue of pathological hallmarks. In this context of *in vivo* GT, IDSsp.SGSH.ApoB was more efficiently delivered to the CNS than the other enzymes, leading to higher SGSH activity restoration and overall improvement of the CNS pathology and behavioural phenotype (Sorrentino et al., 2013). The same group also evaluated the possibility to combine sp modification with the expression of the SGSH enzyme activator. They generated an expression cassette encoding for the chimeric IDSsp.SGSH and the sulfatase-modifying factor 1 (SUMF1), the enzyme mediating the post-translational activation of SGSH. The AAV9-mediated intra-cisterna magna and intra-ventricle injection of the transgenic cassette in WT pigs ($4.5x10^{12}$ vg/Kg) and MPS-IIIA mice ($5.4x10^{12}$ vg/Kg), respectively, showed a safe and synergistic effect of the chimeric SGSH/SUMF1 in terms of CNS distribution and activity of the enzyme. Importantly, treated MPS-IIIA mice showed a significant rescue of CNS pathology (Sorrentino et al., 2019). A similar approach was tested for GLD. Indeed, Pan and colleagues modified the GALC enzyme by replacing the GALCsp with the IDSsp and adding the ApoB binding domain. The IV injection of an AVV9 encoding for the chimeric GALC in PND 2 TWI mice led to an increase in median survival up to 150 days. However, the chimeric GALC enzyme was not detected in the CNS, even if a reduction in the levels of PAS staining was observed in the brain of treated mice (Pan et al., 2019). Moreover, the absence of a control group treated with unmodified enzyme poses a major question if the effect observed is due to GALC delivery or specifically to the modifications of the construct.

Based on the promising results described above, we generated LVs encoding for new chimeric GALC constructs, engineered to increase enzyme expression, secretion,

and BBB crossing leading to enhanced GALC bioavailability. Part of the results of this work has already been published (Ricca, Cascino, et al., 2020). The aim of the work and all the results obtained during this PhD course are described below.

Aim of the work

GLD is a rare and untreatable neurodegenerative LSD caused by the genetic deficiency of the GALC enzyme. The rapid disease progression of the infantile forms and the severe dysfunction of the CNS and PNS pose major issues for the development of effective treatments. HSPC-T, the only available treatment option, is poorly effective. Although promising results and recent progress, the effectiveness of experimental gene/cell therapy approaches to address the complex multi-organ pathology and to ensure adequate timing of intervention has yet to be elucidated.

Previous works anticipate transgene-specific regulation and potential safety concerns associated to GALC overexpression in HSPCs, ultimately resulting in insufficient enzyme secretion by transplanted cells and/or modest enzyme recapture by affected cells (cross-correction). Chimeric lysosomal enzymes with increased secretion and enhanced capability to cross the BBB boost the therapeutic efficacy of GT approaches in murine models of other neurodegenerative LSDs. Therefore, the development of chimeric GALC enzymes with increased bioavailability would be desirable to improve the efficacy of GT approaches for GLD.

The overall goal of the project is to generate proof-of-concept data demonstrating the safety, efficacy, and therapeutic advantage of novel LVs encoding for chimeric GALC enzymes, engineered to enhance enzyme secretion (using alternative sps derived from the more secreted IDS and IDUA lysosomal enzymes) and BBB crossing (by the addition of LDLR-binding domain). We tested the novel constructs in murine TWI neural and hematopoietic stem/progenitor cells and progeny, which are relevant target and/or effector cells in GLD pathology and therapy, respectively.

Our data show the advantage of the chimeric GALC enzymes in terms of protein expression and secretion as compared to the unmodified counterparts. Importantly, the chimeric enzymes were correctly secreted, recaptured, and delivered to the lysosomes of GALC-deficient neural cells, which were metabolically cross-corrected.

These results strongly support the rationale of testing the safety and efficacy of chimeric GALC enzymes in LV-mediated HSPC-GT approach in TWI mice.

We compared Busulfan and total body irradiation as myeloablative conditioning regimens in neonatal mice. The best protocol has been applied in preliminary experiments to test the safety and efficacy of HSPC-GT approaches using the optimized GALC chimeric construct.

The final goal is to overcome the limitations of GALC bioavailability in CNS tissues and develop novel and effective therapeutic strategies for GLD and similar LSDs.

Results

1. WT and TWI neural stem/progenitor cells and progeny and CNS tissues express LDLR and LDL-related proteins.

Chimeric lysosomal enzymes with increased secretion (by sp change) and enhanced capability to cross the BBB (by the addition of alternative receptor-binding domain) boost the therapeutic efficacy of GT in murine models of LSDs with severe CNS involvement (see Introduction, paragraph 3; Gleitz et al., 2018; Sorrentino et al., 2013; Wang et al., 2013). Thus, the use of a similar chimeric GALC enzyme may be crucial to successfully increase GT efficacy in the GLD mouse model.

In the perspective to improve the BBB penetration of the GALC enzyme, we decided to exploit LDLR and LDLR-related proteins (LRP1, LRP2), which are expressed by brain endothelial and CNS cells. The role of these proteins in neurodevelopment and neural cell function is being actively investigated (Auderset et al., 2016; Engel et al., 2019; Marzolo & Farfán, 2011; Safina et al., 2016; Zhao et al., 2016). Furthermore, the addition of an apolipoprotein-derived binding domain, i.e., ApoB and ApoE, has already been shown to enhance the BBB crossing of the chimeric IDUA and IDS enzymes (Gleitz et al., 2018; Sorrentino et al., 2013; Wang et al., 2013).

With a view to add an Apo-derived binding domain to GALC to enhance its bioavailability, we investigated the expression of LDLR, LRP1, and LRP2 in TWI and WT CNS tissues and neural stem/progenitor cell (NSPC)-derived neuronal/glial progeny. As a control, we analysed the expression of M6PR, the canonical receptor mediating the uptake and intracellular targeting of lysosomal enzymes (Braulke & Bonifacino, 2009).

We showed comparable mRNA expression levels of LDLR and M6PR in adult WT and TWI brains (PND 40). Despite the higher mRNA expression of LRP1 and LRP2 in TWI as compared to WT brains (Figure 9A), western blotting (WB) analysis revealed comparable protein expression (Figure 9B).

We performed the same analyses on TWI and WT NSPC-derived neurons/glial cell cultures, to evaluate the expression of these receptors in a system devoid of endothelial cells. We showed comparable expression of M6PR, LDLR, and LRP1 mRNA (Figure 9C) and protein (Figure 9D) in WT and TWI NSPC-derived neuronal/glial cells, while LRP2 mRNA expression was significantly increased in TWI with respect to WT cultures (Figure 9C). Representative immunofluorescence (IF) pictures showed that TWI NSPC-derived astrocytes (GFAP+ cells) and neuronal progenitors (polysialylated

neuronal cell adhesion molecule -PSA-NCAM- positive cells) express M6PR and LRP1, respectively (Figure 9E).

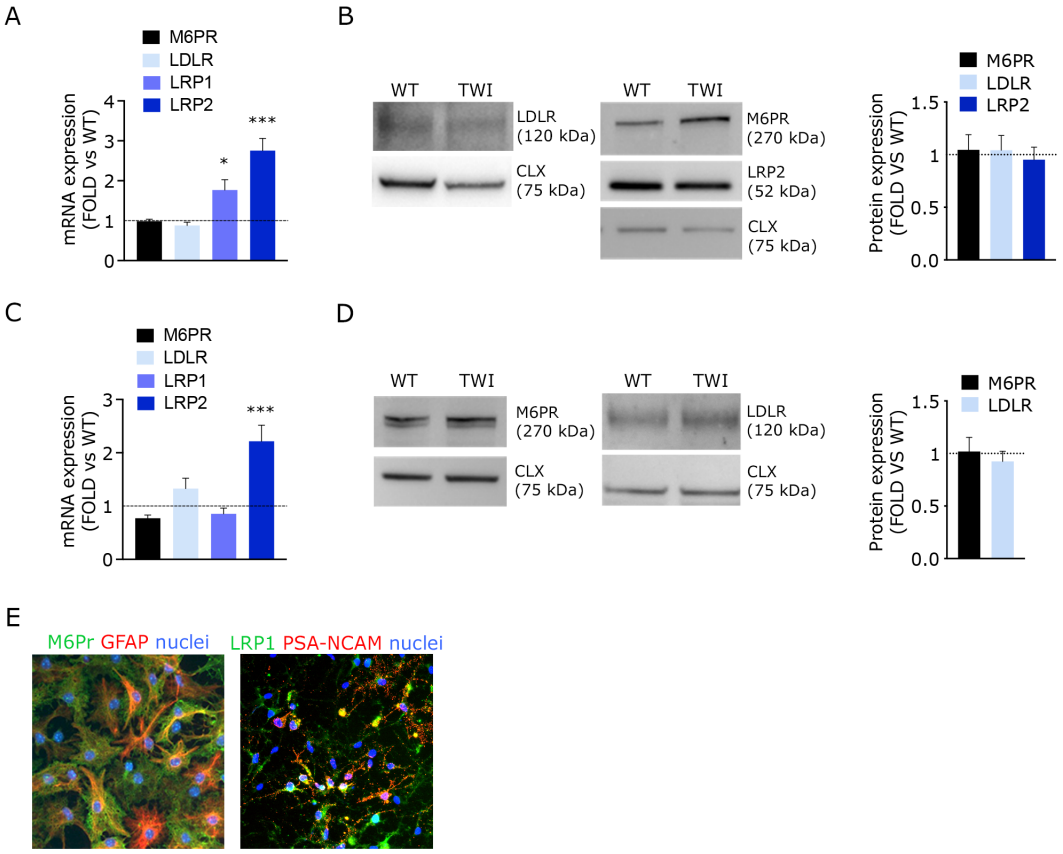

Figure 9. TWI CNS tissues and NSPC-derived progeny express LDLR and LDLR-related proteins. *A. Relative mRNA expression of M6PR, LDLR, LRP1, and LRP2 in the TEL of TWI mice at PND 40. Data are expressed as fold to WT littermates (dotted line) (mean ± SEM; n=3 animals/group). ΔΔCT values were analysed by One-way ANOVA followed by Dunnet's multiple comparison test; *p<0.05, ***p<0.001 vs. WT. B. Representative WB (performed on n=3-6 blots in n=3 different experiments) showing LDLR, LRP2, and M6PR protein in the TEL of WT and TWI mice at PND 40. Calnexin (CLX) was used as normalizer. Data in the graph are expressed as protein expression (M6PR, LDLR or LRP2/CLX), fold to WT (dotted line). Data represent the mean ± SEM; n=3 animals/group. C. Relative mRNA expression of M6PR, LDLR, LRP1, and LRP2 in TWI NSPC-derived neuronal/glial cell cultures. Data are expressed as fold to WT (dotted line) (mean ± SEM; n=3 independent experiments). ΔΔCT values were analysed by One-way ANOVA followed by Dunnet's multiple comparison test, ***p< 0.001 vs. WT. D. Representative WB (performed on n=3 blots in n=3 different experiments) showing M6PR and LDLR protein in WT and TWI NSPC-derived progeny. CLX was used as normalizer. Data in the graph are expressed as protein expression (M6PR or LDLR/CLX), fold to WT (dotted line). Data represent the mean ± SEM; n=3 independent experiments. E. Representative IF merged pictures showing M6PR (green) and LRP1 (green) expression in TWI NSPCs-derived astrocytes (GFAP, red) and* neuronal progenitors (PSA-NCAM, red), respectively. Nuclei stained with Hoechst (blue). 40× magnification. Scale bar, 50 μm. Adapted *from Ricca, Cascino et al., 2020.*

To test whether the LDLR and related proteins expressed by TWI NSPC-derived progeny were functional and adaptable, we treated TWI NSPC cultures with statins, drugs that enhance the expression of LDLR and related proteins. Starting from published protocols (Goto et al., 1997; Pinzõn-Daza et al., 2012), we tested two

statins, Simvastatin (SIM) and Pravastatin (PRA), at 1 and 5 nanomolar (nM) for 24 hours (h). In these pilot experiments, we treated WT NSPCs, in order to establish the optimal treatment scheme resulting in the highest upregulation of LDLR expression without adverse toxicity. SIM (1nM) induced a safe increased expression of all the receptors analysed, up to 8.5x in LDLR mRNA expression (Figure 10A) and 2.5x in LDLR protein expression (Figure 10B) as compared to untreated (UT) cells. TWI NSPCs treated with SIM (1nM) showed increased mRNA expression of all the receptors analysed, with a consistent increase of LDLR (18x) and LRP2 (16x) as compared to UT TWI cells (Figure 10C). Importantly, treated NSPCs showed increased LDLR protein expression (~2x) not only in the total lysate but, most importantly, in the membrane fraction. The action of SIM was specific, as demonstrated by no noticeable changes in the expression of the M6PR protein (Figure 10D).

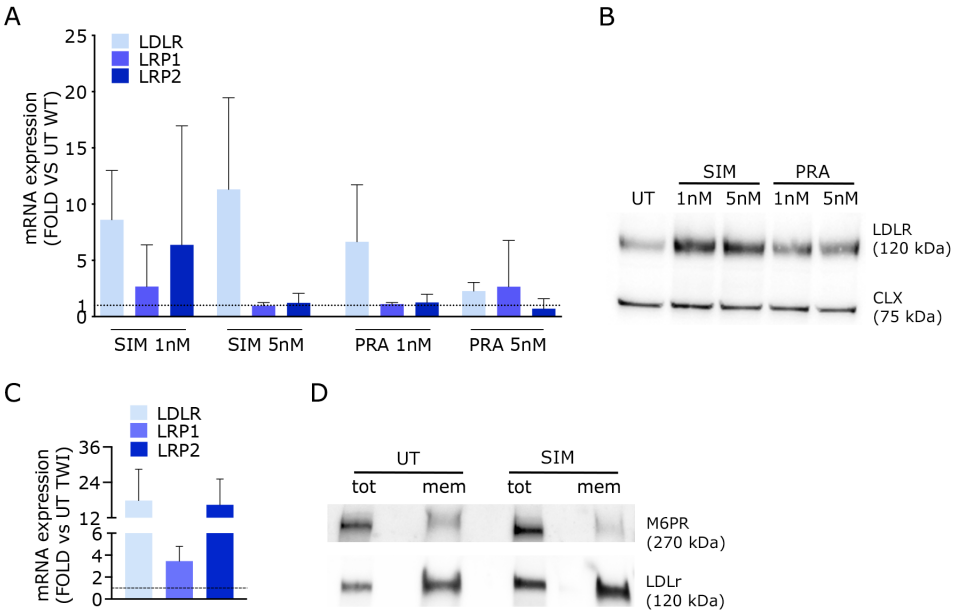

Figure 10. Simvastatin increases LDLR expression in treated WT and TWI NSPCs. *A. Relative mRNA expression of LDLR, LRP1, and LRP2 in WT NSPCs treated with 5 nM and 1 nM of Simvastatin (SIM) and Pravastatin (PRA) for 24 h. Data are expressed as fold to UT WT (dotted line) and represent the mean with range (n=2 independent experiments in duplicate). B. Representative WB (performed on n=2 blots in n=2 different experiments) showing LDLR protein in the total lysate of WT NSPCs, either UT or treated with SIM and PRA (5 and 1 nM, 24 h). CLX was used as normalizer. C. Relative mRNA expression of LDLR, LRP1, and LRP2 in SIM-treated TWI NSPCs. Data are expressed as fold to UT TWI (dotted line) and represent the mean with range (n=2 independent experiments in duplicate). D. Representative WB (performed on n=2 blots in n= 2 different experiments) showing LDLR and M6PR protein in the total lysate (tot) or membrane (mem) fraction isolated from TWI NSPCs, either UT or treated with 1 nM of SIM (24 h). Adapted from Ricca, Cascino et al., 2020.*

Overall, these data show that TWI NSPCs and differentiated progeny (neurons and glial cells) express functional LDLR and LDLR-related proteins, supporting the idea that this receptor-mediated system may be exploited to enhance the availability of a modified GALC enzyme in the CNS.

2 Generation of NSPC- and HSPC-lines overexpressing chimeric GALC enzymes.

2.1 Generation of lentiviral vectors encoding for chimeric GALC constructs.

We generated third generation LVs encoding for the murine *Galc* gene driven by the human phosphoglycerate kinase (PGK) promoter. The *Galc* sequence was fused to the mCherry (CH) fluorescence reporter sequence (LV.GALC-CH, Figure 11A) to facilitate protein detection by IF, WB, and live imaging (Figure 11B), as no commercial antibodies recognising the murine GALC enzyme are available. The CH tag, as previously reported for the hemagglutinin (HA) tag (Neri et al., 2011), does not affect GALC activity. We detected comparable GALC activity in murine TWI NSPCs transduced with the tagged enzyme (LV.GALC-CH, LV.GALC-HA), which was higher than that of UT WT cells expressing physiological levels of unmodified enzyme (Figure 11C). Thus, for the purpose of this study we consider GALC-CH as the wild-type form of the enzyme.

We further engineer the GALC-CH construct by:

- replacing the GALCsp with that of the highly secreted IDS enzyme (LV.IDS.GALC-CH, Figure 11D), with the aim of increasing GALC secretion by transduced cells (Sorrentino et al., 2013);

- adding a tandem repeat of the human ApoE II receptor-binding region (LV.IDS.GALC-CH.APO, Figure 11D), a LDLR-binding domain peptide (Gleitz et al., 2018; Wang et al., 2013) with the aim of enhancing BBB crossing as well as favouring GALC uptake through LDLR- and related proteins that are expressed in non-endothelial cell types, i.e., neural cells (see above).

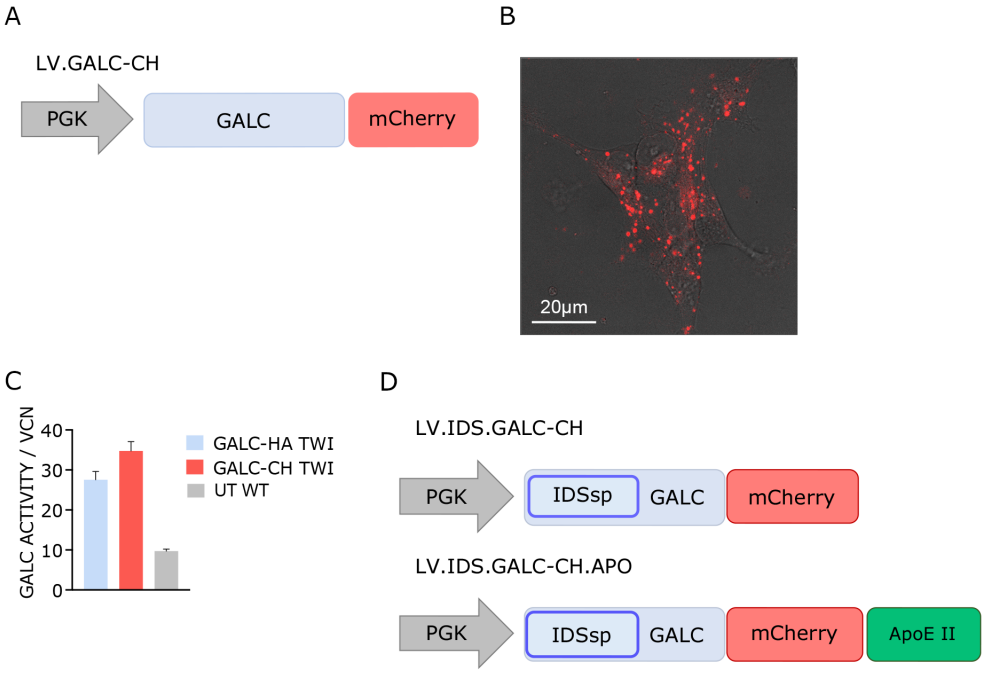

Figure 11. Lentiviral vectors encoding for chimeric GALC constructs. *A. Schematic of LV encoding for murine GALC.mCherry (GALC-CH). B. Representative confocal live imaging picture showing mCherry direct fluorescence in LV-transduced TWI NSPCs expressing GALC-CH. 63× magnification and zoom (~1.5×). Scale bar, 20 µm. C. GALC activity (normalized on VCN) measured in the pellet of LV.GALC-HA- and LV.GALC-CH- transduced TWI NSPCs. Data are the mean ± SEM, n=3 independent experiments in duplicate. D. Schematic of LVs encoding for GALC-CH-derived chimeric constructs (IDS.GALC-CH and IDS.GALC-CH.APO).*

We used the LVs expressing the chimeric enzymes (LV.IDS.GALC-CH and LV.IDS.GALC-CH.APO) or the wild-type version of GALC (LV.GALC-CH) to transduce murine NSPCs and HSPCs derived from TWI mice, which represent relevant target and/or effector cells in GLD pathology and therapy, respectively.

2.2 TWI NSPCs transduction by LVs encoding for chimeric GALC is safe and results in supraphysiological enzymatic activity.

We tested the different LVs in TWI NSPCs at different multiplicities of infection (MOI; 25, 50 and 100) to find the best transduction conditions and to evaluate possible toxicity resulting from the transduction *per se* and/or as a consequence of chimeric GALC overexpression. Results showed a dose-dependent increase of the VCN that ranged between 0.8 and 8 (Figure 12A), with no differences related to the different LVs. All LV-transduced NSPC lines (regardless of the VCN) displayed normal proliferation (not shown) and differentiation capability, as demonstrated by comparable number of neurons (neuron-specific class III beta-tubulin -TUJ1- positive cells; ~15% of total cells), astrocytes (GFAP+ cells; ~60% of total cells), and

oligodendrocytes (oligodendrocytes O4+ cells; ~20% of total cells) generated from UT and LV-transduced cells (Figure 12B).

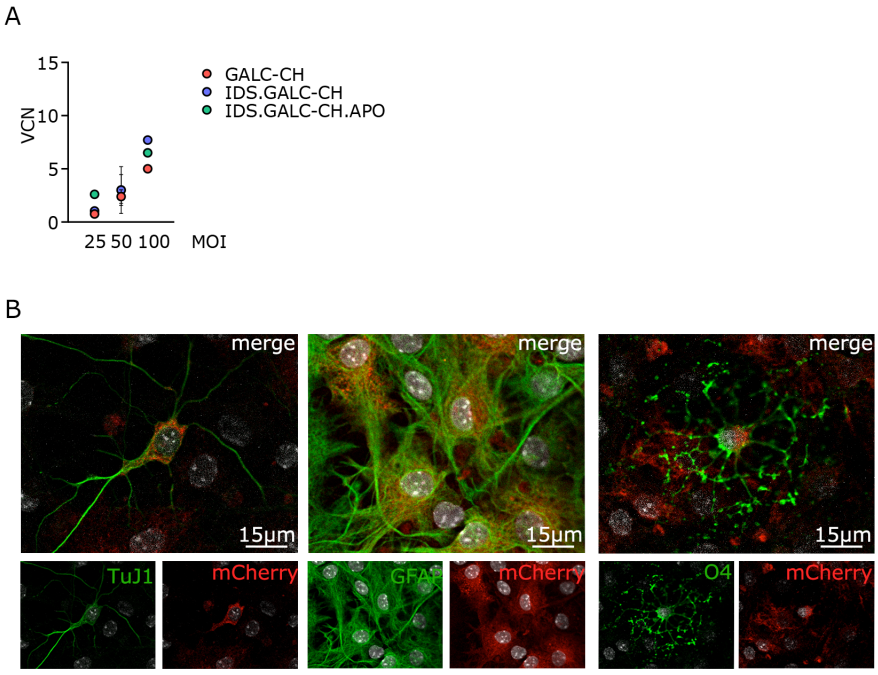

Figure 12. LVs driving the expression of chimeric GALC constructs efficiently transduce NSPCs. *A. VCN measured in LV-transduced TWI NSPCs (transduction at 25, 50, and 100 MOI). Data are expressed as the mean (n < 3) or the mean ± SEM (n=3-4). B. Representative confocal IF pictures showing neurons (TUJ1, green), astrocytes (GFAP, green) and oligodendrocytes (O4, green) expressing IDS.GALC-CH.APO (mCherry, red) in LV-transduced TWI NSPC-derived progeny. Nuclei counterstained with Hoechst (gray, pseudocolor). n=3 independent experiments, 3 coverslips/group/experiment. 40× magnification and zoom. Scale bar, 15 µm.*

Transduced TWI NSPCs showed physiological or supraphysiological GALC activity in the pellet (up to 13×) and supernatant (sup; up to 18×), as compared to UT WT NSPCs (Figure 13A). By normalizing the GALC activity on the VCN, we showed an advantage of IDS.GALC-CH (~1.3×) over the GALC-CH enzyme, while the enzymatic activity was reduced in the pellet of TWI NSPCs expressing IDS.GALC-CH.APO (~0.6×) (Figure 13B-C). Importantly, we detected a consistent increased enzymatic activity in the sup of TWI cells expressing IDS.GALC-CH (~2.7×) and IDS.GALC-CH.APO (~3×) enzymes as compared to those expressing GALC-CH enzyme (Figure 13D-E). Indeed, the percentage of secretion, calculated as enzymatic activity in the sup/total enzymatic activity (pellet+sup) × 100, was enhanced for IDS.GALC-CH (~2×) and even more for the full chimeric IDS.GALC-CH.APO (~6×) as compared to the GALC-CH (Figure 13F-G).

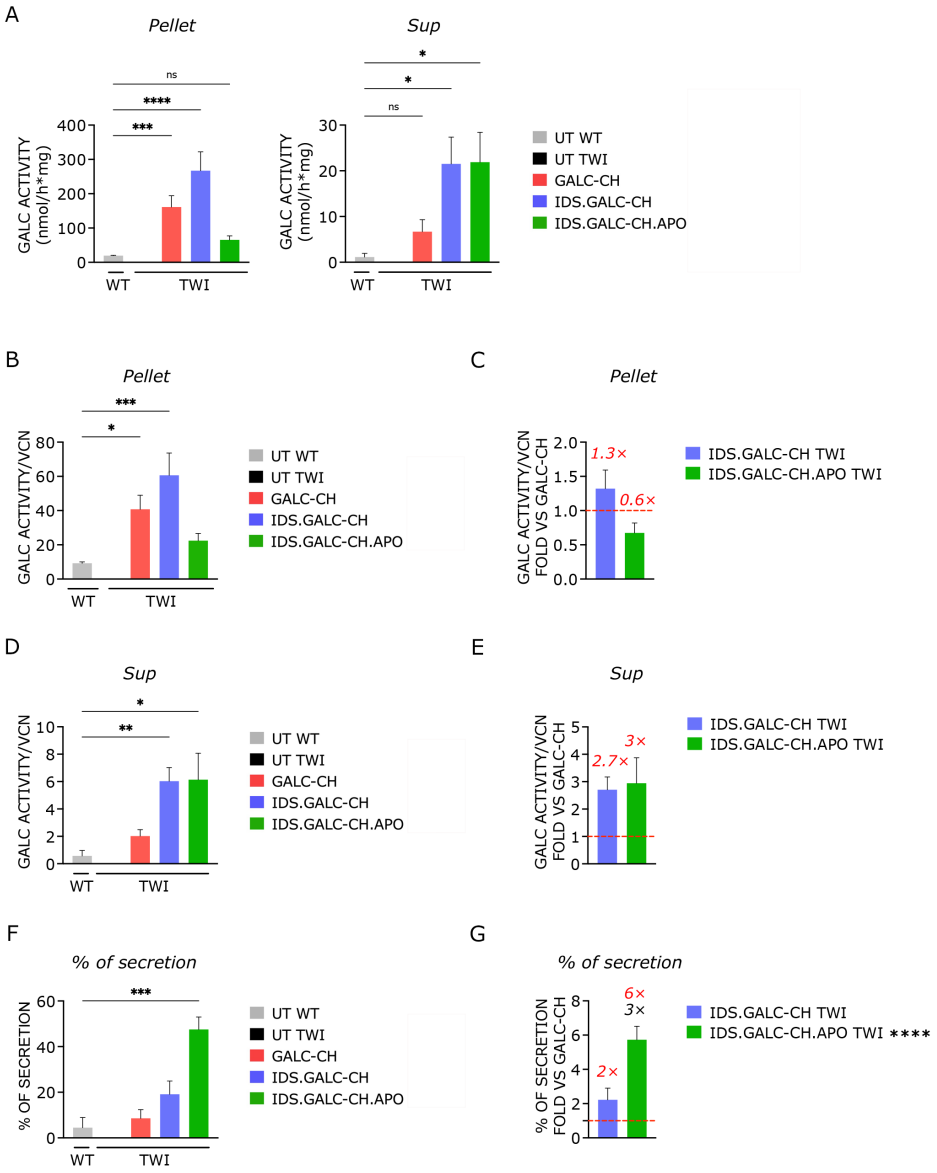

Figure 13. LV-transduced TWI NSPCs express and secrete chimeric GALC enzymes. *A. GALC activity measured in the pellet and sup of UT and LV-transduced TWI NSPCs and UT WT counterpart. Data are the mean ± SEM, n=4 independent experiments in duplicate/triplicate. One-way ANOVA followed by Kruskal Wallis multiple comparison test, * p<0.05, ***p<0.001, ****p<0.0001 vs. UT WT. B. GALC activity (normalized on VCN) measured in the pellet of LV-transduced TWI NSPCs and UT WT counterparts. Data are the mean ± SEM, n=3 independent experiments in duplicate/triplicate. One-way ANOVA followed by Kruskal Wallis multiple comparison test, *p<0.05, ***p<0.001 vs. UT WT. C. GALC activity (normalized on the VCN) reported in the panel B. Data in the graph are expressed as FOLD vs LV-GALC-CH-transduced TWI NSPCs (red dotted line) and represent the mean ± SEM. The fold increase with respect to GALC-CH is indicated in red. D. GALC activity (normalized on VCN) measured in the sup of LV-transduced TWI NSPCs and UT WT counterpart. Data are the mean ± SEM, n=4 independent experiments in duplicate/triplicate. One-way ANOVA followed by Kruskal Wallis multiple comparison test, *p<0.05, **p<0.01 vs. UT WT. E. GALC activity (normalized on the VCN) reported in the panel D. Data in the graph are expressed as FOLD vs. LV.GALC-CH-transduced TWI NSPCs (red dotted line) and represent the mean ± SEM. The fold increase with respect to GALC-CH is indicated in red. F. Percentage of GALC secretion, measured as GALC activity in the sup on total GALC activity (pellet+sup) × 100 in LV-transduced TWI NSPCs. Data are the mean ± SEM, n=4 independent experiments in*

*duplicate/triplicate. One-way ANOVA followed by Kruskal Wallis multiple comparison test, ***p<0.001 vs. UT WT. G. Percentage of GALC secretion reported in the panel F. Data in the graph are expressed as FOLD vs. LV.GALC-CH-transduced TWI NSPCs (red dotted line) and represent the mean ± SEM. One-way ANOVA followed by Dunnet's multiple comparison test, ****p<0.0001 vs. LV.GALC-CH-transduced TWI NSPCs. The fold increases with respect to GALC-CH and IDS.GALC-CH are indicated in red and black, respectively.*

These data suggested that the modifications made in the GALC sequence allow reconstitution of physiological/supraphysiological GALC level without toxicity, and importantly increase enzyme secretion, leading to a higher availability of GALC for cross-correction.

Specifically, GALC precursor is the enzyme form that, once released in extracellular space, can be reuptaken by surrounding cells and be useful for cross-correction (Spratley & Deane, 2016). Thus, we performed WB analysis using an anti-mCherry antibody to evaluate the amount of GALC precursor protein produced and secreted by LV-transduced cells.

We showed increased expression of the IDS.GALC-CH and IDS.GALC-CH.APO precursor proteins with respect to the GALC-CH protein (expected band size 110 kDa: 80 kDa GALC precursor + 30 kDa mCherry) in the pellet (~3x and ~4.5×, respectively) and supernatant (~3.5x and ~5×, respectively) of LV-transduced TWI NSPCs. Importantly, the full chimeric IDS.GALC-CH.APO was more expressed (~1.5×) and secreted (~2×) as compared to the IDS.GALC-CH (Figure 14A-B).

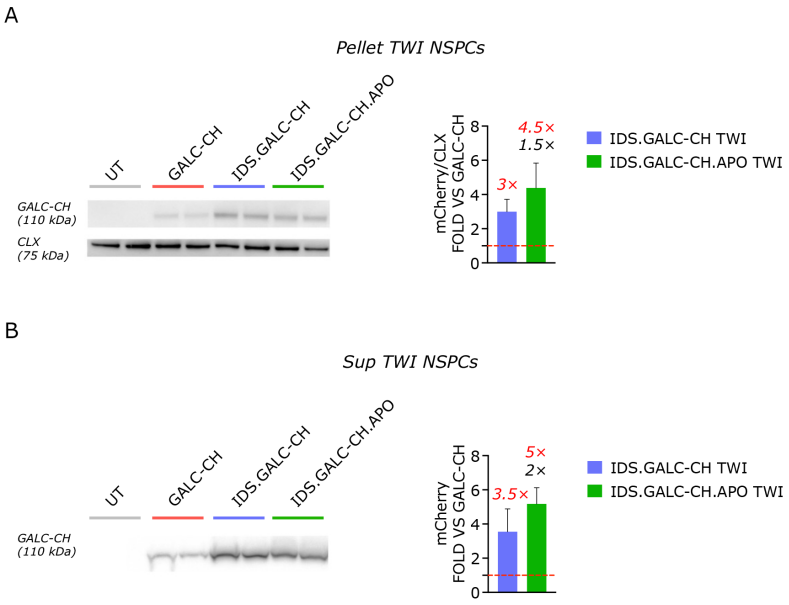

Figure 14. LV-transduced TWI NSPCs express and secrete the GALC precursor protein. *A-B. Representative WB and quantification (performed on n=3-6 blots in n= 3 different experiments) showing the GALC-CH protein (anti-mCherry antibody) in the pellet (A) and sup (B) of LV-transduced TWI NSPCs. The observed band of 110 kDa represents the precursor GALC protein (80 kDa) fused with the mCherry tag (30 kDa). CLX was used as*

normalizer. UT WT NSPCs are included as controls. Data in the graphs are normalized on the VCN and expressed as FOLD: IDS.GALC-CH and IDS.GALC-CH.APO / GALC-CH (red dotted line) and represent the mean ± SEM. The fold increases with respect to GALC-CH and IDS.GALC-CH are indicated in red and black, respectively.

Overall, these analyses suggested an increased IDS.GALC-CH.APO precursor protein expression and secretion.

In the perspective of a direct LV-mediated gene therapy approach (IC-GT) alone or in combination with other therapies (Lattanzi et al., 2010; Ricca et al., 2015), neurons and glial cells, more than NSPCs, are the population that, once corrected, could promote enzymatic reconstitution of CNS tissues. Thus, we differentiated transduced TWI NSPCs and UT counterparts in a mixed neurons/glia cells population to evaluate the GALC activity in differentiated cultures. We demonstrated the safe overexpression and secretion of chimeric GALC enzymes in NSPC-derived differentiated neuronal/glial progeny. Importantly, similarly with data collected from NPSCs, we detected an enhanced secretion of the full chimeric GALC, ~3x and ~2x with respect to GALC-CH and IDS.GALC-CH, respectively (Figure 15A-B).

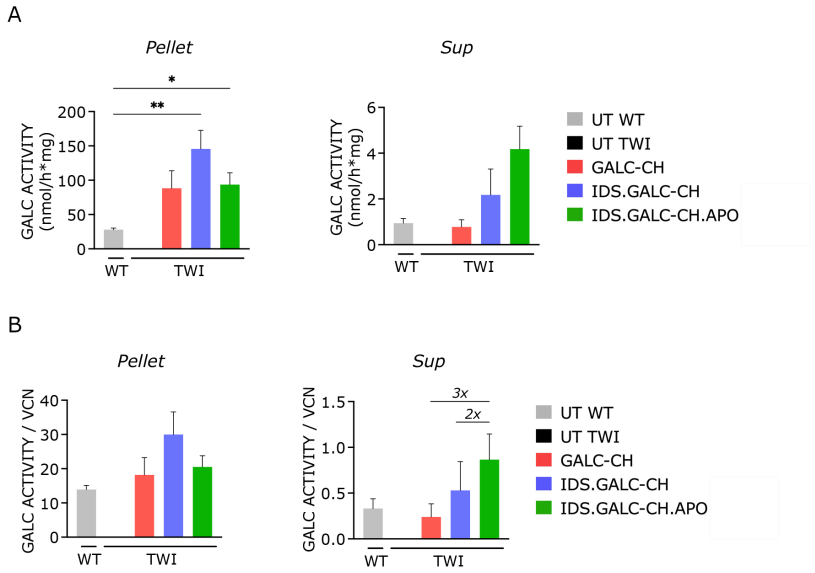

Figure 15. LV-transduced TWI NSPC-derived neuronal/glial progeny overexpress and secrete chimeric GALC enzymes. *A. GALC activity measured in the pellet and sup of UT and LV-transduced TWI NSPC-derived neuronal/glial cells and UT WT counterpart. Data are the mean ± SEM, n=4 independent experiments in duplicate/triplicate. One-way ANOVA followed by Kruskal Wallis multiple comparison test, *p<0.05, ** p<0.01 vs. UT WT. B. GALC activity (normalized on VCN) measured in the pellet and sup of transduced TWI NSPC-derived progeny and UT WT counterpart. Data are the mean ± SEM, n=4 independent experiments in duplicate/triplicate. The fold increase of IDS.GALC-CH.APO with respect to IDS.GALC-CH and GALC-CH is reported.*

To demonstrate the correct localisation of chimeric GALC enzymes in the lysosomal compartment and their ability to clear the GalCer storage that accumulates in UT TWI

differentiated cultures (Figure 16A), we performed confocal IF analysis in LV-transduced TWI NSPC-derived neurons and glial cells and UT TWI controls. We showed the co-localization of mCherry and lysosome-associated membrane protein 1 (LAMP1, glycoprotein highly expressed in lysosomal membranes) signals in transduced TWI cells expressing GALC-CH (Figure 16B), IDS.GALC-CH (Figure 16C) and IDS.GALC-CH.APO enzymes (Figure 16D). Importantly, we observed a substantial clearance of GalCer intracellular storage in transduced cells (Figure 16B–D) as compared to UT TWI counterparts (Figure 16A), confirming that the chimeric GALC enzymes are targeted to lysosomes and are functional.

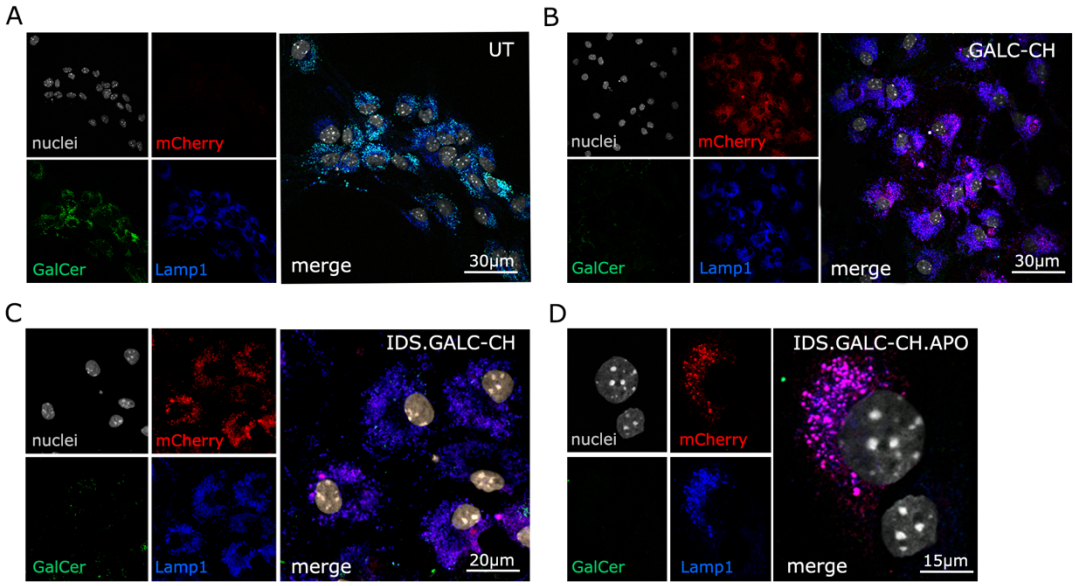

Figure 16. Chimeric GALC enzymes localized in the lysosomal compartment. *A–D. Representative confocal IF images of transduced TWI NSPC-derived progeny showing GALC-CH (B), IDS.GALC-CH (C) and IDS.GALC-CH.APO (D) (mCherry signal, red) localization in lysosomes (LAMP1, blue). Transduced cells show decreased GalCer storage (green) as to UT TWI controls (A). Nuclei stained with Hoechst (gray, pseudocolor); n=2 independent experiments, 2 coverslips/group/experiment. 63× magnification and zoom. Scale bars: 30 µm (A-B), 20 µm (C), 15 µm (D). Ricca, Cascino et al., 2020.*

2.3 TWI HSPCs safely overexpress chimeric GALC enzymes

The safe overexpression and secretion of chimeric GALC enzymes in HSPCs is crucial to favour the enzyme reconstitution of CNS tissues by HSPC-derived myeloid progeny in the context of the HSPC-GT approach (Gentner et al., 2010). To test if chimeric enzymes could provide an advantage in terms of enzyme expression and secretion in this cell type, we isolated HSPCs (lineage negative cells, Lin-) from TWI mice at 5–6 weeks (fully symptomatic stage) and age-matched WT littermates. We transduced HSPCs with the different LVs at MOI 50 and/or 100 using an optimized protocol (Ornaghi et al., 2020, see material and methods). We plated UT and LV-

transduced cells for the colony forming cell (CFC) assay and differentiation in liquid culture (LC) to evaluate the extent of GALC expression as well as a possible toxicity resulting from the transduction procedure and/or related to GALC overexpression, as reported previously (Gentner et al., 2010).

The VCN was evaluated after 14 days of LC, when only integrated LV can be measured (Zonari et al., 2017). VCN values ranged between 1.4 and 14 (Figure 17A). We measured supraphysiological GALC activity in LV-transduced WT and TWI HSPCs (up to 11× and 2.5× the levels of UT WT HSPCs, respectively) (Figure 17B). The transduction and enzyme overexpression were well tolerated, as shown by the comparable number of colonies originated by LV-transduced and UT WT and TWI cells (CFC assay; Figure 17C). By normalizing the enzymatic activity on the VCN, we highlighted a variable but consistent increase of the intracellular GALC activity in WT and TWI cells expressing the GALC-CH and chimeric enzymes as compared to the UT WT counterpart (Figure 17D), suggesting an efficient production and functionality of the chimeric GALC.

In order to test whether the chimeric GALC enzymes were efficiently secreted in the extracellular milieu, thus being potentially available for cross-correction in the context of autologous HSPC-GT, we measured GALC enzymatic activity in the sup of transduced TWI HSPCs. Results showed a moderate increase in the IDS.GALC-CH.APO secretion (~1.5x) with respect to the WT and GALC-CH counterparts (Figure 17E-F). Of note, WB analysis using an anti-mCherry antibody showed the presence of the GALC precursor protein in the sup of LV-transduced TWI HSPCs, indicating that the chimeric GALC precursors were correctly secreted and available in the extracellular environment (Figure 17G).

Finally, we assessed the lysosomal localization of the chimeric GALC enzymes in TWI HSPCs. We labelled HSPCs with anti-mCherry and anti-LAMP1 antibodies and analysed labelled cells and unlabelled controls by ImageStream. This imaging flow cytometry technique combines the sensitivity and quantitative power of cytofluorimetry with the qualitative information of fluorescent microscopy. The results showed a high degree of proximity (an index of co-localization) of the mCherry+ and LAMP1+ signal in >80% of all LV-transduced HSPCs (Figure 17H), suggesting that the chimeric GALC enzymes were correctly sorted to lysosomes.

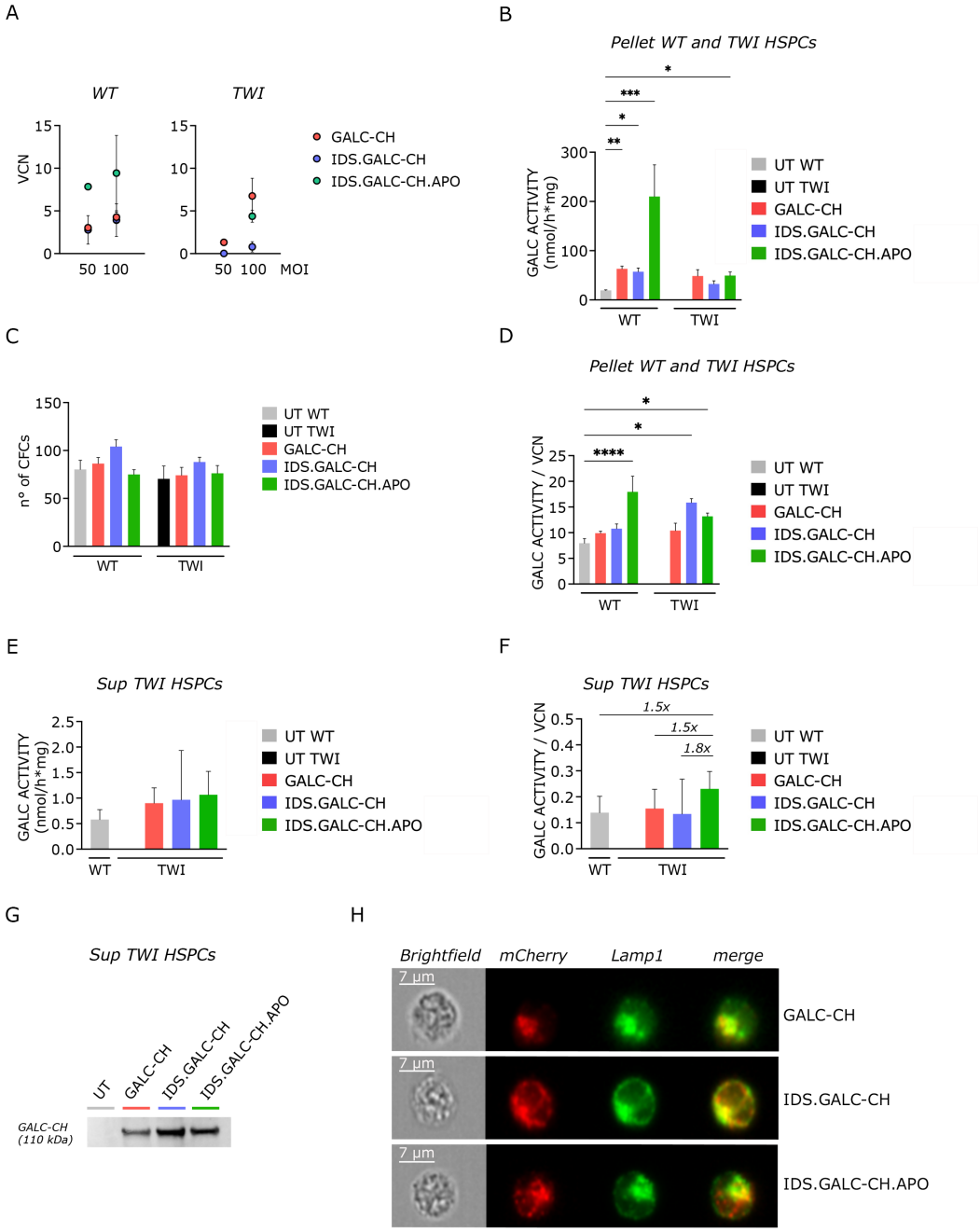

Figure 17. LV-transduced HSPC-progeny express and secrete the chimeric GALC enzymes. *A. VCN measured in WT and TWI HSPCs transduced with the different LVs (50 and/or 100 MOI) after 14 days in culture (liquid cultures, LCs). Data are expressed as the mean (n < 2) or the mean ± SEM (n=3-6). B. GALC activity measured in the pellet of UT and LV-transduced WT and TWI HSPCs (LCs). Data are the mean ± SEM, n=3-6 independent experiments in duplicate/triplicate. One-way ANOVA followed by Kruskal Wallis multiple comparison test, *p< 0.05, ** p<0.01, *** p<0.001 vs. UT WT. C. Number of colonies (CFC assay) originated by UT and LV-transduced WT and TWI HSPCs. Data are expressed as the mean ± SEM, n=4-6 independent experiments in duplicate. D. GALC activity normalized on VCN in the pellet of UT and LV-transduced WT and TWI HSPCs (LCs). Data are expressed as the mean ± SEM, n=4-6 independent experiments in duplicate/triplicate. One-way ANOVA followed by Dunnet's multiple comparison test, *p<0.05, ****p<0.0001 vs. UT WT. E. GALC activity measured in the sup of UT and LV-transduced TWI HSPCs, and UT WT controls (LCs). Data are the mean ± SEM, n=3-4 independent experiments in duplicate/triplicate. F. GALC*

activity normalized on VCN measured in the sup of UT and LV-transduced TWI HSPCs and UT WT counterpart (LCs). The fold increase of IDS.GALC-CH.APO with respect to IDS.GALC-CH and unmodified GALC counterparts is reported. G. Representative WB (n=3 blots in n=2 different experiments) showing the GALC-CH precursor protein (anti-mCherry antibody; 110 kDa) in the sup of transduced TWI HSPC (LCs). Sup collected from UT WT serves as control. H. Representative ImageStream pictures showing LAMP1 (green, pseudocolor) and mCherry (red, pseudocolor) proximity (merge) in transduced TWI HSPCs (LCs) expressing GALC-CH, IDS.GALC-CH, and IDS.GALC-CH.APO; n=2 independent experiments; n= ~1,000/sample cells on average analysed in each experiment. Scale bar, 7 μm.

Overall, these data suggested that TWI HSPCs safely overexpress chimeric GALC enzymes, which are correctly localized to the lysosomal compartment and also secreted as precursor proteins in the extracellular milieu. The chimeric IDS.GALC-CH.APO enzyme showed a slight increase in terms of enzyme expression and secretion as compared to the unmodified GALC enzyme.

2.4 NSPCs and HSPCs safely overexpress optimized chimeric IDUA.GALC-CH.APO construct.

The results obtained in NSPCs and HSPCs suggested an advantage of the IDSsp over the native GALCsp in terms of production and secretion of the chimeric GALC enzymes. Still, they highlighted a moderate enhanced secretion in LV-transduced TWI HSPCs (~1.5x the WT level). In order to further enhance the GALC secretion, and, consequently, its availability in the extracellular milieu, we decided to test a different sp. It is known that the basicity in the N-terminal polar region and the hydrophobicity in the H-core region of the sp positively impact on protein secretion (Knappskog et al., 2007; Kober et al., 2013; Stern et al., 2008; L. Zhang et al., 2005). We screened the sp sequence of several lysosomal enzymes by means of a hydrophobicity/hydrophilicity analysis (using Peptide 2.0 software) and selected the signal peptide of the IDUA enzyme (IDUAsp) for its increased basicity (43% vs. 25%) and hydrophobicity (90% vs. 65%) with respect to the IDSsp. Indeed, the IDUA enzyme is overexpressed in LV.IDUA-transduced murine HSPCs (~100x the normal levels) without apparent toxicity (Visigalli et al., 2010, 2016). We produced a LV encoding for the IDUA.GALC-CH.APO enzyme (see materials and methods for details, Figure 18A) and transduced TWI NSPCs (at 25, 50 and 100 MOI) and HSPCs (at 100 MOI) using the experimental protocols described above.

NSPCs transduced with LV.IDUA.GALC-CH.APO (VCN ranging between 5 and 16, Figure 18B) showed supraphysiological GALC activity in the pellet and sup (up to 13x and 240x the normal levels, respectively) (Figure 18C).

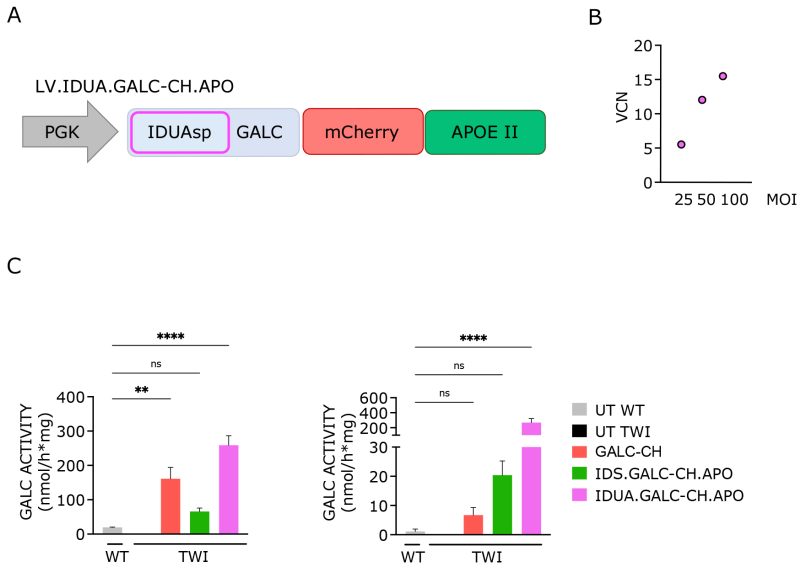

Figure 18. LV-transduced TWI NSPCs overexpress and secrete the IDUA.GALC-CH.APO enzyme. *A. Schematic of LV encoding for the full chimeric GALC enzyme with the IDUAsp (IDUA.GALC-CH.APO). B. VCN measured in LV-transduced TWI NSPCs (transduction at 25, 50, and 100 MOI). Data are expressed as the mean (n=1-2). C. GALC activity measured in the pellet and sup of UT and LV-transduced TWI NSPCs and UT WT counterparts. Data are the mean ± SEM, n=4 independent experiments in duplicate/triplicate. One-way ANOVA followed by Kruskal Wallis multiple comparison test, ** p<0.01, **** p<0.0001 vs. UT WT.*

By normalizing the GALC activity on the VCN we highlighted a reduced intracellular enzymatic activity in NSPCs transduced with LV.IDUA.GALC-CH.APO as compared to GALC-CH (~0.6x), similarly to what observed in LV.IDS.GALC-CH.APO-transduced TWI NSPCs (Figure 19A-B). Of note, WB analysis showed enhanced expression of the IDUA.GALC-CH.APO precursor protein with respect to both GALC-CH (~14x) and IDS.GALC.CH.APO (~3x) (Figure 19C). Also, the secretion of the IDUA.GALC-CH.APO enzyme was increased, as shown by assessing GALC activity (~12x and ~4x of GALC-CH and IDS.GALC.CH.APO, respectively) (Figure 19D-E) and the amount of precursor protein by WB (~11x and ~2x of GALC-CH and IDS.GALC.CH.APO, respectively) (Figure 19F) in the sup of transduced TWI cells. The percentage of secretion was overall enhanced for IDUA.GALC-CH.APO (~6×) as compared to GALC-CH (Figure 19 G-H).

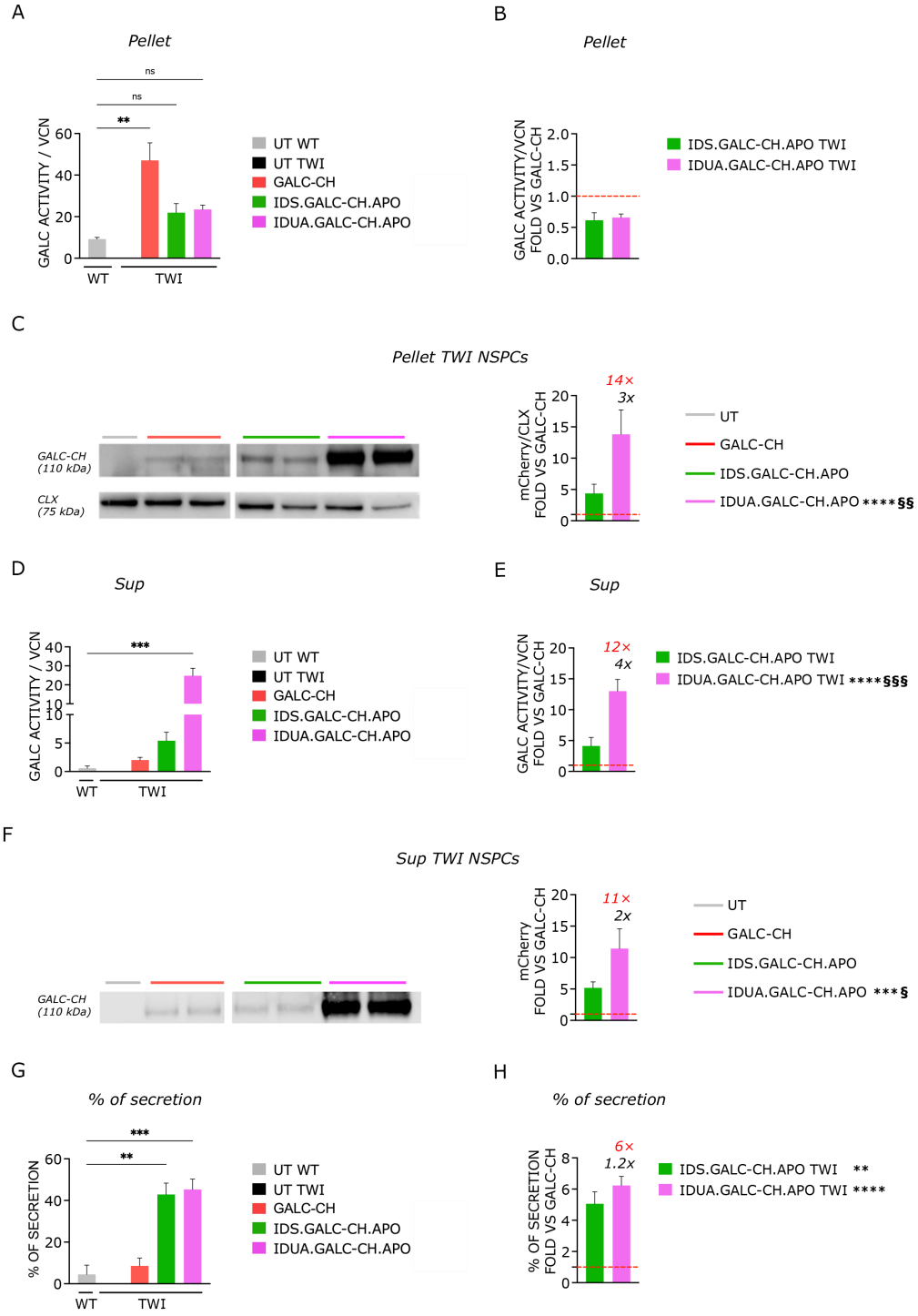

Figure 19. The IDUA.GALC-CH.APO enzyme outperforms the IDS.GALC-CH.APO counterpart in terms of enzyme expression and secretion. A. *GALC activity (normalized on VCN) measured in the pellet of LV-transduced TWI NSPCs and UT WT counterpart. Data are the mean ± SEM, n=4 independent experiments in duplicate/triplicate. One-way ANOVA followed by Kruskal Wallis multiple comparison test, ** p<0.01 vs. UT WT.* B. *GALC activity (normalized on the VCN) reported in the panel C. Data in the graph are expressed as FOLD vs. LV.GALC-CH-transduced TWI NSPCs (red dotted line).* C. *Representative WB (performed on n=3 blots in n=3 different experiments) showing the GALC-CH precursor protein (anti-mCherry antibody, detected band 110 kDa) in the pellet of LV-transduced TWI NSPCs. UT WT NSPCs was included as control. Data in the graphs are normalized on the VCN and expressed as FOLD*

*vs. LV.GALC-CH-transduced TWI NSPCs (red dotted line). Data are the mean ± SEM analysed by One-way ANOVA followed by Dunnet's multiple comparison test, ****p<0.0001 vs. GALC-CH; §§ p<0.01 IDUA.GALC-CH.APO vs. IDS.GALC-CH.APO. The fold increases with respect to GALC-CH and IDS.GALC-CH.APO are indicated in red and black, respectively.* D*. GALC activity (normalized on VCN) measured in the sup of LV-transduced TWI NSPCs and UT WT counterpart. Data are the mean ± SEM, n=4 independent experiments in duplicate/triplicate. One-way ANOVA followed by Kruskal Wallis multiple comparison test, *** p<0.001 vs. UT WT.* E. *GALC activity (normalized on the VCN) reported in the panel F. Data in the graph are expressed as FOLD vs. LV.GALC-CH-transduced TWI NSPCs (red dotted line), analysed by One-way ANOVA followed by Kruskal Wallis multiple comparison test, **** p<0.0001 vs. GALC-CH, §§§ p<0.001 IDUA.GALC-CH.APO vs. IDS.GALC-CH.APO. The fold increases with respect to GALC-CH and IDS.GALC-CH.APO are indicated in red and black, respectively.* F*. Representative WB (performed on n=3 blots in n=3 different experiments) showing the GALC-CH precursor protein (anti-mCherry antibody, detected band 110 kDa) in the sup of LV-transduced TWI NSPCs. UT WT NSPCs was included as control. Data in the graphs are normalized on the VCN and expressed as FOLD vs. LV.GALC-CH-transduced TWI NSPCs (red dotted line). Data are the mean ± SEM analysed by One-way ANOVA followed by Dunnet's multiple comparison test, ***p<0.001 vs. GALC-CH; § p<0.05 IDUA.GALC-CH.APO vs. IDS.GALC-CH.APO. The fold increases with respect to GALC-CH and IDS.GALC-CH.APO are indicated in red and black, respectively.* G*. Percentage of GALC secretion, measured as GALC activity in the sup on total GALC activity (pellet+sup) × 100 in LV-transduced TWI NSPCs. Data are mean ± SEM, n=4 independent experiments in duplicate/triplicate. One-way ANOVA followed by Kruskal Wallis multiple comparison test, **p< 0.01, ***p<0.001 vs. UT WT.* H*. Percentage of GALC secretion reported in the panel G. Data in the graph are expressed as FOLD vs. LV.GALC-CH-transduced TWI NSPCs (red dotted line). Data analysed by One-way ANOVA followed by Kruskal Wallis multiple comparison test, **p<0.01, ****p<0.0001 vs. LV.GALC-CH-transduced TWI NSPCs. The fold increases with respect to GALC-CH and IDS.GALC-CH.APO are indicated in red and black, respectively.*

Overall, these data suggested that the IDUA.GALC-CH.APO precursor protein is more efficiently secreted and available in the extracellular milieu than the GALC-CH and IDS.GALC.CH.APO counterparts, suggesting a superior efficiency of the IDUAsp with respect to IDSsp in favouring the GALC secretory pathway.

Transduction of TWI HSPCs with LV.IDUA.GALC-CH.APO resulted in supraphysiological GALC activity in the pellet and sup, reaching up to 5.4x and 3x the physiological level assessed in UT WT HSPCs, respectively (Figure 20A). Similarly to what described for the other LV constructs, the LV transduction and the consequent GALC overexpression were safe, as demonstrated by comparable number of colonies originated by UT and LV-transduced TWI HSPCs and UT WT counterpart (CFC assay; Figure 20B).

Importantly, by normalizing GALC activity on the VCN we observed an advantage of using IDUAsp in terms of GALC production (~2.8x and ~1.5x of GALC-CH and IDS.GALC-CH.APO, respectively) and secretion (~1.7x and ~1.5x of GALC-CH and IDS.GALC-CH.APO, respectively) (Figure 20C). WB analysis using an anti-mCherry antibody showed the expression of the GALC precursor protein in the sup of transduced HSPCs (Figure 20D), indicating that the IDUA.GALC-CH.APO precursor is correctly secreted and available for potential cross-correction of surrounding cells.

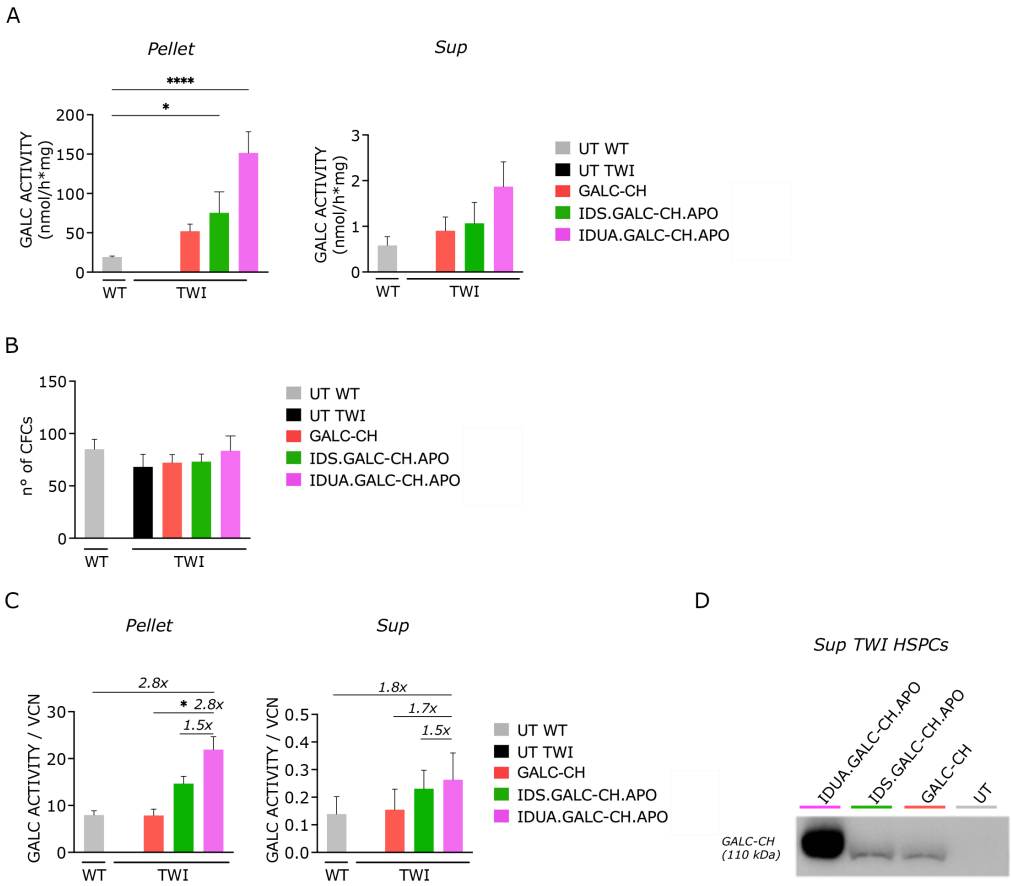

Figure 20. LV-transduced HSPCs overexpress and secrete the IDUA.GALC-CH.APO enzyme. *A. GALC activity measured in the pellet and sup of UT and LV-transduced TWI HSPCs and WT counterpart (LCs). Data are the mean ± SEM, n=3-6 independent experiments in duplicate/triplicate. One-way ANOVA followed by Kruskal Wallis multiple comparison test, *p<0.05, **** p<0.0001 vs. UT WT. B. Number of colonies (assessed in the CFC assay) originated by UT and LV-transduced TWI HSPCs and UT WT counterpart. Data are expressed as the mean ± SEM, n=3-6 independent experiments in duplicate. C. GALC activity normalized on VCN measured in the pellet and sup of UT and LV-transduced TWI HSPCs and UT WT cells as control (LCs). Data are expressed as the mean ± SEM, n=3 independent experiments in duplicate/triplicate, analysed by One-way ANOVA followed by Kruskal Wallis multiple comparison test, *p<0.05 vs. LV.GALC-CH-transduced TWI HSPCs. The fold increase of IDUA.GALC-CH.APO with respect to IDS.GALC-CH.APO and unmodified GALC counterparts is reported. D. Representative WB (performed on n=3 blots in n=2 different experiments) showing the GALC-CH precursor protein (anti-mCherry antibody, observed band 110 kDa) in the sup of LV-transduced TWI HSPCs (LCs). Sup collected from UT WT serves as control.*

Similar to the other chimeric GALC enzymes, the IDUA.GALC-CH.APO enzyme correctly localizes in the lysosomes of the cellular progeny derived from transduced TWI NSPCs and HSPCs (Figure 21A, C). Importantly, in transduced TWI neurons/glial progeny we observed the clearance of GalCer storage that accumulates in UT cells (Figure 21B), suggesting the functionality of the IDUA.GALC-CH.APO enzyme.

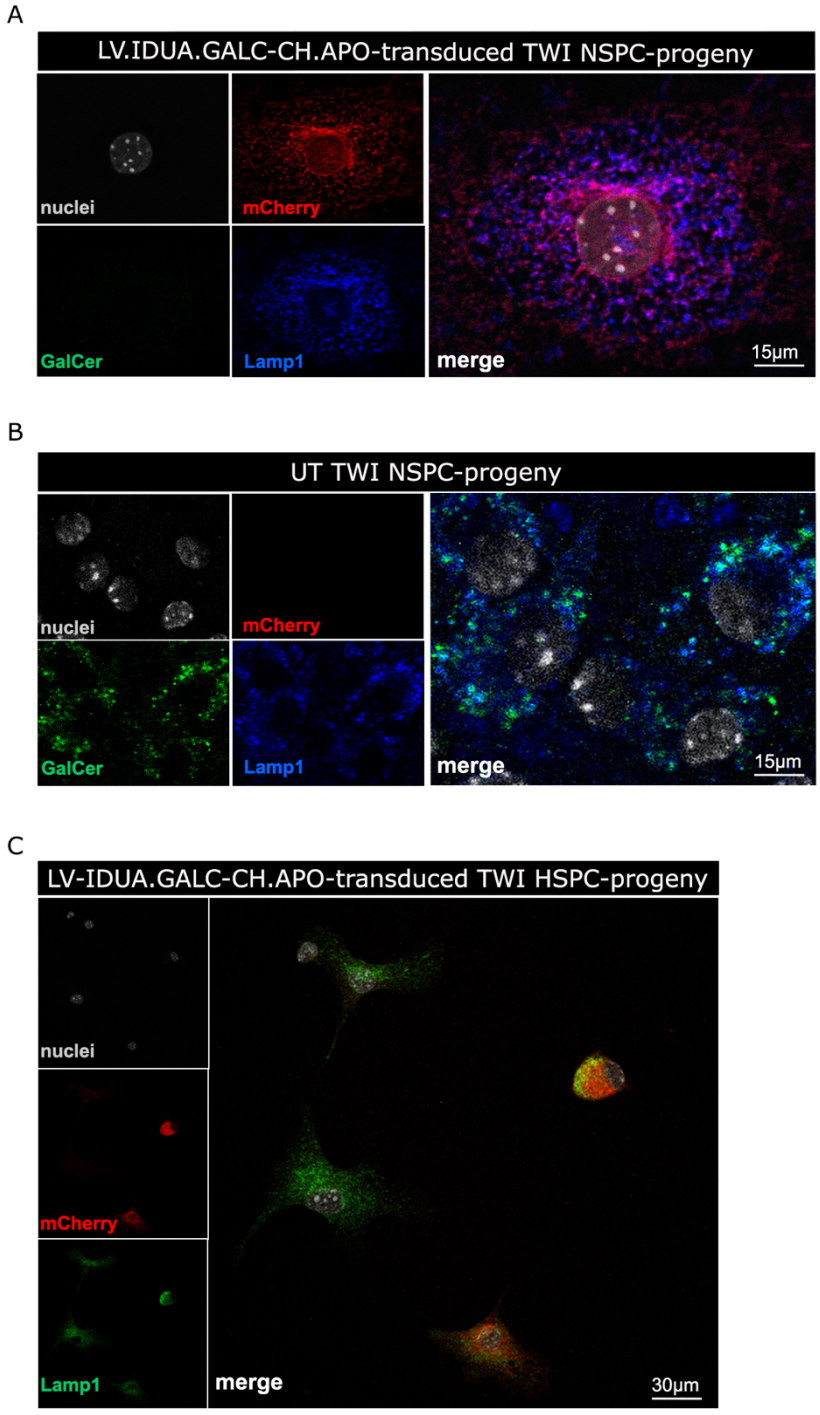

Figure 21. The IDUA.GALC-CH.APO enzyme localizes in the lysosomes of transduced TWI NSPC- and HSPC- derived progeny. *A-C. Representative confocal IF images of LV-transduced TWI NSPC- (A) and HSPC- (C) derived progeny (neurons/glial in A, LCs in C) showing IDUA.GALC-CH.APO (mCherry signal, red) localization in lysosomes (LAMP1, blue in A-B and green in C). Transduced NSPC-derived progeny shows decreased GalCer storage (green) as compared to UT TWI controls (B). Nuclei stained with Hoechst (gray, pseudocolor); n=2 independent experiments, 2 coverslips/group/experiment. 63× magnification and zoom. Scale bars: 15 μm (A-B), 30 μm (C).*

Overall, these data suggested that TWI HSPCs safely overexpress and secrete the IDUA.GALC-CH.APO chimeric enzyme. The chimeric GALC correctly localizes to lysosomal compartment and is functional in clearing the GalCer storage in TWI neurons/glial cells. Importantly, the IDUA.GALC-CH.APO chimeric enzyme showed an additional advantage in terms of intracellular expression and secretion with respect to the unmodified and the IDS.GALC-CH.APO counterparts.

2.5 Chimeric GALC enzymes cross-correct NSPC-derived progeny and reduce intracellular GalCer storage.

We demonstrated the correct production and secretion of chimeric GALC enzymes by LV-transduced TWI NSPCs and HSPCs and identified a clear advantage of the IDUA.GALC-CH.APO enzyme in terms of production and secretion. In the perspective of GT approaches, it is crucial to demonstrate that the chimeric enzymes released by transduced (metabolically corrected) TWI cells can be efficiently reuptaken by GALC-deficient TWI neurons/glial cells and targeted to lysosomes for the clearance of undegraded substrates (cross-correction) (Spratley & Deane, 2016). Thus, we took advantage of our *in vitro* cellular systems to model the cross-correction mechanisms acting in the context of CNS-directed GT approaches (IC-GT and HSPC-GT, respectively). Specifically, we evaluated the ability of chimeric GALC enzymes (with IDSsp and IDUAsp) produced by NSPC- and HSPC-derived progeny to cross-correct GALC-deficient neuronal/glial cells in a direct comparison with the unmodified (GALC-CH) and WT GALC enzymes.

We report in Figure 22A the schematic of cross-correction experiments. NSPCs and HSPCs were cultured for 7 and 14 days, respectively, to obtain lineage-committed progeny (donor cells). The sup was collected from donors every 24 h for the last 3 days of culture and used to treat untransduced TWI NSPC-derived neuron/glial progeny (acceptor cells). We analysed GALC activity in acceptor cells after 3 days of exposure to the sup of donor cells. We used the following donor cell populations:

- UT WT and LV-transduced TWI NSPC-derived neurons/glial cells;
- UT WT and LV-transduced TWI HSPC-derived progeny.

The GALC enzymatic activity measured in the sup of the different donor cell cultures and their VCN are shown in Figure 22B. Note that the GALC activity measured in sup of LV-transduced HSPCs is ~1/10 of that measured in NSPC-derived neurons/glial cells.

In both the donor cell populations we detected a higher secretion of the IDUA.GALC-CH.APO as compared to the other enzymes, confirming the data shown above.

The GALC activity in cross-corrected (XC) TWI cultures treated with the sup of the NSPC-progeny was ~20-25 nmol/h × mg (Figure 22C), representing ~70% of the normal level assessed in WT neurons/glia (Figure 22D). The IDUA.GALC-CH.APO enzyme resulted in a more robust rescue of GALC activity in treated cells (up to 93% the physiological levels).

The GALC activity measured in XC TWI cells treated with the sup of the different HSPC-derived cultures was 6.6 nmol/h × mg (XC UT WT), 12.5 nmol/h × mg (XC GALC-CH TWI), 12.9 nmol/h × mg (XC IDS.GALC-CH.APO TWI) and ~35 nmol/h × mg (XC IDUA.GALC-CH.APO TWI) (Figure 22E), representing ~19%, ~44%, ~41%, and 120% of the normal level assessed in WT neurons/glia, respectively (Figure 22F).

Confocal IF analysis performed in acceptor cells demonstrated the clearance of GalCer storage in all cross-corrected TWI neurons/glial cells (Figure 22G), suggesting that <20% of physiological enzymatic activity is sufficient to completely clear the intracellular storage in GALC-deficient neuronal/glial cells under the *in vitro* culture conditions tested here.

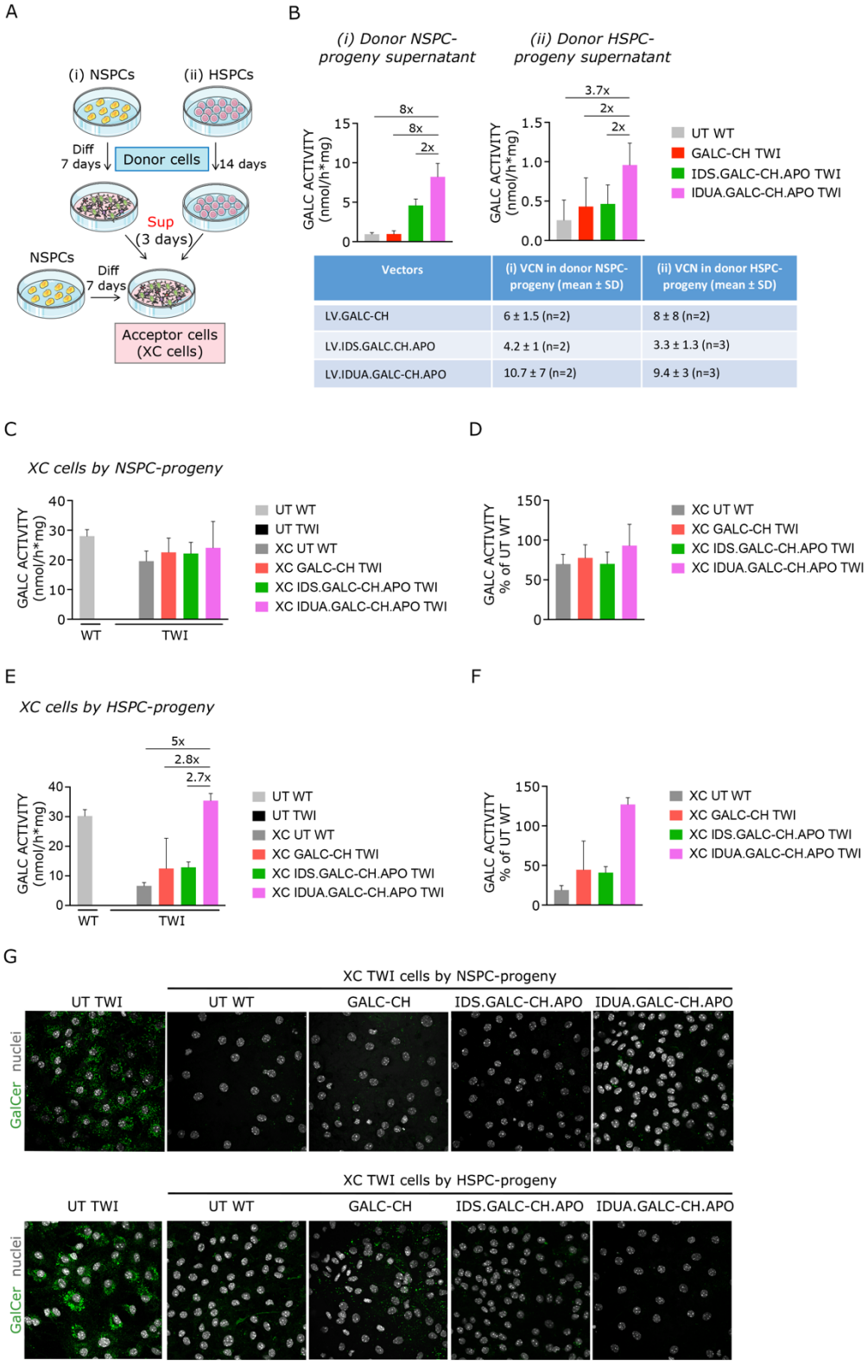

Figure 22. Chimeric GALC enzymes cross-correct TWI NSPC-derived neuronal/glial cells. *A. Schematic of cross-correction experiments. Donor cells: (i) TWI neuronal/glial cells derived from UT WT NSPCs and TWI NSPCs transduced with LV.GALC-CH, LV.IDS.GALC-CH.APO, and LV.IDUA.GALC-CH.APO; (ii) UT WT HSPC-derived progeny and TWI transduced with LV.GALC-CH, LV.IDS.GALC-CH.APO, and LV.IDUA.GALC-CH.APO (LCs). Acceptor cells*

(cross-corrected cells, XC cells): TWI NSPC-derived neuronal/glial cells. XC cells are exposed to fresh medium or to the sup of donor cells during the last 3 days of culture. Donor and XC cells are then collected for analysis. B. GALC activity measured in the sup of donor cells, namely NSPC- (i) and HSPC- (ii) progenies. Data are expressed as the mean ± SEM, n =3-4 independent experiments in duplicate/triplicate, except for TWI NSPC-progeny expressing IDUA.GALC-CH.APO (mean with range, n=2 experiments in duplicate). The fold increase of IDUA.GALC-CH.APO with respect to IDS.GALC-CH.APO and unmodified GALC counterparts is reported. The table reports the VCN (mean ± SD) measured in LV-transduced donor cell and the number of cell preparations used for the cross-correction experiments. C. GALC activity in TWI XC neurons/glia treated with the sup of neuronal/glial donor cells. Data are expressed as the mean ± SEM, n =3-4 independent experiments in duplicate/triplicate, except for TWI NSPC-progeny expressing IDUA.GALC-CH.APO (mean with range, n=2 experiments in duplicate). D. GALC activity reported in the panel C. Data are expressed as FOLD vs. UT WT neuronal/glial cells. E. GALC activity in TWI XC neurons/glia treated with the sup of progeny derived from HSPC donors. Data are expressed as the mean ± SEM, n =3-4 independent experiments in duplicate/triplicate. The fold increase of IDUA.GALC-CH.APO with respect to IDS.GALC-CH.APO and unmodified GALC counterparts is reported. F. GALC activity reported in the panel E. Data are expressed as FOLD vs. UT WT neuronal/glial cells. G. Representative confocal IF pictures showing that TWI XC neurons/glia treated with the sup of donor cells display reduction in GalCer storage (green) as compared to UT TWI cells. Nuclei stained with Hoechst (gray, pseudocolor); n=2–4 independent experiments, 2 coverslips/group/experiment. 63× magnification. Scale bar, 30 μm.

Overall, these data suggested that the chimeric enzymes secreted by transduced NSPC- and HSPC-derived progeny are available in the sup for the uptake by acceptor cells and, importantly, they are able to clear the GalCer storage in GALC-deficient neural progeny, which are metabolically cross-corrected. The data also highlight an advantage of the HSPC-derived IDUA.GALC-CH.APO enzyme in restoring physiological GALC activity in XC TWI neural cells.

Of note, these results show that <20% of the physiological GALC activity is sufficient to clear the intracellular storage in XC TWI neural cells, underlining the limitation of this *in vitro* model to spot an advantage of the chimeric vs. unmodified enzymes, a comparison that can only be fully assessed using *in vivo* GT models.

3. Exploiting chimeric GALC enzymes to optimize *ex vivo* HSPC-GT for GLD.

The enzymatic correction of CNS tissues remains a major challenge in GT approaches for neurodegenerative LSDs: effective therapy requires rapid and robust production of defective enzyme (possibly above the physiological level) coupled to its efficient delivery in this tissue, to prevent demyelination and neuronal damage and to act faster than the disease progression.

Our *in vitro* results demonstrated the higher production and secretion of chimeric GALC enzymes (with IDSsp and even more with IDUAsp) by LV-transduced TWI HSPCs as compared to the unmodified and WT counterparts. Importantly, we observed a full restoration of intracellular GALC activity in TWI neuronal/glial cells

cross-corrected by the IDUA.GALC-CH.APO chimeric enzyme secreted by LV-transduced TWI HSPCs. These data suggest that this advantage could be exploited in the context of an autologous *ex vivo* HSPC-GT approach to achieve an increased bioavailability of chimeric GALC enzyme in CNS tissues. To this end, we designed an experimental plan to test the safety and efficacy of *ex vivo* HSPC-GT approach using the chimeric GALC enzyme in TWI mice, a GLD model with a severe phenotype that recapitulates the most common and severe early infantile form of the disease.

3.1 Design of the therapeutic approach: time of intervention and myeloablative regimen.

To prevent or halt the rapid disease progression that characterizes TWI mice, therapeutic intervention should be performed in the early post-natal life. Because of GALC deficiency, the undegraded and toxic substrate psy accumulates up to 100x the physiological levels in TWI nervous tissues, starting in the very early post-natal days (<PND 10) and with an age-dependent progression and caudal-to-rostral accumulation (Ricca et al., 2015; Santambrogio et al., 2012). Thus, we decided to perform donor cells transplantation at PND 2-3, as compared to PND 6-7 that we tested in our previous work (Ricca et al., 2015).

After HSPCs transplantation, the HSPC-derived myeloid progeny infiltrates the visceral organs, the CNS, and the PNS, providing a stable source of functional enzyme in several LSD animal models (Prasad & Kurtzberg, 2010). The rapidity and level of donor hematopoietic cell (HC) engraftment is related to the myeloablative regimen used to deplete the endogenous HCs in the BM niche and the pool of tissue-resident myeloid cells (Capotondo et al., 2012). Given the widespread pathology that characterizes TWI mice, a fast and robust donor chimerism is critical to ensure relevant therapeutic benefit, especially in the CNS.

Previous data regarding the myeloablation and HSPC-T in newborn mice showed the efficacy of total body irradiation (TBI) as well as the use of the alkylating agent Busulfan (BUS, currently applied in the *ex vivo* HSPC-GT trials in MLD and MPS-I patients; Fumagalli et al., 2022; Gentner et al., 2021) in inducing high levels of engraftment of donor cells derived from the tBM of WT donor mice (Hawkins-Salsbury et al., 2015; Li et al., 2021; Pievani et al., 2015; Reddy et al., 2011; Ricca et al., 2015; Santi et al., 2020; Yeager et al., 1993). As the transplantation of transduced HSPCs (without the committed progenitors present in the tBM) in PND 2-3 TWI mice had never been performed before, we tested both conditioning regimens in TWI mice and WT littermates as controls, to establish the optimal treatment scheme resulting in the highest donor cells chimerism in recipient mice without adverse toxicity. Based

on published data and on pilot dose-response experiments, we decided to use the following regimens: i) TBI at 500 or 400 absorbed radiation dose (RAD) (Hawkins-Salsbury et al., 2015; Li et al., 2021; Reddy et al., 2011); ii) single intraperitoneal injection of 20 mg/Kg of BUS (Pievani et al., 2015; Santi et al., 2020). The following day, mice were transplanted with HCs isolated from WT mice, a setting that models the HSPC-T approach currently available for GLD patients. Specifically, we used: i) WT HSPCs (Lin- fraction) transduced with the LV harbouring green fluorescent protein (GFP), to track the engraftment of donor HCs in host tissues (WT HSPC-GT groups); ii) tBM harvested from transgenic CAG-GFP mice (TgCAG-GFP), which consists of a mixed population of hemopoietic stem cells and committed progenitors expressing GFP (tBM-T groups). We introduced tBM-T groups as positive control, because our previous work showed high level of engraftment of these cells in recipient TWI mice in FVB background (Ricca et al., 2015). Treated WT littermates and UT mice (WT and TWI) were used as controls.

Pilot experiments showed that while both 400 RAD and 500 RAD were sublethal doses in TBI, transplanted mice that had received the highest irradiation dose showed severe motor impairment possibly due to a damage to the developing cerebellum. For this reason, we used 400 RAD in all the following experiments.

Treated mice were monitored to evaluate the growth and survival and analysed one and two months after treatment and at the time of sacrifice to assess:

- the engraftment of transplanted GFP+ HCs: i) by fluorescence-activated cell sorting (FACS) analysis on the peripheral blood (PB) collected one and two months after transplant, by the use of the monoclonal antibody reacting with all isoforms of mouse cluster of differentiation (CD) 45 (CD45), a marker expressed by all HCs excluding mature erythrocytes and platelets; ii) by VCN performed on the BM cells harvest from WT HSPC-GT treated mice at the time of sacrifice; iii) by IF analysis in brain tissues of transplanted mice to evaluate GFP+ donor cells distribution, morphology and activated state;
- the inflammatory status of CNS, a disease-associated pathological feature, in treated and controls groups (by WB analysis);
- the GALC activity in CNS, PNS and peripheral organs (liver, spleen, and BM).

In addition, part of the WT Lin- cells used for the transplant were plated *in vitro* for LC and CFC assays and analysed after 14 days in culture to evaluate the safety (CFC) and the efficacy of transduction (VCN and enzymatic activity on LC).

The experimental protocol and treatment groups are summarized in Figure 23.

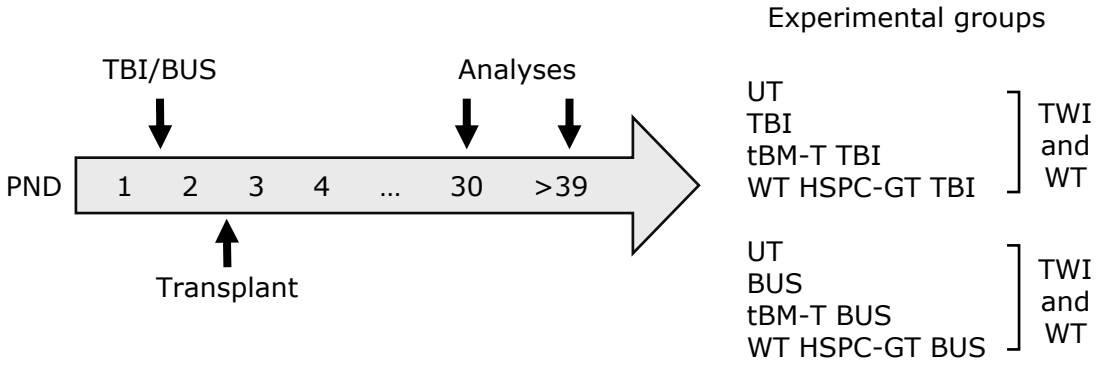

Figure 23. Experimental plan. *Neonatal PND 1-2 TWI and WT mice are myeloablated by total body irradiation (TBI) or by single intraperitoneal injection of Busulfan (BUS, 20 mg/Kg). Transplantation of LV-transduced WT HSPCs expressing GFP (WT HSPC-GT) or total bone marrow isolated from tgCAG-GFP donors (tBM-T) is performed the following day. Treated mice and controls are analysed 1 month after transplant and at the end of the experiment (human disease endpoint; > 39 days, average lifespan of untreated TWI mice).*

3.2 Survival of treated TWI mice and peripheral engraftment of donor HCs.

The median survival of UT TWI mice is 39 days (34-44 days, n=40 mice in the colony observed over 2 years). TBI conditioned TWI mice showed a significantly decrease in the median survival (median lifespan of 27 days; 23-37 days; n=8), differentially from the BUS-treated counterpart (median lifespan of 40.5 days; 38-43 days; n=2) (Figure 24A-B). Total BM-T performed after BUS conditioning determined a significant increase in the survival of TWI mice (median lifespan of 49 days; 43-64 days; n=13) as compared to TBI conditioning (median lifespan of 42 days; 35-44 days; n=5), providing a significant enhanced benefit as compared to UT TWI (Figure 24A). WT HSPC-GT performed after BUS conditioning resulted in a moderate increase in the median survival (median lifespan of 43 days; 41-45 days; n=11) with respect to TBI conditioning (median lifespan of 40 days; 35-44 days; n=8), with an overall less clear advantage over the UT TWI group (Figure 24A-B).

Treated and control mice were weighed weekly to assess their growth following conditioning and transplantation. WT treated mice (n=5 for all the groups) grew similarly regardless of the myeloablation regimen used, maintaining a significant lower weight than the untreated ones (UT WT, n=10). Transplanted TWI mice never achieved the weight of WT controls, regardless of the treatment. The weight of TWI mice transplanted with tBM after BUS conditioning was comparable to UT TWI littermates until PND 39 (the average lifespan of UT TWI mice) and remained stable until the time of sacrifice. Overall, the TBI-conditioned groups showed lower body weight with respect to the BUS-conditioned counterparts (Figure 24C).

Recipient mice were examined at one and two months after transplant to evaluate the engraftment of donor-derived HCs (GFP+CD45+) in the PB by FACS analysis. In

the WT HSPC-GT groups we also evaluated the VCN in the BM collected at the time of sacrifice. In all the tBM-T groups, we achieved variable and stable engraftment, ranging from 20% to 91% of GFP+ donor cells in PB without significantly differences related to the conditioning used. Two treated TWI mice conditioned with Busulfan reached two months of life, starting from 63% and 76% of engrafted donor cells at one month and reaching more than 96% at two months (Figure 24D).

The engraftment of HCs derived from WT Lin- cells (VCN in LCs ~6) in the WT HSPC-GT groups ranged between 2.4% and 56.3%, being significantly lower than the engraftment of HCs derived from tBM (Figure 24E). Since transduction with LV.GFP was safe, as assessed by comparable number of colonies originated by UT and transduced cells and by comparable enzymatic activity measured in LCs of both populations (Figure 24F), the differences observed may indicate a different kinetic of hematopoietic cells reconstitution after treatment. It is known that the early engraftment is mediated by cell populations that are enriched for committed progenitors, while the engraftment of stem cells is a slow process (Jones et al., 1990; Zijlmans et al., 1998). Furthermore, the BUS-conditioned WT HSPC-GT group showed a slight but not significant decrease in the level of engraftment with respect to TBI-conditioned animals, also evaluated by VCN analysis on the BM (Figure 24G).

Importantly, we did not observe differences in the engraftment level between WT and TWI transplanted mice (Figure 24E), suggesting that GALC deficiency does not affect the engraftment of donor-derived HCs.

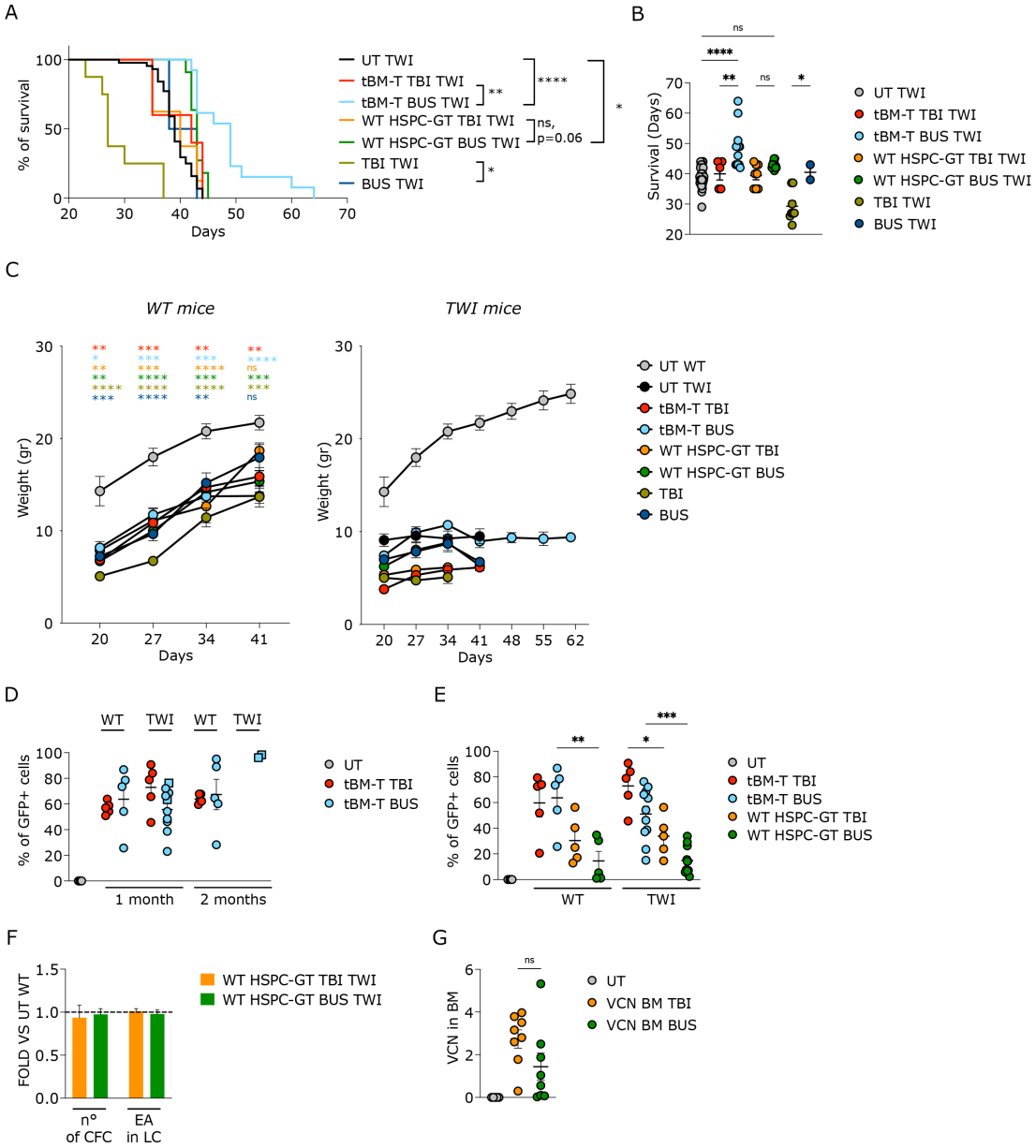

Figure 24. Survival, body weight and peripheral donor-derived cells engraftment of treated TWI mice. *A-B. In the panel A the Kaplan-Meier survival curves plotting the percentage of survival and in the panel B the column graph scatter plotting the survival days of treated and UT TWI mice. UT TWI, n=40; tBM-T TBI TWI, n=5; tBM-T BUS TWI, n=13; WT HSPC-GT TBI TWI, n=8; WT HSPC-GT BUS TWI, n=11; TBI TWI, n=8; BUS TWI, n=2. Data in A are analysed by Log Rank (Mantel Cox) test: *p<0.05; ** p<0,01; **** p<0,0001. Data in B are analysed by One-way ANOVA followed by Tukey's multiple comparisons test: *p<0.05; **p<0.01; **** p<0,0001. C. Body weight of conditioned untransplanted WT and TWI mice (TBI and BUS WT n=8; TBI TWI, n=8; BUS TWI, n=2), transplanted WT (n=5 mice per group), transplanted TWI (all treated mice, see above), and UT littermates (UT WT n=10, UT TWI n=14) was monitored starting at 20 days of age. WT treated mice and UT controls are compared using the One-way ANOVA followed by Tukey's multiple comparisons test: *p<0.05, **p<0.01; *** p<0,001; **** p<0,0001 vs. UT WT. Asterisks indicate statistical significance according to the colour code reported in the figure legend. D. Engraftment of donor-derived GFP+CD45+ cells measured in the PB of treated WT and TWI mice evaluated at one and two months after tBM-T. UT WT mice were used as negative control. E. Engraftment of donor-derived GFP+CD45+ cells measured in the PB of treated WT and TWI mice evaluated one*

*month after donor cells transplant. UT WT mice were used as negative control. Data are analysed by One-way ANOVA followed by Tukey's multiple comparisons test: *p<0.05, **p<0.01, ***p<0.001. F. Data in the graph show: i) comparable number of colonies generated by transduced and UT WT Lin- isolated for HSPCs transplantation (HSPC-GT, n=3 different experiments) after TBI or BUS conditioning; ii) comparable enzymatic activity (EA) detected in UT and transduced LCs derived from WT Lin- isolated for HSPCs transplantation (HSPC-GT, n=3 different experiments) after TBI or BUS conditioning. Data in the graph are expressed as fold vs. UT WT. G. VCN measured in the BM of TWI mice transplanted with WT HSPCs transduced with LV.GFP after TBI or BUS conditioning (n=3 independent experiments). Data are analysed by Unpaired Student t test.*

Overall, these data suggested a better outcome of the transplant in BUS-conditioned animals with respect to the TBI-conditioned groups. The tBM-T performed after BUS conditioning increases the lifespan of treated mice, while the engraftment of WT HSPCs without the support of progenitors is likely too slow a process to give a survival advantage.

3.3 Engraftment of donor-derived HCs in the CNS of treated TWI mice.

The therapeutic efficacy of HSPC-T in treating LSDs with CNS involvement relies on the capacity of donor-derived myeloid cells to stably engraft and differentiate in resident macrophages/microglial cells in the CNS, where they can supply the functional enzyme (Capotondo et al., 2012; Krivit et al., 1998; Soulet & Rivest, 2008). Confocal IF analysis on brain tissues from tBM-T-treated mice (conditioned using BUS and TBI) analyses from 42 days of age (average lifespan of tBM-T TBI TWI mice) showed robust engraftment of donor-derived GFP+ cells starting at one month after transplantation (Figure 25 A-B). High numbers of GFP+ cells were present in the spinal cord (SC) of treated mice. In the brain, the presence of engrafted GFP+ cells decreased moving from the caudal to the rostral areas, confirming a peculiar kinetics of HCs reconstitution (Ricca et al., 2015) that likely reflects the caudal-to-rostral onset and progression of CNS pathology in GLD (Meisingset et al., 2013; Suzuki, 2003). A qualitative assessment of IF images suggested a more widespread and time-dependent distribution of donor-derived cells in BUS-conditioned mice as compared to TBI-conditioned counterparts (Figure 25C). Also, qualitative IF analysis suggested a lower presence of donor-derived HCs in the brain of WT HSPC-GT mice as compared to tBM-T mice. Also in this case, the use of BUS seemed to result in more widespread distribution of engrafted cells (Figure 25D-E).

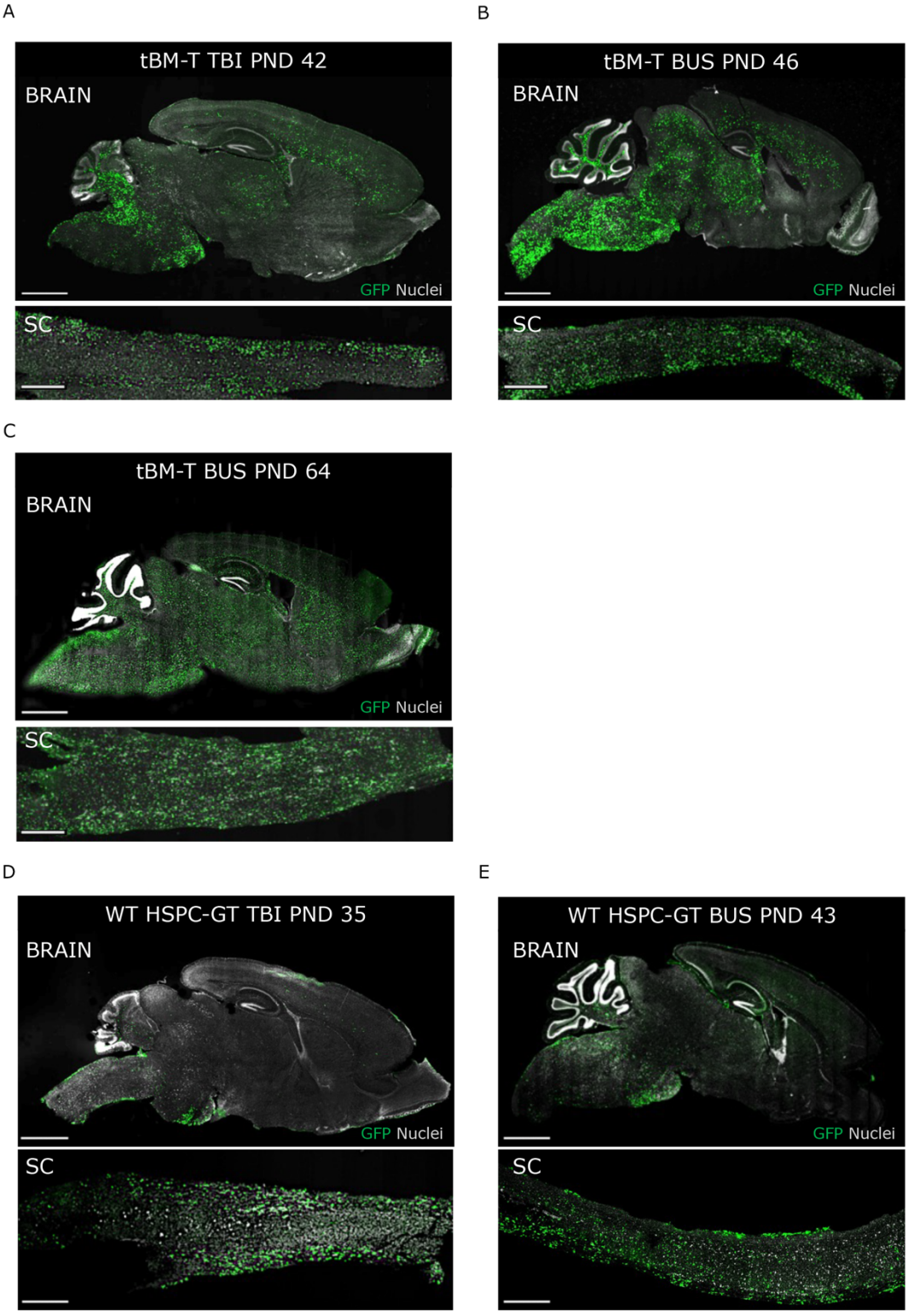

Figure 25. Engraftment of donor HCs in the CNS of transplanted TWI mice. *A-C. Representative reconstructions of sagittal brain and spinal cord (SC) sections of tBM-T TBI TWI mouse analysed at PND 42 (A), tBM-T BUS TWI mouse analysed at PND 46 (B), and tBM-T BUS TWI mouse analysed at PND 64 (C) showing the presence and distribution of engrafted GFP+ cells (green; direct fluorescence). Nuclei stained with Hoechst (gray, pseudocolor). 20X magnification. Scale bars, brain 1500 µm and SC 1000 µm. D-E. Representative reconstruction of brain and SC of WT HSPC-GT TBI TWI mouse at PND 35 (D), WT HSPC-GT BUS TWI mouse*

at PND 43 (E). In green the GFP+ donor derived cells (recognized by anti-GFP antibody); nuclei stained with Hoechst (gray, pseudocolor). 20X magnification. Scale bars, brain 1500 µm and SC 700 µm. IF analysis and brain reconstruction were performed on section derived from all treated mice (2-3 sagittal section/group/experiment).

By confocal IF analysis, we also looked to the morphology of engrafted HCs in the brain of treated mice. The majority of engrafted GFP+ cells displayed an amoeboid shape, which was more pronounced moving from the rostral to the caudal region, without qualitative differences between all the groups (Figure 26A-B). This phenotype is typically associated to the phagocytic/activated state of macrophages/microglial cells, as opposed to the ramified morphology consistent with the physiological resting state of these myeloid cell populations (Rawlinson et al., 2020).

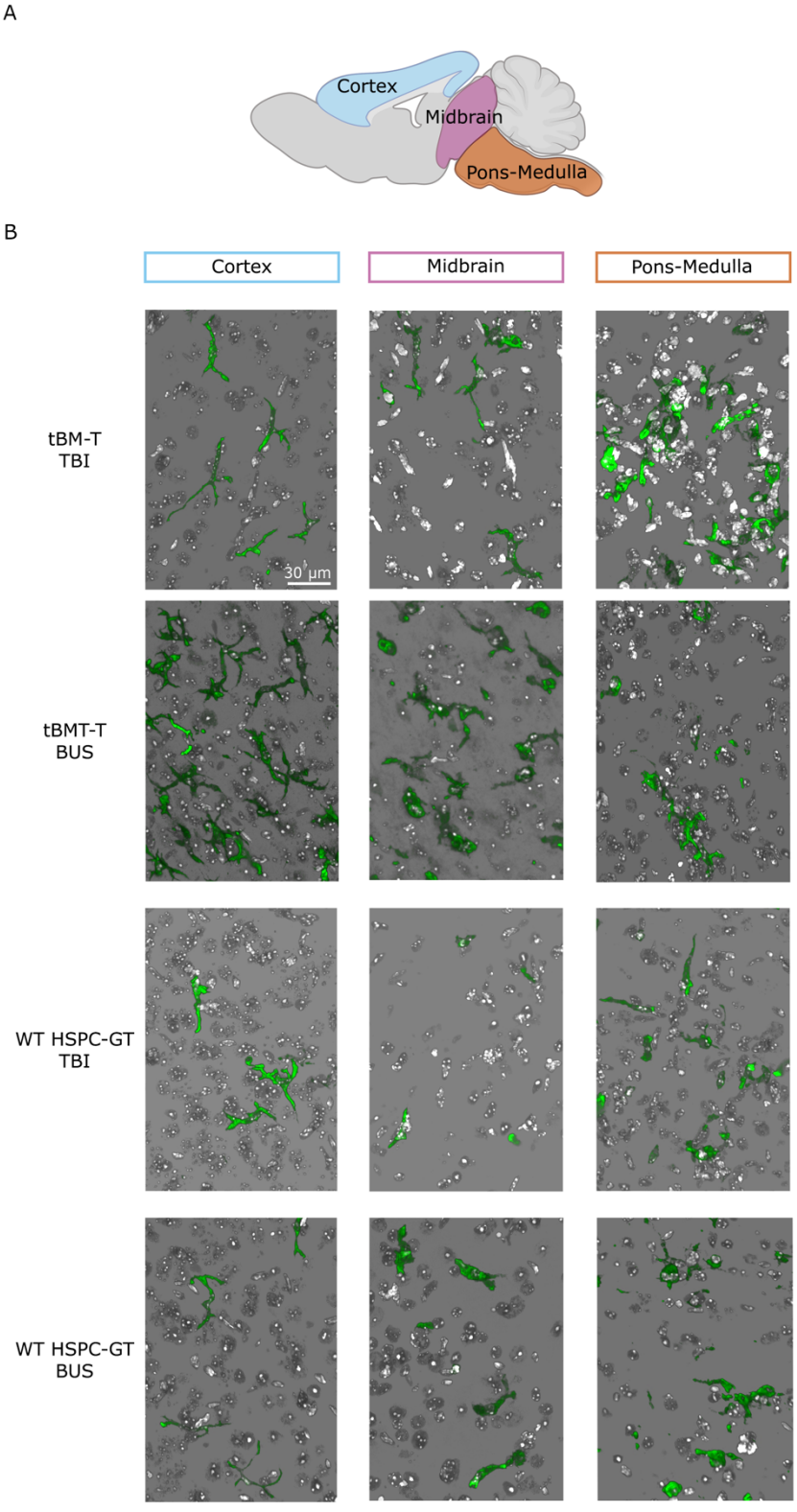

Figure 26. Amoeboid phenotype of GFP+ donor derived cells in the brain of treated TWI mice. *A. Schematic representation of a sagittal section of the mouse brain showing the cortex (light blue), the midbrain (purple) and the pons-medulla (orange) regions. Created with BioRender.com. B. 3D projection of z-stack images showing amoeboid GFP+ donor derived HCs (green) engrafted in the cortex, midbrain, and pons-medulla of all treated TWI groups*

(tBM-T TBI and BUS, WT HSPC-GT TBI and BUS). Nuclei stained with Hoechst (gray, pseudocolor). 40x Magnification. Scale bar 30 µm.

The vast majority of these cells expressed CD68, a marker of activated macrophages/microglia, and the microglial and macrophage-specific ionized calcium-binding adapter molecule 1 (Iba1). Amoeboid (activated) cells co-expressing CD68 and Iba1 are also present in brain tissues of UT TWI mice at the late stages of the diseases. In contrast, highly ramified (resting) Iba1+ microglial cells that are present in physiological conditions do not express CD68 (Figure 27).

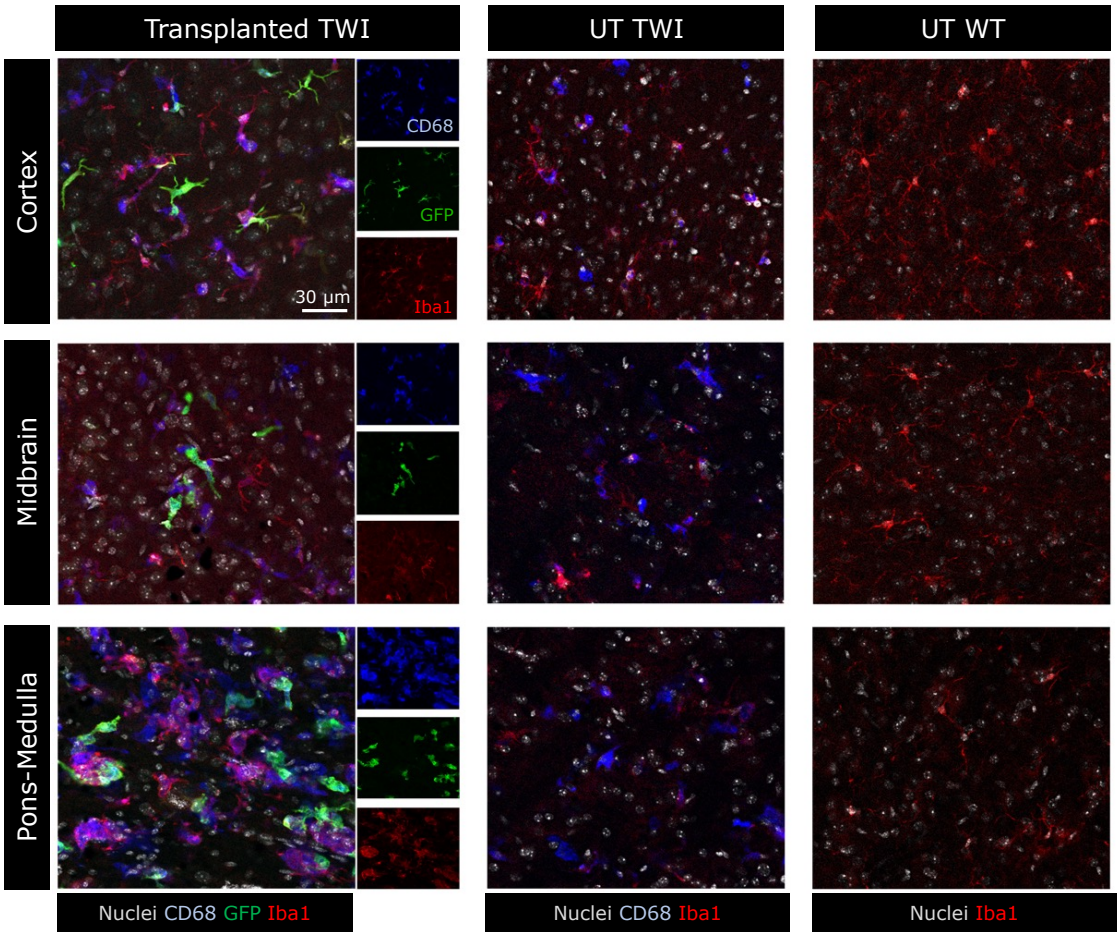

Figure 27. Activated state of donor-derived macrophages/microglial cells. *Representative confocal IF images of WT HSPC-GT BUS TWI mouse showing ameboid donor derived GFP+ HC myeloid progeny (green) engrafted in the cortex, midbrain, and pons-medulla coexpressing CD68 (blue) and Iba1 (red); nuclei stained with Hoechst (gray, pseudocolor). n=2–3 mice/ group, 2-3 sagittal section/group/experiment. 40× magnification. Scale bars: 30 µm*

Overall, these analyses showed a widespread engraftment of transplanted donor HCs in the brain and SC of treated mice, that seems more robust in the tBM-T BUS group as compared to the WT HSPC-GT group. Donor HC-derived myeloid progeny showed the ameboid phenotype indicative of an activated state, regardless of the

treatment and conditioning regime used, suggesting the presence of ongoing neuroinflammation in the treated TWI mice.

3.5 Astrogliosis and microgliosis in treated TWI mice.

Astrogliosis and microgliosis are hallmarks of GLD pathogenesis and contribute to the overall neuroinflammatory state that characterize TWI mice as well patients (Avola et al., 2016; Potter & Petryniak, 2016; Ricca et al., 2015; Santambrogio et al., 2012; Snook et al., 2014). While HSPC-T performed in the clinical practise as well as experimental *ex vivo* HSPC-GT approaches aim to ameliorate this detrimental aspect of GLD pathogenesis, it was demonstrated in transplanted adult mice (WT and transgenic mouse models) that TBI, contrary to BUS conditioning, induces disruption of the BBB and elicits a potent systemic inflammatory response (Wilkinson et al., 2013; Youshani et al., 2019; Yu et al., 2019).

Since no data are available on mice treated in the neonatal age, we wanted to understand the impact of TBI and BUS myeloablative regimens on the astrogliosis and microgliosis in the brain of treated TWI mice in our experimental conditions.

To this end, we performed WB analysis to quantify the expression of GFAP (marker of astrocytes) and Iba1 (marker of microglial cells) proteins. We analysed two different brain regions of treated mice and UT controls: i) the rostral region (RO) comprising the telencephalon (TEL), diencephalon (Di), and midbrain; ii) the caudal region (CA) comprising the cerebellum, pons, and medulla. TBI-treated mice showed increased GFAP and Iba1 expression with respect to the BUS-treated counterpart following tBM- as well as WT HSPCs- transplantation. Also, the expression of these astrocytic and microglial cell markers in the irradiated mice was slightly increased in comparison to those of age-matched UT TWI mice, suggesting a potential aggravation of the pathology-associated brain astrogliosis and microgliosis consequent to irradiation that was not observed in BUS treated mice (Figure 28).

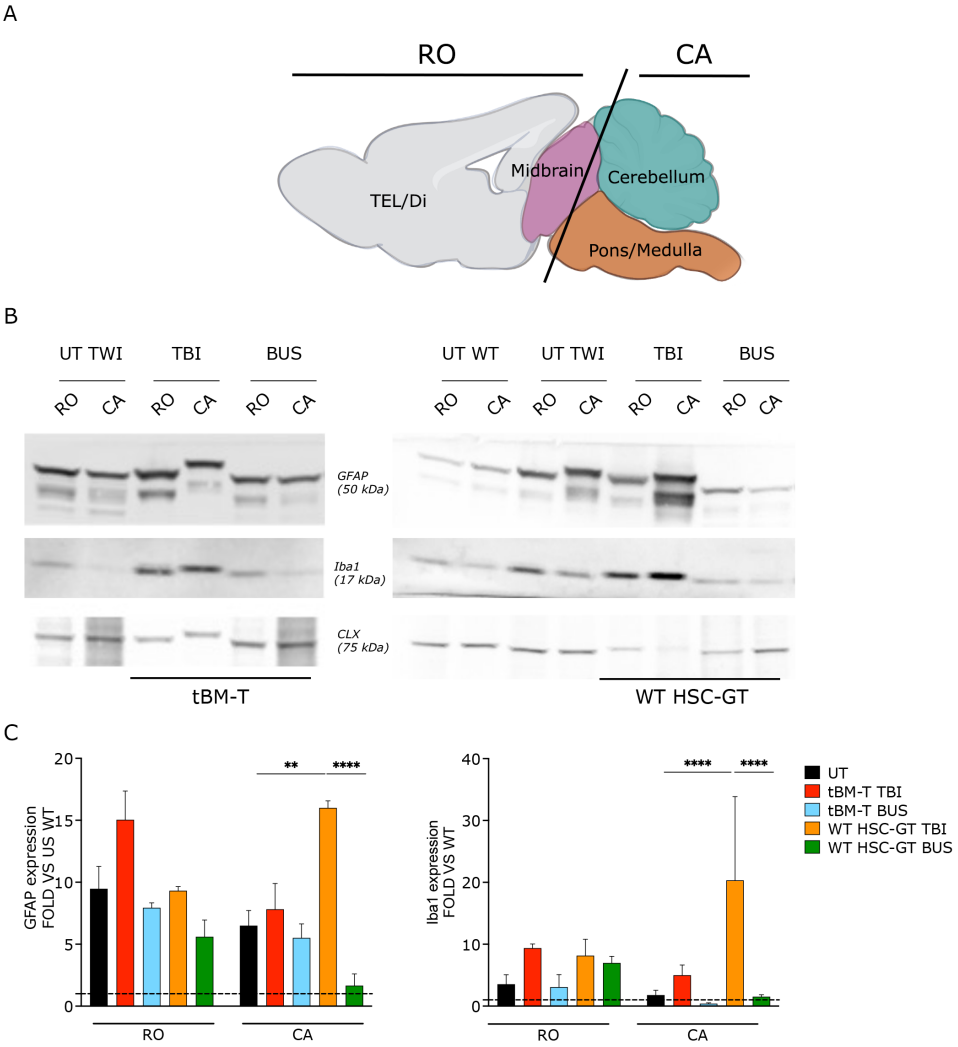

Figure 28. GFAP and Iba1 protein expression in the CNS of treated mice and UT controls. *A. Schematic representation of a sagittal section of the mouse brain showing: the rostral region (RO) comprising the telencephalon (TEL) and diencephalon (Di) (in grey), and the midbrain (in purple); the caudal region (CA) comprising the pons-medulla (in orange) and the cerebellum (in green). Created with BioRender.com. B. Representative WB analysis (performed on n=2-3 blots in n=3 different experiments, 3-5 mice/treatment) showing GFAP and Iba1 protein expression in the RO and CA brain regions of treated mice and UT controls (WT and TWI). CLX was used as normalizer. Data in the graph are expressed as protein expression (GFAP or Iba1/CLX), FOLD vs. UT WT (dotted line), as the mean ± SEM. Two-way ANOVA followed by Tukey's multiple comparison test, **p<0.01, ****p<0.0001.*

3.6 Treatments rescue GALC enzymatic activity in the CNS and periphery of treated TWI mice.

In order to assess the impact of treatments in providing a supply of functional enzyme in all the affected tissues of TWI mice, we evaluated the specific GALC activity in the CNS (caudal and rostral regions), PNS (sciatic nerve, SN), and peripheral organs (liver, spleen, and BM) of treated mice as compared to UT controls.

Overall, BUS-conditioned mice showed a significantly higher rescue of GALC activity with respect to the TBI groups in the CNS and periphery (Figure 29).

Indeed, the peripheral organs of tBM-T- and WT HSPC-GT- treated mice conditioned with BUS showed a substantial reconstitution of GALC activity, which reached ~85-100% of WT levels in the spleen, ~75-85% of WT levels in the liver, and supraphysiological levels in the BM (~110-186% of WT levels). Importantly, we detected substantial GALC activity in the PNS (~35% of WT levels in the SN) and the CNS (~40-50% of WT levels in the SC, ~30-40% of WT levels in the RO and CA brain regions) (Figure 29), indicating the efficacy of the treatments in providing enzymatic supply to the affected tissues.

Overall, the reconstitution of tissue GALC activity (brain, PNS and peripheral organs) in TBI-conditioned mice was ~30% of that achieved in the BUS-treated counterparts, with the exception of the BM of mice treated with tBM-T, which showed comparable and supraphysiological enzymatic reconstitution.

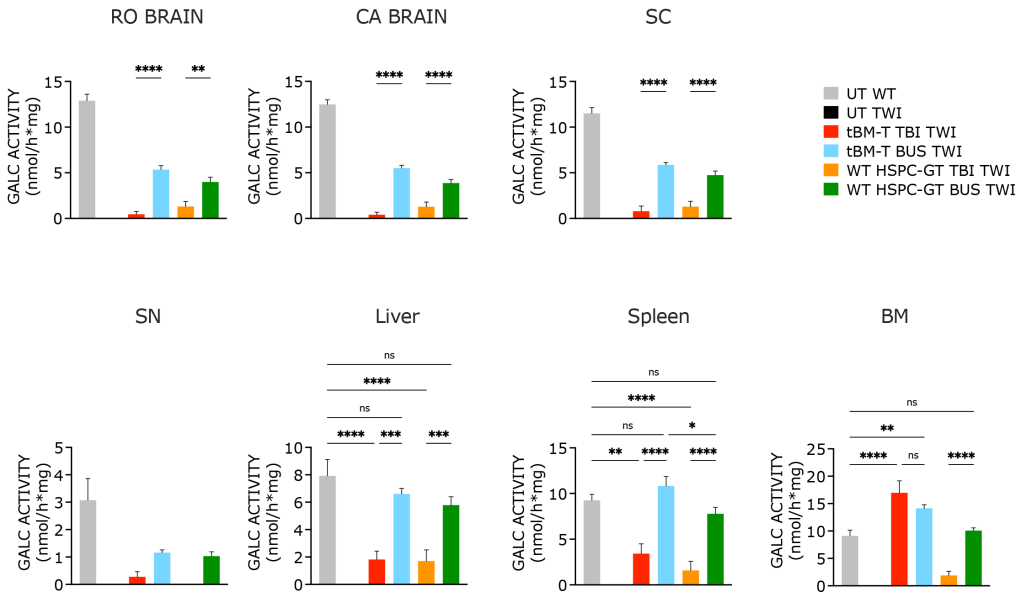

Figure 29. Analyses of GALC enzymatic activity in the tissues of treated mice*. Enzymatic GALC activity measured in CNS tissues (RO and CA regions), PNS tissue (SN), and peripheral organs (liver, spleen, BM) of treated mice (tBM-T TBI and BUS TWI, WT HSPC-GT TBI and BUS TWI) and UT controls (WT and TWI) at the time of sacrifice. Data are expressed as the mean ± SEM; n≥5 mice/group. Two-way ANOVA followed by Tukey's multiple comparison test, *p<0.05, **p<0.01, ***p<0.001, ****p<0.0001.*

Overall, these analyses demonstrate that the use of Busulfan in 2–3-day-old animals is overall more efficient than TBI in terms of GALC activity restoration, leading to a better outcome and increased survival of BUS-conditioned mice.

Thus, we choose BUS as the myeloablative conditioning regimen to be used in the HSPC-GT setting.

3.7 HSPC-GT in neonatal TWI mice.

A fast and robust donor cell engraftment is crucial for the success of *ex vivo* HSPC-GT therapy in GLD mice. The BUS conditioning regimen tested here in PND 1-2 TWI mice resulted in lower chimerism of Lin- cells as compared to tBM in recipient GLD mice, resulting in shorter survival.

Our hypothesis was that the improvement provided by the chimeric GALC enzymes over the unmodified GALC enzyme in terms of GALC production (overexpression) and secretion, coupled to the potential increase of BBB penetration could result in an evident therapeutic advantage in TWI mice even under these stringent conditions.

To test this hypothesis and to collect preliminary indications about the efficacy of the full chimeric enzyme in increasing the survival of treated mice, we transplanted a small cohort of BUS-conditioned TWI mice with TWI HSPCs transduced with the LV.GALC-CH (VCN=8.42; n=4 mice) and LV.IDUA.GALC-CH.APO (VCN=11.85; n=5 mice), the more efficient chimeric GALC construct as shown by *in vitro* results. The GALC overexpression in LV-transduced HSPCs reached ~2.8x and ~13.4x the physiological level assessed in WT HSPCs (Figure 30A). The transduction was safe, as demonstrated by comparable number of colonies generated by transduced cells and UT TWI counterparts (CFC; Figure 30A).

TWI HSPC-GT treated mice showed variable but overall modest donor cell engraftment in the PB one month after transplant (0.9-32% in the GALC-CH group and 9.2-20.5% in the IDUA.GALC-CH.APO group). These data are in line with what observed in TWI mice transplanted with WT HSPCs (Figure 30B).

All the treated mice showed moderate and comparable improvement of lifespan as compared to the UT TWI (median survival 42 days vs. 39 days; Figure 30C-D). The variable and suboptimal donor cell engraftment under these stringent experimental conditions likely hampered the possibility to observe a survival advantage associated to the use of the chimeric over the unmodified GALC enzymes in this small cohort of treated mice, even in the presence of GALC overexpression in the donor cell populations.

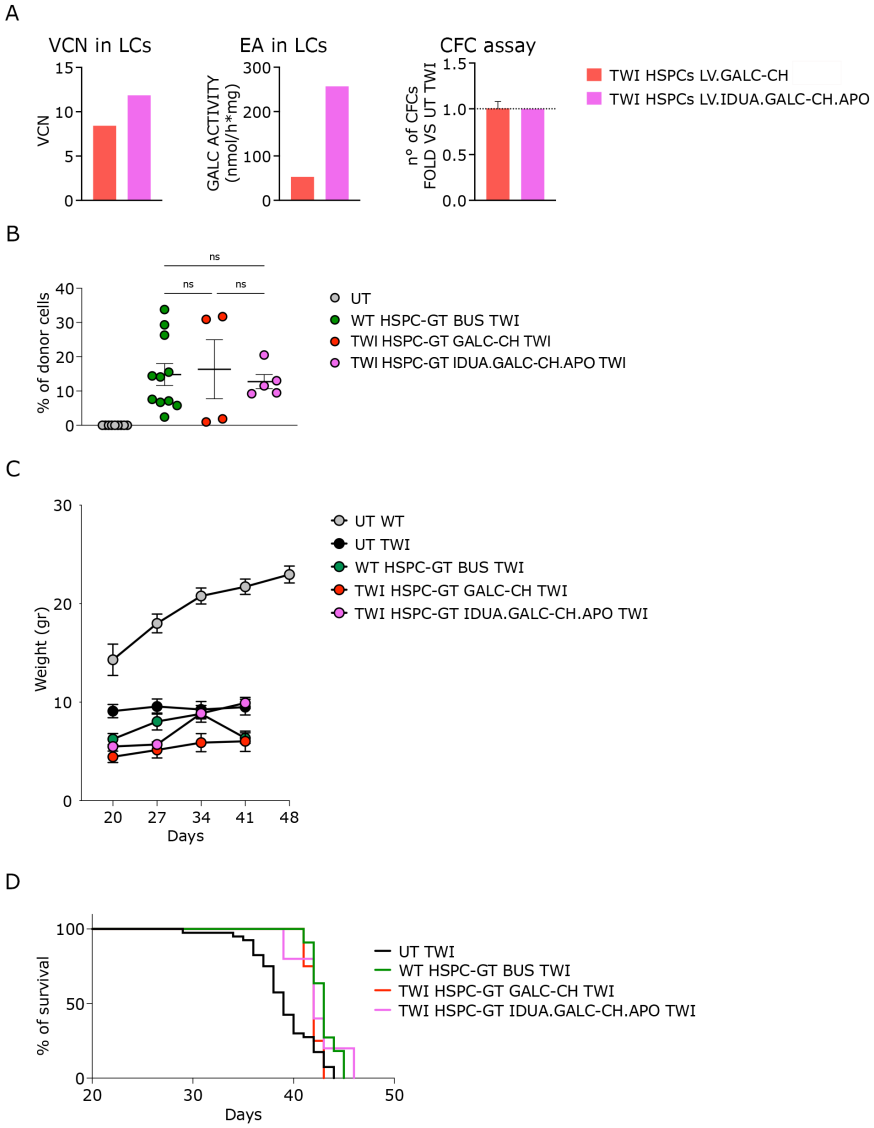

Figure 30. HSPC-GT approach in neonatal TWI mice transplanting TWI HSPCs expressing chimeric and unmodified GALC enzymes. *A. Data in the graph show: the VCN and the enzymatic activity (EA) detected in LCs derived from UT, LV.GALC-CH- and LV.IDUA.GALC-CH.APO- transduced TWI HSPCs and UT TWI counterparts (TWI HSPC-GT groups, n=1 experiment per group); comparable number of colonies generated by transduced and UT TWI HSPCs isolated for transplantation (n=1 experiment per group). B. Engraftment of donor-derived CD45+ cells (GFP+ WT HSPCs; mCherry+ TWI HSPCs) measured in the PB of treated TWI mice evaluated one month after donor cells transplant. UT WT mice were used as negative control. The percentage of WT HSPCs engraftment is referred to the WT HSPC-GT BUS TWI group described above (Figure 24E). Data are analysed by One-way ANOVA followed by Tukey's multiple comparisons test. C. Body weight of treated TWI mice and UT WT and TWI littermates (UT WT n=10, UT TWI n=14), registered starting at 20 days of age. The body weight of the WT HSPC-GT BUS TWI group and UT controls is the same showed above (Figure 24C). D. Kaplan-Meier survival curves plotting the percentage of survival of treated and UT TWI mice. UT TWI, n=40; WT HSPC-GT BUS TWI, n=11; TWI HSPC-GT GALC-CH TWI, n=4; TWI HSPC-GT IDUA.GALC-CH.APO TWI, n=5. The survival of the WT HSPC-GT BUS TWI group and UT TWI is the same showed above (Figure 24A).*

Discussion

Allogeneic HSPC-T is the only therapy available for GLD patients. However, it fails to fully correct the severe CNS pathology of infantile GLD patients, even if performed at the asymptomatic stage (Allewelt et al., 2018). This suboptimal CNS rescue is probably consequent to the insufficient GALC supply in this tissue provided by the transplanted HSPC-derived progeny. GT may ensure a stable, robust, and potentially life-long supply of GALC to all the tissues, including the CNS. The direct injection of different AAV serotypes encoding for the GALC gene is effective in prolonging the survival of GLD animals (mice, dogs, and NHPs) (Bradbury et al., 2018; Hordeaux et al., 2022; Rafi et al., 2020) and are under evaluation in two Phase 1/2 clinical trials (clinical trials ID: NCT04771416, NCT04693598). Still, several concerns on AAV safety remain, primarily the occurrence of hepatocellular carcinoma (Li et al., 2021; Sabatino et al., 2022) and the degeneration of DRG neurons (Bradbury et al., 2020; Hinderer et al., 2018; Hordeaux et al., 2020, 2022; Perez et al., 2020). In addition, the potential genotoxicity associated to AAV gene integrations must be considered (Bijlani et al., 2022; Kaeppel et al., 2013; Li et al., 2021; Russell, 2007; Sabatino et al., 2022).

The LV-mediated GT platform exploited in this study is characterized by high efficiency of gene transfer and low risk of genotoxicity (Biffi et al., 2013; Calabria et al., 2014). It is successfully applied to deliver therapeutic transgenes in pre-clinical studies and in autologous *ex vivo* HSPC-GT Phase I/II clinical trials for genetic blood diseases (Aiuti et al., 2013; Ferrua et al., 2019; Marktel et al., 2019) and MLD (clinical trial ID: NCT01560182), a LSD that shares with GLD the early onset and the severe neurological involvement. Specifically, the use of gene transfer to overexpress the ARSA enzyme in transplanted HSPC-derived myeloid progeny is key to provide a therapeutic advantage in MLD patients (Biffi et al., 2013; Fumagalli et al., 2022; Sessa et al., 2016), in line with the results of pre-clinical studies in MLD mice (Biffi et al., 2006). Of note, in 2020 The European Commission officially announced the full approval of this approach as the world's first LV-based GT (Libmeldy) to treat late infantile or early juvenile forms without clinical manifestations of the disease, or early juvenile form with early clinical manifestations of the disease. The same HSPC-GT platform was applied to treat MPS-I, another neurodegenerative LSD (clinical trial ID: NCT03488394) starting from the promising data obtained in MPS-I mice (Gentner et al., 2021; Visigalli et al., 2010).

Still, enzyme overexpression is differently achieved and tolerated, according to the enzyme itself and the target cell type. While ARSA and IDUA (the defective enzymes in MLD and MPS-I, respectively) are safely overexpressed to >100× the normal levels (Capotondo et al., 2007; Sessa et al., 2016; Visigalli et al., 2016), only modest GALC overexpression (2–3× the normal levels) is reached *in vitro* in HSPCs and progeny (Gentner et al., 2010; Ungari et al., 2015) and neural cells (10–15× the normal levels) (Lattanzi et al., 2010; Neri et al., 2011; Ricca et al., 2015).

A similar difficulty in overexpressing GALC is observed in the brain of treated mice also upon *in vivo* GT (Lattanzi et al., 2014; Meneghini et al., 2016; Ricca et al., 2015), suggesting that supraphysiological levels of GALC activity are hardly to achieve in CNS tissues unless elevated vector doses are used, as shown in *in vivo* AAV-GT approaches (Bradbury et al., 2018; Hordeaux et al., 2022; Rafi et al., 2020). In addition, none of the therapeutic approaches tested in GLD mice so far resulted in full treatment and arrest of the disease progression. Overall, all the pre-clinical evidence suggests that even a good GALC activity reconstitution in the CNS is insufficient to prevent/counteract the complex multi-organ pathology and that an early intervention to provide a consistent and global GALC supply is mandatory to prevent storage accumulation and widespread tissue damage.

The limitation to GALC overexpression also suggests the presence of a species-, tissue- and cell type-specific regulation of the enzyme expression whose mechanisms are poorly elucidated (Chen et al., 1993; Mangiameli et al., 2021; Visigalli et al., 2010). The poor secretion of the enzyme by transduced cells, possible coupled to insufficient/defective uptake by GALC-deficient cells (cross-correction), as suggested by previous studies (Ricca et al., 2015; Weinstock et al., 2020b), could explain the limited benefit of HSPC-T and HSPC-GT in GLD mice (Galbiati et al., 2009; Gentner et al., 2010; Reddy et al., 2011; Ricca et al., 2015; Ungari et al., 2015).

Therefore, in GLD is crucial to maximize GALC expression by transduced cells and/or to enhance tissue bioavailability to boost the efficacy of GT approaches.

Sorrentino and colleagues demonstrated in a murine model of MPS-IIIA (a neurodegenerative LSD) the therapeutic efficacy of a chimeric SGSH enzyme engineered to increase its bioavailability by replacing the SGSHsp with that derived from the highly secreted IDS enzyme (Sorrentino et al., 2013, 2019) and by adding the BBB-binding domain from the ApoB (Sorrentino et al., 2013). We exploited the same strategy to generate LVs carrying chimeric GALC enzymes. Specifically, we substituted the GALCsp with the IDSsp or IDUAsp and used a flexible linker to add the receptor-binding domain of ApoE II. The choice of ApoE II was made based on the reported higher efficacy as compared to ApoB or ApoE I in favouring the BBB

crossing, as demonstrated in MPS-I mice for the chimeric IDUA enzyme (Wang et al., 2013). Moreover, the addition of the ApoE II binding-domain to the IDS enzyme enhanced the correction of CNS pathology in MPS-II mice upon LV-mediated HSPC-GT (Gleitz et al., 2018). Here we showed the expression of LDLR and related proteins in brain tissues and NSPCs-derived neurons/glial cells derived from TWI mice, the common GLD mice model with a severe phenotype that recapitulates the early infantile form of the disease. These data further support the use of ApoE II not only to enhance the transport of the chimeric GALC enzyme across the BBB but also to favour its uptake by GALC-deficient neuronal/glial cells in the CNS. Previous studies described the generation of chimeric GALC enzymes engineered by: i) adding the Tat domain or changing GALCsp with that of IDS (Pan et al., 2019) or with a synthetic sp (Hu et al., 2016) to increase GALC secretion; ii) adding the ApoB binding domain to enhance GALC penetration through the BBB (Pan et al., 2019). The efficacy of these constructs was evaluated in immortal human cell lines (i.e., 293T, HeLa cells) or fibroblasts (from healthy donors and GLD patients), with unclear results in *in vivo* tests on the advantage of chimeric constructs over the unmodified GALC (Hu et al., 2016; Pan et al., 2019; Zhang et al., 2008). The safety and efficacy of chimeric GALC enzymes in NSPCs, HSPCs, and their lineage-committed progeny, which are the therapeutically relevant cell types in the context of GT approaches, have not been extensively studied.

Here, we used optimized transduction protocols to transduce NSPCs and HSPCs derived from TWI mice in order to study the impact of the transduction procedures and the transgene overexpression on the functionality of the transduced cells and their progeny. In LV-transduced HSPCs we obtained VCN values that are 2-10x higher than those reported in a previous study testing chimeric GALC enzymes (Hu et al., 2016), demonstrating robust and consistent transduction efficiency in our experimental conditions. The use of the alternative IDSsp/IDUAsp sequences and the addition of the ApoE II peptide did not hamper the expression, lysosomal localisation, or extracellular secretion of the chimeric GALC enzymes in both HSPCs and NSPCs. The chimeric GALC enzymes showed comparable or higher enzyme activity than their unmodified counterparts. The improved LV design and production could explain the tolerability and absence of toxicity demonstrated here in the overexpression of unmodified and chimeric GALC enzymes by LV-transduced murine HSPCs, which are known to be more sensitive to GALC overexpression than their differentiated myeloid progeny (Gentner et al., 2010). However, different strategies exploiting miRNAs (Chiriaco et al., 2014; Gentner et al., 2010) or myeloid-specific promoters (Ellison et al., 2019; Sergijenko et al., 2013) can still be applied to restrict the transgene

expression to specific cell types, improving the safety and efficacy of HSPC-GT approaches for LSDs. Furthermore, Ungari and colleagues demonstrated that GALC overexpression is more tolerated by human HSPCs than their murine counterpart (Ungari et al., 2015), further supporting the possibility of a clinical development of HSPC-GT with improved LVs to overexpress chimeric GALC enzymes.

The success of GT approaches in all LSDs, including GLD, depends on the extent to which the bioavailability of the enzyme (production and secretion from donor cells) and the uptake by deficient cells can induce an efficient metabolic cross-correction. This is particularly hard to obtain in those tissues that are less accessible to correction due to their specific anatomy and physiology, i.e., CNS, PNS, bone, and heart. Based on these considerations and in light of the encouraging results obtained in different LSD models (Gleitz et al., 2018; Sorrentino et al., 2013, 2019) we engineered the GALC enzyme with the aim of increasing its bioavailability.

Normalizing the GALC activity on the VCN, we showed that the IDSsp modification confers increased secretion to the chimeric GALC enzyme as compared to the unmodified counterpart (~3-5x the physiological level) in transduced TWI NSPCs and differentiated progeny. The addition of ApoE II partially decreases the intracellular GALC activity but does not affect GALC secretion, leading to a net enhanced percentage of secretion of the full chimeric enzyme (IDS.GALC-CH.APO) with respect to unmodified (GALC-CH) and partially modified (IDS.GALC-CH) counterparts. This advantage is less evident in TWI HSPCs (~1.5x the physiological level), while the intracellular GALC activity is slightly increased in LV.IDS.GALC-CH and LV.IDS.GALC-CH.APO transduced TWI cells with respect to those expressing the unmodified enzyme (~1.5-2x), further suggesting the cell type-specificity of enzyme production and secretion already observed in previous studies (Cheng et al., 2021; Güler-Gane et al., 2016).

The use of the mCherry tag allowed us to provide direct evidence for GALC precursor protein production, secretion, and lysosomal localization. In both LV-transduced NSPC- and HSPC-derived progeny all the chimeric GALC enzymes correctly localized in the lysosomal compartment, where they are functional in clearing the GalCer intracellular storage that accumulates in UT TWI neurons/glial cells. The precursor is also the lysosomal enzyme form that can escape the sorting to lysosomes and can be secreted in the extracellular space, where it can be reuptaken by the producing cell or by the surrounding cells in the cross-correction mechanism (Lattanzi et al., 2010; Spratley & Deane, 2016). Thus, achieving an increase in GALC precursor protein secretion represents a very important aspect for the success of GT approaches. By WB analysis, we demonstrated the increased

production and secretion of precursor IDS.GALC-CH.APO as compared to GALC-CH and IDS.GALC-CH enzymes in transduced TWI NSPCs. These data, coupled to the reduced intracellular activity of IDS.GALC-CH.APO detected in TWI NSPCs, suggested an enhanced secretory pathway as a potential consequence of a reduced sorting to the lysosomes. Further analysis of the chimeric GALC enzymes trafficking is needed to confirm this hypothesis.

Taken together, our results show that both LV-transduced NSPCs and HSPCs secrete consistent amounts of the GALC precursor proteins. Based on this promising data, we screened different sp sequences derived from other lysosomal enzymes to identify an alternative sp able to further enhance GALC secretion by both NSPCs and HSCPs. IDUAsp showed increased basicity of the N-terminal polar region and increased hydrophobicity in the H-core region with respect to IDSsp, parameters that are known to enhance protein secretion (Knappskog et al., 2007; Kober et al., 2013; Stern et al., 2008; Zhang et al., 2005). The use of IDUAsp further improved GALC secretion in both LV-transduced TWI NSPCs and HSPCs while preserving a correct lysosomal localization and functionality in clearing the GalCer storage in TWI NSPCs-progeny. Similar to what was observed for the IDS.GALC-CH.APO enzyme, LV-transduced TWI NSPCs showed lower intracellular (~0.6x) and increased extracellular IDUA.GALC-CH.APO activity (~8x) with respect to the unmodified GALC-CH enzyme. More relevant, the IDUA.GALC-CH.APO enzyme showed a 2x higher activity and precursor protein amount with respect to the chimeric IDS.GALC-CH.APO enzyme. The superiority of the new construct was also evident in LV-transduced TWI HSPCs, which showed a 1.5-3x increased intracellular and extracellular GALC activity as compared to the unmodified and IDS.GALC-CH.APO enzymes.

Altogether our data suggested that the IDUA.GALC-CH.APO precursor protein is more efficiently secreted and available in the extracellular milieu than the GALC-CH and IDS.GALC.CH.APO counterparts, suggesting a superior efficiency of IDUAsp with respect to IDSsp in favouring the GALC secretory pathway. Overall, the higher bioavailability of the full chimeric GALC enzymes may reduce the need for a high rate of GALC overexpression, thus decreasing the vector dose necessary to correct HSPCs and thus improving the safety of this approach.

The therapeutic efficacy of the chimeric GALC enzymes produced and secreted by LV-transduced TWI NSPCs and HSPCs was ultimately demonstrated *in vitro* by their capability to cross-correct untransduced TWI NSPC-derived neural progeny, the specific target in GLD pathology. TWI neuronal/glial cells (acceptor cells) displayed a reconstitution of GALC activity ranging from 19% to 100% of the physiological levels (full correction). The extent of cross-correction was comparable in acceptor cells

treated with the sup of neural donor cells transduced with LV.GALC-CH and LV.IDS.GALC-CH.APO (~70% of the normal levels) and cells transduced with LV.IDUA.GALC-CH.APO (~93% of the normal levels). Acceptor cells treated with the sup of LV-transduced HSPC progeny displayed an extent of GALC rescue ranging between ~40% (sup from cells transduced with LV.GALC-CH and LV.IDS.GALC-CH.APO) and 120% of physiological GALC activity (sup from cells transduced with LV.IDUA.GALC-CH.APO). Interestingly, the IDUA.GALC-CH.APO is secreted by LV-transduced TWI HSPCs at a concentration similar to that of WT neurons/glial cells, which results in ~70% of GALC correction in recipient cells. Thus, cross-correction experiments confirmed the superiority of the IDUA.GALC-CH.APO construct in inducing an overall rescue of GALC activity in acceptor cells. All treated cells show a robust clearance of intracellular GalCer storage, further confirming that <20% of physiological GALC enzymatic activity is sufficient to reduce/clear intracellular storage in GALC-deficient neuronal/glial cells *in vitro*. It remains to be defined whether these GALC activity levels are guaranteed on a 'per cell' basis in CNS tissues by the *in vivo*/*ex vivo* GT approaches tested in preclinical studies or planned to reach clinical development.

We did not expect a substantial impact of the ApoE II modification on the outcome of cross-correction *in vitro*. The addition of the ApoE II sequence is expected to favour the uptake of chimeric GALC enzymes by BBB endothelial cells, which express LDLR and related proteins. The potential advantage of using the ApoE II sequence relies on the expected early boost of enzyme in the CNS from the LV-transduced HSPCs engrafted in the BM and periphery, before and/or concomitant to the donor-derived HCs engraftment in the CNS. This aspect needs to be ultimately studied *in vivo* in GLD animal models.

In the perspective of developing a safe and effective therapeutic option for GLD patients, we tested the efficacy of our chimeric GALC constructs in the context of a HSPC-GT approach in neonatal TWI mice. One of the explanations for the suboptimal efficacy of HSPC-T and HSPC-GT experienced so far in this rapidly progressing disease is that the slow pace of microglial/macrophage cells replacement is not sufficient to provide the early supply of GALC enzymatic activity needed for a therapeutic effect in the affected CNS (Capotondo et al., 2012). To counteract/prevent demyelination and neuronal damage in the CNS a therapy should provide a rapid and robust GALC supply, ensuring at the same time its widespread and pervasive delivery in this tissue. Due to the rapid disease progression that also characterizes the TWI mice, related to storage and severe inflammation that starts in the first week of post-natal life (Ricca et al., 2015; Santambrogio et al., 2012), we decided to anticipate the

timing of HSPCs transplantation at PND 2-3 as opposed to PND 6-7, an experimental condition that we tested in our previous work (Ricca et al., 2015). Also, we aimed to explore myeloablative regimens alternative to TBI that could favour the recruitment of HC-derived myeloid progeny in CNS tissues.

TBI and BUS are the two most widely used myeloablative conditioning regimens in murine models to induce the depletion of HCs in the BM niche of recipient mice and favour the donor cell engraftment after transplantation (Hawkins-Salsbury et al., 2015; Li et al., 2021; Pievani et al., 2015; Reddy et al., 2011; Ricca et al., 2015; Santi et al., 2020; Yeager et al., 1993). The kinetic and extent of CNS engraftment of donor HSPCs, either the purified fraction (Lin- cell population) or the total cell population derived from the tBM (that includes the committed progenitors), have been extensively studied in the experimental setting of adult transplantation, and detailed analyses on the morphology and clonality of engrafted donor cells have been provided (Capotondo et al., 2012; Plasschaert et al., 2022; Sailor et al., 2022; Shemer et al., 2018). Donor HSPCs, as purified Lin- (Gentner et al., 2010; Ungari et al., 2015) or derived from tBM (Ricca et al., 2015), engraft the brain of GLD recipient mice (Trs and FVB-TWI) transplanted within the first week of life (PND 7-8). However, no data are available on the brain engraftment of HSPCs transplanted in PND 2-3 TWI mice following either TBI or BUS conditioning. For this reason, we tested both the conditioning regimens to establish the optimal treatment scheme resulting in the highest donor cell chimerism (purified Lin- and tBM-derived cells) in the PB and the brain of recipient mice without adverse toxicity.

Our analyses show an overall better outcome of the transplant in BUS-conditioned vs. TBI-conditioned animals. In the tBM-T groups we achieved variable but stable engraftment of GFP+CD45+ donor cells in the PB of treated WT and TWI mice one month after transplant (from 20% to 91%) without significantly differences related to the conditioning regimen. Nevertheless, BUS-conditioned transplanted TWI mice showed a significantly increased survival with respect to the TBI-conditioned group. The similar engraftment observed in WT and TWI mice undergoing the same treatment suggested that GALC deficiency does not affect the engraftment of donor-derived HCs.

The engraftment of WT Lin- cells in the WT HSPC-GT groups was significantly decreased with respect to the engraftment of WT tBM. Also in this case, no differences between WT and TWI treated mice were detected. These data are in line with previous observations showing that the early engraftment is mediated by cell populations that are enriched for committed progenitors, while the engraftment of stem cells is a slower process (Jones et al., 1990; Zijlmans et al., 1998). BUS-conditioned mice

showed lower donor cell engraftment in the PB with respect to the TBI counterparts but a slight increase in lifespan, also with respect to the UT TWI mice. The levels of WT HSPCs engraftment in TWI transplanted mice after conditioning using TBI and BUS (VCN mean of 2.8 and 1.4 evaluated in the BM, respectively) were lower than those reached in previous works in which HSPCs were transplanted after lethal irradiation at PND 7-8 in GLD murine models, namely the Trs (VCN mean of ~5) (Gentner et al., 2010) and the FVB-TWI (VCN mean of ~7) (Ungari et al., 2015). We could not apply lethal irradiation to PND 2-3 newborn TWI mice as the maximum sublethal dose of 500 RAD tested here already resulted in motor impairment while higher doses of BUS resulted in the death of the transplanted animals.

By IF confocal analysis, we showed the engraftment of donor-derived cells in the brain of all treated TWI mice. We didn't perform a comprehensive quantification of the engrafted cells. Still, our qualitative assessment performed on region-matched tissue slices suggested a more consistent presence of engrafted cells in the BUS-conditioned groups as compared to the TBI counterparts, particularly in the tBM-T BUS group. Donor-derived myeloid progeny showed ameboid phenotype and activated state, regardless of the treatment and conditioning regime used. These data are also confirmed by WB analysis, which showed increased expression of GFAP (marker of astrogliosis) and Iba1 (marker of microgliosis), thus suggesting a persistent inflammation. The expression of GFAP and Iba1 were more pronounced in TBI-conditioned as compared to BUS-conditioned transplanted mice. These data are in line with the knowledge that TBI, contrary to BUS, may disrupt the BBB and elicit a potent inflammatory response in transplanted adult mice (Wilkinson et al., 2013; Youshani et al., 2019; Yu et al., 2019).

In all transplanted animals we detected a partial or total reconstitution of GALC activity, which was significantly higher in the BUS-conditioned vs. TBI-conditioned animals. BUS-conditioned TWI mice transplanted with tBM and WT HSPCs showed ~30-40% of the physiological GALC activity in brain tissues. These values are in line with those reported in previous studies in which different GLD murine models were transplanted with tBM (Gentner et al., 2010; Ricca et al., 2015; Ungari et al., 2015). Importantly, we detected ~35% of physiological GALC levels in the PNS of BUS-conditioned groups, while GALC activity was significantly lower in the tBM-T TBI TWI mice and undetectable in the WT HSPCS-GT TBI TWI group. Finally, BUS-conditioned mice showed full rescue of GALC activity in the peripheral organs (liver, spleen) that was not reached in the TBI-conditioned counterparts. The GALC activity levels reached in the tBM-T TBI TWI mice were lower than those observed in our previous work in which FVB-TWI mice were transplanted with tBM at PND 7 (Ricca et al.,

2015), while they are comparable to those obtained in the BUS-conditioned groups. These data suggest different kinetics of hematopoietic cell engraftment in relation to the different timing of conditioning and transplantation in newborn mice.

Based on these data, we choose BUS as myeloablative regimen to test the efficacy of the full chimeric IDUA.GALC-CH.APO construct over the unmodified counterpart in the context of autologous HSPC-GT approach in PND 2–3 TWI mice. A small cohort of transplanted mice was monitored for body weight and survival. Transduced TWI HSPCs safely overexpressed the unmodified and chimeric GALC enzymes, reaching up to 2.8x and 13.4x the physiological levels assessed in UT WT HSPCs in the LV.GALC-CH-transduced TWI cells and LV.IDUA.GALC-CH.APO-transduced TWI cells, respectively. These values of GALC activity are 1.8x and 8.4x higher than those reported in previous studies, where LV.GALC-transduced TWI HSPCs reached only 1.6x of the physiological levels with higher/comparable VCN (~15) (Ungari et al., 2015), further suggesting a potential advantage of the chimeric vs. the unmodified GALC enzymes. Preliminary data collected from these few mice (n=4-5 mice per group) showed low level of donor cell engraftment (13-16%), without significant differences between the two groups. Also, comparable engraftment levels were obtained by transplanting LV-transduced TWI or LV-transduced WT HSPCs in recipient TWI mice. In these stringent conditions, we did not observe an advantage of the chimeric GALC construct over the unmodified one in terms of survival of the treated mice.

Overall, the results of this study show relevant findings on the feasibility, efficacy, and safety of LV-mediated (over)expression of functional chimeric GALC enzymes – modified to enhance enzyme secretion and bioavailability – in murine neural and hematopoietic cell types, that are the specific target and/or the effector cells in GT strategies. We could not demonstrate the advantage of using LV-transduced HSPCs overexpressing chimeric vs. native GALC enzymes in the context of HSPC-GT *in vivo* in the severe TWI murine model. The most likely explanation for this is that the low level of donor cells engraftment obtained using the stringent experimental conditions tested here does not provide the threshold of GALC supply that is needed to delay the disease onset and slow down the disease progression, thus hampering the possibility to make any comparison in terms of treatment efficacy. Further cohorts of treated animals are needed to quantify the levels of donor cell engraftment in the brain and the enzymatic activity of chimeric GALC enzymes in all the tissues, especially in the CNS. In the CNS, we plan to analyse the GALC activity in the freshly isolated engrafted donor cell population as well as in the neuronal and glial

counterparts taking advantage of brain dissociation protocols optimized in our laboratory. In this way, we expect to gain a better understanding of the threshold of GALC activity achieved in the CNS upon transplantation of LV-transduced TWI HSPCs (chimeric vs. unmodified GALC) in direct comparison to WT HSPCs, and the degree of cross-correction in the neuronal and glial counterparts.

The achievement of a robust donor cell chimerism (>75%) is key to evaluate the efficacy of chimeric GALC constructs in the HSPC-GT setting in this murine model. The transient treatment with Pexidartinib (PLX), a small molecule that inhibits the colony stimulating factor 1 receptor (CSF1R), favours the depletion of resident microglia and enhances the engraftment of donor-derived myeloid progeny in the brain of mice transplanted in adulthood (Hohsfield et al., 2021; Huang et al., 2018; Sailor et al., 2022). Thus, the use of PLX could be helpful to speed up and enhance donor cell engraftment in the brain of transplanted TWI mice. Pilot experiments in newborn TWI mice will be necessary to evaluate the dose of PLX that results in the highest engraftment of donor cells without adverse toxicity.

As an additional backup (or parallel) strategy, we could consider using a conditional GALC murine model with a milder phenotype and prolonged lifespan (Weinstock, et al., 2020a) that would expand the window of therapeutic intervention, ultimately allow the assessment of the advantage of chimeric GALC enzymes vs. the native counterpart in terms of production and bioavailability in CNS tissues upon HSPC-GT.

Materials and methods

1 Animals

Mouse colonies are maintained in the animal facility of the San Raffaele Scientific Institute, Milano, Italy. All procedures are performed according to protocols approved by the 'Institutional Committee for the Good Animal Experimentation' of the San Raffaele Scientific Institute (IACUC #791 and IACUC #1145) and are reported to the Ministry of Health, as required by Italian law.

1.1 The twitcher mouse model

The TWI mouse bears an autosomal recessive mutation in the *Galc* gene resulting in a premature stop codon and no residual GALC activity (Suzuki & Suzuki, 1983). The most commonly used TWI mice are on a C57BL/6J background (Jackson laboratory, Bar Harbor, Maine, 04609, USA). The mutation consists in G to A transition at codon 355 of the *Galc* gene, changing it from tryptophan to a stop codon (p.W355*).

Heterozygous (HET) mice have a normal phenotype. Homozygous TWI and WT littermates are obtained by strict brother/sister mating of HET animals, since TWI do not mate because of precocious death and abnormalities in spermatogenesis (Luddi et al., 2017). The genotype of newborn mice is determined by polymerase chain reaction (PCR) specific for the twitcher mutation (Sakai et al., 1996).

TWI mice appear normal at birth and develop tremors at PND 21. At this time TWI mice show a mild phenotype, with modest resting tremors and initial paralysis of hind legs, which rapidly progress to severe resting tremors ('twitching'), weight loss, paralysis, and subsequent wasting of hind legs and weakness of facial muscles. At around PND 30, TWI mice display a severe condition with compromised walking ability and feeding difficulty. The PNS is severely demyelinated, while the CNS shows a patchy demyelination (Taniike & Suzuki, 1994). The median survival of TWI mice in our colony is 39 days (n=40 mice analysed over 2 years), with a range between 34 and 44 days that reflects the variability of the disease progression. HET mice retain a half of physiological GALC activity and are indistinguishable from WT mice (Suzuki & Suzuki, 1995).

1.2 Genotyping of TWI mice

DNA extraction is performed from mouse finger biopsies. Tissues are digested with Proteinase K (Sigma) at 20 mg/ml concentration at 56°C overnight (o/n) diluted in 150 µl of lysis buffer. Details of lysis buffer are shown in the table below (Table 1).

	Concentration	**Provider**
Tris-HCL	10 mM	Tris Sigma; HCL Carlo Erba
KCL	50 mM	Fluka
$MgCl_2$	1.5 mM	Merck
Gelatine type A	0.01%	Sigma
NP40	0.45%	Calbiochem
Tween20	0.45%	Sigma

Table 1. Details of lysis buffer composition.

After inhibition of proteinase K for 10 minutes (min) at 96°C, the genotype is determined by PCR followed by amplified fragment digestion at 37 °C for 1 hour (h).

The primers are acquired from Eurofins Genomics. The forward primer (FW) for the reaction is designed on an intronic sequence 230 base pair (bp) upstream the mutation (FW: 5'-CACTTAATTTTCTCCAGTCAT-3'), while the reverse primer (REV) has a complementary sequence of the exon downstream the mutation site (RW: 5'-TAGATGGCCCACTGTCTTCAGGTGATA-3'). The mutation forms a restriction site for the enzyme EcoRV. Details of the PCR and digestion reactions are shown in Tables 2 and 3.

PCR Reaction MIX			**Thermal cycle**			
	Concentration	Provider	Step 1	94 °C	10 min	1 cycle
DNA	10 µl from digestion					
GoTaq Buffer 5X	5X	Promega	Step 2	95 °C	30 sec	40 cycles
dNTPs 10 mM	0.24 mM	Promega		56 °C	30 sec	
Primer FW+REV 10 uM	0.2 uM	Eurofins Genomics		72 °C	30 sec	
GoTaq polymerase 5u/µl	1.25 u	Promega	Step 3	72 °C	10 min	1 cycle
H_2O RNase-free	Up to 25 µl					

Table 2. Details of PCR reaction constituents and thermal cycle to identify mice genotypes. *dNTP: Deoxyribonucleotide triphosphate.*

Digestion Reaction MIX		
	Concentration	Provider
DNA	25 µl from previous PCR	
Buffer 3.1	10X	BioLabs
EcoRV 20u/µl (NEB)	0.28 u/µl	BioLabs
H_2O RNase-free	Up to 25 µl	

Table 3. Details of digestion reaction performed after PCR.

The products are separated by electrophoresis in 3% Low Range Ultra Agarose gel (Bio-Rad, 1316107). EcoRV digestion of WT DNA results in the generation of a band of 260 bp; HET restriction pattern shows 2 bands: one corresponding to the WT allele (260 bp) and the other corresponding to the mutant allele (234 bp); homozygous restriction pattern shows only the band corresponding to the mutant allele (234 bp). A representative agarose gel of PCR products after EcoRV digestion is shown below (Figure 31).

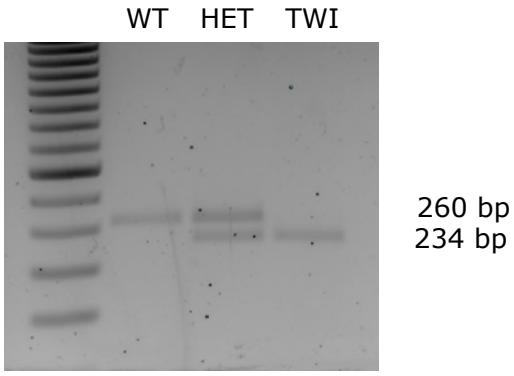

Figure 31. Representative gel showing band pattern corresponding to specific genotypes.

1.3 The transgenic GFP mouse model.

Transgenic CAG-GFP mice (TgCAG-GFP, background C57BL/6-Tg (CAG-eGFP)1Osb/J) were purchased from The Jackson Laboratory (Bar Harbor, ME USA). The enhanced GFP (eGFP) cDNA is under control of a CAG promoter, leading to a widespread eGFP fluorescence. CAG-GFP mice are used as tBM donors.

2 Lentiviral vectors: production and titration.

We used vesicular stomatitis virus (VSV)-pseudotyped third-generation LVs, produced by transient four-plasmid co-transfection into 293T cells and purified by ultracentrifugation, as described (Amendola et al., 2005; Vigna et al., 2005)

LVs carry the sequence of unmodified and chimeric GALC enzymes under the human PGK promoter (Ricca, Cascino, et al., 2020).

All the plasmids were synthesized by Gene Script (New Jersey, United States), which performed the cloning strategies according to our indications.

The GALC-CH plasmid was obtained by inserting the mCherry sequence (mCherry Monomeric derivative of DsRed fluorescent protein; sequence author: Clontech (TaKaRa), link:

https://www.snapgene.com/resources/plasmidfiles/?set=fluorescent_protein_genes_and_plasmids&plasmid=mCherry) downstream of the murine *Galc* cDNA (Neri et al., 2011) using the following linker: TRTRPLE.

Chimeric GALC enzymes are obtained from the GALC-CH as follows:

- The GALCsp (MANSQPKASQQRQAKVMTAAAGSASRVAVPLLLCALLVPGGA) is substituted with that derived from IDS (IDSsp:MPPPRTGRGLLWLGLVLSSVCVALG) or IDUA (IDUAsp: MRPLRPRAALLALLASLLAAPPVAPAE) enzymes;
- A tandem repeat of the ApoE II receptor-binding region, from aa 141 to 149 (LRKLRKRLL LRKLRKRLL) is added downstream of the mCherry sequence using a flexible linker (LGGGGSGGGGSGGGGSGGGGS).

The LV carrying the expression of GFP under the human PGK promoter was used as control (LV.GFP; Meneghini et al., 2016).

All the procedures relative to LV preparation and titration have been previously described (Amendola et al., 2005; Ornaghi et al., 2020), and were performed in collaboration with Doctor Lucia Sergi Sergi, Doctor Luigi Tiradani and Doctor Francesca Ornaghi (SR-Tiget). Briefly, LVs were produced by transient four-plasmid cotransfection into 293T cells, purified by ultra-centrifugation (Vigna et al., 2005) and their expression titers were estimated on human cells (293T) by limiting dilution. The copies of integrated vector (VCN) per cell were obtained by quantitative droplet dd-PCR as described below (paragraph 5.2). Specifically, the titer was calculated as VCN × number of plated cells × dilution of vector and expressed as transducing units (TU)/ml. Vector particle was measured by HIV-1 gag p24 antigen immunocapture (NEN Life Science Products). Vector infectivity was calculated as the ratio between titer and particle and expressed as TU/ng of p24. The titer and infectivity of the different LVs are reported below (Table 4).

Vector	Titer (TU/ml)	Infectivity (TU/ng)
LV.GALC-CH	5.08×10^9	4.57×10^4
LV.IDS.GALC-CH	2.55×10^{10}	2.3×10^5
LV.IDS.GALC-CH.APO	5×10^9	1.2×10^5
LV.IDUA.GALC-CH.APO	$4{,}93 \times 10^9$	1.8×10^4
LV.GFP	$2{,}93 \times 10^9$	2.67×10^4

Table 4. Titer and infectivity of LVs used in this study.

3 NSPC and HSPC isolation, culturing, and characterization.

3.1 Establishment of murine neural stem/progenitor cell (NSPC) lines.

NSPC cultures were established as previously described (Gritti et al., 2009; Ricca et al., 2022). Neonates (PND 0-2) TWI and WT mice were anaesthetised in crushed ice before being decapitated. Brains were removed and transferred in a Petri dish containing PBS + Glucose (0.6%, Sigma) + Penicillin/Streptomycin (P/S, Lonza) (1%). The olfactory bulbs were removed, a coronal slice comprising the periventricular subventricular zone (SVZ) of the forebrain lateral ventricles was cut and the periventricular tissue was carefully dissected using fine forceps. After two steps of centrifugation at 500 x g for 10 min and cells dissociation in dulbecco's modified eagle medium (DMEM, Life Technologies), primary cells are counted and plated with an approximate final cell density of ~0.5–1 x 10^5 cells/cm^2. A pool of SVZs from 3 mice originated a primary cell suspension. Primary cells were plated in chemically defined serum free medium (control medium, see Table 5) containing a mix of hormones (see Table 6) and the growth factors, fibroblast growth factor 2 (FGF2) and epidermal growth factor (EGF) (Peprotech; 10 and 20 ng/mL, respectively; growth medium). Under these culture conditions, a small population of cells proliferates to form floating clonal primary spheres (neurospheres). In order to generate a NSPC line, seven-day-old primary spheres were collected, mechanically dissociated to a single cell suspension, and plated in growth medium (2 x 10^3 cells/cm^2). This procedure was repeated twice; bulk cultures were then generated by plating cells in growth medium (10^4 cells/cm^2).

Details of the control medium composition are shown in the tables below:

Control medium		
	Concentration	**Provider**
WATER	Up to 500 ml	
DMEM/F12	10x	GIBCO
Glucose	30%	Sigma
NaHCO3	7.5%	GIBCO
HEPES	1M	GIBCO
GLUTAMAX	200Mm	GIBCO
HORMONE MIX	10X	

Table 5. Details of control medium composition.

HORMONE MIX		
	Concentration	**Provider**
WATER	Up to 800 ml	
DMEM/F12	10x	GIBCO
Glucose	30%	Sigma
$NaHCO_3$	7.5%	GIBCO
HEPES	1M	GIBCO

human recombinant insulin solution	10 mg/mL	Sigma
Putrescine	1 mg/mL	Sigma
Apo-transferrin	1 mg/mL	Sigma
Progesterone	3mM	Sigma
Sodium selenite	3mM	Sigma

Table 6. Details of hormone mix composition.

3.2 Differentiation of NSPCs into neurons and glia.

WT and TWI-derived serially passaged NSPCs were plated on matrigel-coated coverslips (SACCO) (3.5 x 10^4 cells/cm^2) in growth medium. After 48 h cells were collected as a population enriched in proliferating and undifferentiated cells (precursor cells) or the medium was replaced with progenitor medium (control medium + FGF2) to continue differentiation. After 2 days, cells were collected as population enriched in lineage-committed progenitors (progenitor cells) or the medium was replaced with control medium + 2% fetal bovine serum (FBS, Euroclone) to obtain, after 5 days, differentiated neuronal/glial population (differentiated cells). After LV transduction (see paragraph 3.3) pellet and sup of LV-transduced and UT TWI and UT WT counterparts were collected for analyses (enzymatic activity and VCN measurement, WB, gene expression, IF).

For IF analysis, *in vitro* cultures were plaited onto matrigel-coated glass coverslips and, at the end of the experiment, were fixed with 4% paraformaldehyde (PFA, Santa Cruz Biotechnology) and processed for IF as previously described (Gritti et al., 2009; Ricca et al., 2022). Neurons, astrocytes, and oligodendrocytes were revealed by positivity for TuJ1, GFAP and O4 markers, respectively. IF assay and antibody dilutions are described below (paragraph 7.1, Table 8).

3.3 LV-mediated gene transfer in NSPCs.

LV transduction was performed on serially subcultured NSPCs (passages 4-13). NSPCs were plated in growth medium 8 h before transduction (3 x 10^4 cells/cm^2) and incubated o/n with LV, at 25, 50 or 100 MOI. LV-containing medium was then replaced with fresh medium to allow the formation of neurospheres, which were subcultured every 4 days by mechanical dissociation to establish stable LV-transduced NSPC lines. After 3 subcultures, LV-transduced TWI NSPCs and UT TWI and WT counterparts (controls) were differentiated and NSPCs and derived progeny are analysed for: i) VCN (see paragraph 5.2); ii) GALC enzymatic activity (see paragraph 6.1) in the pellet and sup of NSPCs and progeny; iii) WB analysis (see paragraph 6.2) to detect chimeric GALC precursor proteins in the pellet and sup of

NSPCs and differentiated progeny; iv) IF analysis (see paragraph 7.1) to evaluate the lysosomal localization of chimeric GALC enzymes and their capability to clear GalCer intracellular storage that accumulate in UT TWI NSPC-derived progeny (see chapter results, Figure 16A and 21B).

A summary of NSPCs establishment, differentiation, treatment, and analyses is show in Figure 32.

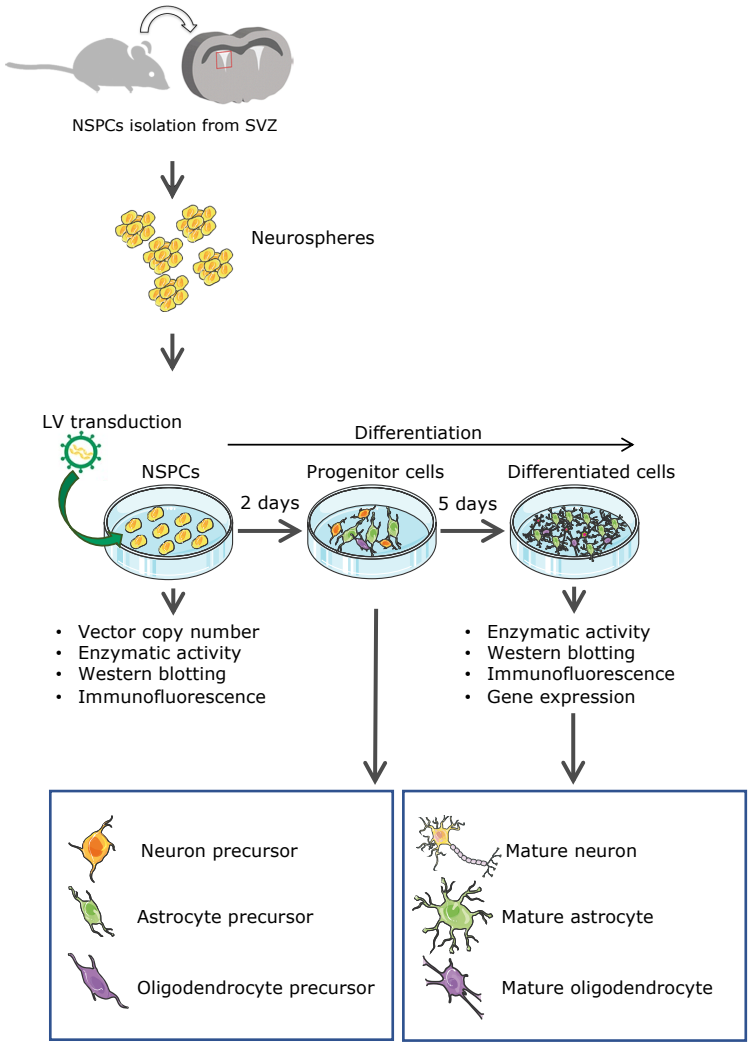

Figure 32. Representative scheme of NSPCs isolation, culturing, and differentiation*. WT and TWI NSPCs are isolated from SVZ of neonatal mice and cell cultures are established. Pellet and sup of LV-transduced TWI cells and UT WT and TWI counterparts, from precursor and differentiated cultures, are collected for analyses.*

3.3.4 Treatment of NSPCs with statins.

WT NSPCs were plated (6 x 10^4 cells/cm^2) in growth medium for 24 h. Cells were then exposed to Simvastatin or Pravastatin (Sigma-Aldrich) at 1 and 5 nM for 24 h. Cells were collected for WB (see paragraph 6.2) and Real-time (RT)-PCR analyses (see paragraph 5.1). Simvastatin at 1 nM was chosen to treat TWI NSPCs for the membrane-bound LDLR protein analysis. Cells were collected for Cell Surface Protein

Biotinylation and Avidin Pull-Down (see paragraph 6.3) and WB analysis (see paragraph 6.2).

3.4 Isolation and transduction of murine hematopoietic stem/progenitor cells (HSPCs).

HSPC cultures were established as previously described (Gentner et al., 2010; Ornaghi et al., 2020). TWI and WT adult mice (5–6 weeks) were euthanized with CO_2, and BM was harvested by flushing femurs and tibias with PBS. Murine HSPCs were purified using a lineage cell depletion kit (Miltenyi; LS columns, Miltenyi), following the manufacturer's instructions. Briefly, BM cells were magnetically labelled with a cocktail of biotinylated antibodies against a panel of antigens expressed by mature HCs (like T and B cells, monocytes/macrophages, granulocytes and erythrocytes and their committed precursors). The selection by Anti-Biotin MicroBeads allowed the separation of Lineage negative (Lin-) fraction. The purity of enriched Lin- cells was assessed by FACS analysis, labelling 2 x 10^5 Lin- and Lin+ cells with CD3/Ly-6G(Ly6C)/CD11b/CD45R(B220)/Ter119 APC Cy7 antibody (Biolegend), following the manufacturer's instructions.

For LV transduction, Lin- cells were plated (1 x 10^5 cells/cm^2) in StemSpan serum-free medium (Stemcell) supplemented with cytokines (murine stem cell factor -mSCF-, 5 ng/ml; human FMS-related tyrosine kinase 3 ligand -hFlt3L-, 10 ng/ml; murine IL3, 10 ng/ ml; murine thrombopoietin -mTPO-, 50 ng/ml; all from Peprotech) in the presence of LVs at MOI 50 and 100 for 12 h (Ornaghi et al., 2020). The day after transduction, Lin- cells were plated for: i) the CFC assay, 4 x 10^3 cells/ml in murine Methocult (StemCell; in duplicate); ii) LC, 3 x 10^4 cells/cm^2 in RPMI medium (Corning), 10% FBS (Euroclone), 1% P/S (Lonza), 1% l-glutamine (Lonza), and cytokines (mSCF, 5 ng/ml; hFlt3L, 10 ng/ml; mIL3, 10 ng/ml; mTPO, 50 ng/ml; all from Peprotech).

After 14 days in culture, CFC and LC were counted, and bulk populations are collected and analysed for VCN and enzymatic activity. LC was also analysed for IF and ImageStream (see paragraphs 7.1 and 7.4, respectively). The pellet of TWI and WT LCs (LV-transduced and UT WT and TWI cells) and the sup of LV-transduced TWI cells and UT WT and TWI controls were collected: i) to measure GALC enzymatic activity (see paragraph 6.1); ii) to detect chimeric GALC precursor (by WB; see paragraph 6.2); iii) to be used as donor medium for cross-correction experiments (see paragraph 3.7). Eight single colonies/plate (CFC assay) were picked to analyse the efficiency of transduction by VCN analysis.

3.7 Cross-correction of TWI NSPC-derived neuronal/glial progeny.

TWI-derived serially passaged NSPCs were plated (3.5 x 10^4 cells/cm^2) onto an adhesive substrate (Matrigel, SACCO) in growth medium and differentiated as described above (see paragraph 3.2). In the last 72 h of culture, cells were treated with the sup collected from the following populations of donor cells: i) UT WT and LV-transduced TWI NSPC-derived neurons/glial cells (for VCN values of donor cells see Figure 22); ii) UT WT and LV-transduced TWI HSPC-derived progeny (LCs after 14 days in culture; for VCN values of donor cells see the Figure22). See Figure 22 for the schematic of cross-correction experiments.

UT TWI and WT cultures were treated with fresh medium as controls. Donor and acceptor cells were collected for IF (see paragraph 7.1) and GALC activity (see paragraph 6.1) analyses.

4 In vivo studies.

4.1 Myeloablative regimen.

From 16 to 24 hours before transplantation, PND 1-2 TWI and WT pups were conditioned with sublethal TBI at 500 or 400 RAD or with a single intraperitoneal injection of 20 mg/kg of BUS (Busilvex 6 mg/ml, Pierre Fabre, Boulogne-Billancourt, France). UT TWI and WT littermates were used as controls.

4.2 Treatments.

Total bone marrow transplant (tBM-T): four- to eight-week-old tgCAG-GFP mice were euthanized with CO_2 and tBM was flushed from tibias and femurs with PBS and then centrifuged at 800 x g for 5 min. Red blood cells in the tBM pellet were lysed with double-distilled water (ddH2O) for 10 seconds (sec). PBS + 10% FBS was added to stop the reaction and the cell suspension was flowed through a 40 μm cell strainer (BD Biosciences). After centrifugation (800 x g for 5 min), cells were suspended in PBS (5 × 10^6 cells/50 μL) and immediately injected into myeloablated recipient mice. Donor BM cells were GFP+ and expressed physiological levels of GALC activity (13.9 ± 0.8 nmol/h x mg; n= 3).

Hematopoietic stem/progenitor cell gene therapy (HSPC-GT): WT and TWI HSPCs (Lin- cells) were isolated as described above (paragraph 3.4). The day after transduction with different vectors (LV.GFP, 50 MOI; LV.GALC-CH, and LV.IDUA.GALC-CH.APO, 100 MOI), HSPCs were suspended in PBS (5 × 10^5 cells/50 μL) and immediately injected into myeloablated recipient mice. HSPCs were also plated for *in vitro* characterization as described above (LC and CFC assays).

Neonatal (PND 2-3) recipient mice were anesthetized on ice for one min to induce a transient hypothermia. tBM and HSPCs were injected into the temporal vein using a U-100 insulin syringe (DB Micro-Fine, 0.3 ml). After injection, pups were warmed up by putting them under a heat lamp for around 1 min. The procedure takes less than 3 min for each mouse, then neonates are immediately returned to parental cures. The survival after the procedure is >95%. Experimental animals of both sexes were randomly assigned to groups before sex could be identified.

4.3 Monitoring of treated mice.

The body weight was monitored once a week starting from PND 20.

Treated mice were analysed at different time points after treatment and at the time of sacrifice to assess:

- the engraftment of transplanted HCs: i) by FACS analysis on the PB collected from the tail vein one and two months after transplant, by the use of the monoclonal antibody reacting with all isoforms of mouse CD45, a marker expressed by all HCs excluding mature erythrocytes and platelets (see paragraph 6.4); ii) by VCN analysis (see paragraph 5.2) performed on BM cells harvested from HSPC-GT treated mice at the time of sacrifice; iii) by IF analysis in CNS tissues to evaluate GFP+ donor cells distribution and morphology (see paragraph 7.1);
- the inflammatory status of CNS tissues, a disease-associated pathological feature, in treated and controls groups (by WB analysis, see paragraph 6.2);
- GALC activity (see paragraph 6.1) in CNS, PNS and peripheral organs (liver, spleen, and BM).

Mice were euthanized when they reached the human disease endpoint (weight loss >30% in one week, inability to move, eat and drink). UT TWI and WT littermates were included as controls. No sex-related differences in treatment outcomes were observed. Mice were provided with the antibiotic Gentamycin (final concentration 320 mg/mL) (ITALFARMACO) in drinking water from the day of conditioning for the following two months.

4.4 Tissue collection and processing.

Treated and control mice were anaesthetised with Ketamine-Xylazine (from SIGMA, 100 e 10 mg/Kg, respectively) and intracardially perfused via the descending aorta with 0.9% NaCl + 25,000 heparin sodium I.U./ml. Brain, SC, SN, liver, spleen, and BM tissues were collected for enzymatic activity.

The two brain hemispheres were separated, and each hemisphere was again divided into two parts. An integra hemisphere part was used for IF analysis (see paragraph 7.1). For the other, a cut was made thus separating: the rostral region (RO) comprising the telencephalon, diencephalon, and midbrain; the caudal region (CA) comprising the cerebellum, pons, and medulla. The RO and CA regions were analysed for enzymatic activity (see paragraph 6.1) and WB (see paragraph 6.2). Spinal cord was collected as a whole and then sagittally halved. The BM was collected as described in paragraph 4.2 and immediately frozen for subsequent enzymatic activity and VCN analyses (see paragraph 5.2).

For IF analysis, sections of the brain and spinal cord tissues were fixed for 24 h in 4% PFA and included in 4% agarose. Serial coronal vibratome sections (6 series, 40 µm-thick) were processed as described below (see paragraph 7.1).

For biochemical and molecular assays, tissues were quickly frozen in liquid nitrogen.

5 Molecular biology analyses.

5.1 Total mRNA extraction and RT-PCR.

Total RNA was extracted from WT and TWI NSPCs pellets by RNeasy mini Kit (Qiagen), following the manufacturer's instructions. Brain tissues from age-matched WT and TWI mice were treated with Qiazol and homogenized and total RNA was extracted using the RNeasy Lipid Tissue miniKit (Qiagen), following the manufacturer's instructions.

The quantity of RNA was determined by 260/280 nm OD reading on a NanoDrop ND-1000 Spectrophotometer (NanoDrop, Pero, Italy). Reverse transcription was carried out using 1 µg of total RNA and the Quantitect Reverse Transcriptase kit (Qiagen, Hilden, Germany).

qPCR was performed in Optical 96-well Fast Thermal Cycling Plates (Applied Biosystems) on ViiA7 Real-Time PCR System (Applied Biosystems), using the following thermal cycling conditions: one cycle at 95°C for 15 min, 40 cycles at 95°C for 50 sec and 60°C for 1 min. Each sample was run in duplicate in a total volume of 12.5 µl/reaction, containing 6.25 µl 2× Universal PCR Master Mix (Applied Biosystems), 1 µl of template cDNA and 1.25 µl of probe and primers (TaqMan Gene Expression Assays, Applied Biosystems) listed in Table 7.

The SDS 2.2.1 software was used to extract raw data. Relative expression of mRNA for the target genes was performed by the comparative CT (ΔΔCT) method using

glyceraldehyde-3-phosphate dehydrogenase (*Gapdh*) housekeeping gene as control. Briefly, ΔCt was calculated for each sample as the Ct of the gene of interest minus the Ct of the normalizer (*Gapdh*). The ΔΔCt was then determined as the ΔCt of each sample minus the average of the ΔCt of controls. Finally, the fold change was expressed as 2^(-ΔΔCt), for each sample.

Probe+Primers for Taqman RT-PCR		
M6PR	Mannose-6-Phosphate receptor	Mm04208409_gH
LDLR	Low density lipoprotein receptor	Mm01177349_m1
LRP1	Low density lipoprotein receptor-related protein 1	Mm00464608_m1
LRP2	Low density lipoprotein receptor-related protein 2	Mm01328171_m1
GAPDH	Glyceraldehyde-3-Phosphate Dehydrogenase	Mm99999915_g1

Table 7. List of commercial primers and probes used.

3.5.2 Quantification of the vector copy number (VCN).

Genomic DNA from murine 293T cells, NSPCs and HSPCs (bulk population of LC and CFC) was extracted from cellular pellets (mini kit Qiagen), following the manufacturer's instructions. DNA was quantified by 260/280 nm optical density (OD) reading on the NanoDrop ND-1000 Spectrophotometer (Euroclone). DNA from single colonies (CFC assay) was extracted by using QuickExtract DNA extraction solution (Lucigen), following the manufacturer's instructions.

The VCN was quantified by quantitative droplet dd-PCR, as described (Ornaghi et al., 2020). Briefly, VCN were normalized to genomic DNA content, which was assessed using the murine semaphorin 3A (sema3A, Biorad) and the human telomerase (TELO, Life Technologies) genes.

Each sample was run in duplicate in a total volume of 22 µl/reaction, containing 11 µl ddPCR supermix for probes (Biorad), 5 µl of template DNA (3 ng/µl - 15 ng tot) and 20x of probes-primers mix (custom primers and probes listed below) amplifying the PSI (ψ) sequence of the LV backbone and a fragment of the murine or human reference sequence (sema3A or TELO).

Gene primers and probes:

Sema3A primers/HEX probe set
Forward primer: 5'-ACC GAT TCC AGA TGA TTG GC-3'
Reverse primer: 5'-TCC ATA TTA ATG CAG TGC TTG C-3'
HEX probe: 5'- (HEX) - AGA GGC CTG TCC TGC AGC TCA TGG-(BHQ-1) - 3'

TELO primers/Vic-TAMRA probe set

Forward primer: 5’-GGCACACGTGGCTTTTCG-3’
Reverse primer: 5’-GGTGAACCTCGTAAGTTTATGCAA-3’
Vic-TAMRA probe: 5’-TCAGGACGTCGAGTGGACACGGTG-3’

HIV primers/FAM probe set
Forward primer: 5’-TACTGACGCTCTCGCACC-3’
Reverse primer: 5’-TCTCGACGCAGGACTCG-3’
FAM probe: 5’-ATCTCTCTCCTTCTAGCCTC-3’

In QuantaSoftTMsoftware, copy number was determined by calculating the ratio of the target molecule concentration to the reference molecule concentration, times the ploidy of reference species.

6 Biochemical analyses.

6.1 Measurement of GALC enzymatic activity.

GALC activity was measured in the pellet and sup of NSPCs and differentiated cells and HSPCs (LCs), and in tissues collected from treated and control mice. Samples sizes are indicated in the legend of each figure in the results. UT WT and TWI cells were included in all the experiments as controls.

Samples prepared at SR-Tiget were sent to the Università degli Studi di Perugia (Dipartimento di Medicina Sperimentale e Scienze Biochimiche, Sezione di Biochimica e Biologia Molecolare; in collaboration with Doctor Francesco Morena and Doctor Sabata Martino) for determination of specific GALC activity, as previously described (Martino et al., 2009). The assay was performed using 2–7.5 µg of sample proteins with the artificial fluorogenic substrate 4-methylumbelliferone-β-galactopyranoside (1.5 mM) resuspended in 0.1/0.2 mol/L citrate/phosphate buffer, pH 4.0, and $AgNO_3$ (11 mM) at 37 °C. The enzymatic reaction was stopped by adding 0.2 M pH10.6 Glycine/NaOH. The fluorescence of liberated 4-methylumbelliferone was measured on a spectrofluorometer (λ excitation 360 nm, λ emission 446 nm). Total protein content was measured using the Bradford Protein Assay kit with bovine serum albumin (BSA) as the reference standard.

3.6.2 Western blotting (WB).

Cell pellets and tissues: for protein extraction, cell pellets and tissues were lysed using RIPA buffer (50 mM Tris–HCl pH 7.4, 150 mM NaCl, 0.5% sodium deoxycholate, 0.1% SDS, 2 mM EDTA) containing protease and phosphatase inhibitors (Roche, 25×

and 10×, respectively). Tissues were lysed with a homogenizer. The samples were incubated twice in ice (15 min each), vortexed (few sec) between incubations, and finally centrifuged at 4°C 12,000 x g (15 min). Protein content was measured using the DCTM protein assay and the MultiskanTM Go microplate spectrophotometer, using the quick start BSA standard set (Bio-Rad) as the reference standard. Equal protein amount from different samples was incubated with SDS-PAGE loading buffer (NuPage, Invitrogen) for 5 min at 95 °C before use in WB analysis. SDS-PAGE of protein extracts was performed with Novex NuPAGE SDS-PAGE system according to the manufacturer instructions and proteins were transferred on nitrocellulose membranes using the iBlot2 Gel Transfer Device (all Invitrogen). After blocking with TBST (Tris-HCl pH 7.5 200 mM, NaCl 1.5 M, 0.1% Tween 20) plus 5% milk, membranes were hybridized with primary antibodies (reported in Table 8) o/n at 4 °C, washed 3 times (10 min each, RT) with TBST and incubated with species-specific horseradish peroxidase (HRP)-conjugated secondary antibody (listed in Table 8) for 1 h RT. After 3 washes (10 min each, RT), the membranes were developed using ClarityTM ECL western blotting substrate (Bio-Rad) and the alliance western blot imaging system (Alliance UVItec Ltd, Cambridge). Quantification of WB was performed using the ImageJ software as described in section 30.13 of the ImageJ User Guide version 1.43.

Cell supernatants: sup were collected from: i) LV-transduced TWI NSPC and UT WT and TWI cultures and differentiated progeny, plated at the same cell density; ii) transduced TWI HSPCs and UT WT and TWI after 14 days in culture (LCs). Proteins were collected by adding four volumes of acetone and incubating the samples o/n at −20°C. After centrifugation at 4°C, 4,000 x g (20 min), the resulting pellets were resuspended in 50 µl of PBS. Equal volume from different samples was incubated with SDS-PAGE loading buffer (NuPage, Invitrogen) for 15 min RT before use in WB analysis. The primary and secondary antibodies used are listed in Table 8.

6.3 Cell surface protein biotinylation and avidin pull-down.

NSPCs (5 × 10^6 cells in a T75 flask) were plated in growth medium. Cells were collected after 24 h and centrifuged twice (800 x g, 5 min/each) with cold PBS, 0.1 mM $CaCl_2$, 1 mM $MgCl_2$ (PBS-CM, Sigma). Cells were treated with biotin (Thermo Fisher Scientific) in cold PBS-CM (1 mg/ml, 1:200; 1 h at 4°C, mild shaking in darkness). After 3 washing with cold PBS-CM/100 mM glycine (Sigma), cells were rinsed with cold PBS-CM and lysed in RIPA lysis buffer supplemented with phosphatase and proteases inhibitors (10× and 25×, respectively), 1 h at 4°C in a rotating wheel. Protein concentration was measured using the DCTM protein assay

and the MultiskanTM Go microplate spectrophotometer. Thirty µg of total lysate was used in WB as control (total lysate). The remaining lysate was incubated with neutravidin agarose resin (Thermo Fisher Scientific; 40 µl/sample) and resuspended in RIPA buffer plus 1/5 of inhibitors (400 µl/sample; 4°C, 2 h in mild shaking). Samples treated with neutravidin agarose resin or biotin were used as controls. Samples were washed 3 times with PBS/0.1% Triton X-100 (5 min/each, mild shaking at 4°C) and centrifuged at 6,000 x g (5 min/each, 4°C). Samples were released by adding 50 µl of 4× reducing SDS-PAGE loading buffer, heating at 99°C for 10 min, and centrifuging at 12,000 x g (2 min) to collect the supernatant. Pull-down of biotinylated proteins (membrane fraction) was immunoblotted by WB. The primary and secondary antibodies used are listed in Table 8.

6.4 Cytofluorimetric analyses of PB and BM samples.

PB was collected from treated and UT mice, and 20 µl of each sample was incubated for 30 min at 4°C with rat anti-mouse CD45-VioBlue (dilution 1:50; Miltenyi Biotec, Bergisch Gladbach, Germany) and for the following 15 min in ice with 1 mL of ammonium-chloride-potassium (ACK, Thermo Fisher Scientific) buffer for red blood cell lysis, following the manufacturer's instructions. The GFP and mCherry signals were measured by direct fluorescence. Samples were centrifuged at 800 x g for 5 min and resuspended in FACS buffer (PBS, 5% FBS, 1% BSA). Cell suspensions were analysed for CD45 and GFP or mCherry positivity using a flow cytometer (Canto II, BD Biosciences or Cytoflex, Beckman Coulter, respectively). Data were analysed using the FlowJo software.

7 Imaging.

7.1 Immunofluorescence (IF) analysis.

Cells: cells were fixed in 4% PFA, rinsed with PBS, incubated with blocking solution containing 10% normal goat serum (NGS, Sigma-Aldrich) and 0.1% Triton X-100 (Sigma) in PBS for 30 min (RT) and incubated o/n at 4 °C with primary antibodies diluted in blocking solution (full permeabilization). To reveal GalCer accumulation and O4, the blocking step was performed using 10% NGS/0.1% Triton X-100 in PBS for 10 min and with only PBS/10% NGS for 20 min (RT), followed by o/n incubation at 4 °C with primary antibodies diluted in PBS/10% NGS (partial permeabilization). After 3 washes (5 min each), antibody staining was revealed using species-specific fluorophore-conjugated secondary antibodies diluted in 1% NGS in PBS (incubation at RT, 1 h). Finally, nuclei were counterstained with Hoechst (10 µg/ml in PBS,

Thermofisher) for 5 min (RT, in darkness). Coverslips were mounted on glass slides using Fluorsave (Calbiochem). Cells incubated only with secondary antibodies were used as negative controls. The primary and secondary antibodies are listed in Table 8.

Tissues: after 3 washes with PBS (5 min each), free-floating vibratome sections were incubated with blocking solution containing 10% NGS/0.3% Triton X-100 in PBS for 1 h (RT) and then incubated o/n at 4°C with the primary antibodies diluted in blocking solution. After 3 washes (5 min each), antibody staining was revealed using species-specific fluorophore-conjugated secondary antibodies diluted in 1% NGS in PBS (RT, 2 h). Tissue sections were counterstained with Hoechst for nuclei (10 min at RT, in darkness), washed in PBS, collected, and mounted on glass slides using Fluorsave. Samples incubated only with secondary antibodies were used as negative controls. All the washes and incubations were performed in mild shaking. The primary and secondary antibodies are listed in Table 8.

7.2 Image acquisition.

Samples were visualized with a Nikon Eclipse E600 microscope and images were acquired at 20× or 40× magnification (scale bars are specified in the legends to figures) with Nikon DS Ri-2 camera, using NIS-Elements F imaging software (Nikon, Japan). ImageJ was used to count immunoreactive cells which were normalized on the total number of nuclei. Cells were counted in 3–5 non-overlapping fields/coverslip (100–200 cells/sample), 2–3 coverslips/experiment, n=3 experiments.

Confocal images were acquired at 20×, 40× and 63× magnification (scale bars are specified in the legends to figures) with a Leica TCS SP8 and Maving RS-G4 confocal microscopes and analysed with LasX and Imaris software, respectively. The number of samples was specified in the legend to each figure in the results.

7.3 Live imaging.

TWI NSPCs transduced with LV.GALC-CH were plated (3 x 10^5 cells/cm^2) onto matrigel-coated glass coverslips (Zeta) and cultured for 48 h in growth medium. Coverslips were transferred in an Oko-Lab stage incubator and confocal images were acquired at 63× magnification with a Leica TCS SP8 confocal microscope. For analysis, the LasX software was used.

7.4 ImageStream analysis.

After 14 days in culture, LV-transduced HSPCs (LCs; 3 × 10^6 cells) were centrifuged and resuspended in 500 µl of PBS/4% PFA (10 min, RT), rinsed in PBS,

and incubated with PBS/0.1% Triton X-100 (10 min at RT, mild shaking). After washing in PBS, cells were incubated for 1 h in blocking solution containing MACS buffer (PBS/0.5% BSA/2 mM EDTA) and 10% NGS (mild shaking) and o/n at 4°C with primary antibodies diluted in blocking solution (anti mCherry, anti-LAMP1). Antibody staining was revealed using species-specific fluorophore-conjugated secondary antibodies diluted in MACS buffer/1% NGS (1 h at RT). Nuclei were counterstained with Hoechst (4 µM in PBS). After washing in EDTA 2 mM, pellets were resuspended in 50 µl of MACS buffer. The primary and secondary antibodies used are listed in Table 8.

Labelled cells were analysed using the ImageStreamX MarkII System (Amnis, Luminex) and IDEAS 6.2 software. At least 20,000 events were collected for each sample (60× magnification, scale bars are specified in the legends to figures). Single-stained samples were used for compensation. Cells in focus were gated using the gradient root mean square feature (Gradient RMS) and single cells were identified using area and aspect ratio features on the brightfield image. Cells with high contrast in the brightfield channel (likely debris or apoptotic cells) and cells with saturation count > 0 were excluded from the analyses. A mask for LAMP1 was created: a first spot mask was used for the identification of spots with a size ≥ 5 pixels and a spot to cell-background ratio ≥ 6. A threshold function of 70% was then applied on the spot mask and a further intensity function was used to exclude all spots ≤ 100. Only cells with intense mCherry signal (an indication of efficient LV transduction) were considered for the analysis. The mask for mCherry was created as that for LAMP1. A threshold function of 70% was then applied and a further intensity function was used to exclude all spots ≤ 150. LAMP1 and mCherry masks were combined to create an overlapping mask and the presence of 0 or at least 1 overlapping mask (proximity or co-localization mask) was quantified in each sample. We analysed ~1,000/sample cells on average (28–2,604 cells).

Primary antibodies	**Provider**	**Dilution**		
		IF	**Image Stream**	**WB**
Hybridoma rat anti-Lamp1	DSHB	1:300	1:300	-
Monoclonal mouse anti-GalCer	Millipore	1:300	-	-
Monoclonal mouse anti-GFAP	Millipore	1:1,000	-	1:100,000
Monoclonal rabbit anti-mCherry	Abcam	-	-	1:1,000
Monoclonal mouse anti-Tuj1	Serotec	1:200	-	-
Monoclonal mouse anti-O4	Millipore	1:200	-	-
Monoclonal rat anti-CD68	Serotec	1:200	-	-

Monoclonal mouse anti-PSA-NCAM				
Polyclonal rabbit anti-calnexin	Sigma	-	-	1:3,000
Polyclonal rabbit anti-GFP	Thermo Fisher Scientific	1:1,000	-	-
Polyclonal rabbit anti-Iba1	Wako	1:100	-	1:1,000
Polyclonal rabbit anti-LDLR	Biovision	-	-	1:1,000
Polyclonal rabbit anti-LRP1	Santa Cruz	1:200	-	-
Polyclonal rabbit anti-LRP2	Santa Cruz	1:200	-	1:200
Polyclonal rabbit anti-M6Pr	Cell Signaling	1:300	-	1:300
Polyclonal rabbit anti-mCherry	Abcam	1:1,000	1:1,000	-
Secondary antibodies	**Provider**	**Dilution**		
		IF	**Image Stream**	**WB**
ALEXA 488 anti-mouse	Thermo Fisher Scientific	1:1,000	1:1,000	-
ALEXA 488 anti-rabbit	Thermo Fisher Scientific	1:1,000	-	-
ALEXA 546 anti-rabbit	Thermo Fisher Scientific	1:2,000	-	-
ALEXA 594 anti-rabbit	Thermo Fisher Scientific	1:2,000	-	-
ALEXA 647 anti-rat	Thermo Fisher Scientific	1:500	1:500	-
HRP anti mouse	Chemicon	-	-	1:5,000
HRP anti rabbit	Chemicon	-	-	1:5,000

Table 8. List of the primary and secondary antibodies used for biochemical and imaging analyses.

8 Statistics

All data were analysed with Graph Pad Prism version 9.2 for Macintosh and expressed as the mean ± std.error of the mean (SEM) ($n \geq 3$) or as the mean + range ($n < 3$). Student's t test, One or Two-Way ANOVA followed by appropriate post tests are used (statistical significance: $p<0.05$). Survival curves are analysed by Log Rank (Mantel–Cox) test. The number of samples and the statistical tests used are indicated in the legends to each figure (see Results).

References

Abordo-Adesida, E., Follenzi, A., Barcia, C., Sciascia, S., Castro, M. G., Naldini, L., & Lowenstein, P. R. (2005). Stability of lentiviral vector-mediated transgene expression in the brain in the presence of systemic antivector immune responses. *Human Gene Therapy*, *16*(6), 741–751. https://doi.org/10.1089/HUM.2005.16.741

Aiuti, A., Biasco, L., Scaramuzza, S., Ferrua, F., Cicalese, M. P., Baricordi, C., Dionisio, F., Calabria, A., Giannelli, S., Castiello, M. C., Bosticardo, M., Evangelio, C., Assanelli, A., Casiraghi, M., Di Nunzio, S., Callegaro, L., Benati, C., Rizzardi, P., Pellin, D., … Naldini, L. (2013). Lentiviral hematopoietic stem cell gene therapy in patients with wiskott-aldrich syndrome. *Science*, *341*(6148). https://doi.org/10.1126/SCIENCE.1233151/SUPPL_FILE/AIUTI.SM.PDF

Allewelt, H., Taskindoust, M., Troy, J., Page, K., Wood, S., Parikh, S., Prasad, V. K., & Kurtzberg, J. (2018). Long-Term Functional Outcomes after Hematopoietic Stem Cell Transplant for Early Infantile Krabbe Disease. *Biology of Blood and Marrow Transplantation : Journal of the American Society for Blood and Marrow Transplantation*, *24*(11), 2233–2238. https://doi.org/10.1016/J.BBMT.2018.06.020

Amendola, M., Venneri, M. A., Biffi, A., Vigna, E., & Naldini, L. (2005). Coordinate dual-gene transgenesis by lentiviral vectors carrying synthetic bidirectional promoters. *Nature Biotechnology*, *23*(1), 108–116. https://doi.org/10.1038/NBT1049

Anzil, A. P., Blinzinger, K., Mehraein, P., Dohn, G., & Neuhauser, G. (1972). Cytoplasmic inclusions in a child affected with Krabbe's disease (globoid leucodystrophy) and in the rabbit injected with galactocerebrosides. *Journal of Neuropathology and Experimental Neurology*, *31*(2), 370–388. https://doi.org/10.1097/00005072-197204000-00011

Auderset, L., Cullen, C. L., & Young, K. M. (2016). Low Density Lipoprotein-Receptor Related Protein 1 Is Differentially Expressed by Neuronal and Glial Populations in the Developing and Mature Mouse Central Nervous System. *PloS One*, *11*(6). https://doi.org/10.1371/JOURNAL.PONE.0155878

Avola, R., Graziano, A. C. E., Pannuzzo, G., Alvares, E., & Cardile, V. (2016). Krabbe's leukodystrophy: Approaches and models in vitro. *Journal of Neuroscience Research*, *94*(11), 1284–1292. https://doi.org/10.1002/JNR.23846

Babcock, M. C., Mikulka, C. R., Wang, B., Chandriani, S., Chandra, S., Xu, Y., Webster, K., Feng, Y., Nelvagal, H. R., Giaramita, A., Yip, B. K., Lo, M., Jiang, X., Chao, Q., Woloszynek, J. C., Shen, Y., Bhagwat, S., Sands, M. S., & Crawford, B. E. (2021). Substrate reduction therapy for Krabbe disease and metachromatic leukodystrophy using a novel ceramide galactosyltransferase inhibitor. *Scientific Reports*, *11*(1). https://doi.org/10.1038/S41598-021-93601-1

Bagshaw, R. D., Mahuran, D. J., & Callahan, J. W. (2005). A proteomic analysis of lysosomal integral membrane proteins reveals the diverse composition of the organelle. *Molecular & Cellular Proteomics : MCP*, *4*(2), 133–143. https://doi.org/10.1074/MCP.M400128-MCP200

Bajaj, L., Lotfi, P., Pal, R., Ronza, A. di, Sharma, J., & Sardiello, M. (2019). Lysosome biogenesis in health and disease. *Journal of Neurochemistry*, *148*(5), 573–589. https://doi.org/10.1111/JNC.14564

Ballabio, A., & Bonifacino, J. S. (2020). Lysosomes as dynamic regulators of cell and organismal homeostasis. *Nature Reviews. Molecular Cell Biology*, *21*(2), 101–118. https://doi.org/10.1038/S41580-019-0185-4

Ballabio, A., & Gieselmann, V. (2009). Lysosomal disorders: from storage to cellular damage. *Biochimica et Biophysica Acta*, *1793*(4), 684–696. https://doi.org/10.1016/J.BBAMCR.2008.12.001

Bascou, N., Derenzo, A., Poe, M. D., & Escolar, M. L. (2018). A prospective natural history study of Krabbe disease in a patient cohort with onset between 6 months and 3 years of life. *Orphanet Journal of Rare Diseases*, *13*(1). https://doi.org/10.1186/S13023-018-0872-9

Bell, P., Moscioni, A. D., McCarter, R. J., Wu, D., Gao, G., Hoang, A., Sanmiguel, J. C., Sun, X., Wivel, N. A., Raper, S. E., Furth, E. E., Batshaw, M. L., & Wilson, J. M. (2006). Analysis of tumors arising in male B6C3F1 mice with and without AAV vector delivery to liver. *Molecular Therapy : The Journal of the American Society of Gene Therapy*, *14*(1), 34–44. https://doi.org/10.1016/J.YMTHE.2006.03.008

Belleri, M., & Presta, M. (2016). Endothelial cell dysfunction in globoid cell leukodystrophy. *Journal of Neuroscience Research*, *94*(11), 1359–1367. https://doi.org/10.1002/JNR.23744

Belleri, M., Ronca, R., Coltrini, D., Nico, B., Ribatti, D., Poliani, P. L., Giacomini, A., Alessi, P., Marchesini, S., Santos, M. B., Bongarzone, E. R., & Presta, M. (2013). Inhibition of angiogenesis by β-galactosylceramidase deficiency in globoid cell leukodystrophy. *Brain : A Journal of Neurology*, *136*(Pt 9), 2859–

2875. https://doi.org/10.1093/BRAIN/AWT215

Bellettato, C. M., & Scarpa, M. (2010). Pathophysiology of neuropathic lysosomal storage disorders. *Journal of Inherited Metabolic Disease*, *33*(4), 347–362. https://doi.org/10.1007/S10545-010-9075-9

Ben-Yoseph, Y., Hungerford, M., & Nadler, H. L. (1980). The interrelations between high- and low-molecular weight forms of normal and mutant (Krabbe-disease) galactocerebrosidase. *The Biochemical Journal*, *189*(1), 9–15. https://doi.org/10.1042/BJ1890009

Bickel, U., Kang, Y. S., Yoshikawa, T., & Pardridge, W. M. (1994). In vivo demonstration of subcellular localization of anti-transferrin receptor monoclonal antibody-colloidal gold conjugate in brain capillary endothelium. *The Journal of Histochemistry and Cytochemistry : Official Journal of the Histochemistry Society*, *42*(11), 1493–1497. https://doi.org/10.1177/42.11.7930531

Biffi, A., Capotondo, A., Fasano, S., Del Carro, U., Marchesini, S., Azuma, H., Malaguti, M. C., Amadio, S., Brambilla, R., Grompe, M., Bordignon, C., Quattrini, A., & Naldini, L. (2006). Gene therapy of metachromatic leukodystrophy reverses neurological damage and deficits in mice. *The Journal of Clinical Investigation*, *116*(11), 3070–3082. https://doi.org/10.1172/JCI28873

Biffi, A., Montini, E., Lorioli, L., Cesani, M., Fumagalli, F., Plati, T., Baldoli, C., Martino, S., Calabria, A., Canale, S., Benedicenti, F., Vallanti, G., Biasco, L., Leo, S., Kabbara, N., Zanetti, G., Rizzo, W. B., Mehta, N. A. L., Cicalese, M. P., … Naldini, L. (2013). Lentiviral hematopoietic stem cell gene therapy benefits metachromatic leukodystrophy. *Science (New York, N.Y.)*, *341*(6148). https://doi.org/10.1126/SCIENCE.1233158

Bijlani, S., Pang, K. M., Sivanandam, V., Singh, A., & Chatterjee, S. (2022). The Role of Recombinant AAV in Precise Genome Editing. *Frontiers in Genome Editing*, *3*. https://doi.org/10.3389/FGEED.2021.799722

Biswas, S., & Levine, S. M. (2002). Substrate-reduction therapy enhances the benefits of bone marrow transplantation in young mice with globoid cell leukodystrophy. *Pediatric Research*, *51*(1), 40–47. https://doi.org/10.1203/00006450-200201000-00009

Blau, N. (2014). *Physician's Guide to the Diagnosis, Treatment, and Follow-Up of Inherited Metabolic Diseases.* (C. D. V. Nenad Blau, Marinus Duran, K Michael Gibson (ed.)). Springer Berlin, Heidelberg. https://doi.org/10.1007/978-3-642-40337-8

Boado, R. J., Golden, P. L., Levin, N., & Pardridge, W. M. (1998). Up-regulation of blood-brain barrier short-form leptin receptor gene products in rats fed a high fat diet. *Journal of Neurochemistry*, *71*(4), 1761–1764. https://doi.org/10.1046/J.1471-4159.1998.71041761.X

Boado, R. J., Hui, E. K. W., Lu, J. Z., & Pardridge, W. M. (2013). IgG-enzyme fusion protein: pharmacokinetics and anti-drug antibody response in rhesus monkeys. *Bioconjugate Chemistry*, *24*(1), 97–104. https://doi.org/10.1021/BC3005123

Boado, R. J., Hui, E. K. W., Lu, J. Z., Sumbria, R. K., & Pardridge, W. M. (2013). Blood-brain barrier molecular trojan horse enables imaging of brain uptake of radioiodinated recombinant protein in the rhesus monkey. *Bioconjugate Chemistry*, *24*(10), 1741–1749. https://doi.org/10.1021/BC400319D

Boado, R. J., Hui, E. K. W., Lu, J. Z., Zhou, Q. H., & Pardridge, W. M. (2011). Reversal of lysosomal storage in brain of adult MPS-I mice with intravenous Trojan horse-iduronidase fusion protein. *Molecular Pharmaceutics*, *8*(4), 1342–1350. https://doi.org/10.1021/MP200136X

Boado, R. J., Ka-Wai Hui, E., Zhiqiang Lu, J., & Pardridge, W. M. (2014). Insulin receptor antibody-iduronate 2-sulfatase fusion protein: Pharmacokinetics, anti-drug antibody, and safety pharmacology in Rhesus monkeys. *Biotechnology and Bioengineering*, *111*(11), 2317–2325. https://doi.org/10.1002/bit.25289

Boado, R. J., & Pardridge, W. M. (2017). Brain and Organ Uptake in the Rhesus Monkey in Vivo of Recombinant Iduronidase Compared to an Insulin Receptor Antibody-Iduronidase Fusion Protein. *Molecular Pharmaceutics*, *14*(4), 1271–1277. https://doi.org/10.1021/ACS.MOLPHARMACEUT.6B01166

Böckenhoff, A., Cramer, S., Wölte, P., Knieling, S., Wohlenberg, C., Gieselmann, V., Galla, H. J., & Matzner, U. (2014). Comparison of five peptide vectors for improved brain delivery of the lysosomal enzyme arylsulfatase A. *The Journal of Neuroscience : The Official Journal of the Society for Neuroscience*, *34*(9), 3122–3129. https://doi.org/10.1523/JNEUROSCI.4785-13.2014

Borda, J. T., Alvarez, X., Mohan, M., Ratterree, M. S., Phillippi-Falkenstein, K., Lackner, A. A., & Bunnell, B. A. (2008). Clinical and immunopathologic alterations in rhesus macaques affected with globoid cell leukodystrophy. *The American Journal of Pathology*, *172*(1), 98–111. https://doi.org/10.2353/AJPATH.2008.070404

Bradbury, A. M., Bagel, J. H., Nguyen, D., Lykken, E. A., Salvador, J. P., Jiang, X., Swain, G. P., Assenmacher, C. A., Hendricks, I. J., Miyadera, K., Hess, R. S., Ostrager, A., ODonnell, P., Sands, M. S., Ory, D. S., Shelton, G. D., Bongarzone, E. R., Gray, S. J., & Vite, C. H. (2020). Krabbe disease

successfully treated via monotherapy of intrathecal gene therapy. *The Journal of Clinical Investigation*, *130*(9), 4906. https://doi.org/10.1172/JCI133953

Bradbury, A. M., Bongarzone, E. R., & Sands, M. S. (2021a). Krabbe disease: New hope for an old disease. *Neuroscience Letters*, *752*. https://doi.org/10.1016/j.neulet.2021.135841

Bradbury, A. M., Bongarzone, E. R., & Sands, M. S. (2021b). Krabbe disease: New hope for an old disease. *Neuroscience Letters*, *752*. https://doi.org/10.1016/J.NEULET.2021.135841

Bradbury, A. M., Rafi, M. A., Bagel, J. H., Brisson, B. K., Marshall, M. S., Pesayco Salvador, J., Jiang, X., Swain, G. P., Prociuk, M. L., Odonnell, P. A., Fitzgerald, C., Ory, D. S., Bongarzone, E. R., Shelton, G. D., Wenger, D. A., & Vite, C. H. (2018). AAVrh10 Gene Therapy Ameliorates Central and Peripheral Nervous System Disease in Canine Globoid Cell Leukodystrophy (Krabbe Disease). *Human Gene Therapy*, *29*(7), 785–801. https://doi.org/10.1089/HUM.2017.151

Braulke, T., & Bonifacino, J. S. (2009). Sorting of lysosomal proteins. *Biochimica et Biophysica Acta*, *1793*(4), 605–614. https://doi.org/10.1016/J.BBAMCR.2008.10.016

Burlina, A. B., Polo, G., Salviati, L., Duro, G., Zizzo, C., Dardis, A., Bembi, B., Cazzorla, C., Rubert, L., Zordan, R., Desnick, R. J., & Burlina, A. P. (2018). Newborn screening for lysosomal storage disorders by tandem mass spectrometry in North East Italy. *Journal of Inherited Metabolic Disease*, *41*(2), 209–219. https://doi.org/10.1007/S10545-017-0098-3

Calabria, A., Leo, S., Benedicenti, F., Cesana, D., Spinozzi, G., Orsini, M., Merella, S., Stupka, E., Zanetti, G., & Montini, E. (2014). VISPA: a computational pipeline for the identification and analysis of genomic vector integration sites. *Genome Medicine*, *6*(9). https://doi.org/10.1186/S13073-014-0067-5

Cantore, A., Fraldi, A., Meneghini, V., & Gritti, A. (2022). In vivo Gene Therapy to the Liver and Nervous System: Promises and Challenges. *Frontiers in Medicine*, *8*. https://doi.org/10.3389/FMED.2021.774618

Cantore, A., Ranzani, M., Bartholomae, C. C., Volpin, M., Valle, P. Della, Sanvito, F., Sergi, L. S., Gallina, P., Benedicenti, F., Bellinger, D., Raymer, R., Merricks, E., Bellintani, F., Martin, S., Doglioni, C., D'Angelo, A., Driessche, T. Vanden, Chuah, M. K., Schmidt, M., … Naldini, L. (2015). Liver-directed lentiviral gene therapy in a dog model of hemophilia B. *Science Translational Medicine*, *7*(277). https://doi.org/10.1126/SCITRANSLMED.AAA1405

Cantuti-Castelvetri, L., Givogri, M. I., Zhu, H., Smith, B., Lopez-Rosas, A., Qiu, X.,

Van Breemen, R., & Bongarzone, E. R. (2011). Axonopathy is a compounding factor in the pathogenesis of Krabbe disease. *Acta Neuropathologica*, *122*(1), 35–48. https://doi.org/10.1007/s00401-011-0814-2

Cantuti-Castelvetri, L., Zhu, H., Givogri, M. I., Chidavaenzi, R. L., Lopez-Rosas, A., & Bongarzone, E. R. (2012). Psychosine induces the dephosphorylation of neurofilaments by deregulation of PP1 and PP2A phosphatases. *Neurobiology of Disease*, *46*(2), 325–335. https://doi.org/10.1016/J.NBD.2012.01.013

Cantuti Castelvetri, L., Givogri, M. I., Hebert, A., Smith, B., Song, Y., Kaminska, A., Lopez-Rosas, A., Morfini, G., Pigino, G., Sands, M., Brady, S. T., & Bongarzone, E. R. (2013). The sphingolipid psychosine inhibits fast axonal transport in Krabbe disease by activation of GSK3β and deregulation of molecular motors. *The Journal of Neuroscience : The Official Journal of the Society for Neuroscience*, *33*(24), 10048–10056. https://doi.org/10.1523/JNEUROSCI.0217-13.2013

Capotondo, A., Cesani, M., Pepe, S., Fasano, S., Gregori, S., Tononi, L., Venneri, M. A., Brambilla, R., Quattrini, A., Ballabio, A., Cosma, M. P., Naldini, L., & Biffi, A. (2007). Safety of arylsulfatase A overexpression for gene therapy of metachromatic leukodystrophy. *Human Gene Therapy*, *18*(9), 821–836. https://doi.org/10.1089/HUM.2007.048

Capotondo, A., Milazzo, R., Politi, L. S., Quattrini, A., Palini, A., Plati, T., Merella, S., Nonis, A., Di Serio, C., Montini, E., Naldini, L., & Biffi, A. (2012). Brain conditioning is instrumental for successful microglia reconstitution following hematopoietic stem cell transplantation. *Proceedings of the National Academy of Sciences of the United States of America*, *109*(37), 15018–15023. https://doi.org/10.1073/PNAS.1205858109

Cesana, D., Ranzani, M., Volpin, M., Bartholomae, C., Duros, C., Artus, A., Merella, S., Benedicenti, F., Sergi Sergi, L., Sanvito, F., Brombin, C., Nonis, A., Serio, C. Di, Doglioni, C., Von Kalle, C., Schmidt, M., Cohen-Haguenauer, O., Naldini, L., & Montini, E. (2014). Uncovering and dissecting the genotoxicity of self-inactivating lentiviral vectors in vivo. *Molecular Therapy : The Journal of the American Society of Gene Therapy*, *22*(4), 774–785. https://doi.org/10.1038/MT.2014.3

Chandler, R. J., La Fave, M. C., Varshney, G. K., Trivedi, N. S., Carrillo-Carrasco, N., Senac, J. S., Wu, W., Hoffmann, V., Elkahloun, A. G., Burgess, S. M., & Venditti, C. P. (2015). Vector design influences hepatic genotoxicity after adeno-associated virus gene therapy. *The Journal of Clinical Investigation*, *125*(2), 870–880. https://doi.org/10.1172/JCI79213

Chen, Y. Q., Rafi, M. A., De Gala, G., & Wenger, D. A. (1993). Cloning and expression of cDNA encoding human galactocerebrosidase, the enzyme deficient in globoid cell leukodystrophy. *Human Molecular Genetics*, *2*(11), 1841–1846. https://doi.org/10.1093/HMG/2.11.1841

Chen, Y. Q., & Wenger, D. A. (1993). Galactocerebrosidase from human urine: purification and partial characterization. *Biochimica et Biophysica Acta*, *1170*(1), 53–61. https://doi.org/10.1016/0005-2760(93)90175-9

Chen, Y., Zheng, S., Tecedor, L., & Davidson, B. L. (2018). Overcoming Limitations Inherent in Sulfamidase to Improve Mucopolysaccharidosis IIIA Gene Therapy. *Molecular Therapy : The Journal of the American Society of Gene Therapy*, *26*(4), 1118–1126. https://doi.org/10.1016/J.YMTHE.2018.01.010

Cheng, K. W., Wang, F., Lopez, G. A., Singamsetty, S., Wood, J., Dickson, P. I., & Chou, T. F. (2021). Evaluation of artificial signal peptides for secretion of two lysosomal enzymes in CHO cells. *The Biochemical Journal*, *478*(12), 2309–2319. https://doi.org/10.1042/BCJ20210015

Chiriaco, M., Farinelli, G., Capo, V., Zonari, E., Scaramuzza, S., Di Matteo, G., Sergi, L. S., Migliavacca, M., Hernandez, R. J., Bombelli, F., Giorda, E., Kajaste-Rudnitski, A., Trono, D., Grez, M., Rossi, P., Finocchi, A., Naldini, L., Gentner, B., & Aiuti, A. (2014). Dual-regulated lentiviral vector for gene therapy of X-linked chronic granulomatosis. *Molecular Therapy : The Journal of the American Society of Gene Therapy*, *22*(8), 1472–1483. https://doi.org/10.1038/MT.2014.87

Corre, G., Seye, A., Frin, S., Ferrand, M., Winkler, K., Luc, C., Dorange, F., Rocca, C. J., & Galy, A. (2022). Lentiviral standards to determine the sensitivity of assays that quantify lentiviral vector copy numbers and genomic insertion sites in cells. *Gene Therapy*, *29*(9), 536–543. https://doi.org/10.1038/S41434-022-00315-8

Coutinho, M. F., Santos, J. I., & Alves, S. (2016). Less Is More: Substrate Reduction Therapy for Lysosomal Storage Disorders. *International Journal of Molecular Sciences*, *17*(7). https://doi.org/10.3390/IJMS17071065

D'auria, L., Reiter, C., Ward, E., Moyano, A. L., Marshall, M. S., Nguyen, D., Scesa, G., Hauck, Z., Van Breemen, R., Givogri, M. I., & Bongarzone, E. R. (2017). Psychosine enhances the shedding of membrane microvesicles: Implications in demyelination in Krabbe's disease. *PloS One*, *12*(5). https://doi.org/10.1371/JOURNAL.PONE.0178103

Das, D., Deb, B., Malakar, A. K., & Chakraborty, S. (2020). Allele frequency analysis of GALC gene causing Krabbe disease in human and its codon usage.

Gene, *747*. https://doi.org/10.1016/J.GENE.2020.144673

Desnick, R. J., & Schuchman, E. H. (2012). Enzyme replacement therapy for lysosomal diseases: lessons from 20 years of experience and remaining challenges. *Annual Review of Genomics and Human Genetics*, *13*, 307–335. https://doi.org/10.1146/ANNUREV-GENOM-090711-163739

Dolcetta, D., Amadio, S., Guerrini, U., Givogri, M. I., Perani, L., Galbiati, F., Sironi, L., Del Carro, U., Roncarolo, M. G., & Bongarzone, E. R. (2005). Myelin deterioration in Twitcher mice: motor evoked potentials and magnetic resonance imaging as in vivo monitoring tools. *Journal of Neuroscience Research*, *81*(4), 597–604. https://doi.org/10.1002/JNR.20574

Donsante, A., Vogler, C., Muzyczka, N., Crawford, J. M., Barker, J., Flotte, T., Campbell-Thompson, M., Daly, T., & Sands, M. S. (2001). Observed incidence of tumorigenesis in long-term rodent studies of rAAV vectors. *Gene Therapy*, *8*(17), 1343–1346. https://doi.org/10.1038/SJ.GT.3301541

Ehmann, P., & Lantos, J. D. (2019). Ethical issues with testing and treatment for Krabbe disease. *Developmental Medicine and Child Neurology*, *61*(12), 1358–1361. https://doi.org/10.1111/dmcn.14258

Ellison, S. M., Liao, A., Wood, S., Taylor, J., Youshani, A. S., Rowlston, S., Parker, H., Armant, M., Biffi, A., Chan, L., Farzaneh, F., Wynn, R., Jones, S. A., Heal, P., Gaspar, H. B., & Bigger, B. W. (2019). Pre-clinical Safety and Efficacy of Lentiviral Vector-Mediated Ex Vivo Stem Cell Gene Therapy for the Treatment of Mucopolysaccharidosis IIIA. *Molecular Therapy. Methods & Clinical Development*, *13*, 399–413. https://doi.org/10.1016/J.OMTM.2019.04.001

Eng, C. M., Guffon, N., Wilcox, W. R., Germain, D. P., Lee, P., Waldek, S., Caplan, L., Linthorst, G. E., & Desnick, R. J. (2001). Safety and efficacy of recombinant human alpha-galactosidase A replacement therapy in Fabry's disease. *The New England Journal of Medicine*, *345*(1), 9–16. https://doi.org/10.1056/NEJM200107053450102

Engel, D. F., Grzyb, A. N., de Oliveira, J., Pötzsch, A., Walker, T. L., Brocardo, P. S., Kempermann, G., & de Bem, A. F. (2019). Impaired adult hippocampal neurogenesis in a mouse model of familial hypercholesterolemia: A role for the LDL receptor and cholesterol metabolism in adult neural precursor cells. *Molecular Metabolism*, *30*, 1–15. https://doi.org/10.1016/J.MOLMET.2019.09.002

Escolar, M. L., Poe, M. D., Provenzale, J. M., Richards, K. C., Allison, J., Wood, S., Wenger, D. A., Pietryga, D., Wall, D., Champagne, M., Morse, R., Krivit, W., Kurtzberg, J., Porter, F. L. E.), & Child, G. (2005). Transplantation of

Umbilical-Cord Blood in Babies with Infantile Krabbe's Disease From the Program for Neurodevelopmen-tal Function in Rare Disorders, Clinical Cen-ter for the Study of Development and Learn-ing (M. *N Engl J Med*, *352*, 2069–2081. http://www.nejm.org

Favret, J. M., Weinstock, N. I., Feltri, M. L., & Shin, D. (2020). Pre-clinical Mouse Models of Neurodegenerative Lysosomal Storage Diseases. *Frontiers in Molecular Biosciences*, *7*. https://doi.org/10.3389/FMOLB.2020.00057

Ferrua, F., Cicalese, M. P., Galimberti, S., Giannelli, S., Dionisio, F., Barzaghi, F., Migliavacca, M., Bernardo, M. E., Calbi, V., Assanelli, A. A., Facchini, M., Fossati, C., Albertazzi, E., Scaramuzza, S., Brigida, I., Scala, S., Basso-Ricci, L., Pajno, R., Casiraghi, M., … Aiuti, A. (2019). Lentiviral haemopoietic stem/progenitor cell gene therapy for treatment of Wiskott-Aldrich syndrome: interim results of a non-randomised, open-label, phase 1/2 clinical study. *The Lancet. Haematology*, *6*(5), e239–e253. https://doi.org/10.1016/S2352-3026(19)30021-3

Filocamo, M., & Morrone, A. (2011). Lysosomal storage disorders: molecular basis and laboratory testing. *Human Genomics*, *5*(3), 156–169. https://doi.org/10.1186/1479-7364-5-3-156

Fujikawa, A., Tsuchiya, K., Katase, S., Kurosaki, Y., & Hachiya, J. (2001). Diffusion-weighted MR imaging of Carmofur-induced leukoencephalopathy. *European Radiology*, *11*(12), 2602–2606. https://doi.org/10.1007/S003300100955

Fuller, M., Meikle, P. J., & Hopwood, J. J. (2006). Epidemiology of lysosomal storage diseases: an overview. *Fabry Disease: Perspectives from 5 Years of FOS*. https://www.ncbi.nlm.nih.gov/books/NBK11603/

Fumagalli, F., Calbi, V., Natali Sora, M. G., Sessa, M., Baldoli, C., Rancoita, P. M. V., Ciotti, F., Sarzana, M., Fraschini, M., Zambon, A. A., Acquati, S., Redaelli, D., Attanasio, V., Miglietta, S., De Mattia, F., Barzaghi, F., Ferrua, F., Migliavacca, M., Tucci, F., … Aiuti, A. (2022). Lentiviral haematopoietic stem-cell gene therapy for early-onset metachromatic leukodystrophy: long-term results from a non-randomised, open-label, phase 1/2 trial and expanded access. *Lancet (London, England)*, *399*(10322), 372–383. https://doi.org/10.1016/S0140-6736(21)02017-1

Futerman, A. H., & Van Meer, G. (2004). The cell biology of lysosomal storage disorders. *Nature Reviews. Molecular Cell Biology*, *5*(7), 554–565. https://doi.org/10.1038/NRM1423

Galbiati, F., Givogri, M. I., Cantuti, L., Lopez Rosas, A., Cao, H., van Breemen, R., & Bongarzone, E. R. (2009). Combined hematopoietic and lentiviral gene-

transfer therapies in newborn Twitcher mice reveal contemporaneous neurodegeneration and demyelination in Krabbe disease. *Journal of Neuroscience Research*, *87*(8), 1748–1759. https://doi.org/10.1002/JNR.22006

Galbiati, F., Basso, V., Cantuti, L., Givogri, M. I., Lopez-Rosas, A., Perez, N., Vasu, C., Cao, H., Van Breemen, R., Mondino, A., & Bongarzone, E. R. (2007). Autonomic denervation of lymphoid organs leads to epigenetic immune atrophy in a mouse model of Krabbe disease. *The Journal of Neuroscience : The Official Journal of the Society for Neuroscience*, *27*(50), 13730–13738. https://doi.org/10.1523/JNEUROSCI.3379-07.2007

Garcia-Ruiz, C., Morales, A., & Fernández-Checa, J. C. (2015). Glycosphingolipids and cell death: one aim, many ways. *Apoptosis : An International Journal on Programmed Cell Death*, *20*(5), 607–620. https://doi.org/10.1007/S10495-015-1092-6

Garcia-Segura, L. M., Rodriguez, J. R., & Torres-Aleman, I. (1997). Localization of the insulin-like growth factor I receptor in the cerebellum and hypothalamus of adult rats: an electron microscopic study. *Journal of Neurocytology*, *26*(7), 479–490. https://doi.org/10.1023/A:1018581407804

Gentner, B., Tucci, F., Galimberti, S., Fumagalli, F., De Pellegrin, M., Silvani, P., Camesasca, C., Pontesilli, S., Darin, S., Ciotti, F., Sarzana, M., Consiglieri, G., Filisetti, C., Forni, G., Passerini, L., Tomasoni, D., Cesana, D., Calabria, A., Spinozzi, G., … Bernardo, M.-E. (2021). Hematopoietic Stem- and Progenitor-Cell Gene Therapy for Hurler Syndrome. *The New England Journal of Medicine*, *385*(21), 1929–1940. https://doi.org/10.1056/NEJMOA2106596

Gentner, B., Visigalli, I., Hiramatsu, H., Lechman, E., Ungari, S., Giustacchini, A., Schira, G., Amendola, M., Quattrini, A., Martino, S., Orlacchio, A., Dick, J. E., Biffi, A., & Naldini, L. (2010). Identification of hematopoietic stem cell-specific miRNAs enables gene therapy of globoid cell leukodystrophy. *Science Translational Medicine*, *2*(58). https://doi.org/10.1126/SCITRANSLMED.3001522

Giacomini, A., Ackermann, M., Belleri, M., Coltrini, D., Nico, B., Ribatti, D., Konerding, M. A., Presta, M., & Righi, M. (2015). Brain angioarchitecture and intussusceptive microvascular growth in a murine model of Krabbe disease. *Angiogenesis*, *18*(4), 499–510. https://doi.org/10.1007/S10456-015-9481-6

Gieselmann, V. (2005). What can cell biology tell us about heterogeneity in lysosomal storage diseases? *Acta Paediatrica (Oslo, Norway : 1992). Supplement*, *94*(447), 80–86. https://doi.org/10.1111/J.1651-

2227.2005.TB02118.X

Gillmore, J. D., Gane, E., Taubel, J., Kao, J., Fontana, M., Maitland, M. L., Seitzer, J., O'Connell, D., Walsh, K. R., Wood, K., Phillips, J., Xu, Y., Amaral, A., Boyd, A. P., Cehelsky, J. E., McKee, M. D., Schiermeier, A., Harari, O., Murphy, A., … Lebwohl, D. (2021). CRISPR-Cas9 In Vivo Gene Editing for Transthyretin Amyloidosis. *The New England Journal of Medicine*, *385*(6), 493–502. https://doi.org/10.1056/NEJMOA2107454

Giugliani, R., Giugliani, L., De Oliveira Poswar, F., Donis, K. C., Corte, A. D., Schmidt, M., Boado, R. J., Nestrasil, I., Nguyen, C., Chen, S., & Pardridge, W. M. (2018). Neurocognitive and somatic stabilization in pediatric patients with severe Mucopolysaccharidosis Type I after 52 weeks of intravenous brain-penetrating insulin receptor antibody-iduronidase fusion protein (valanafusp alpha): an open label phase 1-2 trial. *Orphanet Journal of Rare Diseases*, *13*(1). https://doi.org/10.1186/S13023-018-0849-8

Giugliani, R., Vairo, F., Kubaski, F., Poswar, F., Riegel, M., Baldo, G., & Saute, J. A. (2018). Neurological manifestations of lysosomal disorders and emerging therapies targeting the CNS. *The Lancet. Child & Adolescent Health*, *2*(1), 56–68. https://doi.org/10.1016/S2352-4642(17)30087-1

Gleitz, H. F., Liao, A. Y., Cook, J. R., Rowlston, S. F., Forte, G. M., D'Souza, Z., O'Leary, C., Holley, R. J., & Bigger, B. W. (2018). Brain-targeted stem cell gene therapy corrects mucopolysaccharidosis type II via multiple mechanisms. *EMBO Molecular Medicine*, *10*(7). https://doi.org/10.15252/EMMM.201708730

Goertsen, D., Flytzanis, N. C., Goeden, N., Chuapoco, M. R., Cummins, A., Chen, Y., Fan, Y., Zhang, Q., Sharma, J., Duan, Y., Wang, L., Feng, G., Chen, Y., Ip, N. Y., Pickel, J., & Gradinaru, V. (2022). AAV capsid variants with brain-wide transgene expression and decreased liver targeting after intravenous delivery in mouse and marmoset. *Nature Neuroscience*, *25*(1), 106–115. https://doi.org/10.1038/S41593-021-00969-4

Gong, Y., Berenson, A., Laheji, F., Gao, G., Wang, D., Ng, C., Volak, A., Kok, R., Kreouzis, V., Dijkstra, I. M., Kemp, S., Maguire, C. A., & Eichler, F. (2019). Intrathecal Adeno-Associated Viral Vector-Mediated Gene Delivery for Adrenomyeloneuropathy. *Human Gene Therapy*, *30*(5), 544–555. https://doi.org/10.1089/HUM.2018.079

Gonzalez, E. A., & Baldo, G. (2017). Gene Therapy for Lysosomal Storage Disorders. *Http://Dx.Doi.Org/10.1177/2326409816689786*, *5*, 232640981668978. https://doi.org/10.1177/2326409816689786

Goto, D., Okimoto, T., Ono, M., Shimotsu, H., Abe, K., Tsujita, Y., & Kuwano, M.

(1997). Upregulation of low density lipoprotein receptor by gemfibrozil, a hypolipidemic agent, in human hepatoma cells through stabilization of mRNA transcripts. *Arteriosclerosis, Thrombosis, and Vascular Biology*, *17*(11), 2707–2712. https://doi.org/10.1161/01.ATV.17.11.2707

Gowrishankar, S., Cologna, S. M., Givogri, M. I., & Bongarzone, E. R. (2020). Deregulation of signalling in genetic conditions affecting the lysosomal metabolism of cholesterol and galactosyl-sphingolipids. *Neurobiology of Disease*, *146*. https://doi.org/10.1016/J.NBD.2020.105142

Gray, S. J., Nagabhushan Kalburgi, S., McCown, T. J., & Jude Samulski, R. (2013). Global CNS gene delivery and evasion of anti-AAV-neutralizing antibodies by intrathecal AAV administration in non-human primates. *Gene Therapy*, *20*(4), 450–459. https://doi.org/10.1038/GT.2012.101

Graziano, A. C. E., & Cardile, V. (2015). History, genetic, and recent advances on Krabbe disease. *Gene*, *555*(1), 2–13. https://doi.org/10.1016/J.GENE.2014.09.046

Graziano, A. C. E., Pannuzzo, G., Avola, R., & Cardile, V. (2016). Chaperones as potential therapeutics for Krabbe disease. *Journal of Neuroscience Research*, *94*(11), 1220–1230. https://doi.org/10.1002/JNR.23755

Gritti, A., Molin, M. D., Foroni, C., & Bonfanti, L. (2009). Effects of developmental age, brain region, and time in culture on long-term proliferation and multipotency of neural stem cell populations. *The Journal of Comparative Neurology*, *517*(3), 333–349. https://doi.org/10.1002/CNE.22153

Grosso, A. Del, Galliani, M., Angella, L., Santi, M., Tonazzini, I., Parlanti, G., Signore, G., & Cecchini, M. (2019). Brain-targeted enzyme-loaded nanoparticles: A breach through the blood-brain barrier for enzyme replacement therapy in Krabbe disease. *Science Advances*, *5*(11). https://doi.org/10.1126/SCIADV.AAX7462

Güler-Gane, G., Kidd, S., Sridharan, S., Vaughan, T. J., Wilkinson, T. C. I., & Tigue, N. J. (2016). Overcoming the Refractory Expression of Secreted Recombinant Proteins in Mammalian Cells through Modification of the Signal Peptide and Adjacent Amino Acids. *PloS One*, *11*(5). https://doi.org/10.1371/JOURNAL.PONE.0155340

Gurda, B. L., & Vite, C. H. (2019). Large animal models contribute to the development of therapies for central and peripheral nervous system dysfunction in patients with lysosomal storage diseases. *Human Molecular Genetics*, *28*(R1), R119–R131. https://doi.org/10.1093/HMG/DDZ127

Haq, E., Contreras, M. A., Giri, S., Singh, I., & Singh, A. K. (2006). Dysfunction of

peroxisomes in twitcher mice brain: a possible mechanism of psychosine-induced disease. *Biochemical and Biophysical Research Communications*, *343*(1), 229–238. https://doi.org/10.1016/J.BBRC.2006.02.131

Haq, E., Giri, S., Singh, I., & Singh, A. K. (2003). Molecular mechanism of psychosine-induced cell death in human oligodendrocyte cell line. *Journal of Neurochemistry*, *86*(6), 1428–1440. https://doi.org/10.1046/J.1471-4159.2003.01941.X

Hawkins-Salsbury, J. A., Shea, L., Jiang, X., Hunter, D. A., Miguel Guzman, A., Reddy, A. S., Qin, E. Y., Li, Y., Gray, S. J., Ory, D. S., & Sands, M. S. (2015). Mechanism-based combination treatment dramatically increases therapeutic efficacy in murine globoid cell leukodystrophy. *The Journal of Neuroscience : The Official Journal of the Society for Neuroscience*, *35*(16), 6495–6505. https://doi.org/10.1523/JNEUROSCI.4199-14.2015

Hayashi, T., & Su, T. P. (2004). Sigma-1 receptors at galactosylceramide-enriched lipid microdomains regulate oligodendrocyte differentiation. *Proceedings of the National Academy of Sciences of the United States of America*, *101*(41), 14949–14954. https://doi.org/10.1073/PNAS.0402890101

Hemsley, K. M., & Hopwood, J. J. (2010). Lessons learnt from animal models: pathophysiology of neuropathic lysosomal storage disorders. *Journal of Inherited Metabolic Disease*, *33*(4), 363–371. https://doi.org/10.1007/S10545-010-9078-6

Hill, C. H., Cook, G. M., Spratley, S. J., Fawke, S., Graham, S. C., & Deane, J. E. (2018). The mechanism of glycosphingolipid degradation revealed by a GALC-SapA complex structure. *Nature Communications*, *9*(1). https://doi.org/10.1038/S41467-017-02361-Y

Hill, C. H., Graham, S. C., Read, R. J., & Deane, J. E. (2013). Structural snapshots illustrate the catalytic cycle of β-galactocerebrosidase, the defective enzyme in Krabbe disease. *Proceedings of the National Academy of Sciences of the United States of America*, *110*(51), 20479–20484. https://doi.org/10.1073/PNAS.1311990110

Hill, C. H., Viuff, A. H., Spratley, S. J., Salamone, S., Christensen, S. H., Read, R. J., Moriarty, N. W., Jensen, H. H., & Deane, J. E. (2015). Azasugar inhibitors as pharmacological chaperones for Krabbe disease. *Chemical Science*, *6*(5), 3075–3086. https://doi.org/10.1039/C5SC00754B

Hinderer, C., Katz, N., Buza, E. L., Dyer, C., Goode, T., Bell, P., Richman, L. K., & Wilson, J. M. (2018). Severe Toxicity in Nonhuman Primates and Piglets Following High-Dose Intravenous Administration of an Adeno-Associated Virus

Vector Expressing Human SMN. *Human Gene Therapy*, *29*(3), 285–298. https://doi.org/10.1089/HUM.2018.015

Hoffmann, G. F., Lindner, M., & Loeber, J. G. (2014). 50 years of newborn screening. *Journal of Inherited Metabolic Disease*, *37*(2), 163–164. https://doi.org/10.1007/S10545-014-9688-5

Hohsfield, L. A., Najafi, A. R., Ghorbanian, Y., Soni, N., Crapser, J. D., Figueroa Velez, D. X., Jiang, S., Royer, S. E., Kim, S. J., Henningfield, C. M., Anderson, A. J., Gandhi, S. P., Mortazavi, A., Inlay, M. A., & Green, K. N. (2021). Subventricular zone/white matter microglia reconstitute the empty adult microglial niche in a dynamic wave. *ELife*, *10*. https://doi.org/10.7554/ELIFE.66738

Hordeaux, J., Buza, E. L., Dyer, C., Goode, T., Mitchell, T. W., Richman, L., Denton, N., Hinderer, C., Katz, N., Schmid, R., Miller, R., Choudhury, G. R., Horiuchi, M., Nambiar, K., Yan, H., Li, M., & Wilson, J. M. (2020). Adeno-Associated Virus-Induced Dorsal Root Ganglion Pathology. *Human Gene Therapy*, *31*(15–16), 808–818. https://doi.org/10.1089/HUM.2020.167

Hordeaux, J., Hinderer, C., Goode, T., Katz, N., Buza, E. L., Bell, P., Calcedo, R., Richman, L. K., & Wilson, J. M. (2018). Toxicology Study of Intra-Cisterna Magna Adeno-Associated Virus 9 Expressing Human Alpha-L-Iduronidase in Rhesus Macaques. *Molecular Therapy. Methods & Clinical Development*, *10*, 79–88. https://doi.org/10.1016/J.OMTM.2018.06.003

Hordeaux, J., Jeffrey, B. A., Jian, J., Choudhury, G. R., Michalson, K., Mitchell, T. W., Buza, E. L., Chichester, J., Dyer, C., Bagel, J., Vite, C. H., Bradbury, A. M., & Wilson, J. M. (2022). Efficacy and Safety of a Krabbe Disease Gene Therapy. *Human Gene Therapy*, *33*(9–10), 499–517. https://doi.org/10.1089/HUM.2021.245

Hossain, M. A., Higaki, K., Saito, S., Ohno, K., Sakuraba, H., Nanba, E., Suzuki, Y., Ozono, K., & Sakai, N. (2015). Chaperone therapy for Krabbe disease: potential for late-onset GALC mutations. *Journal of Human Genetics*, *60*(9), 539–545. https://doi.org/10.1038/JHG.2015.61

Hu, P., Li, Y., Nikolaishvili-Feinberg, N., Scesa, G., Bi, Y., Pan, D., Moore, D., Bongarzone, E. R., Sands, M. S., Miller, R., & Kafri, T. (2016). Hematopoietic Stem cell transplantation and lentiviral vector-based gene therapy for Krabbe's disease: Present convictions and future prospects. *Journal of Neuroscience Research*, *94*(11), 1152–1168. https://doi.org/10.1002/JNR.23847

Huang, Y., Xu, Z., Xiong, S., Sun, F., Qin, G., Hu, G., Wang, J., Zhao, L., Liang, Y. X., Wu, T., Lu, Z., Humayun, M. S., So, K. F., Pan, Y., Li, N., Yuan, T. F., Rao,

Y., & Peng, B. (2018). Repopulated microglia are solely derived from the proliferation of residual microglia after acute depletion. *Nature Neuroscience*, *21*(4), 530–540. https://doi.org/10.1038/S41593-018-0090-8

Ida, H., Umezawa, F., Kasai, E., Eto, Y., & Maekawa, K. (1982). An accumulation of galactocerebroside in kidney from mouse globoid cell leukodystrophy (twitcher). *Biochemical and Biophysical Research Communications*, *109*(3), 634–638. https://doi.org/10.1016/0006-291X(82)91987-8

Igisu, H., Takahashi, H., Suzuki, K., & Suzuki, K. (1983). Abnormal accumulation of galactosylceramide in the kidney of twitcher mouse. *Biochemical and Biophysical Research Communications*, *110*(3), 940–944. https://doi.org/10.1016/0006-291X(83)91053-7

Ijichi, K., Brown, G. D., Moore, C. S., Lee, J. P., Winokur, P. N., Pagarigan, R., Snyder, E. Y., Bongarzone, E. R., & Crocker, S. J. (2013). MMP-3 mediates psychosine-induced globoid cell formation: implications for leukodystrophy pathology. *Glia*, *61*(5), 765–777. https://doi.org/10.1002/GLIA.22471

Issa, S. S., Shaimardanova, A. A., Valiullin, V. V., Rizvanov, A. A., & Solovyeva, V. V. (2022). Mesenchymal Stem Cell-Based Therapy for Lysosomal Storage Diseases and Other Neurodegenerative Disorders. *Frontiers in Pharmacology*, *13*. https://doi.org/10.3389/FPHAR.2022.859516

Itoh, M., Hayashi, M., Fujioka, Y., Nagashima, K., Morimatsu, Y., & Matsuyama, H. (2002). Immunohistological study of globoid cell leukodystrophy. *Brain and Development*, *24*(5), 284–290. https://doi.org/10.1016/S0387-7604(02)00057-8

Jatana, M., Giri, S., & Singh, A. K. (2002). Apoptotic positive cells in Krabbe brain and induction of apoptosis in rat C6 glial cells by psychosine. *Neuroscience Letters*, *330*(2), 183–187. https://doi.org/10.1016/S0304-3940(02)00655-9

Jefferies, W. A., Brandon, M. R., Hunt, S. V., Williams, A. F., Gatter, K. C., & Mason, D. Y. (1984). Transferrin receptor on endothelium of brain capillaries. *Nature*, *312*(5990), 162–163. https://doi.org/10.1038/312162A0

Jones, R. J., Wagner, J. E., Celano, P., Zicha, M. S., & Sharkis, S. J. (1990). Separation of pluripotent haematopoietic stem cells from spleen colony-forming cells. *Nature*, *347*(6289), 188–189. https://doi.org/10.1038/347188A0

Jones, S. A., Cheillan, D., Chakrapani, A., Church, H. J., Heales, S., Wu, T. H. Y., Morton, G., Roberts, P., Sluys, E. F., & Burlina, A. (2022). Application of a Novel Algorithm for Expanding Newborn Screening for Inherited Metabolic Disorders across Europe. *International Journal of Neonatal Screening*, *8*(1).

https://doi.org/10.3390/IJNS8010020

Jones, B. V, Barron, T. F., & Towfighi, J. (1999). Optic Nerve Enlargement in Krabbe's Disease. *AJNR Am J Neuroradiol*, *20*, 1228–1231.

Kaeppel, C., Beattie, S. G., Fronza, R., Van Logtenstein, R., Salmon, F., Schmidt, S., Wolf, S., Nowrouzi, A., Glimm, H., Von Kalle, C., Petry, H., Gaudet, D., & Schmidt, M. (2013). A largely random AAV integration profile after LPLD gene therapy. *Nature Medicine*, *19*(7), 889–891. https://doi.org/10.1038/NM.3230

Kanazawa, T., Nakamura, S., Momoi, M., Yamaji, T., Takematsu, H., Yano, H., Sabe, H., Yamamoto, A., Kawasaki, T., & Kozutsumi, Y. (2000). Inhibition of cytokinesis by a lipid metabolite, psychosine. *The Journal of Cell Biology*, *149*(4), 943–950. https://doi.org/10.1083/JCB.149.4.943

Knappskog, S., Ravneberg, H., Gjerdrum, C., Trösße, C., Stern, B., & Pryme, I. F. (2007). The level of synthesis and secretion of Gaussia princeps luciferase in transfected CHO cells is heavily dependent on the choice of signal peptide. *Journal of Biotechnology*, *128*(4), 705–715. https://doi.org/10.1016/J.JBIOTEC.2006.11.026

Kobayashi, T., Shinnoh, N., Goto, I., & Kuroiwa, Y. (1985). Hydrolysis of galactosylceramide is catalyzed by two genetically distinct acid beta-galactosidases. *The Journal of Biological Chemistry*, *260*(28), 14982–14987. https://doi.org/10.1016/s0021-9258(18)95690-5

Kobayashi, T., Yamanaka, T., Jacobs, J. M., Teixeira, F., & Suzuki, K. (1980). The Twitcher mouse: an enzymatically authentic model of human globoid cell leukodystrophy (Krabbe disease). *Brain Research*, *202*(2), 479–483. https://doi.org/10.1016/0006-8993(80)90159-6

Kober, L., Zehe, C., & Bode, J. (2013). Optimized signal peptides for the development of high expressing CHO cell lines. *Biotechnology and Bioengineering*, *110*(4), 1164–1173. https://doi.org/10.1002/BIT.24776

Kofler, J., Beltran-Quintero, M. L., Rugari, A., Zuccoli, G., Klotz, S., & Escolar, M. L. (2022). Improved Brain Pathology and Progressive Peripheral Neuropathy in a 15 Year Old Survivor of Infantile Krabbe Disease Treated With Umbilical Cord Transplantation. *Frontiers in Molecular Neuroscience*, *15*. https://doi.org/10.3389/FNMOL.2022.888231

Kozutsumi, Y., Kanazawa, T., Sun, Y., Yamaji, T., Yamamoto, H., & Takematsu, H. (2002). Sphingolipids involved in the induction of multinuclear cell formation. *Biochimica et Biophysica Acta - Molecular and Cell Biology of Lipids*, *1582*(1–3), 138–143. https://doi.org/10.1016/S1388-1981(02)00148-8

Krabbe, K. (1916). A new familial, infantule form of diffuse brain-sclerosis. *Brain*,

39(1–2), 74–114. https://doi.org/10.1093/BRAIN/39.1-2.74

Krivit, W., Shapiro, E. G., Peters, C., Wagner, J. E., Cornu, G., Kurtzberg, J., Wenger, D. A., Kolodny, E. H., Vanier, M. T., Loes, D. J., Dusenbery, K., & Lockman, L. A. (1998). Hematopoietic stem-cell transplantation in globoid-cell leukodystrophy. *The New England Journal of Medicine*, *338*(16), 1119–1127. https://doi.org/10.1056/NEJM199804163381605

Kurata, T., Miyazaki, K., Morimoto, N., Kawai, H., Ohta, Y., Ikeda, Y., & Abe, K. (2013). Atorvastatin and pitavastatin reduce oxidative stress and improve IR/LDL-R signals in Alzheimer's disease. *Neurological Research*, *35*(2), 193–205. https://doi.org/10.1179/1743132812Y.0000000127

Kwon, J. M., Matern, D., Kurtzberg, J., Wrabetz, L., Gelb, M. H., Wenger, D. A., Ficicioglu, C., Waldman, A. T., Burton, B. K., Hopkins, P. V, & Orsini, J. J. (2018). Consensus guidelines for newborn screening, diagnosis and treatment of infantile Krabbe disease. In *Orphanet Journal of Rare Diseases* (Vol. 13, Issue 1). BioMed Central Ltd. https://doi.org/10.1186/s13023-018-0766-x

Lattanzi, A., Neri, M., Maderna, C., di Girolamo, I., Martino, S., Orlacchio, A., Amendola, M., Naldini, L., & Gritti, A. (2010). Widespread enzymatic correction of CNS tissues by a single intracerebral injection of therapeutic lentiviral vector in leukodystrophy mouse models. *Human Molecular Genetics*, *19*(11), 2208–2227. https://doi.org/10.1093/HMG/DDQ099

Lattanzi, A., Salvagno, C., Maderna, C., Benedicenti, F., Morena, F., Kulik, W., Naldini, L., Montini, E., Martino, S., & Gritti, A. (2014). Therapeutic benefit of lentiviral-mediated neonatal intracerebral gene therapy in a mouse model of globoid cell leukodystrophy. *Human Molecular Genetics*, *23*(12), 3250–3268. https://doi.org/10.1093/HMG/DDU034

Leal, A. F., Espejo-Mojica, A. J., Sánchez, O. F., Ramírez, C. M., Reyes, L. H., Cruz, J. C., & Almériga-Díaz, C. J. (2020). Lysosomal storage diseases: current therapies and future alternatives. *Journal of Molecular Medicine (Berlin, Germany)*, *98*(7), 931–946. https://doi.org/10.1007/S00109-020-01935-6

Lee, W. C., Courtenay, A., Troendle, F. J., Stallings-Mann, M. L., Dickey, C. A., Delucia, M. W., Dickson, D. W., & Eckman, C. B. (2005). Enzyme replacement therapy results in substantial improvements in early clinical phenotype in a mouse model of globoid cell leukodystrophy. *FASEB Journal : Official Publication of the Federation of American Societies for Experimental Biology*, *19*(11), 1549–1551. https://doi.org/10.1096/FJ.05-3826FJE

Lee, W. C., Kang, D., Causevic, E., Herdt, A. R., Eckman, E. A., & Eckman, C. B. (2010). Molecular characterization of mutations that cause globoid cell

leukodystrophy and pharmacological rescue using small molecule chemical chaperones. *The Journal of Neuroscience : The Official Journal of the Society for Neuroscience*, *30*(16), 5489–5497. https://doi.org/10.1523/JNEUROSCI.6383-09.2010

Lee, W. C., Tsoi, Y. K., Dickey, C. A., DeLucia, M. W., Dickson, D. W., & Eckman, C. B. (2006). Suppression of galactosylceramidase (GALC) expression in the twitcher mouse model of globoid cell leukodystrophy (GLD) is caused by nonsense-mediated mRNA decay (NMD). *Neurobiology of Disease*, *23*(2), 273–280. https://doi.org/10.1016/J.NBD.2006.03.005

Lee, W. C., Tsoi, Y. K., Troendle, F. J., DeLucia, M. W., Ahmed, Z., Dicky, C. A., Dickson, D. W., & Eckman, C. B. (2007). Single-dose intracerebroventricular administration of galactocerebrosidase improves survival in a mouse model of globoid cell leukodystrophy. *FASEB Journal : Official Publication of the Federation of American Societies for Experimental Biology*, *21*(10), 2520–2527. https://doi.org/10.1096/FJ.06-6169COM

Lenders, M., & Brand, E. (2018). Effects of Enzyme Replacement Therapy and Antidrug Antibodies in Patients with Fabry Disease. *Journal of the American Society of Nephrology : JASN*, *29*(9), 2265–2278. https://doi.org/10.1681/ASN.2018030329

LeVine, S. M., Pedchenko, T. V., Bronshteyn, I. G., & Pinson, D. M. (2000). L-cycloserine slows the clinical and pathological course in mice with globoid cell leukodystrophy (twitcher mice). *Journal of Neuroscience Researchournal of Neuroscience Research*, *60*, 231–236. https://doi.org/10.1002/(SICI)1097-4547(20000415)60:2<231::AID-JNR12>3.0.CO;2-E

LeVine, S. M., & Tsau, S. (2022). Substrate Reduction Therapy for Krabbe Disease: Exploring the Repurposing of the Antibiotic D-Cycloserine. *Frontiers in Pediatrics*, *9*. https://doi.org/10.3389/FPED.2021.807973

Li, M. (2018). Enzyme Replacement Therapy: A Review and Its Role in Treating Lysosomal Storage Diseases. *Pediatric Annals*, *47*(5), e191–e197. https://doi.org/10.3928/19382359-20180424-01

Li, Y., Miller, C. A., Shea, L. K., Jiang, X., Guzman, M. A., Chandler, R. J., Ramakrishnan, S. M., Smith, S. N., Venditti, C. P., Vogler, C. A., Ory, D. S., Ley, T. J., & Sands, M. S. (2021). Enhanced Efficacy and Increased Long-Term Toxicity of CNS-Directed, AAV-Based Combination Therapy for Krabbe Disease. *Molecular Therapy : The Journal of the American Society of Gene Therapy*, *29*(2), 691–701. https://doi.org/10.1016/J.YMTHE.2020.12.031

Li, Y., Xu, Y., Benitez, B. A., Nagree, M. S., Dearborn, J. T., Jiang, X., Guzman, M.

A., Woloszynek, J. C., Giaramita, A., Yip, B. K., Elsbernd, J., Babcock, M. C., Lo, M., Fowler, S. C., Wozniak, D. F., Vogler, C. A., Medin, J. A., Crawford, B. E., & Sands, M. S. (2019). Genetic ablation of acid ceramidase in Krabbe disease confirms the psychosine hypothesis and identifies a new therapeutic target. *Proceedings of the National Academy of Sciences of the United States of America*, *116*(40), 20097–20103. https://doi.org/10.1073/PNAS.1912108116

Liao, H. C., Spacil, Z., Ghomashchi, F., Escolar, M. L., Kurtzberg, J., Orsini, J. J., Turecek, F., Scott, C. R., & Gelb, M. H. (2017). Lymphocyte Galactocerebrosidase Activity by LC-MS/MS for Post-Newborn Screening Evaluation of Krabbe Disease. *Clinical Chemistry*, *63*(8), 1363–1369. https://doi.org/10.1373/CLINCHEM.2016.264952

Liao, P., Gelinas, J., & Sirrs, S. (2014). Phenotypic variability of Krabbe disease across the lifespan. *The Canadian Journal of Neurological Sciences. Le Journal Canadien Des Sciences Neurologiques*, *41*(1), 5–12. https://doi.org/10.1017/S0317167100016188

Lin, D., Donsante, A., Macauley, S., Levy, B., Vogler, C., & Sands, M. S. (2007). Central nervous system-directed AAV2/5-mediated gene therapy synergizes with bone marrow transplantation in the murine model of globoid-cell leukodystrophy. *Molecular Therapy : The Journal of the American Society of Gene Therapy*, *15*(1), 44–52. https://doi.org/10.1038/SJ.MT.6300026

Lin, D., Fantz, C. R., Levy, B., Rafi, M. A., Vogler, C., Wenger, D. A., & Sands, M. S. (2005). AAV2/5 vector expressing galactocerebrosidase ameliorates CNS disease in the murine model of globoid-cell leukodystrophy more efficiently than AAV2. *Molecular Therapy : The Journal of the American Society of Gene Therapy*, *12*(3), 422–430. https://doi.org/10.1016/J.YMTHE.2005.04.019

Linthorst, G. E., Hollak, C. E. M., Donker-Koopman, W. E., Strijland, A., & Aerts, J. M. F. G. (2004). Enzyme therapy for Fabry disease: neutralizing antibodies toward agalsidase alpha and beta. *Kidney International*, *66*(4), 1589–1595. https://doi.org/10.1111/J.1523-1755.2004.00924.X

Luciani, M., Gritti, A., & Meneghini, V. (2020). Human iPSC-Based Models for the Development of Therapeutics Targeting Neurodegenerative Lysosomal Storage Diseases. *Frontiers in Molecular Biosciences*, *7*. https://doi.org/10.3389/FMOLB.2020.00224

Luddi, A., Gori, M., Crifasi, L., Marrocco, C., Belmonte, G., Costantino-Ceccarini, E., & Piomboni, P. (2017). Impaired spermatogenesis in the twitcher mouse: A morphological evaluation from the seminiferous tubules to epididymal transit.

Systems Biology in Reproductive Medicine, *63*(2), 77–85. https://doi.org/10.1080/19396368.2016.1271918

Luzi, P., Rafi, M. A., Victoria, T., Baskin, G. B., & Wenger, D. A. (1997). Characterization of the rhesus monkey galactocerebrosidase (GALC) cDNA and gene and identification of the mutation causing globoid cell leukodystrophy (Krabbe disease) in this primate. *Genomics*, *42*(2), 319–324. https://doi.org/10.1006/GENO.1997.4744

Luzi, P., Rafi, M. A., & Wenger, D. A. (1995a). Structure and organization of the human galactocerebrosidase (GALC) gene. *Genomics*, *26*(2), 407–409. https://doi.org/10.1016/0888-7543(95)80230-J

Luzi, P., Rafi, M. A., & Wenger, D. A. (1995b). Characterization of the large deletion in the GALC gene found in patients with Krabbe disease. *Human Molecular Genetics*, *4*(12), 2335–2338. https://doi.org/10.1093/HMG/4.12.2335

Luzi, P., Rafi, M. A., Zaka, M., Curtis, M., Vanier, M. T., & Wenger, D. A. (2001). Generation of a mouse with low galactocerebrosidase activity by gene targeting: a new model of globoid cell leukodystrophy (Krabbe disease). *Molecular Genetics and Metabolism*, *73*(3), 211–223. https://doi.org/10.1006/MGME.2001.3194

Macarov, M., Zlotogora, J., Meiner, V., Khatib, Z., Sury, V., Mengistu, G., Bargal, R., Shmueli, E., Meidan, B., & Zeigler, M. (2011). Genetic screening for Krabbe disease: Learning from the past and looking to the future. *American Journal of Medical Genetics, Part A*, *155*(3), 574–576. https://doi.org/10.1002/ajmg.a.33815

Mangiameli, E., Cecchele, A., Morena, F., Sanvito, F., Matafora, V., Cattaneo, A., della Volpe, L., Gnani, D., Paulis, M., Susani, L., Martino, S., Di Micco, R., Bachi, A., & Gritti, A. (2021). Human iPSC-based neurodevelopmental models of globoid cell leukodystrophy uncover patient- and cell type-specific disease phenotypes. *Stem Cell Reports*, *16*(6), 1478–1495. https://doi.org/10.1016/J.STEMCR.2021.04.011

Marcus, J., & Popko, B. (2002). Galactolipids are molecular determinants of myelin development and axo-glial organization. *Biochimica et Biophysica Acta - General Subjects*, *1573*(3), 406–413. https://doi.org/10.1016/S0304-4165(02)00410-5

Markmann, S., Thelen, M., Cornils, K., Schweizer, M., Brocke-Ahmadinejad, N., Willnow, T., Heeren, J., Gieselmann, V., Braulke, T., & Kollmann, K. (2015). Lrp1/LDL Receptor Play Critical Roles in Mannose 6-Phosphate-Independent Lysosomal Enzyme Targeting. *Traffic (Copenhagen, Denmark)*, *16*(7), 743–

759. https://doi.org/10.1111/TRA.12284

Marktel, S., Scaramuzza, S., Cicalese, M. P., Giglio, F., Galimberti, S., Lidonnici, M. R., Calbi, V., Assanelli, A., Bernardo, M. E., Rossi, C., Calabria, A., Milani, R., Gattillo, S., Benedicenti, F., Spinozzi, G., Aprile, A., Bergami, A., Casiraghi, M., Consiglieri, G., … Ferrari, G. (2019). Intrabone hematopoietic stem cell gene therapy for adult and pediatric patients affected by transfusion-dependent ß-thalassemia. *Nature Medicine*, *25*(2), 234–241. https://doi.org/10.1038/S41591-018-0301-6

Marques, A. R. A., & Saftig, P. (2019). Lysosomal storage disorders - challenges, concepts and avenues for therapy: beyond rare diseases. *Journal of Cell Science*, *132*(2). https://doi.org/10.1242/JCS.221739

Marshall, M. S., Issa, Y., Jakubauskas, B., Stoskute, M., Elackattu, V., Marshall, J. N., Bogue, W., Nguyen, D., Hauck, Z., Rue, E., Karumuthil-Melethil, S., Zaric, V., Bosland, M., van Breemen, R. B., Givogri, M. I., Gray, S. J., Crocker, S. J., & Bongarzone, E. R. (2018). Long-Term Improvement of Neurological Signs and Metabolic Dysfunction in a Mouse Model of Krabbe's Disease after Global Gene Therapy. *Molecular Therapy : The Journal of the American Society of Gene Therapy*, *26*(3), 874–889. https://doi.org/10.1016/J.YMTHE.2018.01.009

Martino, G., & Pluchino, S. (2006). The therapeutic potential of neural stem cells. *Nature Reviews. Neuroscience*, *7*(5), 395–406. https://doi.org/10.1038/NRN1908

Martino, S., Tiribuzi, R., Tortori, A., Conti, D., Visigalli, I., Lattanzi, A., Biffi, A., Gritti, A., & Orlacchio, A. (2009). Specific determination of β-galactocerebrosidase activity via competitive inhibition of β-galactosidase. *Clinical Chemistry*, *55*(3), 541–548. https://doi.org/10.1373/clinchem.2008.115873

Marzolo, M. P., & Farfán, P. (2011). New insights into the roles of megalin/LRP2 and the regulation of its functional expression. *Biological Research*, *44*(1), 89–105. https://doi.org/10.4067/S0716-97602011000100012

Massaro, G., Geard, A. F., Liu, W., Coombe-tennant, O., Waddington, S. N., Baruteau, J., Gissen, P., & Rahim, A. A. (2021). Gene Therapy for Lysosomal Storage Disorders: Ongoing Studies and Clinical Development. *Biomolecules*, *11*(4). https://doi.org/10.3390/BIOM11040611

Matsuda, J., Vanier, M. T., Saito, Y., Tohyama, J., Suzuki, K., & Suzuki, K. (2001). A mutation in the saposin A domain of the sphingolipid activator protein (prosaposin) gene results in a late-onset, chronic form of globoid cell leukodystrophy in the mouse. *Human Molecular Genetics*, *10*(11), 1191–1199.

https://doi.org/10.1093/HMG/10.11.1191

Matthes, F., Andersson, C., Stein, A., Eistrup, C., Fogh, J., Gieselmann, V., Wenger, D. A., & Matzner, U. (2015). Enzyme replacement therapy of a novel humanized mouse model of globoid cell leukodystrophy. *Experimental Neurology*, *271*, 36–45. https://doi.org/10.1016/J.EXPNEUROL.2015.04.020

Meisingset, T. W., Ricca, A., Neri, M., Sonnewald, U., & Gritti, A. (2013). Region- and age-dependent alterations of glial-neuronal metabolic interactions correlate with CNS pathology in a mouse model of globoid cell leukodystrophy. *Journal of Cerebral Blood Flow and Metabolism : Official Journal of the International Society of Cerebral Blood Flow and Metabolism*, *33*(7), 1127–1137. https://doi.org/10.1038/JCBFM.2013.64

Meneghini, V., Lattanzi, A., Tiradani, L., Bravo, G., Morena, F., Sanvito, F., Calabria, A., Bringas, J., Fisher-Perkins, J. M., Dufour, J. P., Baker, K. C., Doglioni, C., Montini, E., Bunnell, B. A., Bankiewicz, K., Martino, S., Naldini, L., & Gritti, A. (2016). Pervasive supply of therapeutic lysosomal enzymes in the CNS of normal and Krabbe-affected non-human primates by intracerebral lentiviral gene therapy. *EMBO Molecular Medicine*, *8*(5), 489–510. https://doi.org/10.15252/EMMM.201505850

Mikulka, C. R., & Sands, M. S. (2016). Treatment for Krabbe's disease: Finding the combination. *Journal of Neuroscience Research*, *94*(11), 1126–1137. https://doi.org/10.1002/JNR.23822

Milani, M., Canepari, C., Liu, T., Biffi, M., Russo, F., Plati, T., Curto, R., Patarroyo-White, S., Drager, D., Visigalli, I., Brombin, C., Albertini, P., Follenzi, A., Ayuso, E., Mueller, C., Annoni, A., Naldini, L., & Cantore, A. (2022). Liver-directed lentiviral gene therapy corrects hemophilia A mice and achieves normal-range factor VIII activity in non-human primates. *Nature Communications*, *13*(1). https://doi.org/10.1038/S41467-022-30102-3

Miranda, C. O., Teixeira, C. A., Liz, M. A., Sousa, V. F., Franquinho, F., Forte, G., Di Nardo, P., Pinto-Do-Ó, P., & Sousa, M. M. (2011). Systemic delivery of bone marrow-derived mesenchymal stromal cells diminishes neuropathology in a mouse model of Krabbe's disease. *Stem Cells (Dayton, Ohio)*, *29*(11), 1738–1751. https://doi.org/10.1002/STEM.724

Modlich, U., Navarro, S., Zychlinski, D., Maetzig, T., Knoess, S., Brugman, M. H., Schambach, A., Charrier, S., Galy, A., Thrasher, A. J., Bueren, J., & Baum, C. (2009). Insertional transformation of hematopoietic cells by self-inactivating lentiviral and gammaretroviral vectors. *Molecular Therapy : The Journal of the American Society of Gene Therapy*, *17*(11), 1919–1928.

https://doi.org/10.1038/MT.2009.179

Molino, Y., David, M., Varini, K., Jabès, F., Gaudin, N., Fortoul, A., Bakloul, K., Masse, M., Bernard, A., Drobecq, L., Lécorché, P., Temsamani, J., Jacquot, G., & Khrestchatisky, M. (2017). Use of LDL receptor-targeting peptide vectors for in vitro and in vivo cargo transport across the blood-brain barrier. *FASEB Journal : Official Publication of the Federation of American Societies for Experimental Biology*, *31*(5), 1807–1827. https://doi.org/10.1096/FJ.201600827R

Montini, E., Cesana, D., Schmidt, M., Sanvito, F., Bartholomae, C. C., Ranzani, M., Benedicenti, F., Sergi, L. S., Ambrosi, A., Ponzoni, M., Doglioni, C., Di Serio, C., Von Kalle, C., & Naldini, L. (2009). The genotoxic potential of retroviral vectors is strongly modulated by vector design and integration site selection in a mouse model of HSC gene therapy. *The Journal of Clinical Investigation*, *119*(4), 964–975. https://doi.org/10.1172/JCI37630

Morimoto, H., Kida, S., Yoden, E., Kinoshita, M., Tanaka, N., Yamamoto, R., Koshimura, Y., Takagi, H., Takahashi, K., Hirato, T., Minami, K., & Sonoda, H. (2021). Clearance of heparan sulfate in the brain prevents neurodegeneration and neurocognitive impairment in MPS II mice. *Molecular Therapy : The Journal of the American Society of Gene Therapy*, *29*(5), 1853–1861. https://doi.org/10.1016/J.YMTHE.2021.01.027

Mullin, M. J., Wilkinson, C., Hiles, I., & Smith, K. J. (2021). Improved secretion of recombinant human IL-25 in HEK293 cells using a signal peptide-pro-peptide domain derived from Trypsin-1. *Biotechnology Letters*, *43*(4), 757–765. https://doi.org/10.1007/S10529-020-03072-Z

Nagano, S., Yamada, T., Shinnoh, N., Furuya, H., Taniwaki, T., & Kira, J. I. (1998). Expression and processing of recombinant human galactosylceramidase. *Clinica Chimica Acta*, *276*(1), 53–61. https://doi.org/10.1016/S0009-8981(98)00095-3

Naldini, L. (2019). Genetic engineering of hematopoiesis: current stage of clinical translation and future perspectives. *EMBO Molecular Medicine*, *11*(3). https://doi.org/10.15252/EMMM.201809958

Neri, M., Ricca, A., Di Girolamo, I., Alcala'-Franco, B., Cavazzin, C., Orlacchio, A., Martino, S., Naldini, L., & Gritti, A. (2011). Neural stem cell gene therapy ameliorates pathology and function in a mouse model of globoid cell leukodystrophy. *Stem Cells (Dayton, Ohio)*, *29*(10), 1559–1571. https://doi.org/10.1002/STEM.701

Nguyen, G. N., Everett, J. K., Kafle, S., Roche, A. M., Raymond, H. E., Leiby, J.,

Wood, C., Assenmacher, C. A., Merricks, E. P., Long, C. T., Kazazian, H. H., Nichols, T. C., Bushman, F. D., & Sabatino, D. E. (2021). A long-term study of AAV gene therapy in dogs with hemophilia A identifies clonal expansions of transduced liver cells. *Nature Biotechnology*, *39*(1), 47–55. https://doi.org/10.1038/S41587-020-0741-7

Nicaise, A. M., Bongarzone, E. R., & Crocker, S. J. (2016). A microglial hypothesis of globoid cell leukodystrophy pathology. *Journal of Neuroscience Research*, *94*(11), 1049–1061. https://doi.org/10.1002/JNR.23773

Okuyama, T., Eto, Y., Sakai, N., Nakamura, K., Yamamoto, T., Yamaoka, M., Ikeda, T., So, S., Tanizawa, K., Sonoda, H., & Sato, Y. (2021). A Phase 2/3 Trial of Pabinafusp Alfa, IDS Fused with Anti-Human Transferrin Receptor Antibody, Targeting Neurodegeneration in MPS-II. *Molecular Therapy : The Journal of the American Society of Gene Therapy*, *29*(2), 671–679. https://doi.org/10.1016/J.YMTHE.2020.09.039

Olsen, A. S. B., & Færgeman, N. J. (2017). Sphingolipids: membrane microdomains in brain development, function and neurological diseases. *Open Biology*, *7*(5). https://doi.org/10.1098/RSOB.170069

Ornaghi, F., Sala, D., Tedeschi, F., Maffia, M. C., Bazzucchi, M., Morena, F., Valsecchi, M., Aureli, M., Martino, S., & Gritti, A. (2020). Novel bicistronic lentiviral vectors correct β-Hexosaminidase deficiency in neural and hematopoietic stem cells and progeny: implications for in vivo and ex vivo gene therapy of GM2 gangliosidosis. *Neurobiology of Disease*, *134*. https://doi.org/10.1016/J.NBD.2019.104667

Orsini, J. J. (2019). Newborn screening for Krabbe disease: perceived and current ethical issues. In *Developmental Medicine and Child Neurology* (Vol. 61, Issue 12, p. 1354). https://doi.org/10.1111/dmcn.14265

Orsini, J. J., Escolar, M. L., Wasserstein, M. P., & Caggana, M. (2018). Krabbe Disease. *GeneReviews*®. https://pubmed.ncbi.nlm.nih.gov/20301416/

Orsini, J. J., Kay, D. M., Saavedra-Matiz, C. A., Wenger, D. A., Duffner, P. K., Erbe, R. W., Biski, C., Martin, M., Krein, L. M., Nichols, M., Kurtzberg, J., Escolar, M. L., Adams, D. J., Arnold, G. L., Iglesias, A., Galvin-Parton, P., Kronn, D. F., Kwon, J. M., Levy, P. A., … Caggana, M. (2016). Newborn screening for Krabbe disease in New York State: The first eight years' experience. *Genetics in Medicine*, *18*(3), 239–248. https://doi.org/10.1038/gim.2015.211

Paciotti, S., Persichetti, E., Pagliardini, S., Deganuto, M., Rosano, C., Balducci, C., Codini, M., Filocamo, M., Menghini, A. R., Pagliardini, V., Pasqui, S., Bembi, B., Dardis, A., & Beccari, T. (2012). First pilot newborn screening for four

lysosomal storage diseases in an Italian region: identification and analysis of a putative causative mutation in the GBA gene. *Clinica Chimica Acta; International Journal of Clinical Chemistry*, *413*(23–24), 1827–1831. https://doi.org/10.1016/J.CCA.2012.07.011

Pan, X., Sands, S. A., Yue, Y., Zhang, K., Levine, S. M., & Duan, D. (2019). An Engineered Galactosylceramidase Construct Improves AAV Gene Therapy for Krabbe Disease in Twitcher Mice. *Human Gene Therapy*, *30*(9), 1039–1051. https://doi.org/10.1089/HUM.2019.008

Pardridge, W. M. (2022). Blood-brain barrier delivery for lysosomal storage disorders with IgG-lysosomal enzyme fusion proteins. *Advanced Drug Delivery Reviews*, *184*. https://doi.org/10.1016/J.ADDR.2022.114234

Pardridge, W. M., Kang, Y. S., Buciak, J. L., & Yang, J. (1995). Human insulin receptor monoclonal antibody undergoes high affinity binding to human brain capillaries in vitro and rapid transcytosis through the blood-brain barrier in vivo in the primate. *Pharmaceutical Research*, *12*(6), 807–816. https://doi.org/10.1023/A:1016244500596

Parenti, G., Andria, G., & Ballabio, A. (2015a). Lysosomal storage diseases: from pathophysiology to therapy. *Annual Review of Medicine*, *66*, 471–486. https://doi.org/10.1146/ANNUREV-MED-122313-085916

Parenti, G., Andria, G., & Valenzano, K. J. (2015b). Pharmacological Chaperone Therapy: Preclinical Development, Clinical Translation, and Prospects for the Treatment of Lysosomal Storage Disorders. *Molecular Therapy : The Journal of the American Society of Gene Therapy*, *23*(7), 1138–1148. https://doi.org/10.1038/MT.2015.62

Parenti, G., Medina, D. L., & Ballabio, A. (2021). The rapidly evolving view of lysosomal storage diseases. *EMBO Molecular Medicine*, *13*(2). https://doi.org/10.15252/EMMM.202012836

Pastores, G. M., & Sathe, S. (2006). A chaperone-mediated approach to enzyme enhancement as a therapeutic option for the lysosomal storage disorders. *Drugs in R&D*, *7*(6), 339–348. https://doi.org/10.2165/00126839-200607060-00003

Peake, R. W. A., & Bodamer, O. A. (2017). Newborn Screening for Lysosomal Storage Disorders. *J Pediatr Genet*, *6*, 51–60. https://doi.org/10.1055/s-0036-1593843

Pellegatta, S., Tunici, P., Poliani, P. L., Dolcetta, D., Cajola, L., Colombelli, C., Ciusani, E., Di Donato, S., & Finocchiaro, G. (2006). The therapeutic potential of neural stem/progenitor cells in murine globoid cell leukodystrophy is

conditioned by macrophage/microglia activation. *Neurobiology of Disease*, *21*(2), 314–323. https://doi.org/10.1016/J.NBD.2005.07.016

Penati, R., Fumagalli, F., Calbi, V., Bernardo, M. E., & Aiuti, A. (2017). Gene therapy for lysosomal storage disorders: recent advances for metachromatic leukodystrophy and mucopolysaccaridosis I. *Journal of Inherited Metabolic Disease*, *40*(4), 543–554. https://doi.org/10.1007/S10545-017-0052-4

Pereira, D. M., Valentão, P., & Andrade, P. B. (2018). Tuning protein folding in lysosomal storage diseases: the chemistry behind pharmacological chaperones. *Chemical Science*, *9*(7), 1740–1752. https://doi.org/10.1039/C7SC04712F

Perez, B. A., Shutterly, A., Chan, Y. K., Byrne, B. J., & Corti, M. (2020). Management of Neuroinflammatory Responses to AAV-Mediated Gene Therapies for Neurodegenerative Diseases. *Brain Sciences*, *10*(2). https://doi.org/10.3390/BRAINSCI10020119

Pievani, A., Azario, I., Antolini, L., Shimada, T., Patel, P., Remoli, C., Rambaldi, B., Valsecchi, M. G., Riminucci, M., Biondi, A., Tomatsu, S., & Serafini, M. (2015). Neonatal bone marrow transplantation prevents bone pathology in a mouse model of mucopolysaccharidosis type I. *Blood*, *125*(10), 1662–1671. https://doi.org/10.1182/blood-2014-06

Pinzõn-Daza, M. L., Garzõn, R., Couraud, P. O., Romero, I., Weksler, B., Ghigo, D., Bosia, A., & Riganti, C. (2012). The association of statins plus LDL receptor-targeted liposome-encapsulated doxorubicin increases in vitro drug delivery across blood-brain barrier cells. *British Journal of Pharmacology*, *167*(7), 1431–1447. https://doi.org/10.1111/J.1476-5381.2012.02103.X

Plasschaert, R. N., DeAndrade, M. P., Hull, F., Nguyen, Q., Peterson, T., Yan, A., Loperfido, M., Baricordi, C., Barbarossa, L., Yoon, J. K., Dogan, Y., Unnisa, Z., Schindler, J. W., van Til, N. P., Biasco, L., & Mason, C. (2022). High-throughput analysis of hematopoietic stem cell engraftment after intravenous and intracerebroventricular dosing. *Molecular Therapy : The Journal of the American Society of Gene Therapy*, *30*(10). https://doi.org/10.1016/J.YMTHE.2022.05.022

Platt, F. M., d'Azzo, A., Davidson, B. L., Neufeld, E. F., & Tifft, C. J. (2018). Lysosomal storage diseases. *Nature Reviews. Disease Primers*, *4*(1). https://doi.org/10.1038/S41572-018-0025-4

Platt, F. M., & Lachmann, R. H. (2009). Treating lysosomal storage disorders: current practice and future prospects. *Biochimica et Biophysica Acta*, *1793*(4), 737–745. https://doi.org/10.1016/J.BBAMCR.2008.08.009

Potter, G. B., & Petryniak, M. A. (2016). Neuroimmune mechanisms in Krabbe's disease. *Journal of Neuroscience Research*, *94*(11), 1341–1348. https://doi.org/10.1002/JNR.23804

Potter, G. B., Santos, M., Davisson, M. T., Rowitch, D. H., Marks, D. L., Bongarzone, E. R., & Petryniak, M. A. (2013). Missense mutation in mouse GALC mimics human gene defect and offers new insights into krabbe disease. *Human Molecular Genetics*, *22*(17), 3397–3414. https://doi.org/10.1093/hmg/ddt190

Prasad, V. K., & Kurtzberg, J. (2010). Cord blood and bone marrow transplantation in inherited metabolic diseases: scientific basis, current status and future directions. *British Journal of Haematology*, *148*(3), 356–372. https://doi.org/10.1111/J.1365-2141.2009.07974.X

Qin, E. Y., Hawkins-Salsbury, J. A., Jiang, X., Reddy, A. S., Farber, N. B., Ory, D. S., & Sands, M. S. (2012). Bone marrow transplantation increases efficacy of central nervous system-directed enzyme replacement therapy in the murine model of globoid cell leukodystrophy. *Molecular Genetics and Metabolism*, *107*(1–2), 186–196. https://doi.org/10.1016/J.YMGME.2012.05.021

Rabinowitz, J., Chan, Y. K., & Samulski, R. J. (2019). Adeno-associated Virus (AAV) versus Immune Response. *Viruses*, *11*(2). https://doi.org/10.3390/V11020102

Rafi, M. A., Luzi, P., & Wenger, D. A. (2020). Conditions for combining gene therapy with bone marrow transplantation in murine Krabbe disease. *BioImpacts : BI*, *10*(2), 105–115. https://doi.org/10.34172/BI.2020.13

Rafi, M. A., Rao, H. Z., Luzi, P., Curtis, M. T., & Wenger, D. A. (2012). Extended normal life after AAVrh10-mediated gene therapy in the mouse model of Krabbe disease. *Molecular Therapy : The Journal of the American Society of Gene Therapy*, *20*(11), 2031–2042. https://doi.org/10.1038/MT.2012.153

Rafi, M. A., Zhi Rao, H., Passini, M. A., Curtis, M., Vanier, M. T., Zaka, M., Luzi, P., Wolfe, J. H., & Wenger, D. A. (2005). AAV-mediated expression of galactocerebrosidase in brain results in attenuated symptoms and extended life span in murine models of globoid cell leukodystrophy. *Molecular Therapy : The Journal of the American Society of Gene Therapy*, *11*(5), 734–744. https://doi.org/10.1016/J.YMTHE.2004.12.020

Rawlinson, C., Jenkins, S., Thei, L., Dallas, M. L., & Chen, R. (2020). Post-Ischaemic Immunological Response in the Brain: Targeting Microglia in Ischaemic Stroke Therapy. *Brain Sciences*, *10*(3). https://doi.org/10.3390/BRAINSCI10030159

Reddy, A. S., Kim, J. H., Hawkins-Salsbury, J. A., Macauley, S. L., Tracy, E. T.,

Vogler, C. A., Han, X., Song, S. K., Wozniak, D. F., Fowler, S. C., Klein, R. S., & Sands, M. S. (2011). Bone marrow transplantation augments the effect of brain- and spinal cord-directed adeno-associated virus 2/5 gene therapy by altering inflammation in the murine model of globoid-cell leukodystrophy. *The Journal of Neuroscience : The Official Journal of the Society for Neuroscience*, *31*(27), 9945–9957. https://doi.org/10.1523/JNEUROSCI.1802-11.2011

Reghupaty, S. C., & Sarkar, D. (2019). Current Status of Gene Therapy in Hepatocellular Carcinoma. *Cancers*, *11*(9). https://doi.org/10.3390/CANCERS11091265

Ribbens, J., Whiteley, G., Furuya, H., Southall, N., Hu, X., Marugan, J., Ferrer, M., & Maegawa, G. H. B. (2013). A high-throughput screening assay using Krabbe disease patient cells. *Analytical Biochemistry*, *434*(1), 15–25. https://doi.org/10.1016/J.AB.2012.10.034

Ribitsch, I., Baptista, P. M., Lange-Consiglio, A., Melotti, L., Patruno, M., Jenner, F., Schnabl-Feichter, E., Dutton, L. C., Connolly, D. J., van Steenbeek, F. G., Dudhia, J., & Penning, L. C. (2020). Large Animal Models in Regenerative Medicine and Tissue Engineering: To Do or Not to Do. *Frontiers in Bioengineering and Biotechnology*, *8*. https://doi.org/10.3389/FBIOE.2020.00972

Ricca, A., Cascino, F., & Gritti, A. (2022). Isolation and Culture of Neural Stem/Progenitor Cells from the Postnatal Periventricular Region. *Methods in Molecular Biology (Clifton, N.J.)*, *2389*, 11–31. https://doi.org/10.1007/978-1-0716-1783-0_2

Ricca, A., Cascino, F., Morena, F., Martino, S., & Gritti, A. (2020). In vitro Validation of Chimeric β-Galactosylceramidase Enzymes With Improved Enzymatic Activity and Increased Secretion. *Frontiers in Molecular Biosciences*, *7*. https://doi.org/10.3389/FMOLB.2020.00167

Ricca, A., Rufo, N., Ungari, S., Morena, F., Martino, S., Kulik, W., Alberizzi, V., Bolino, A., Bianchi, F., Del Carro, U., Biffi, A., & Gritti, A. (2015). Combined gene/cell therapies provide long-term and pervasive rescue of multiple pathological symptoms in a murine model of globoid cell leukodystrophy. *Human Molecular Genetics*, *24*(12), 3372–3389. https://doi.org/10.1093/HMG/DDV086

Ruoppolo, M., Malvagia, S., Boenzi, S., Carducci, C., Dionisi-Vici, C., Teofoli, F., Burlina, A., Angeloni, A., Aronica, T., Bordugo, A., Bucci, I., Camilot, M., Carbone, M. T., Cardinali, R., Carducci, C., Cassanello, M., Castana, C., Cazzorla, C., Ciatti, R., … Uccheddu, A. P. (2022). Expanded Newborn

Screening in Italy Using Tandem Mass Spectrometry: Two Years of National Experience. *International Journal of Neonatal Screening*, *8*(3). https://doi.org/10.3390/IJNS8030047

Russell, D. W. (2007). AAV vectors, insertional mutagenesis, and cancer. *Molecular Therapy : The Journal of the American Society of Gene Therapy*, *15*(10), 1740–1743. https://doi.org/10.1038/SJ.MT.6300299

Rydell-Törmänen, K., & Johnson, J. R. (2019). The Applicability of Mouse Models to the Study of Human Disease. *Methods in Molecular Biology (Clifton, N.J.)*, *1940*, 3–22. https://doi.org/10.1007/978-1-4939-9086-3_1

Sabatino, D. E., Bushman, F. D., Chandler, R. J., Crystal, R. G., Davidson, B. L., Dolmetsch, R., Eggan, K. C., Gao, G., Gil-Farina, I., Kay, M. A., McCarty, D. M., Montini, E., Ndu, A., & Yuan, J. (2022). Evaluating the state of the science for adeno-associated virus integration: An integrated perspective. *Molecular Therapy : The Journal of the American Society of Gene Therapy*, *30*(8), 2646–2663. https://doi.org/10.1016/J.YMTHE.2022.06.004

Safina, D., Schlitt, F., Romeo, R., Pflanzner, T., Pietrzik, C. U., Narayanaswami, V., Edenhofer, F., & Faissner, A. (2016). Low-density lipoprotein receptor-related protein 1 is a novel modulator of radial glia stem cell proliferation, survival, and differentiation. *Glia*, *64*(8), 1363–1380. https://doi.org/10.1002/GLIA.23009

Saftig, P., & Klumperman, J. (2009). Lysosome biogenesis and lysosomal membrane proteins: trafficking meets function. *Nature Reviews. Molecular Cell Biology*, *10*(9), 623–635. https://doi.org/10.1038/NRM2745

Sailor, K. A., Agoranos, G., López-Manzaneda, S., Tada, S., Gillet-Legrand, B., Guerinot, C., Masson, J. B., Vestergaard, C. L., Bonner, M., Gagnidze, K., Veres, G., Lledo, P. M., & Cartier, N. (2022). Hematopoietic stem cell transplantation chemotherapy causes microglia senescence and peripheral macrophage engraftment in the brain. *Nature Medicine*, *28*(3), 517–527. https://doi.org/10.1038/S41591-022-01691-9

Sakai, N., Fukushima, H., Inui, K., Fu, L., Nishigaki, T., Yanagihara, I., Tatsumi, N., Ozono, K., & Okada, S. (1998). Human galactocerebrosidase gene: Promoter analysis of the 5'-flanking region and structural organization. *Biochimica et Biophysica Acta - Gene Structure and Expression*, *1395*(1), 62–67. https://doi.org/10.1016/S0167-4781(97)00140-1

Sakai, N., Inui, K., Tatsumi, N., Fukushima, H., Nishigaki, T., Taniike, M., Nishimoto, J., Tsukamoto, H., Yanagihara, I., Ozono, K., & Okada, S. (1996). Molecular cloning and expression of cDNA for murine galactocerebrosidase and

mutation analysis of the twitcher mouse, a model of Krabbe's disease. *Journal of Neurochemistry*, *66*(3), 1118–1124. https://doi.org/10.1046/J.1471-4159.1996.66031118.X

Sands, M. S., & Davidson, B. L. (2006). Gene therapy for lysosomal storage diseases. *Molecular Therapy : The Journal of the American Society of Gene Therapy*, *13*(5), 839–849. https://doi.org/10.1016/J.YMTHE.2006.01.006

Santambrogio, S., Ricca, A., Maderna, C., Ieraci, A., Aureli, M., Sonnino, S., Kulik, W., Aimar, P., Bonfanti, L., Martino, S., & Gritti, A. (2012). The galactocerebrosidase enzyme contributes to maintain a functional neurogenic niche during early post-natal CNS development. *Human Molecular Genetics*, *21*(21), 4732–4750. https://doi.org/10.1093/HMG/DDS313

Santi, L., De Ponti, G., Dina, G., Pievani, A., Corsi, A., Riminucci, M., Khan, S., Sawamoto, K., Antolini, L., Gregori, S., Annoni, A., Biondi, A., Quattrini, A., Tomatsu, S., & Serafini, M. (2020). Neonatal combination therapy improves some of the clinical manifestations in the Mucopolysaccharidosis type I murine model. *Molecular Genetics and Metabolism*, *130*(3), 197–208. https://doi.org/10.1016/J.YMGME.2020.05.001

Sasaki, M., Sakuragawa, N., Takashima, S., Hanaoka, S., & Arima, M. (1991). MRI and CT findings in Krabbe disease. *Pediatric Neurology*, *7*(4), 283–288. https://doi.org/10.1016/0887-8994(91)90046-N

Schulze, H., & Sandhoff, K. (2011). Lysosomal lipid storage diseases. *Cold Spring Harbor Perspectives in Biology*, *3*(6), 1–19. https://doi.org/10.1101/CSHPERSPECT.A004804

Schwarze, S. R., Ho, A., Vocero-Akbani, A., & Dowdy, S. F. (1999). In vivo protein transduction: delivery of a biologically active protein into the mouse. *Science (New York, N.Y.)*, *285*(5433), 1569–1572. https://doi.org/10.1126/SCIENCE.285.5433.1569

Sergijenko, A., Langford-Smith, A., Liao, A. Y., Pickford, C. E., McDermott, J., Nowinski, G., Langford-Smith, K. J., Merry, C. L., Jones, S. A., Wraith, J. E., Wynn, R. F., Wilkinson, F. L., & Bigger, B. W. (2013). Myeloid/Microglial driven autologous hematopoietic stem cell gene therapy corrects a neuronopathic lysosomal disease. *Molecular Therapy : The Journal of the American Society of Gene Therapy*, *21*(10), 1938–1949. https://doi.org/10.1038/MT.2013.141

Sessa, M., Lorioli, L., Fumagalli, F., Acquati, S., Redaelli, D., Baldoli, C., Canale, S., Lopez, I. D., Morena, F., Calabria, A., Fiori, R., Silvani, P., Rancoita, P. M. V., Gabaldo, M., Benedicenti, F., Antonioli, G., Assanelli, A., Cicalese, M. P., del Carro, U., … Biffi, A. (2016). Lentiviral haemopoietic stem-cell gene therapy in

early-onset metachromatic leukodystrophy: an ad-hoc analysis of a non-randomised, open-label, phase 1/2 trial. *Lancet (London, England)*, *388*(10043), 476–487. https://doi.org/10.1016/S0140-6736(16)30374-9

Sevin, C., & Deiva, K. (2021). Clinical Trials for Gene Therapy in Lysosomal Diseases With CNS Involvement. *Frontiers in Molecular Biosciences*, *8*. https://doi.org/10.3389/FMOLB.2021.624988

Shemer, A., Grozovski, J., Tay, T. L., Tao, J., Volaski, A., Süß, P., Ardura-Fabregat, A., Gross-Vered, M., Kim, J. S., David, E., Chappell-Maor, L., Thielecke, L., Glass, C. K., Cornils, K., Prinz, M., & Jung, S. (2018). Engrafted parenchymal brain macrophages differ from microglia in transcriptome, chromatin landscape and response to challenge. *Nature Communications*, *9*(1). https://doi.org/10.1038/S41467-018-07548-5

Shihabuddin, L. S., & Cheng, S. H. (2011). Neural stem cell transplantation as a therapeutic approach for treating lysosomal storage diseases. *Neurotherapeutics : The Journal of the American Society for Experimental NeuroTherapeutics*, *8*(4), 659–667. https://doi.org/10.1007/S13311-011-0067-8

Shin, D., Feltri, M. L., & Wrabetz, L. (2016). Altered Trafficking and Processing of GALC Mutants Correlates with Globoid Cell Leukodystrophy Severity. *The Journal of Neuroscience : The Official Journal of the Society for Neuroscience*, *36*(6), 1858–1870. https://doi.org/10.1523/JNEUROSCI.3095-15.2016

Siddiqi, Z. A., Sanders, D. B., & Massey, J. M. (2006a). Peripheral neuropathy in Krabbe disease: effect of hematopoietic stem cell transplantation. *Neurology*, *67*(2), 268–272. https://doi.org/10.1212/01.WNL.0000230156.01228.33

Siddiqi, Z. A., Sanders, D. B., & Massey, J. M. (2006b). Peripheral neuropathy in Krabbe disease: electrodiagnostic findings. *Neurology*, *67*(2), 263–267. https://doi.org/10.1212/01.WNL.0000230153.34613.84

Sikonja, J., Groselj, U., Scarpa, M., la Marca, G., Cheillan, D., Kölker, S., Zetterström, R. H., Kožich, V., Cam, Y. Le, Gumus, G., Bottarelli, V., van der Burg, M., Dekkers, E., Battelino, T., Prevot, J., Schielen, P. C. J. I., & Bonham, J. R. (2022). Towards Achieving Equity and Innovation in Newborn Screening across Europe. *International Journal of Neonatal Screening*, *8*(2). https://doi.org/10.3390/IJNS8020031

Smith, B., Galbiati, F., Castelvetri, L. C., Givogri, M. I., Lopez-Rosas, A., & Bongarzone, E. R. (2011). Peripheral neuropathy in the Twitcher mouse involves the activation of axonal caspase 3. *ASN Neuro*, *3*(4), 213–222. https://doi.org/10.1042/AN20110019

Snook, E. R., Fisher-Perkins, J. M., Sansing, H. A., Lee, K. M., Alvarez, X., MacLean, A. G., Peterson, K. E., Lackner, A. A., & Bunnell, B. A. (2014). Innate immune activation in the pathogenesis of a murine model of globoid cell leukodystrophy. *The American Journal of Pathology*, *184*(2), 382–396. https://doi.org/10.1016/J.AJPATH.2013.10.011

Solomon, M., & Muro, S. (2017). Lysosomal enzyme replacement therapies: Historical development, clinical outcomes, and future perspectives. *Advanced Drug Delivery Reviews*, *118*, 109–134. https://doi.org/10.1016/J.ADDR.2017.05.004

Sorrentino, N. C., Cacace, V., De Risi, M., Maffia, V., Strollo, S., Tedesco, N., Nusco, E., Romagnoli, N., Ventrella, D., Huang, Y., Liu, N., Kalled, S. L., Choi, V. W., De Leonibus, E., & Fraldi, A. (2019). Enhancing the Therapeutic Potential of Sulfamidase for the Treatment of Mucopolysaccharidosis IIIA. *Molecular Therapy. Methods & Clinical Development*, *15*, 333–342. https://doi.org/10.1016/J.OMTM.2019.10.009

Sorrentino, N. C., D'Orsi, L., Sambri, I., Nusco, E., Monaco, C., Spampanato, C., Polishchuk, E., Saccone, P., De Leonibus, E., Ballabio, A., & Fraldi, A. (2013). A highly secreted sulphamidase engineered to cross the blood-brain barrier corrects brain lesions of mice with mucopolysaccharidoses type IIIA. *EMBO Molecular Medicine*, *5*(5), 675–690. https://doi.org/10.1002/EMMM.201202083

Soulet, D., & Rivest, S. (2008). Bone-marrow-derived microglia: myth or reality? *Current Opinion in Pharmacology*, *8*(4), 508–518. https://doi.org/10.1016/J.COPH.2008.04.002

Spada, M., Pagliardini, S., Yasuda, M., Tukel, T., Thiagarajan, G., Sakuraba, H., Ponzone, A., & Desnick, R. J. (2006). High incidence of later-onset fabry disease revealed by newborn screening. *American Journal of Human Genetics*, *79*(1), 31–40. https://doi.org/10.1086/504601

Spencer, B. J., & Verma, I. M. (2007). Targeted delivery of proteins across the blood-brain barrier. *Proceedings of the National Academy of Sciences of the United States of America*, *104*(18), 7594–7599. https://doi.org/10.1073/PNAS.0702170104

Spiegel, S., & Milstien, S. (2003). Sphingosine-1-phosphate: an enigmatic signalling lipid. *Nature Reviews. Molecular Cell Biology*, *4*(5), 397–407. https://doi.org/10.1038/NRM1103

Spratley, S. J., & Deane, J. E. (2016). New therapeutic approaches for Krabbe disease: The potential of pharmacological chaperones. *Journal of Neuroscience Research*, *94*(11), 1203–1219. https://doi.org/10.1002/JNR.23762

Srivastava, A. (2016). In vivo tissue-tropism of adeno-associated viral vectors. *Current Opinion in Virology*, *21*, 75–80. https://doi.org/10.1016/J.COVIRO.2016.08.003

Stern, B., Olsen, L. C., Tröße, C., Ravneberg, H., & Pryme, I. F. (2008). Improving mammalian cell factories: The selection of signal peptide has a major impact on recombinant protein synthesis and secretion in mammalian cells. *Trends in Cell & Molecular Biology*, *2*, 1–17. http://www.researchtrends.net/tia/abstract.asp?tid=55&in=0&vn=2&aid=2346

Storck, S. E., Meister, S., Nahrath, J., Meißner, J. N., Schubert, N., Di Spiezio, A., Baches, S., Vandenbroucke, R. E., Bouter, Y., Prikulis, I., Korth, C., Weggen, S., Heimann, A., Schwaninger, M., Bayer, T. A., & Pietrzik, C. U. (2016). Endothelial LRP1 transports amyloid-β(1-42) across the blood-brain barrier. *The Journal of Clinical Investigation*, *126*(1), 123–136. https://doi.org/10.1172/JCI81108

Sugie, K., Koori, T., Yamamoto, A., Ogawa, M., Hirano, M., Inoue, K., Nonaka, I., & Nishino, I. (2003). Characterization of Danon disease in a male patient and his affected mother. *Neuromuscular Disorders*, *13*(9), 708–711. https://doi.org/10.1016/S0960-8966(03)00105-6

Sun, A. (2018). Lysosomal storage disease overview. *Annals of Translational Medicine*, *6*(24), 476.-476. https://doi.org/10.21037/ATM.2018.11.39

Suzuki, K., & Suzuki, K. (1983). The twitcher mouse. A model of human globoid cell leukodystrophy (krabbe's disease). *The American Journal of Pathology*, *111*(3), 394–397. https://pubmed.ncbi.nlm.nih.gov/6859223/

Suzuki, K., & Suzuki, K. (1990). Myelin pathology in the twitcher mouse. *Annals of the New York Academy of Sciences*, *605*(1), 313–324. https://doi.org/10.1111/J.1749-6632.1990.TB42405.X

Suzuki, K., & Suzuki, Y. (1970). Globoid cell leucodystrophy (Krabbe's disease): deficiency of galactocerebroside beta-galactosidase. *Proceedings of the National Academy of Sciences of the United States of America*, *66*(2), 302–309. https://doi.org/10.1073/PNAS.66.2.302

Suzuki, K. (2003). Globoid cell leukodystrophy (Krabbe's disease): update. *Journal of Child Neurology*, *18*(9), 595–603. https://doi.org/10.1177/08830738030180090201

Suzuki, Kinuko, & Taniike, M. (1995). Murine model of genetic demyelinating disease: the twitcher mouse. *Microscopy Research and Technique*, *32*(3), 204–214. https://doi.org/10.1002/JEMT.1070320304

Suzuki, Kunihiko, & Suzuki, K. (1995). The twitcher mouse: a model for Krabbe

disease and for experimental therapies. *Brain Pathology (Zurich, Switzerland)*, *5*(3), 249–258. https://doi.org/10.1111/J.1750-3639.1995.TB00601.X

Svennerholm, L., & Vanier, M.-T. (1980). *Krabbe disease: a galactosylsphingosine (psychosine) lipidosis.* https://doi.org/10.1016/S0022-2275(20)39839-4

Takahashi, H., Igisu, H., Suzuki, K., & Suzuki, K. (1983). Murine globoid cell leukodystrophy (the twitcher mouse). The presence of characteristic inclusions in the kidney and lymph nodes. *The American Journal of Pathology*, *112*(2), 147. /pmc/articles/PMC1916262/?report=abstract

Tan, E. Y., Boelens, J. J., Jones, S. A., & Wynn, R. F. (2019). Hematopoietic Stem Cell Transplantation in Inborn Errors of Metabolism. *Frontiers in Pediatrics*, *7*. https://doi.org/10.3389/FPED.2019.00433

Tanaka, N., Kida, S., Kinoshita, M., Morimoto, H., Shibasaki, T., Tachibana, K., & Yamamoto, R. (2018). Evaluation of cerebrospinal fluid heparan sulfate as a biomarker of neuropathology in a murine model of mucopolysaccharidosis type II using high-sensitivity LC/MS/MS. *Molecular Genetics and Metabolism*, *125*(1–2), 53–58. https://doi.org/10.1016/J.YMGME.2018.07.013

Taniike, M., & Suzuki, K. (1994). Spacio-temporal progression of demyelination in twitcher mouse: with clinico-pathological correlation. *Acta Neuropathologica*, *88*(3), 228–236. https://doi.org/10.1007/BF00293398

Tappino, B., Biancheri, R., Mort, M., Regis, S., Corsolini, F., Rossi, A., Stroppiano, M., Lualdi, S., Fiumara, A., Bembi, B., Di Rocco, M., Cooper, D. N., & Filocamo, M. (2010). Identification and characterization of 15 novel GALC gene mutations causing Krabbe disease. *Human Mutation*, *31*(12). https://doi.org/10.1002/HUMU.21367

Tominaga, K., Matsuda, J., Kido, M., Naito, E., Yokota, I., Toida, K., Ishimura, K., Suzuki, K., & Kuroda, Y. (2004). Genetic background markedly influences vulnerability of the hippocampal neuronal organization in the "twitcher" mouse model of globoid cell leukodystrophy. *Journal of Neuroscience Research*, *77*(4), 507–516. https://doi.org/10.1002/JNR.20190

Toyoshima, E., Yeager, A. M., Brennan, S., Santos, G. W., Moser, H. W., & Mayer, R. F. (1986). Nerve conduction studies in the Twitcher mouse (murine globoid cell leukodystrophy). *Journal of the Neurological Sciences*, *74*(2–3), 307–318. https://doi.org/10.1016/0022-510X(86)90116-4

Ullman, J. C., Arguello, A., Getz, J. A., Bhalla, A., Mahon, C. S., Wang, J., Giese, T., Bedard, C., Jin Kim, D., Blumenfeld, J. R., Liang, N., Ravi, R., Nugent, A. A., Davis, S. S., Ha, C., Duque, J., Tran, H. L., Wells, R. C., Lianoglou, S., … Henry, A. G. (2020). Brain delivery and activity of a lysosomal enzyme using a

blood-brain barrier transport vehicle in mice. In *Sci. Transl. Med* (Vol. 12). http://stm.sciencemag.org/

Ungari, S., Montepeloso, A., Morena, F., Cocchiarella, F., Recchia, A., Martino, S., Gentner, B., Naldini, L., & Biffi, A. (2015). Design of a regulated lentiviral vector for hematopoietic stem cell gene therapy of globoid cell leukodystrophy. *Molecular Therapy. Methods & Clinical Development*, *2*, 15038. https://doi.org/10.1038/MTM.2015.38

Vandamme, C., Adjali, O., & Mingozzi, F. (2017). Unraveling the Complex Story of Immune Responses to AAV Vectors Trial After Trial. *Human Gene Therapy*, *28*(11), 1061–1074. https://doi.org/10.1089/HUM.2017.150

Vandamme, T. (2014). Use of rodents as models of human diseases. *Journal of Pharmacy & Bioallied Sciences*, *6*(1), 2–9. https://doi.org/10.4103/0975-7406.124301

Vanier, M. T., & Svennerholm, L. (1974). Chemical pathology of Krabbe's disease. I. Lipid composition and fatty acid patterns of phosphoglycerides in brain. *Acta Paediatrica Scandinavica*, *63*(4), 494–500. https://doi.org/10.1111/J.1651-2227.1974.TB04838.X

Victoria, T., Rafi, M. A., & Wenger, D. A. (1996). Cloning of the canine GALC cDNA and identification of the mutation causing globoid cell leukodystrophy in West Highland White and Cairn terriers. *Genomics*, *33*(3), 457–462. https://doi.org/10.1006/GENO.1996.0220

Vigna, E., Amendola, M., Benedicenti, F., Simmons, A. D., Follenzi, A., & Naldini, L. (2005). Efficient Tet-dependent expression of human factor IX in vivo by a new self-regulating lentiviral vector. *Molecular Therapy : The Journal of the American Society of Gene Therapy*, *11*(5), 763–775. https://doi.org/10.1016/J.YMTHE.2004.11.017

Visigalli, I., Delai, S., Ferro, F., Cecere, F., Vezzoli, M., Sanvito, F., Chanut, F., Benedicenti, F., Spinozzi, G., Wynn, R., Calabria, A., Naldini, L., Montini, E., Cristofori, P., & Biffi, A. (2016). Preclinical Testing of the Safety and Tolerability of Lentiviral Vector-Mediated Above-Normal Alpha-L-Iduronidase Expression in Murine and Human Hematopoietic Cells Using Toxicology and Biodistribution Good Laboratory Practice Studies. *Human Gene Therapy*, *27*(10), 813–829. https://doi.org/10.1089/HUM.2016.068

Visigalli, I., Delai, S., Politi, L. S., Di Domenico, C., Cerri, F., Mrak, E., D'Isa, R., Ungaro, D., Stok, M., Sanvito, F., Mariani, E., Staszewsky, L., Godi, C., Russo, I., Cecere, F., Del Carro, U., Rubinacci, A., Brambilla, R., Quattrini, A., … Biffi, A. (2010). Gene therapy augments the efficacy of hematopoietic cell

transplantation and fully corrects mucopolysaccharidosis type I phenotype in the mouse model. *Blood*, *116*(24), 5130–5139. https://doi.org/10.1182/BLOOD-2010-04-278234

Visigalli, I., Moresco, R. M., Belloli, S., Politi, L. S., Gritti, A., Ungaro, D., Matarrese, M., Turolla, E., Falini, A., Scotti, G., Naldini, L., Fazio, F., & Biffi, A. (2009). Monitoring disease evolution and treatment response in lysosomal disorders by the peripheral benzodiazepine receptor ligand PK11195. *Neurobiology of Disease*, *34*(1), 51–62. https://doi.org/10.1016/J.NBD.2008.12.019

von Heijne, G. (1990). The signal peptide. *The Journal of Membrane Biology*, *115*(3), 195–201. https://doi.org/10.1007/BF01868635

Wakabayashi, T., Shimada, Y., Akiyama, K., Higuchi, T., Fukuda, T., Kobayashi, H., Eto, Y., Ida, H., & Ohashi, T. (2015). Hematopoietic Stem Cell Gene Therapy Corrects Neuropathic Phenotype in Murine Model of Mucopolysaccharidosis Type II. *Human Gene Therapy*, *26*(6), 357–366. https://doi.org/10.1089/HUM.2014.158

Walkley, S. U. (2007). Pathogenic mechanisms in lysosomal disease: a reappraisal of the role of the lysosome. *Acta Paediatrica (Oslo, Norway : 1992)*, *96*(455), 26–32. https://doi.org/10.1111/J.1651-2227.2007.00202.X

Wang, D., El-Amouri, S. S., Dai, M., Kuan, C. Y., Hui, D. Y., Brady, R. O., & Pan, D. (2013). Engineering a lysosomal enzyme with a derivative of receptor-binding domain of apoE enables delivery across the blood-brain barrier. *Proceedings of the National Academy of Sciences of the United States of America*, *110*(8), 2999–3004. https://doi.org/10.1073/PNAS.1222742110

Wasserstein, M. P., Andriola, M., Arnold, G., Aron, A., Duffner, P., Erbe, R. W., Escolar, M. L., Estrella, L., Galvin-Parton, P., Iglesias, A., Kay, D. M., Kronn, D. F., Kurtzberg, J., Kwon, J. M., Langan, T. J., Levy, P. A., Naidich, T. P., Orsini, J. J., Pellegrino, J. E., … Caggana, M. (2016). Clinical outcomes of children with abnormal newborn screening results for Krabbe disease in New York State. *Genetics in Medicine*, *18*(12), 1235–1243. https://doi.org/10.1038/GIM.2016.35

Weinstock, N. I., Kreher, C., Favret, J., Nguyen, D., Bongarzone, E. R., Wrabetz, L., Laura Feltri, M., & Shin, D. (2020a). Brainstem development requires galactosylceramidase and is critical for pathogenesis in a model of Krabbe disease. *Nature Communications*, *11*(1). https://doi.org/10.1038/s41467-020-19179-w

Weinstock, N. I., Shin, D., Dhimal, N., Hong, X., Irons, E. E., Silvestri, N. J., Reed, C. B., Nguyen, D., Sampson, O., Cheng, Y. C., Lau, J. T. Y., Bongarzone, E. R.,

Kofler, J., Escolar, M. L., Gelb, M. H., Wrabetz, L., & Feltri, M. L. (2020b). Macrophages Expressing GALC Improve Peripheral Krabbe Disease by a Mechanism Independent of Cross-Correction. *Neuron*, *107*(1), 65-81.e9. https://doi.org/10.1016/J.NEURON.2020.03.031

Wenger, D.A, Escolar, M. ., Luzi, P., & Rafi, M. . (2019). *Krabbe disease (Globoid Cell Leukodystrophy) | The Online Metabolic and Molecular Bases of Inherited Disease | OMMBID | McGraw Hill Medical*. https://ommbid.mhmedical.com/content.aspx?bookid=2709&sectionid=225546481

Wenger, D. A., Rafi, M. A., & Luzi, P. (1997). Molecular genetics of Krabbe disease (globoid cell leukodystrophy): diagnostic and clinical implications. *Human Mutation*, *10*(4), 268–279. https://doi.org/10.1002/(sici)1098-1004(1997)10:4<268::aid-humu2>3.0.co;2-d

Wenger, D. A., Rafi, M. A., Luzi, P., Datto, J., & Costantino-Ceccarini, E. (2000). Krabbe disease: genetic aspects and progress toward therapy. *Molecular Genetics and Metabolism*, *70*(1), 1–9. https://doi.org/10.1006/MGME.2000.2990

Wenger, D. A., Victoria, T., Rafi, M. A., Luzi, P., Vanier, M. T., Vite, C., Patterson, D. F., & Haskins, M. H. (1999). Globoid cell leukodystrophy in cairn and West Highland white terriers. *The Journal of Heredity*, *90*(1), 138–142. https://doi.org/10.1093/JHERED/90.1.138

White, A. B., Galbiati, F., Givogri, M. I., Lopez Rosas, A., Qiu, X., Van Breemen, R., & Bongarzone, E. R. (2011). Persistence of psychosine in brain lipid rafts is a limiting factor in the therapeutic recovery of a mouse model for Krabbe disease. *Journal of Neuroscience Research*, *89*(3), 352–364. https://doi.org/10.1002/JNR.22564

White, A. B., Givogri, M. I., Lopez-Rosas, A., Cao, H., Van Breemen, R., Thinakaran, G., & Bongarzone, E. R. (2009). Psychosine accumulates in membrane microdomains in the brain of krabbe patients, disrupting the raft architecture. *The Journal of Neuroscience : The Official Journal of the Society for Neuroscience*, *29*(19), 6068–6077. https://doi.org/10.1523/JNEUROSCI.5597-08.2009

Wicks, S. E., Londot, H., Zhang, B., Dowden, J., Klopf-Eiermann, J., Fisher-Perkins, J. M., Trygg, C. B., Scruggs, B. A., Zhang, X., Gimble, J. M., Bunnell, B. A., & Pistell, P. J. (2011). Effect of intrastriatal mesenchymal stromal cell injection on progression of a murine model of Krabbe disease. *Behavioural Brain Research*, *225*(2), 415–425. https://doi.org/10.1016/J.BBR.2011.07.051

Wilkinson, F. L., Sergijenko, A., Langford-Smith, K. J., Malinowska, M., Wynn, R. F., & Bigger, B. W. (2013). Busulfan conditioning enhances engraftment of hematopoietic donor-derived cells in the brain compared with irradiation. *Molecular Therapy : The Journal of the American Society of Gene Therapy*, *21*(4), 868–876. https://doi.org/10.1038/MT.2013.29

Won, J. S., Kim, J., Paintlia, M. K., Singh, I., & Singh, A. K. (2013). Role of endogenous psychosine accumulation in oligodendrocyte differentiation and survival: implication for Krabbe disease. *Brain Research*, *1508*, 44–52. https://doi.org/10.1016/J.BRAINRES.2013.02.024

Wong, L. F., Goodhead, L., Prat, C., Mitrophanous, K. A., Kingsman, S. M., & Mazarakis, N. D. (2006). Lentivirus-mediated gene transfer to the central nervous system: therapeutic and research applications. *Human Gene Therapy*, *17*(1), 1–9. https://doi.org/10.1089/HUM.2006.17.1

Wraith, J. E., Beck, M., Lane, R., Van Der Ploeg, A., Shapiro, E., Xue, Y., Kakkis, E. D., & Guffon, N. (2007). Enzyme replacement therapy in patients who have mucopolysaccharidosis I and are younger than 5 years: results of a multinational study of recombinant human alpha-L-iduronidase (laronidase). *Pediatrics*, *120*(1). https://doi.org/10.1542/PEDS.2006-2156

Wright, M. D., Poe, M. D., DeRenzo, A., Shilpa Haldal, B., & Escolar, M. L. (2017). *Developmental outcomes of cord blood transplantation for Krabbe disease*.

Xu, M., Motabar, O., Ferrer, M., Marugan, J. J., Zheng, W., & Ottinger, E. A. (2016). Disease models for the development of therapies for lysosomal storage diseases. *Annals of the New York Academy of Sciences*, *1371*(1), 15–29. https://doi.org/10.1111/NYAS.13052

Yamada, T., Okamura, S., Okazaki, T., Ushiroyama, T., Yanagawa, Y., Ueki, M., Sugimoto, O., Yamazaki, H., Sugino, M., & Masui, Y. (1989). Leukoencephalopathy following treatment with carmofur: a case report and review of the Japanese literature. *Asia-Oceania Journal of Obstetrics and Gynaecology*, *15*(2), 161–168. https://doi.org/10.1111/J.1447-0756.1989.TB00171.X

Yeager, A. M., Shinn, C., Shinohara, M., & Pardoll, D. M. (1993). Hematopoietic cell transplantation in the twitcher mouse. The effects of pretransplant conditioning with graded doses of busulfan. *Transplantation*, *56*(1), 185–190. https://doi.org/10.1097/00007890-199307000-00034

Youshani, A. S., Rowlston, S., O'Leary, C., Forte, G., Parker, H., Liao, A., Telfer, B., Williams, K., Kamaly-Asl, I. D., & Bigger, B. W. (2019). Non-myeloablative busulfan chimeric mouse models are less pro-inflammatory than head-shielded

irradiation for studying immune cell interactions in brain tumours. *Journal of Neuroinflammation*, *16*(1). https://doi.org/10.1186/S12974-019-1410-Y

Yu, K., Youshani, A. S., Wilkinson, F. L., O'Leary, C., Cook, P., Laaniste, L., Liao, A., Mosses, D., Waugh, C., Shorrock, H., Pathmanaban, O., Macdonald, A., Kamaly-Asl, I., Roncaroli, F., & Bigger, B. W. (2019). A nonmyeloablative chimeric mouse model accurately defines microglia and macrophage contribution in glioma. *Neuropathology and Applied Neurobiology*, *45*(2), 119–140. https://doi.org/10.1111/NAN.12489

Zaka, M., & Wenger, D. A. (2004). Psychosine-induced apoptosis in a mouse oligodendrocyte progenitor cell line is mediated by caspase activation. *Neuroscience Letters*, *358*(3), 205–209. https://doi.org/10.1016/j.neulet.2003.12.126

Zhang, L., Leng, Q., & Mixson, A. J. (2005). Alteration in the IL-2 signal peptide affects secretion of proteins in vitro and in vivo. *The Journal of Gene Medicine*, *7*(3), 354–365. https://doi.org/10.1002/JGM.677

Zhang, X. Y., Dinh, A., Cronin, J., Li, S. C., & Reiser, J. (2008). Cellular uptake and lysosomal delivery of galactocerebrosidase tagged with the HIV Tat protein transduction domain. *Journal of Neurochemistry*, *104*(4), 1055–1064. https://doi.org/10.1111/J.1471-4159.2007.05030.X

Zhao, Y., Li, D., Zhao, J., Song, J., & Zhao, Y. (2016). The role of the low-density lipoprotein receptor-related protein 1 (LRP-1) in regulating blood-brain barrier integrity. *Reviews in the Neurosciences*, *27*(6), 623–634. https://doi.org/10.1515/REVNEURO-2015-0069

Zheng, C. X., Wang, S. M., Bai, Y. H., Luo, T. T., Wang, J. Q., Dai, C. Q., Guo, B. L., Luo, S. C., Wang, D. H., Yang, Y. L., & Wang, Y. Y. (2018). Lentiviral Vectors and Adeno-Associated Virus Vectors: Useful Tools for Gene Transfer in Pain Research. *Anatomical Record (Hoboken, N.J. : 2007)*, *301*(5), 825–836. https://doi.org/10.1002/AR.23723

Zhou, S., Mody, D., DeRavin, S. S., Hauer, J., Lu, T., Ma, Z., Abina, S. H. B., Gray, J. T., Greene, M. R., Cavazzana-Calvo, M., Malech, H. L., & Sorrentino, B. P. (2010). A self-inactivating lentiviral vector for SCID-X1 gene therapy that does not activate LMO2 expression in human T cells. *Blood*, *116*(6), 900–908. https://doi.org/10.1182/BLOOD-2009-10-250209

Zijlmans, J. M., Visser, J. W. M., Laterveer, L., Kleiverda, K., Heemskerk, D. P. M., Kluin, P. M., Willemze, R., & Fibbe, W. E. (1998). The early phase of engraftment after murine blood cell transplantation is mediated by hematopoietic stem cells. *Proceedings of the National Academy of Sciences of*

the United States of America, *95*(2), 725–729. https://doi.org/10.1073/PNAS.95.2.725

Zizioli, D., Guarienti, M., Tobia, C., Gariano, G., Borsani, G., Bresciani, R., Ronca, R., Giacopuzzi, E., Preti, A., Gaudenzi, G., Belleri, M., Di Salle, E., Fabrias, G., Casas, J., Ribatti, D., Monti, E., & Presta, M. (2014). Molecular cloning and knockdown of galactocerebrosidase in zebrafish: new insights into the pathogenesis of Krabbe's disease. *Biochimica et Biophysica Acta*, *1842*(4), 665–675. https://doi.org/10.1016/J.BBADIS.2014.01.008

Zlotogora, J., Chakraborty, S., Knowlton, R. G., & Wenger, D. A. (1990). Krabbe disease locus mapped to chromosome 14 by genetic linkage. *American Journal of Human Genetics*, *47*(1), 37. /pmc/articles/PMC1683747/?report=abstract

Zonari, E., Desantis, G., Petrillo, C., Boccalatte, F. E., Lidonnici, M. R., Kajaste-Rudnitski, A., Aiuti, A., Ferrari, G., Naldini, L., & Gentner, B. (2017). Efficient Ex Vivo Engineering and Expansion of Highly Purified Human Hematopoietic Stem and Progenitor Cell Populations for Gene Therapy. *Stem Cell Reports*, *8*(4), 977–990. https://doi.org/10.1016/J.STEMCR.2017.02.010